Sistemas miméticos de los cuerpos laminares epidérmicos para el tratamiento de la piel

Verónica Moner del Moral

UNIVERSITAT DE BARCELONA

iQAC CSIC
CONSEJO SUPERIOR DE INVESTIGACIONES CIENTÍFICAS

Tesis Doctoral
2018

Sistemas miméticos de los cuerpos laminares epidérmicos para el tratamiento de la piel

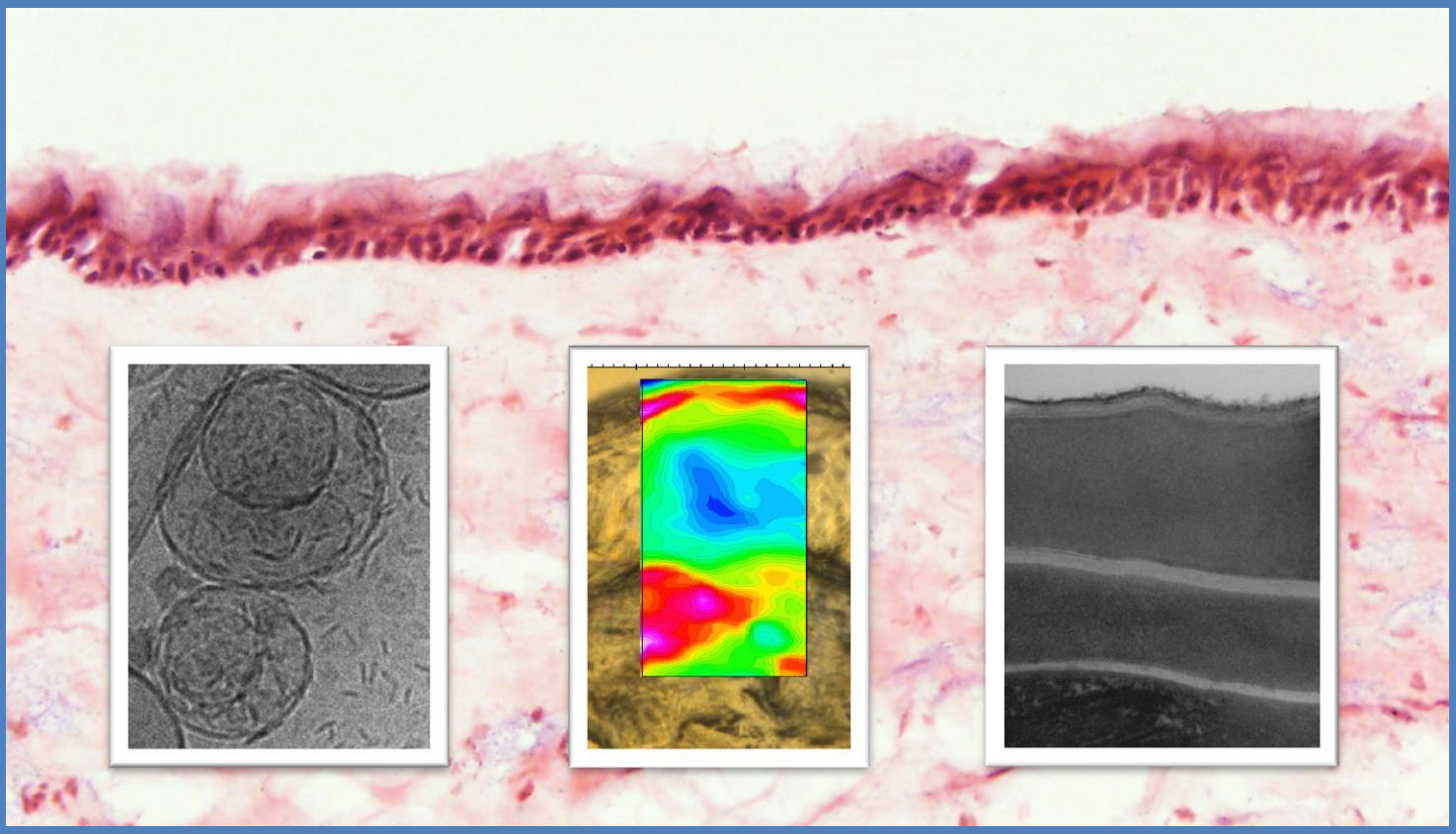

Verónica Moner del Moral

UNIVERSIDAD DE BARCELONA

FACULTAD DE FARMACIA Y CIENCIAS DE LA ALIMENTACIÓN

CONSEJO SUPERIOR DE INVESTIGACIONES CIENTIFICAS

INSTITUTO DE QUÍMICA AVANZADA DE CATALUÑA (IQAC-CSIC)

Departamento de Tensioactivos y Nanobiotecnología

Sistemas miméticos de los cuerpos laminares epidérmicos para el tratamiento de la piel

Verónica Moner del Moral

Barcelona, 2018

PROGRAMA DE DOCTORADO:

Investigación, Desarrollo y Control de Medicamentos

Sistemas miméticos de los cuerpos laminares epidérmicos para el tratamiento de la piel

Memoria presentada por Verónica Moner del Moral para optar al título de doctora por la Universidad de Barcelona.

Verónica Moner del Moral

La presente Tesis Doctoral ha sido realizada en el Departamento de Tensioactivos y Nanobiotecnología del Instituto de Química Avanzada de Cataluña del Consejo Superior de Investigaciones Científicas (IQAC-CSIC) bajo la dirección de la Dra. Olga López Serrano y de la tutoría de Dr. Alfonso del Pozo Carrascosa del Departamento de Farmacia y Tecnología Farmacéutica de la Universidad de Barcelona, que autorizan su presentación:

Dra. Olga López Serrano

Dr. Alfonso del Pozo Carrascosa

Barcelona, 2018

Esta tesis doctoral ha sido realizada con el apoyo de:

- Proyecto “Sistemas lipídicos avanzados para la vehiculización de antioxidantes en aplicaciones dermatológicas”. Ministerio de Economía y Competitividad (MINECO), Gobierno de España. *Ref. CTQ2013-44998-P.*
- Ayudas para contratos predoctorales para la formación de doctores, concedida por el Ministerio de Economía y Competitividad (MINECO). Gobierno de España. *Ref. BES-2014-068519.*
- Ayudas a la movilidad predoctoral para la realización de estancias breves en centros de I+D, concedida por el Ministerio de Economía y Competitividad (MINECO). Gobierno de España. *Ref. EEBB-I-17-11990.*

Para mis padres

AGRADECIMIENTOS

Quisiera agradecer a todas las personas que han contribuido directa o indirectamente a la realización de esta tesis. Especialmente, a mi directora, por su apoyo, dedicación y por contagiarme su pasión por la investigación científica. Muchas gracias Olga por aceptarme en tu grupo, por tus correcciones y por enseñarme tanto. Eres un ejemplo a seguir.

A Merce por revisarme los manuscritos, sus sugerencias y ayuda durante la tesis. A Estitxu y Rosana por todos esos buenos momentos que hemos pasado en el laboratorio 2228, vuestro apoyo y consejos, sois geniales. A Gelen, Kirian, Laia, Jeremie, Ana, Lucyanna, Montse, Martha y Alfonso, con vosotros el tiempo pasa rápido. Gracias por todas las vivencias que hemos compartido tanto dentro como fuera del laboratorio. ¡Por muchas margaritas más!

I want to thank Kateřina Vávrová for giving me a great support during the time that I spent in her lab. I would also like to thank Lukáš Opálka for sharing with me his great knowledge about the synthesis of acylceramides. I will never forget the weeks working together on the permeation experiments.

I want to thank Ibraheem Youself for his help during the experiment at Synchrotron Alba. I am very grateful for your lessons about PCA and the Unscrambler Program.

A Alfonso del Pozo por aceptar ser mi tutor y haberme cedido por una temporada el Tewameter y el Corneometer. Muchas gracias por todo.

A Ana Calpena por su ayuda en el experimento con los ratones.

A Carmen López-Iglesias y Lidia Delgado por su apoyo en las técnicas de microscopía electrónica.

A Jaume Caelles por su dedicación y ayuda en las técnicas de SAXS y GISAXS.

A Adriana Garcia-Herrera por enseñarme a interpretar las histologías.

A mis padres, por estar siempre ahí cuando los necesito de manera totalmente incondicional. Os tengo que agradecer el esfuerzo y sacrificio que habéis hecho para darme lo mejor.

A Irene, por escucharme y decirme siempre lo que opina me guste o no. Eres especial y una de las personas más importantes en mi vida.

A mis amigas, por su apoyo y palabras de ánimo sobre todo en la recta final de la tesis.

Y por último, a Sergi, por sus consejos, sus palabras de ánimo y darme valor. Lo esencial es invisible a los ojos, y eso es exactamente lo que tú me das. Gracias por compartir tu vida conmigo.

“En algún lugar algo increíble espera ser descubierto”

Carl Sagan

ÍNDICE

ABREVIATURAS

Las abreviaturas siguen su descripción del inglés.

AWD	Porcentaje de agua liberada durante la fase de desorción
Cryo-TEM	Criomicroscopía electrónica de transmisión
CerEOS	(*N*-(32-linoleoyloxy-triacontanoyl)-sphingosine
Cer3b	*N*-oleoil fitoesfingosina
DHPC	Dihexanoilfosfatidilcolina
DLS	Dispersión dinámica de luz
DPPC	Dipalmitoilfosfatidilcolina
Elisa	Ensayo por inmunoabsorción ligado a enzimas
FSTEM	Criosustitución aplicada a la microscopía electrónica de transmisión
FFAs	Ácidos grasos libres
FTIRM	Microespectroscopía infrarroja con transformada de Fourier
GISAXS	Dispersión de rayos X con incidencia rasante y detección a ángulos pequeño
H&E	Hematoxilina-Eosina
HPLC	Cromatografía líquida de alta eficacia
LBms	Sistema mimético de los cuerpos laminares
LPP	Periodicidad laminar larga
PCA	Análisis de componentes principales
SAXS	Dispersión de rayos X a ángulos pequeños
SC	Estrato córneo
SDT	Test de absorción-desorción

SPP	Periodicidad laminar corta
TEWL	Pérdida transepidérmica de agua
WHC	Capacidad de retención de agua
WSC	Capacidad de absorción de agua

PLANTEAMIENTO GENERAL

El SC es la capa más superficial de la epidermis. Su función es actuar como barrera evitando la pérdida de agua y la entrada de microorganismos. Está formado por unas 15-20 capas de corneocitos rodeados por lípidos que se organizan en forma de láminas. Estos lípidos son ceramidas, ácidos grasos libres, colesterol, sulfato de colesterol y esteres de colesterol. Los orgánulos responsables de la formación de esta estructura lipídica intercelular son los cuerpos laminares epidérmicos. Se trata de vesículas derivadas del aparato de Golgi que contienen múltiples láminas en su interior y miden aproximadamente 200-300nm de diámetro. Secretan su contenido, principalmente precursores de los lípidos del SC, en el espacio intercelular del estrato granuloso-SC donde forman la matriz lipídica en forma de láminas de este tejido. En muchas enfermedades de la piel, la función de los cuerpos laminares está alterada y como consecuencia se observa una composición lipídica irregular y una barrera cutánea ineficiente que puede ser causa y efecto de la propia enfermedad. Por ejemplo, tanto en psoriasis como en dermatitis atópica se encuentra una deficiencia en ciertos lípidos especialmente ceramidas y ácidos grasos libres.

El estudio sobre la biofísica y autoagregación de los lípidos nos ha permitido diseñar sistemas lipídicos complejos con un tamaño, morfología, estructura, composición y comportamiento fásico específicos. Las bicelas son nanoestructuras discoidales formadas por fosfolípidos de cadena larga (DPPC) y fosfolípidos de cadena corta (DHPC) que se sitúan en la zona plana y en los bordes de la estructura discoidal, respectivamente. Estos sistemas presentan una gran versatilidad morfológica y estructural modulada por la temperatura, la concentración lipídica o la relación molar entre los lípidos, haciéndolos candidatos idóneos para aplicaciones farmacéuticas y dermatológicas. Por otro lado, los bicosomas surgen como estrategia para proteger las bicelas en entornos de alta dilución en agua. Para ello, las bicelas son encapsuladas en vesículas fosfolipídicas formando así los bicosomas. Estas estructuras también están siendo aplicadas en la vía tópica.

Esta tesis parte de los resultados obtenidos por nuestro grupo de investigación en proyectos anteriores. El objetivo principal ha sido desarrollar un nuevo sistema lipídico que imite la composición y la estructura de los cuerpos laminares epidérmicos con el propósito de que estas estructuras puedan imitar también la función de estos orgánulos epidérmicos mejorando la función barrera.

En este sentido, se diseñó un sistema lipídico con morfología similar a la de los cuerpos laminares epidérmicos: láminas lipídicas encapsuladas en vesículas. Llamaremos a este sistema LBms, por su abreviación del inglés: "Lamellar Body mimetic system". Inicialmente este sistema se formó con mezclas de Cer3b, ácido esteárico, colesterol, sulfato de colesterol y palmitato de colesterol y se caracterizó su tamaño, morfología y estructura. Se evaluó el efecto de este sistema *in vitro* sobre piel previamente deslipidizada e *in vivo* tanto en voluntarios con barrera cutánea comprometida como en un modelo animal de dermatitis inducida. También se estudió como el tratamiento con este sistema afecta a los lípidos, proteínas y ácidos nucleicos de la piel. Se ha descrito que en las capas más externas de la piel predominan ceramidas de cadena alquílica larga como la CerEOS. Ésta ceramida tiene un papel imprescindible en la organización característica de los lípidos del SC y por tanto en el mantenimiento de la función barrera de la piel. En base a los resultados obtenidos con el LBms que incluye Cer3b (cadena alquílica corta) y el conocimiento del papel relevante de la CerEOS, se decidió incluir esta ceramida en el sistema y se comparó el efecto de estos sistemas con distinto tipo de ceramida en la reparación de la barrera cutánea. Para ello, se estudió *in vitro* tanto el perfil de penetración de un permeante modelo como la pérdida de agua a través del SC después de tratar la piel con los diferentes sistemas lipídicos. Finalmente, para mimetizar en mayor medida la complejidad composicional del SC se preparó un nuevo sistema que incorporaba una mezcla de ceramidas extraídas del SC humano y una mezcla de ácidos grasos de cadena larga y se estudió *in vitro* la capacidad de este sistema para reparar la estructura lipídica del SC.

1. INTRODUCCIÓN

1. INTRODUCCIÓN

1.1. La piel

1.1.1. Fisiología y función de la piel

La piel es el órgano más grande del cuerpo humano, representando más del 10% de la masa corporal total (Schaefer y col., 1996). Su función es actuar como barrera física evitando la pérdida de agua y protegiendo al organismo del medio que lo rodea. Además, controla la regulación térmica corporal a través del sistema vascular y de las glándulas sudoríparas, regula procesos endocrinos e inmunológicos y contiene una extensa red neurosensorial que nos mantiene en contacto con el entorno. Estas funciones son primordiales para la vida y requieren la específica composición y estructura que caracteriza a este órgano. Anatómicamente, la piel está dividida en SC, epidermis, dermis e hipodermis (figura 1).

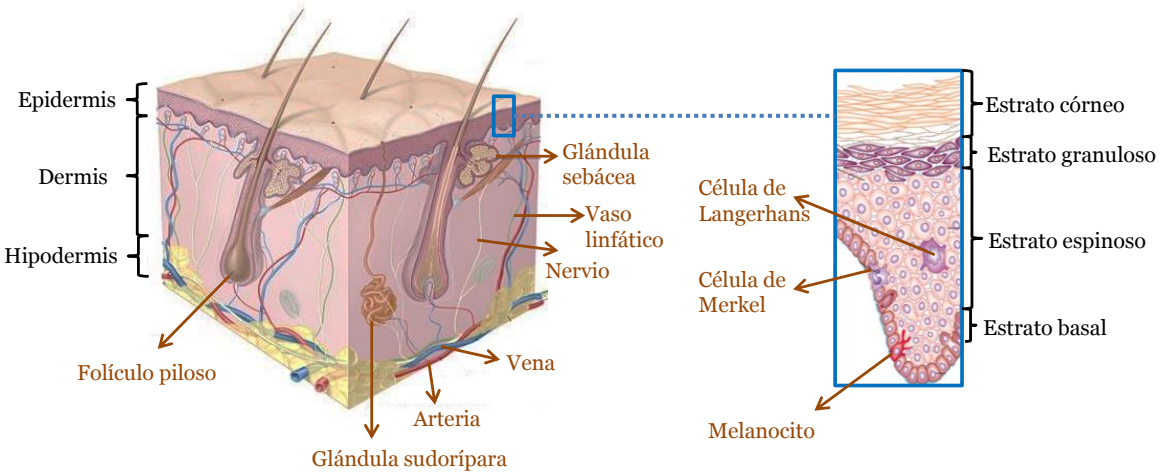

Figura 1. Esquema de la piel indicando las capas cutáneas.

El SC es la capa más externa de la piel y es donde se localiza la función barrera cutánea (Elias, 1991). Tiene un espesor de 10-20µm y está formado por células planas, anucleadas y cornificadas (corneocitos) separadas por una matriz lipídica ordenada en láminas. Se compone aproximadamente de un 15% de agua, un 70% de proteínas y un 15% de lípidos (Downing y col., 1987; Smith y col., 1982). Hasta hace pocos años se le consideraba parte de la epidermis, sin embargo, actualmente se considera independiente de ésta debido a las características funcionales y estructurales específicas que presenta. La estructura del SC fue descrita por primera vez por Peter

Elias como un modelo de “ladrillos y cemento” donde los ladrillos son los corneocitos y el cemento que los rodea se refiere a la matriz lipídica ordenada en láminas (Elias, 1988).

La epidermis es una capa cuyo espesor depende de su localización anatómica oscilando entre 50-100μm. Está formada por tres capas: estrato granuloso, estrato espinoso y estrato basal (Schaefer y col., 1996). Los queratinocitos representan casi la totalidad de las células de la epidermis pero también están presentes otras células como los melanocitos, las células de Langerhans y las células de Merkel.

La dermis es la capa más extensa de la piel (de 1 a 2mm) y se trata de un tejido fibroelástico situado debajo de la epidermis que proporciona elasticidad y resistencia física. Por la dermis circulan vasos sanguíneos y linfáticos y también existen terminaciones nerviosas (Schaefer y col., 1996). Las células propias del tejido son los fibroblastos que se encargan de producir el tejido conectivo y también contiene células móviles involucradas en las respuestas inmunes e inflamatorias como son los mastocitos o los linfocitos. Además, en esta capa se encuentran proteínas estructurales como el colágeno y la elastina (Pons Gimier y col., 1995). El colágeno es la principal proteína estructural y proporciona integridad a este tejido, muestra un ordenamiento característico en la piel y cualquier cambio en su ordenamiento u organización conlleva alteraciones en el tejido. Estas alteraciones pueden causar la pérdida de resistencia y flexibilidad cutánea, la aparición de arrugas o incluso desordenes de la función barrera (Costa y col., 2009; Varani y col., 2006; Waller y col., 2006).

La hipodermis es la capa más interna de la piel y su grosor es variable según la zona anatómica, sexo y edad. Está formada principalmente por tejido adiposo que sirve de almacén de energía, de aislante térmico y protege al tejido de agresiones externas (Pons Gimier y col., 1995).

1.1.2. Barrera cutánea

La función barrera cutánea se localiza en el SC y se atribuye principalmente al contenido y a la composición de los lípidos intercelulares y, sobre todo, a la estructura organizada en láminas que adquieren estos lípidos que rodean a las células de esta capa de la piel, los corneocitos (Elias, 1991; Madison, 2003). Por otro lado, los corneocitos son ricos en queratina y están interconectados entre sí por estructuras proteicas denominadas corneodesmosomas que contribuyen a la cohesión del tejido (Chapman y col., 1990; Serre y col., 1991). Los corneocitos están envueltos por una cubierta proteica

llamada envoltura celular cornificada, formada por proteínas estructurales unidas por enlaces covalentes a una capa de lípidos, principalmente ceramidas (Wertz y col., 1989). Esta capa de lípidos juega un papel importante como soporte para la organización de las bicapas laminares extracelulares, necesaria para la función barrera (Lazo y col., 1995; Marekov y col., 1998).

La estructura laminar del SC está formada aproximadamente por un 50% de ceramidas, un 25% de colesterol, un 15-20% de ácidos grasos libres, un 3-5% de sulfato de colesterol y un 1-2% de ésteres de colesterol (Schaefer y col., 1996). Estudios de SAXS demostraron que la estructura laminar lipídica del SC está organizada en dos fases laminares coexistentes de 130Å y 60Å denominadas LPP y SPP, respectivamente (Bouwstra y col., 1991). También se ha demostrado *in vitro* utilizando membranas lipídicas que ésta organización de los lípidos es esencial para una correcta función barrera (Bouwstra y col., 2010).

Los lípidos del SC provienen de los cuerpos laminares también denominados cuerpos de Odland. Se trata de orgánulos ovoides (~300nm) formados por vesículas que contienen en su interior múltiples láminas formadas por los precursores de los lípidos del SC (fosfolípidos, glucosilceramidas, esfingomielina y colesterol), enzimas y péptidos antimicrobianos (Elias y col., 2005; Feingold y col., 2014; Menon y col., 1992). Durante la diferenciación de los queratinocitos, debido a cambios en la concentración de calcio local, los cuerpos laminares derivados del aparato de Golgi se mueven hasta el ápice de las células, se fusionan con la membrana plasmática y secretan su contenido en el espacio extracelular en la frontera estrato granuloso-SC por exocitosis, según el modelo de Landman (figura 2) (Landmann, 1986). Los lípidos secretados se procesan posteriormente y se organizan en el espacio intercelular del SC o en la envoltura del corneocito.

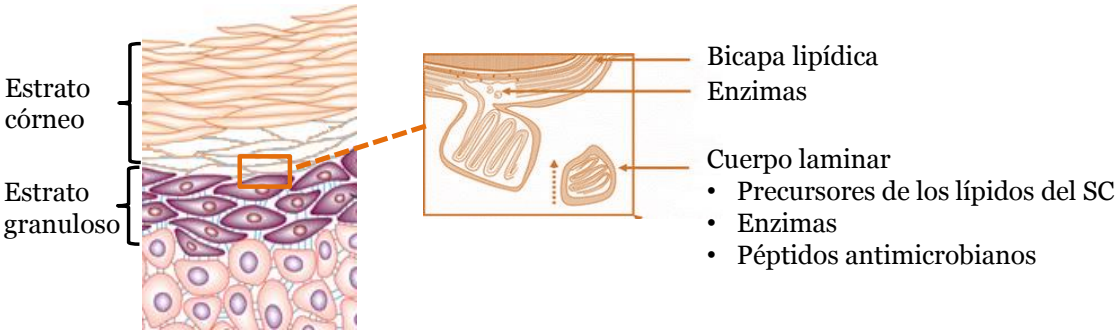

Figura 2. Esquema de la secreción del contenido de los cuerpos laminares en la frontera estrato granuloso-SC.

Recientemente, se ha propuesto otro modelo para describir la secreción de los lípidos por parte de los cuerpos laminares denominado "membrane-folding model" descrito por Norlén y col. que propone una secreción de los lípidos a través de un sistema tuboloreticular que asocia el aparato de Golgi con el espacio extracelular (den Hollander y col., 2015; Norlén, 2015).

1.1.2.1. Ceramidas en el estrato córneo

Los lípidos con un papel más relevante en el SC son las ceramidas, que representan sobre el 50% del peso de los lípidos en esta capa (Schurer y col., 1991). Las ceramidas son un grupo estructuralmente heterogéneo y complejo de esfingolípidos que contiene bases C18-esfingoides unidas mediante enlaces amida con nohidroxi-, α-hidroxi- o ω-hidroxiácidos. Las ceramidas se diferencian unas de otras por la arquitectura de su grupo cabeza, tipo y grado de hidroxilación junto con la longitud de la cadena *N*-acil (que varía entre 16 y 30-40 átomos de carbono) y la presencia de una acilación adicional en la posición ω del grupo *N*-acil (Bouwstra y col., 2010).

La nomenclatura inicial de las ceramidas estaba basada en una serie de números del 1 al 8 según su polaridad (así la 1 corresponde con la especie más apolar) de acuerdo con las fracciones de ceramidas extraídas de SC humano separadas mediante cromatografía de capa fina de alta resolución (HPTLC) (Ponec y col., 2003; Robson y col., 1994; Stewart y col., 1999; Wertz y col., 1985). Más tarde, con el descubrimiento de nuevas estructuras de ceramidas en SC humano mediante cromatografía líquida acoplada a la espectrometría de masas (LC/MS) fue necesario establecer una nueva nomenclatura más detallada basada en su estructura molecular (según el tipo de base y el tipo de ácido graso enlazado). Esta clasificación fue propuesta por Motta (Motta y col., 1993) y ampliada por Masukawa (Masukawa y col., 2008) y Rabionet (Rabionet y col., 2014). La base puede ser de cuatro tipos: esfingosina (S), fitoesfingosina (P), 6-hidroxiesfingosina (H) y dihidroesfingosina (dS) y el ácido graso esterificado a la amida de cualquiera de estas bases puede ser nohidroxi- (N), α-hidroxi- (A) o ácido linoleico enlazado a ω-hidroxiácidos (EO) (van Smeden y col., 2011). La figura 3 muestra las diferentes estructuras de las ceramidas que resultan en 12 subclases diferentes. En la tabla 1 se compara los nombres de las ceramidas según las dos clasificaciones descritas.

Las ceramidas pueden formar parte de la estructura laminar del SC como especies libres o pueden encontrarse unidas covalentemente a las proteínas de la envoltura

celular de los corneocitos. Estas ceramidas unidas son principalmente ω-hidroxiceramidas con ácidos grasos de cadena ultra larga (Macheleidt y col., 2002).

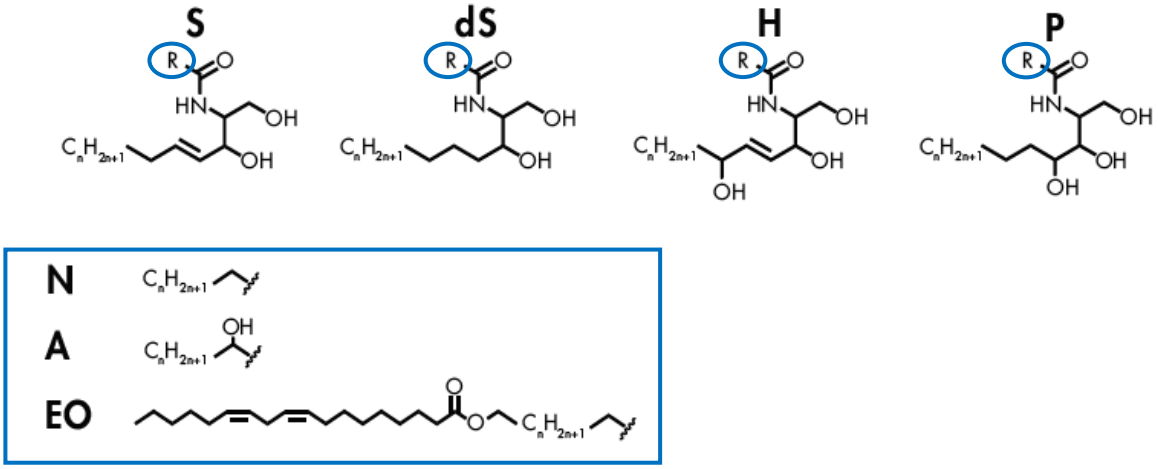

Figura 3. Estructura de las ceramidas. Se clasifican según su tipo de base (S, dS, H o P) donde R representa una de las tres cadenas de ácidos grasos (N, A o EO) (van Smeden y col., 2011).

Clasificación según polaridad	Clasificación según estructura molecular
1	EOS
2	NS
3	NP
4	EOH
5	AS
6	AP
7	AH
8	NH

Tabla 1. Nombre de las ceramidas según el tipo de clasificación utilizada.

1.1.3. Deterioro de la función barrera en disfunciones cutáneas: dermatitis atópica

En diversas enfermedades cutáneas se ha observado un aumento o disminución en la formación y/o secreción de los cuerpos laminares (Elias y col., 2014; Fartasch y col., 1999; Ghadially y col., 1996; Milner y col., 1992). En algunos casos estos cuerpos laminares presentan un déficit en las enzimas que procesan los precursores de los lípidos que luego formarán parte de la estructura laminar del SC (Chan y col., 2011). Por lo tanto, la piel enferma se caracteriza por tener una composición y organización lipídica alterada y consecuentemente una función barrera comprometida. Cuando la barrera cutánea está dañada, la piel es más susceptible a la penetración de agentes externos y/o patógenos provocando una respuesta inmune (Kuo y col., 2013). Además, la piel enferma se caracteriza por tener un TEWL mayor que la piel sana tanto en las zonas que presentan las lesiones como en las no lesionadas (Jensen y col., 2004).

Por ejemplo, la dermatitis atópica es una enfermedad cutánea compleja, inflamatoria y crónica, que ocurre típicamente en individuos con una historia familiar de atopía. Se caracteriza por presentar lesiones de dermatitis, prurito y piel seca que evolucionan con un curso crónico y brotes intermitentes que alternan con periodos de remisión (Spergel y col., 2003). Es una patología muy común que afecta entre un 10-20% de la población pediátrica y entre un 1-3% de la población adulta a nivel mundial (Nutten, 2015). La piel atópica se caracteriza por tener una disminución de los lípidos del SC totales. Se observa una reducción tanto en las ceramida 1 y 3 como los ácidos grasos de cadena alquílica larga y también un aumento en el colesterol (di Nardo y col., 1998; Smeden y col., 2014). Además, la piel atópica presenta un déficit en la secreción de péptidos antimicrobianos por parte de los cuerpos laminares (Elias y col., 2014). Estos péptidos juegan un papel muy importante previniendo la infección por microorganismos.

1.2. Modelos de piel con función barrera deteriorada

El uso de diferentes modelos *in vitro* e *in vivo* que mimetizan el comportamiento de la piel con una barrera cutánea deteriorada son generalmente utilizados para evaluar la eficacia y posibles efectos de toxicidad sistémica de productos desarrollados para el tratamiento de patologías de la piel.

Existen diferentes metodologías para alterar la función barrera del SC. Se utilizan métodos químicos como la aplicación de disolventes orgánicos (Tsai y col., 2001) o tensioactivos (Effendy y col., 1995; Nielsen, 2005) y métodos mecánicos como el “tape-

stripping" que consiste en retirar capas del SC secuencialmente por medio de la aplicación de tiras de cinta adhesiva (Sekkat y col., 2004; Simonsen y col., 2007). También se utilizan modelos animales principalmente en ratón que permiten no solo mimetizar una barrera deteriorada sino reproducir la enfermedad cutánea. Se han descrito diferentes modelos para dermatitis atópica como son el modelo de ratón NC/Nga (Suto y col., 1999), el modelo de dermatitis inducida por la sucesiva aplicación de haptenos una vez los animales han sido sensibilizados (Man y col., 2008; Matsumoto y col., 2004) o modelos de ratón transgénicos que bien sobreexpresan o carecen de moléculas selectivas (Bäckman y col., 2002; Chan y col., 2001; Konishi y col., 2002). Todos estos modelos muestran características de la dermatitis humana y su estudio ha resultado en una mejor comprensión de la patogénesis de esta enfermedad.

En los trabajos 1, 5 y 6 que han dado lugar a esta tesis se han utilizado mezclas de cloroformo-metanol para simular *in vitro* una barrera cutánea deteriorada. En el trabajo 2 se ha utilizado un parche (Finn Chambers®, SmartPractice) con una solución de lauril sulfato de sodio al 2% durante 2 horas para inducir una irritación en la piel *in vivo*. En los trabajos 3 y 4 se ha utilizado un modelo de dermatitis inducida *in vivo* mediante la aplicación de oxazolona en el dorso de ratones sin pelo siguiendo el protocolo descrito por Man y col. (Man y col., 2008).

1.3. Sistemas lipídicos para el tratamiento de la piel

Dada la relevancia de los lípidos en el mantenimiento de la función barrera cutánea, se han descrito sistemas lipídicos de diferente composición y estructura para el tratamiento de la piel. De entre ellos, aquellos que tienen la bicapa lipídica como principal unidad estructural se describen como los más apropiados. Los liposomas son probablemente los más utilizados para aplicaciones cutáneas. Se trata de vesículas constituidas por una o varias bicapas fosfolipídicas concéntricas, con un compartimento acuoso en su interior. Su tamaño es variable entre 20nm-1µm. Normalmente, se preparan con fosfolípidos naturales o sintéticos, siendo la fosfatidilcolina el más utilizado ya que es el principal componente de las membranas biológicas. La habilidad de los fosfolípidos de adoptar una configuración en bicapas en medio acuoso se debe a que son moléculas anfipáticas, es decir, tienen un extremo polar o hidrofílico que se orienta hacia la parte acuosa y un extremo no polar o hidrofóbico que rechaza la fase acuosa y se orienta hacia el interior de la bicapa. Inicialmente, fueron utilizados como modelos de membrana (Bangham y col., 1974) y más tarde como vehículos de trasporte de diversas sustancias (Mezei y col., 1982), tanto

en industria farmacéutica como cosmética. Tienen la función de favorecer la penetración y reducir la toxicidad del fármaco encapsulado y de liberarlo sostenidamente (Knepp y col., 1990). Sin embargo, el uso de liposomas como vehículo en la vía transdérmica tiene limitaciones ya que el SC es una barrera muy eficaz que dificulta el paso de numerosas moléculas. La principal barrera para la difusión a través de la piel reside en la estructura laminar intercelular del SC con espacios entre 6 y 13nm, de modo que es difícil que los liposomas debido a su tamaño atraviesen los espacios intercelulares del SC por difusión pasiva (Dreier y col., 2016). Se han descrito diferentes estrategias para conseguir una mayor penetración, como la combinación de lípidos con tensioactivos, alcoholes y otras moléculas (El Maghraby y col., 2000; Touitou y col., 2000). Bajo estas circunstancias las vesículas se rompen o desagregan en las primeras capas del SC. En determinadas condiciones, pese a sus limitaciones, si se aplican en SC dañado o si se preparan con lípidos extraídos del SC (El Maghraby, 2016), los liposomas son capaces de penetrar en mayor medida.

Otro sistema que ha demostrado efectos beneficiosos sobre la piel son los sistemas de micelas mixtas lípido-tensioactivo. Estas estructuras tienen un tamaño entorno a 10nm por lo que son capaces de pasar a través de los espacios intercelulares del SC (Lasic, 1992). La desventaja de estos sistemas es que contienen tensioactivos. Estas moléculas tienen un efecto irritante sobre la piel pudiendo solubilizar parte de los lípidos de la barrera, entre otros efectos (Deo y col., 2001; López y col., 1998).

Las bicelas también se han propuesto recientemente para aplicaciones dermatológicas. Se trata de nanoagregados lipídicos discoidales formados por al menos dos tipos de fosfolípidos, uno con cadenas alquílicas largas y otro con cadenas cortas, dispersos en solución acuosa (Sanders y col., 1992). En general los fosfolípidos de cadena larga (DPPC o DMPC) se ensamblan formando una bicapa plana, mientras que los fosfolípidos de cadena corta (DHPC) se colocan en el borde estabilizando la estructura. Normalmente tienen forma de disco y presentan un tamaño entre 10-50nm de diámetro y entre 4-6nm de grosor de la bicapa (Barbosa‐Barros y col., 2008). Aunque el tamaño y morfología de las nanoestructuras depende de la composición lipídica, de la relación molar entre el fosfolípido de cadena larga y el fosfolípido de cadena corta (q=DXPC/DHPC), de la concentración lipídica y de la temperatura (Struppe y col., 1998; van Dam y col., 2006). La figura 4 muestra una representación de una bicela y la estructura molecular de los fosfolípidos típicos que la forman. Una de las grandes ventajas de las bicelas frente a otros sistemas laminares es su capacidad de alinearse espontáneamente en un campo magnético, lo que las hace adecuadas para estudios

estructurales y conformacionales de péptidos y proteínas usando resonancia magnética nuclear (Sanders y col., 1994).

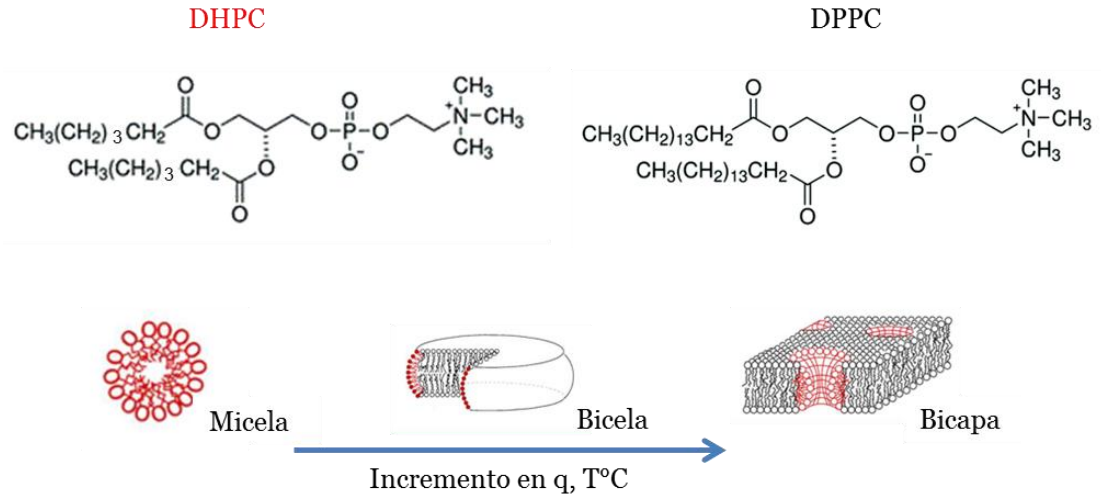

Figura 4. Esquema representativo de las diferentes estructuras según q o T°C y estructura molecular de los fosfolípidos que forman las bicelas.

Nuestro grupo de investigación es pionero en la aplicación de estos sistemas en estudios relacionados con la piel (Barbosa - Barros y col., 2012; Rodríguez y col., 2015). Diferentes trabajos han demostrado el potencial de estos sistemas para encapsular sustancias de interés farmacológico y para liberarlas a través de la piel (Rubio y col., 2010; Rubio y col., 2011). También se ha observado que estos sistemas pueden modular la función barrera cutánea, aumentando o reforzando su permeabilidad (Barbosa - Barros y col., 2012). Debido a su pequeño tamaño y morfología discoidal son capaces de penetrar a través de los espacios intercelulares del SC (Rodríguez y col., 2010).

Se sabe que estas estructuras son estables hasta una concentración lipídica total del 3% (Struppe y col., 1998). Sin embargo, cuando este porcentaje disminuye (dilución), las bicelas se transforman en estructuras más grandes ya que el DHPC pasa al agua para restablecer el equilibrio monomérico, esto induce un incremento en la relación molar en las estructuras y un aumento de su diámetro que lleva a la fusión de las bicelas para formar vesículas (Barbosa-Barros y col., 2008). Diversos autores han diseñado varios métodos para estabilizar la morfología discoidal de las bicelas en condiciones de alta dilución, como el uso de bicelas formadas por fosfolípidos cargados (Losonczi y col.,

1998) y mezclas de lípidos conjugados con polietilenglicol (Liu y col., 2014). Estos métodos de estabilización podrían limitar la funcionalidad de las bicelas. Con el fin de evitar esta limitación y poder mantener la estructura de las bicelas en medios con gran contenido de agua, se crearon los llamados "bicosomas" (Rodríguez y col., 2010).

Los bicosomas son nanoestructuras formadas por bicelas encapsuladas por una vesícula de alrededor de 150-250nm de diámetro (figura 5) (Rodríguez y col., 2010). Los fosfolípidos típicos utilizados para formar estas estructuras son los ya mencionados para la formación de las bicelas y además, los que forman la vesícula que encapsula las bicelas. Esta vesícula exterior está formada por fosfolípidos compuestos por dos ácidos grasos cuyas cadenas alquílicas pueden tener enlaces saturados o insaturados. En general estos fosfolípidos de la vesícula exterior suelen ser mezclas que contienen un 80-90% de fosfatidilcolinas formados mayoritariamente por ácido palmítico o ácido esteárico como ácido saturado y principalmente ácido linoleico o linolénico como ácido insaturado. El 10-20% restante de la vesícula exterior suele ser el colesterol. Aunque los bicosomas se diseñaron para poder usar las bicelas en entornos de alta dilución, se ha evaluado también su aplicación en la vía tópica. Se han incluido en los bicosomas diferentes antioxidantes tales como el β-caroteno o el complejo de Mn y se ha estudiado el efecto anti-radicalario que tienen estos sistemas en la piel, así como su utilidad previniendo la degradación de colágeno inducida por radiación IR (Fernández y col., 2016a; Fernández y col., 2016b).

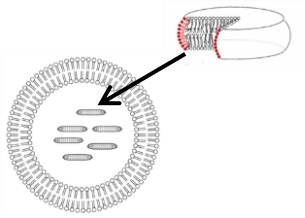

Figura 5. Esquema de un bicosoma.

Siguiendo la línea de investigación dermatológica y debido a que los bicosomas recuerdan en estructura a los cuerpos laminares epidérmicos, en esta tesis se propone un nuevo sistema lipídico para mimetizar a estos orgánulos endógenos. Así, en el nuevo sistema lipídico que denominamos LBms, se incluyeron lípidos del SC con una relación molar entre ellos similar a la que presenta la piel, lípidos con efecto antimicrobiano y lípidos que podrían regular el pH de la piel ya que se sabe que la piel atópica presenta un pH básico que podría hacerla susceptible a la colonización de microorganismos

(Rippke y col., 2004). Además, se pretende que este sistema que mimetiza la morfología, estructura y composición de los cuerpos laminares epidérmicos pueda imitar también la función de estos orgánulos reparando la barrera cutánea.

A lo largo de esta tesis se han utilizado un gran número de técnicas que han permitido caracterizar el sistema mimético de los cuerpos laminares epidérmicos y evaluar su efecto en piel con barrera cutánea deteriorada tanto *in vitro* como *in vivo*.

1.4. Técnicas de caracterización de los sistemas lipídicos

1.4.1. Dispersión dinámica de la luz

La dispersión dinámica de la luz (DLS, del inglés "Dynamic light Scattering") es una técnica utilizada para medir el tamaño y la polidispersidad de partículas en solución (Goldburg, 1999). Esta técnica consiste en hacer incidir un haz de radiación con determinada longitud de onda λ (633nm) y vector de onda $q=2\pi/\lambda$ en una suspensión de partículas. Al interactuar la radiación con las partículas, una parte de la energía se absorbe, otra se transmite sin modificar el vector de onda incidente y otra se dispersa por todo el espacio. La luz dispersada a un cierto ángulo θ se recoge en un detector. Estudiando la radiación dispersada por la muestra en función del vector de onda de difusión $q=(4\pi/\lambda)\sin(\theta/2)$, suponiendo que la energía incidente es igual a la energía transmitida, y correlacionando las intensidades de dispersión a diferentes tiempos se puede obtener una función de autocorrelación.

Para partículas esféricas monodispersas, la función de autocorrelación puede ser ajustada a la siguiente función exponencial dependiendo del tiempo, t:

$$g(t)= A \exp(-2t/t_R)+B$$

Donde A es una constante instrumental, B es la línea base y t_R es el tiempo de relajación. El t_R se relaciona con un coeficiente de difusión (D) mediante la ecuación:

$$t_R=1/Dq^2$$

Aplicando la ecuación de Stokes-Einstein, a cada coeficiente de difusión se puede asociar un radio hidrodinámico característico R.

$$D=k_BT/6\pi\eta R$$

Donde k_B es la constante de Boltzman, T es la temperatura absoluta y η es la viscosidad del sistema.

En términos generales todos los equipos de dispersión de luz tienen los mismos componentes: fuente de radiación, atenuador de la luz, detector situado al ángulo de dispersión y un correlador (figura 6).

En esta tesis, se utilizó la tecnología no invasiva de retrodispersión ("Non Invasive Back Scatter", NIBS). Con esta tecnología, la detección de la dispersión se realiza a un ángulo de 173°, tal como muestra la figura 6. Así, se elimina o se puede reducir el efecto llamado dispersión múltiple donde la luz dispersada por una partícula es a la vez dispersada por otras partículas dando un error en la medida. Esta estrategia permite la medida de muestras concentradas como es el caso de los diferentes sistemas lipídicos formados en esta tesis.

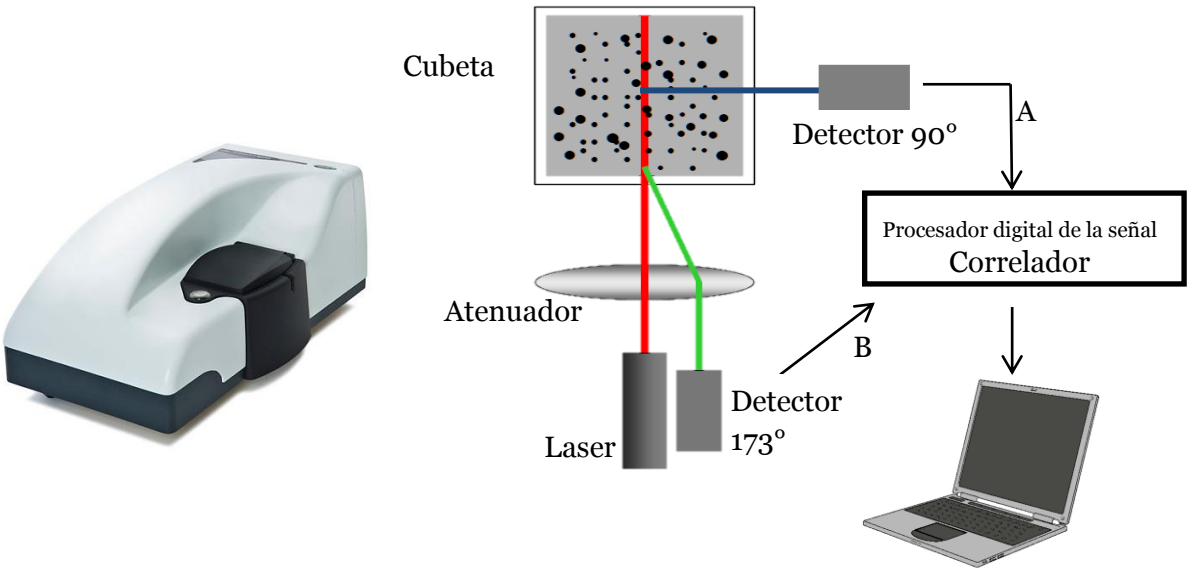

Figura 6. Fotografía del equipo Zetasizer Nano ZS (Malvern Instruments, Inglaterra) y esquema del equipo con la posibilidad de detección de la luz dispersada a 90° o 173°.

Las medidas de DLS se llevaron a cabo utilizando el Zetasizer Nano ZS (Malvern Instruments, Inglaterra) en el Instituto de Química Avanzada de Cataluña (IQAC-CSIC).

1.4.2. Dispersión de rayos X: SAXS

La dispersión de rayos X es una técnica en la que se hace incidir un haz de radiación monocromática sobre la muestra dando como resultado un patrón de dispersión. Este

patrón muestra las diferentes intensidades de rayos X dispersados a diferentes ángulos, lo que permite calcular las dimensiones, la forma y la organización de las partículas. La intensidad de dispersión a ángulos pequeños (SAXS, del inglés "Small Angle X-ray Scattering") nos da información sobre la estructura macromolecular (1-200nm). La figura 7 representa la disposición de la muestra y del detector, y el perfil de dispersión que se puede obtener a ángulo pequeño.

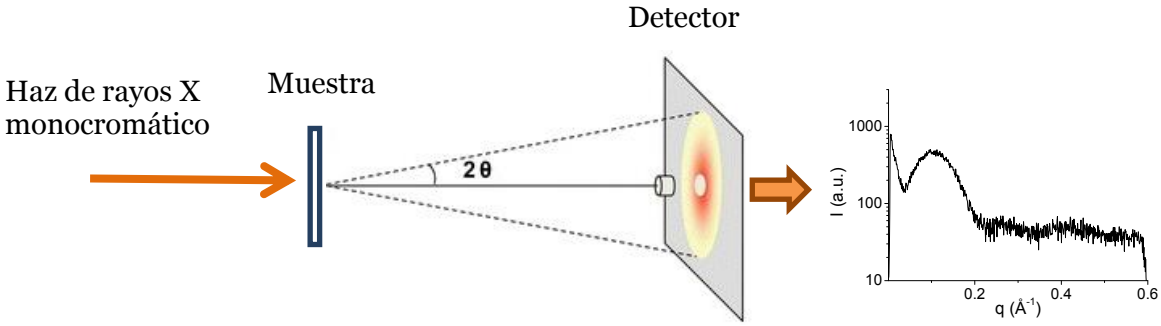

Figura 7. Representación esquemática de una medida de SAXS y perfil de dispersión.

La intensidad de dispersión I (en unidades arbitrarias) se mide en función del módulo del vector de dispersión q (en $Å^{-1}$) que se define como:

$$|q|=(4\pi\sin\theta)/\lambda$$

donde θ es el ángulo de dispersión y λ es la longitud de onda de la radiación (1.542 Å).

La posición de los picos de dispersión está directamente relacionada con la distancia de repetición (d) de la estructura molecular como define la ley de Bragg (Bragg, 1913):

$$2d\sin\theta=n\lambda$$

donde n es el orden de difracción y d es la distancia de repetición. Para estructuras laminares apiladas, los picos están posicionados a distancias equidistantes, de esta forma:

$$q_n=2\pi n/d$$

donde q_n es el módulo del vector de dispersión que indica la posición del n orden de difracción.

En esta tesis, la distancia laminar de repetición (d) fue estimada a partir del análisis de los picos por la ley de Bragg, y se relacionó con la anchura de las bicapas lipídicas como en los estudios con liposomas y otros modelos de bicapa (Rappolt y col., 2004).

Las medidas de SAXS se llevaron a cabo utilizando el equipo SAXS S3-MICRO (Hecus GmbH, Graz, Austria) del Servicio de SAXS del Instituto de Química Avanzada de Cataluña (IQAC-CSIC) con la colaboración del Sr. Jaume Caelles.

1.4.3. Criomicroscopía electrónica de transmisión

La técnica de criomicroscopía electrónica de transmisión (cryo-TEM, del inglés "Cryogenic Transmission Electron Microscopy") permite visualizar directamente las muestras vitrificadas a temperaturas muy bajas (alrededor de -170°C). La vitrificación es una técnica de criofijación basada en una congelación muy rápida que evita la formación de cristales de hielo que pueden generar daños en las estructuras que se quieren visualizar. Esta técnica permite obtener imágenes directas de agregados lipídicos en solución acuosa (Almgren y col., 2000). El proceso de vitrificación de las muestras se realiza de forma automatizada con el aparato Vitrobot (FEI Company, Eindhoven, Holanda) (figura 8A), donde una pequeña cantidad de muestra se coloca en una rejilla de cobre recubierta con una película de carbono. Después se absorbe la muestra sobrante ("blotting") quedando una película fina de muestra sobre la rejilla. A continuación, la muestra se vitrifica sumergiéndola inmediatamente en etano líquido (-180°C) y se almacena en nitrógeno líquido (-196°C) hasta ser examinada. Para examinar la muestra, ésta se transfiere a un microscopio Tecnai F20 TEM (FEI Company, Eindhoven, Holanda) (figura 8B) mediante un soporte de criotransferencia. Las imágenes se tomaron a 200 kV y a temperatura entre -170 y -175°C.

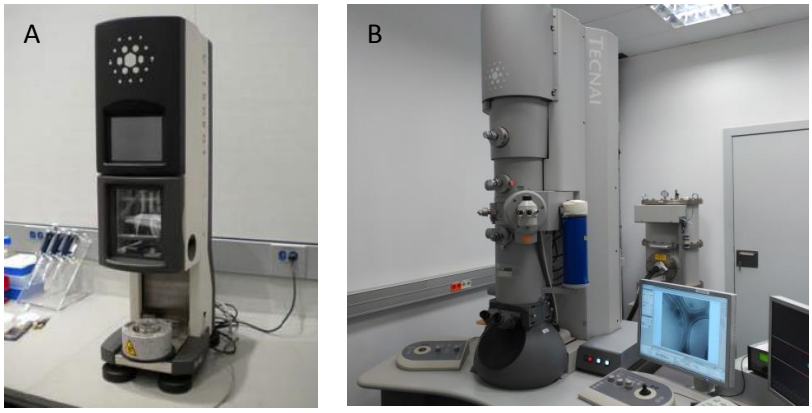

Figura 8. (A) Fotografía del Vitrobot utilizado para la vitrificación de las muestras. (B) Fotografía del microscopio Tecnai F20 TEM utilizado para visualizar las muestras.

La morfología y tamaño de los diferentes sistemas lipídicos formados en ésta tesis fueron estudiados mediante ésta técnica, ya que permite la visualización de estructuras pequeñas en medio acuoso.

La preparación de las muestras y la posterior visualización por microscopía electrónica se han realizado en la unidad de Crio-Microscopía Electrónica de los Centros Científicos y Tecnológicos de la Universidad de Barcelona (CCiT-UB), bajo la asistencia técnica tanto de la Dra. Carmen López y como la Dra. Lídia Delgado.

1.5. Técnicas para evaluar la función barrera cutánea

1.5.1. *In vitro*

1.5.1.1. Criosustitución aplicada a la microscopía electrónica de transmisión

La criosustitución aplicada a la microscopía electrónica de transmisión (FSTEM, del inglés "Freeze-Substitution Transmission Electron Microscopy") se utiliza para visualizar la ultraestructura de la piel y los lípidos del SC (van den Bergh y col., 1997). La criosustitución consiste en el intercambio (sustitución) del agua del medio por un disolvente orgánico y la posterior inclusión de la muestra en una resina. El tiempo de sustitución depende de la capacidad de retención de agua del disolvente usado, del tamaño de la muestra, de la temperatura de criosustitución y de la composición química de la muestra. Usualmente se criosustituye en 3 días.

En esta tesis se han seguido los siguientes pasos para la preparación de las muestras:

- Fijación química con glutaraldehído.
- Post-fijación química donde se añade tetróxido de rutenio para contrastar los lípidos del SC y que se puedan observar con microscopio electrónico.
- Criofijación en nitrógeno líquido (-196°C).
- Criosustitución. Se hace mediante un sistema automatizado de substitución ("Automatic Freeze Substitution", AFS) donde se intercambia el agua del medio por un disolvente orgánico. Como disolvente orgánico se utilizó metanol y se incluyó tetróxido de osmio (entre otros compuestos) para que los lípidos y las estructuras de la piel se puedan observar mediante TEM.
- Inclusión del tejido en una resina (Lowicryl HM20).
- Polimerización de la resina bajo radiación UVA (48h a -50°C).

- Finalmente, se hacen cortes ultrafinos con un ultramicrotomo (Ultracut UCT, Leica, Viena, Austria) y se visualizan en un TEM Hitachi 600.

Esta técnica permitió observar la microestructura de la piel antes y después del tratamiento con el LBms aplicado tanto *in vitro* como *in vivo*.

La preparación de los tejidos y la posterior visualización de las muestras por microscopía electrónica se han realizado en la unidad de Crio-Microscopía Electrónica de los Centros Científicos y Tecnológicos de la Universidad de Barcelona (CCiT-UB), bajo la asistencia técnica de la Dra. Lídia Delgado.

1.5.1.2. Dispersión de rayos X: GISAXS

La técnica de SAXS nos permite estudiar tanto la estructura de los sistemas, como vimos en la sección 1.4.2, como la organización laminar de los lípidos del SC. La disposición de la muestra con respecto al haz incidente permite una incidencia en transmisión o en ángulo rasante (GI, "Grazing-Incidence") (Levine y col., 1989). En general la incidencia rasante se utiliza para muestras poco concentradas. En el caso del SC, los lípidos representan solo el 15% por lo que si se dispone la muestra en transmisión la señal será débil. En cambio, si los rayos X, que pueden proceder de fuente convencional o radiación sincrotrón, inciden en la muestra a ángulo rasante, el camino del haz a través de la muestra es mayor por lo que se obtiene una señal más intensa. Cuando los experimentos se hacen con fuente de luz convencional es especialmente interesante utilizar la disposición a ángulo rasante y tiempos de exposición largos, para aumentar la intensidad de la luz dispersada. Para realizar los experimentos, que requieren vacío para evitar la dispersión del aire, se utiliza una cámara de humedad (Pons Pons, 2012) que mantiene la muestra hidratada. En la figura 9 se muestra la disposición de la muestra y el perfil de dispersión que se puede obtener a ángulo pequeño. La obtención de los espectros es igual que la descrita en el apartado de caracterización de los sistemas lipídicos. Las distancias laminares de repetición fueron estimadas a partir de los picos por la ley de Bragg (Bragg, 1913).

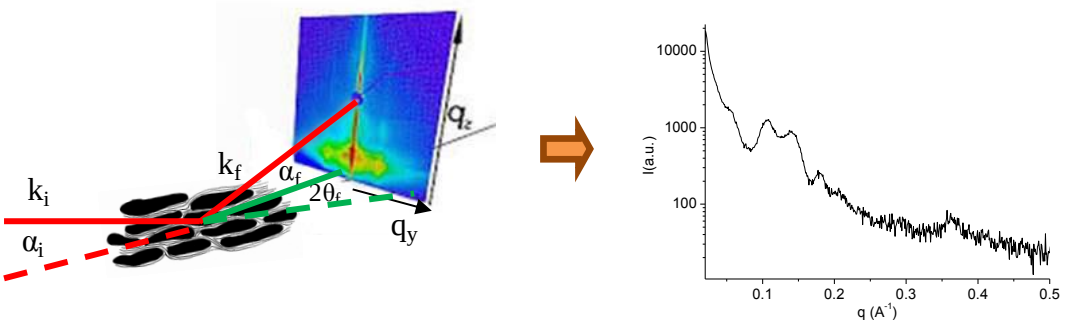

Figura 9. Representación esquemática de una medida de GISAXS y perfil de dispersión.

Para tomar las medidas de GISAXS se utilizó el equipo del IQAC-CSIC utilizado y descrito en el apartado 1.4.2.

1.5.1.3. Microespectroscopia de infrarrojo con transformada de Fourier y fuente sincrotrón

La espectroscopia de infrarrojo con transformada de Fourier (FTIR, del inglés "Fourier Transform Infrared") se basa en la interacción de la radiación IR con la muestra. El IR se divide en tres regiones: IR cercano, medio y lejano. De estos tres el IR medio que comprende entre los 4000 cm^{-1} y 400 cm^{-1}, es el de mayor interés en el análisis de los compuestos orgánicos como es el caso de las moléculas de la piel. Cada molécula o grupo funcional absorbe luz IR a una longitud de onda determinada, por lo que esta técnica nos proporciona información sobre las distintas vibraciones moleculares.

Esta técnica se ha utilizado en estudios anteriores para evaluar la penetración de diferentes sistemas lipídicos en la piel utilizando lípidos deuterados para formar estos sistemas (Rodríguez y col., 2012) o incluyendo en éstos determinados activos (Fernández y col., 2015). Tanto los lípidos deuterados con enlaces carbono-deuterio como estos activos con enlaces metal-carbonilo tienen vibraciones a longitudes de onda diferentes de las observadas para los componentes de la piel por lo que se pueden monitorizar fácilmente dentro del tejido (Fernández y col., 2016b).

Acoplando un microscopio a la espectroscopia de IR y utilizando radiación sincrotrón, la cual ofrece un alto brillo (que se define como cantidad de potencia por unidad de frecuencia, área y ángulo sólido) y un tamaño de foco pequeño, es posible obtener mapas químicos mostrando la distribución de las diferentes moléculas de la piel a altas

resoluciones (figura S3, artículo 4). Es decir, esta técnica no solo permite el estudio de penetración de sustancias tales cómo fármacos o sistemas lipídicos con bandas de absorción diferentes a las del tejido cutáneo, sino que también permite analizar los efectos que pueden tener estas sustancias sobre el tejido. Esta técnica también se utiliza para detectar cambios patológicos, por ejemplo el diagnóstico de cáncer en etapas tempranas del melanoma (Mordechai y col., 2004; Tfayli y col., 2005).

En esta tesis la técnica FTIR se ha utilizado para estudiar el efecto del sistema mimético de los cuerpos laminares a nivel bioquímico en piel con dermatitis inducida. Se ha comparado piel sana, piel con dermatitis y piel con dermatitis después de ser tratada con el sistema lipídico mediante PCA, un tipo de análisis estadístico multivariante. Este análisis requiere de un proceso matemático que transforma un set de datos en términos de nuevas variables no-correlacionadas llamadas componentes principales. Las componentes se ordenan por la cantidad de variancia original que describen, por lo que es útil para reducir la dimensionalidad de un conjunto de datos. Se utiliza el menor número de componentes que explica la mayor variancia. Normalmente se seleccionan las dos o tres primeras que deben explicar al menos un 80% de la variancia. Los resultados se representan en mapa de casos, "scores", valores que toman las muestras en el nuevo espacio, siendo posible observar relaciones entre ellas. También se representan en mapa de variables "loadings". Cuanto mayor sea un "loading" más tendrá en común esta variable con el componente principal por lo tanto indica la importancia que tiene cada variable en cada componente. Por lo tanto, el PCA nos permite determinar semejanzas o diferencias espectrales entre las muestras.

Las medidas de FTIR se han llevado a cabo con el microscopio Hyperion 3000 acoplado a un espectrómetro Vertex 70 (Bruker, Alemania) (figura 10). Los experimentos se han realizado en la línea Miras del Sincrotrón Alba (Barcelona, España) en colaboración con el Dr. Ibraheem Yousef. El análisis de PCA se ha realizado con el programa Unscrambler X 10.5 (CAMO).

Figura 10. Fotografía del equipo utilizado en la línea Miras del Sincrotrón Alba.

1.5.1.4. Permeabilidad cutánea

Las celdas de Franz representan desde su desarrollo en 1975, uno de los principales métodos utilizados para evaluar la penetración transepitelial y la liberación de fármacos (Schaefer y col., 1996). La figura 11 muestra un esquema del montaje de una celda de Franz. Las celdas constan de dos cámaras, una donadora y otra receptora, separadas por una membrana de origen animal, humana o sintética que permite evaluar la difusión de moléculas biológicamente activas de una cámara a otra. En el compartimiento donador se adiciona una solución o sistema lipídico que contiene el activo y en el receptor, que es agitado magnéticamente, se toman las muestras correspondientes, que posteriormente son cuantificadas mediante técnicas analíticas como el HPLC.

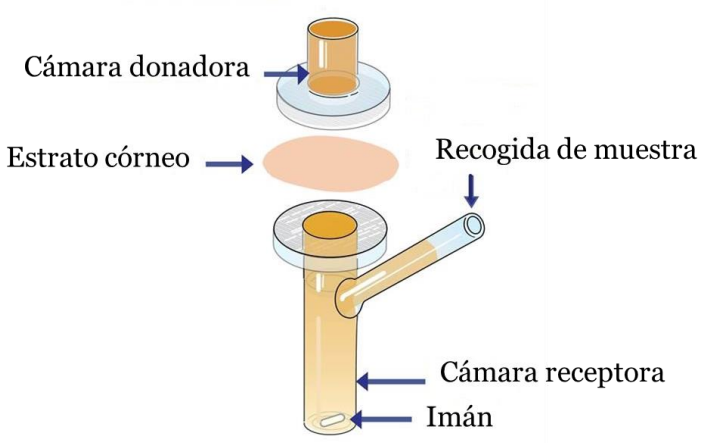

Figura 11. Esquema del montaje de una celda de Franz.

En esta tesis se han utilizado celdas de Franz para evaluar cambios en la permeabilidad de la piel. Para ello se ha estudiado la permeabilidad de la teofilina a través de SC deslipidizado y tratado con diferentes sistemas lipídicos. La teofilina se utiliza normalmente como marcador de la permeabilidad *in vitro* ya que tiene un tamaño molecular pequeño y muestra una lipofilia equilibrada, probablemente penetra la membrana mediante difusión simple (Opálka y col., 2016; Vávrová y col., 2007). Se han utilizado celdas estáticas con un compartimiento receptor de 6.6ml de volumen y un área de 1cm^2. Como membrana se ha utilizado SC humano. La integridad de la función barrera del SC se ha controlado mediante medidas de TEWL una vez colocado sobre la celda. Durante todo el experimento, las celdas están sumergidas en un baño termostatizado a 32°C para mimetizar la temperatura de la piel. Primero se aplica el

tratamiento durante 12h, luego se retira el sistema que queda sobre la superficie, se añade una solución de teofilina al 2% y se recogen alícuotas del fluido receptor cada hora durante 5 horas a excepción de la primera hora que se recogen cada 15min. Las muestras de fluido se analizan mediante el HPLC Prominence (Shimadzu, Japón) de fase inversa para determinar el contenido de teofilina. Con los datos del HPLC, el área de la celda y en función del tiempo se calcula el flujo de teofilina (μg/cm²/h) a través del SC.

El estudio de permeabilidad y el análisis de las muestras mediante HPLC se realizó en la Facultad de Farmacia de la Universidad Charles en Hradec Králové, República Checa, en colaboración con el Dr. Lukáš Opálka y la Dra. Kateřina Vávrová.

1.5.2. *In vivo*

Las técnicas para evaluar la función barrera cutánea *in vivo* pueden ser en animales de laboratorio o en voluntarios humanos. En ambos casos conviene que los sujetos permanezcan en salas con control de temperatura y humedad relativa durante la realización de las pruebas. Los voluntarios deben permanecer en la sala durante un periodo mínimo de 15min previos a la realización de las medidas para mantener estables las condiciones fisiológicas, evitar sudoración y disminuir las variables inter-día de los experimentos. Además, los voluntarios no deben aplicarse productos cosméticos hidratantes en el área de piel que se quiere estudiar desde una semana antes ni durante el tiempo que dure el estudio.

1.5.2.1. Pérdida transepidérmica de agua

La piel ejerce su función como barrera no sólo protegiendo al cuerpo de posibles agresiones externas, sino también controlando la pérdida de moléculas de agua de su interior. Este flujo transcutáneo de agua depende de la permeabilidad intrínseca de la piel y del medio ambiente, y se denomina pérdida de agua transepidérmica (TEWL, del inglés “Transepidermal Water Loss”). La medida de TEWL ha sido universalmente aceptada para evaluar la función barrera de la piel y consiste en determinar la cantidad de vapor de agua que atraviesa el SC hacia el exterior (Nangia y col., 1998; Werner y col., 1985). Valores elevados de TEWL (>25 g/m²h) indican que la barrera se encuentra deteriorada, ya sea por alteraciones físicas del SC o debido a tratamiento con agentes químicos (Branco y col., 2005). Existen diferentes evaporímetros para medir el TEWL.

En esta tesis se ha utilizado el Tewameter TM210 (figura 12A) y el Aquaflux AF200 (figura 12B). Para tomar las medidas, en ambos aparatos, el cabezal del sensor se debe colocar de modo perpendicular a la superficie de la piel y ejercer una presión constante.

El tewameter utiliza un sensor de cámara abierta. El sensor permite medir el gradiente de evaporación del agua de la piel indirectamente por dos pares de sensores (temperatura y humedad relativa) que se ubican en el interior de la cámara. En cambio, la cámara de medición del Aquaflux está cerrada. Un extremo se pone en contacto con la piel y en el otro extremo hay un condensador cuya temperatura se mantiene por debajo del punto de congelación del agua. El condensador elimina continuamente el vapor de agua que se origina en la piel y lo almacena como hielo. Esto mantiene una baja humedad en el condensador, mientras que la humedad en la superficie de la piel aumenta al aumentar la tasa de evaporación del agua. El gradiente de evaporación del agua se calcula a partir del valor proporcionado por sensores de temperatura y humedad, y del valor que proviene del condensador.

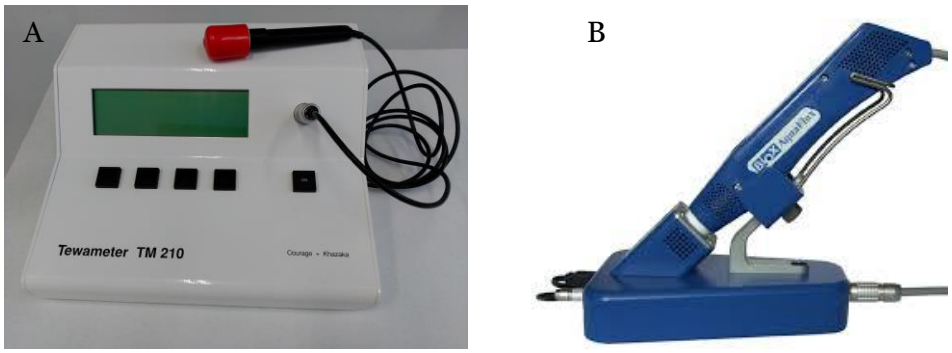

Figura 12. (A) Fotografía del Tewameter TM 210 (Courage & Khazaka). (B) Fotografía del AquaFlux AF200 (Biox Systems Ltd).

Las medidas con Tewameter (cedido por el Dr. Alfonso del Pozo) se realizaron en el Instituto de Química Avanzada de Cataluña (IQAC-CSIC). Las medidas con AquaFlux se realizaron en la facultad de farmacia de la Universidad Charles en Hradec Karlové, República Checa, con la colaboración del Dr. Lukás Olpálka.

1.5.2.2. Capacitancia de piel

El grado de hidratación cutánea es un parámetro utilizado en la caracterización de la piel. Un SC hidratado es sinónimo de elasticidad y buena apariencia de la piel. Cuando la hidratación se altera, se produce un incremento de la velocidad de descamación de los corneocitos, aparición de arrugas y pérdida de elasticidad, entre otros fenómenos. En esta tesis, se ha utilizado el Corneometer CM 825 (figura 13). Este instrumento está constituido por una sonda cilíndrica que contiene en su extremo dos circuitos paralelos a modo de condensadores recubiertos por una membrana plástica. Para hacer las medidas la sonda se debe colocar perpendicularmente sobre la superficie de la piel ejerciendo siempre la misma presión. Mediante este instrumento se mide la capacitancia (capacidad de un cuerpo para almacenar una carga eléctrica) de un medio dieléctrico, en este caso la piel (Clarys y col., 1999). Esta técnica se basa en el hecho de que el agua tiene una constante dieléctrica muy superior a la de los otros compuestos existentes en la epidermis por lo que cualquier variación en el contenido acuoso del SC ocasionará un cambio en su constante dieléctrica, alterando la capacitancia de la piel. Por lo tanto, se evalúa el contenido acuoso de la piel.

Las lecturas de hidratación son dadas por el equipo en unidades arbitrarias. Se considera piel seca valores inferiores a 30u.a y piel hidratada valores superiores a 60u.a (Barel y col., 2013).

Figura 13. Fotografía del Corneometer CM 825 (izquierda) y fotografía mostrando cómo se realiza una medida con la sonda (derecha).

Estas medidas se llevaron a cabo en el Instituto de Química Avanzada de Cataluña (IQAC-CSIC). El equipo fue cedido por el Dr. Alfonso del Pozo.

1.5.2.3. Test dinámicos de hidratación

Los test dinámicos de hidratación se utilizan para llevar a cabo un análisis funcional de la piel *in vivo*. Existen diferentes tipos: test de absorción-desorción (SDT) (Tagami, 2014; Tagami y col., 1982), test de acumulación de humedad (MAT) (van Neste, 1990) y "plastic occlusion stress test" (POST) (Berardesca y col., 1990). En esta tesis se utilizó el SDT que consiste en evaluar la cinética de hidratación y deshidratación del SC después de aplicar agua a saturación en una superficie de piel definida y durante un tiempo prefijado. Es un test simple y rápido que proporciona información de diferentes parámetros como son: la capacidad que tiene la piel de retener agua (WHC), la capacidad de absorción de agua (WSC) y la cantidad de agua liberada a través del SC a lo largo de la fase de desorción (AWD) (Pellacani y col., 2001). La figura 14 muestra un ejemplo de curva obtenida indicando como se calculan los diferentes parámetros. Este test ha sido utilizado por otros autores para estudiar el comportamiento de piel enferma (dermatitis atópica y psoriasis) (Borroni y col., 1989; Pellacani y col., 2001). También se utiliza comúnmente para estudiar el efecto que tienen diferentes irritantes sobre la piel y para evaluar la eficacia de diversos humectantes en piel con barrera cutánea deteriorada (Sindhvananda y col., 1993; Treffel y col., 1995).

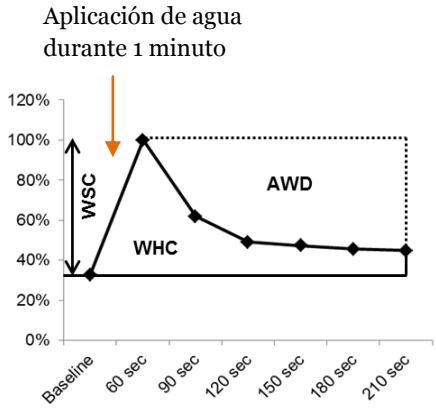

Figura 14. Ejemplo de curva obtenida mediante el test de absorción-desorción. Se aplica 1ml de agua en una zona de piel delimitada durante 1 minuto. Después de este tiempo se mide la capacitancia cada 30s hasta un máximo de 2.5min. La primera medida de capacitancia (Baseline) representa el valor de prehidratación. La curva se construye utilizando el valor de hidratación máxima (60s) como 100% y el resto de valores se calculan de acuerdo a este (Pellacani y col., 2001).

Las medidas para realizar este test se hicieron con Corneometer CM 825, igual que en la sección 1.5.2.2 en el Instituto de Química Avanzada de Cataluña (IQAC-CSIC).

1.6. Técnicas para evaluar la inflamación

La inflamación de la piel provocada por irritantes y alérgenos puede determinarse por análisis del suero sanguíneo y por evaluación de las muestras del tejido. La oxazolona es un hapteno que se une a las proteínas cutáneas y el continuo contacto con este antígeno desencadena una reacción de hipersensibilidad crónica mediada por linfocitos Th2 que producen citocinas e IgE (Liu y col., 2013). Por lo tanto, la cuantificación en suero sanguíneo de estas citocinas e IgE mediante ensayo de Elisa son buenos marcadores para evaluar el grado de inflamación. El ensayo de Elisa se basa en el uso de antígenos o anticuerpos marcados con una enzima, de forma que los conjugados resultantes tengan actividad tanto inmunológica como enzimática. Al estar uno de los componentes marcado con una enzima e insolubilizado sobre un soporte o pocillo la reacción antígeno-anticuerpo queda inmovilizada y, por tanto, es fácilmente detectada mediante la adición de un sustrato específico que al actuar la enzima produce un color observable a simple vista y cuantificable mediante el uso de un espectrofotómetro (Hoffman, 1973).

La inflamación de la piel también puede evaluarse mediante análisis histológico del tejido. La tinción de H&E es uno de los métodos más populares de tinción utilizado en histología y medicina diagnóstica. Mediante esta tinción se evalúa el grado de inflamación de la piel, ya que se puede determinar el grosor epidérmico (a mayor grosor, mayor inflamación), la presencia de edema (acumulación de líquido en el espacio extracelular), paraqueratosis (presencia de núcleos celulares en el SC) e infiltrado epidérmico de linfocitos.

En esta tesis se ha determinado el grado de inflamación que presentan los ratones con dermatitis inducida por oxazolona mediante cuantificación de IgE en suero sanguíneo. Para ello se ha utilizado el kit “mouse IgE Elisa” (Termo Scientific) siguiendo las instrucciones del fabricante. También se ha evaluado la inflamación histológicamente mediante la tinción H&E.

El ensayo Elisa se ha llevado a cabo en el Instituto de Química Avanzada de Cataluña (IQAC-CSIC). Las fotos de las histologías se han adquirido en el servicio de anatomía patológica del Hospital Clínico de Barcelona con la colaboración de la Dra. Adriana Garcia Herrera.

2. OBJETIVOS

2. OBJETIVOS

El objetivo principal de esta tesis ha sido producir un sistema lipídico que mimetice a los cuerpos laminares epidérmicos para tratar disfunciones cutáneas.

Con este fin se han establecido unos objetivos más específicos.

- Mimetizar los cuerpos laminares epidérmicos en morfología, estructura y composición.
- Incorporar diferentes ceramidas al sistema lipídico.
- Caracterizar el sistema lipídico.
- Evaluar si el sistema lipídico es capaz de reparar *in vitro* e *in vivo* la barrera cutánea.
- Estudiar la permeabilidad de la piel después de ser tratada con el sistema lipídico.
- Estudiar el efecto que produce el tratamiento con el sistema lipídico en la piel a nivel bioquímico.
- Evaluar el efecto antinflamatorio del tratamiento con el sistema lipídico en un modelo animal de dermatitis inducida.

Los objetivos propuestos en esta tesis han dado lugar a varios resultados que se han publicado en los artículos detallados en la siguiente sección.

En el artículo 1 se ha producido un sistema lipídico mimético y se ha caracterizado mediante diferentes técnicas. También se ha evaluado su efecto *in vitro* en piel previamente deslipidizada. El efecto del sistema *in vivo* se ha evaluado en voluntarios con piel irritada por un tensioactivo y por consiguiente con barrera cutánea comprometida (artículo 2) y en un modelo animal de dermatitis inducida (artículo 3). En el artículo 3 también se ha evaluado el efecto antinflamatorio del tratamiento con el sistema lipídico. En el artículo 4 se ha estudiado el efecto que tiene el sistema lipídico en la piel a nivel bioquímico en cuanto a lípidos, proteínas y ácidos nucleicos. Por otro lado, en el artículo 5 se ha incorporado CerEOS al sistema lipídico y se ha estudiado *in vitro* la permeabilidad de la piel después de ser tratada con el sistema. También se ha comparado este sistema con el descrito en el artículo 1 que incluía Cer3b. Y finalmente, en el artículo 6 se ha añadido complejidad a la composición del sistema lipídico añadiendo una mezcla de ceramidas extraídas de SC humano y ácidos grasos de cadena alquílica larga, y se ha estudiado la capacidad que tiene este sistema para reparar *in vitro* la estructura laminar del SC.

En la sección de resultados se adjuntan dichos artículos con un breve resumen.

3. RESULTADOS

3. RESULTADOS

Los resultados de la presente tesis doctoral están reflejados en los artículos científicos que se muestran a continuación acompañados con un breve resumen.

ARTÍCULO 1: **Lamellar body mimetic system: An up-to-down repairing strategy of the stratum corneum lipid structure.** V. Moner, E. Fernández, G. Rodríguez, M. Cócera, L. Barbosa-Barros, A. de la Maza y O. López. *International Journal of Pharmaceutics*, 2016, 510(1), 135-143.

ARTÍCULO 2: **Sorption-desorption test for the functional assessment of skin treated with a lipid system that mimics epidermal lamellar bodies.** V. Moner, E. Fernández, A. del Pozo, G. Rodríguez, M. Cócera, A. de la Maza y O. López. *Contact Dermatitis*, 2017, 77(1), 25-34.

ARTÍCULO 3: **A lamellar body mimetic system for the treatment of oxazolone-induced atopic dermatitis in hairless mice.** V. Moner, E. Fernández, A. Calpena, A. Garcia-Herrera, M. Cócera y O. López. *Journal of Dermatological Science*, 2018, 90(2), 172-179.

ARTÍCULO 4: **Synchrotron FTIR microspectroscopy to study different skin conditions.** V. Moner, I. Yousef, E. Fernández, M. Cócera, K. Talló, A. Calpena y O. López. *Journal of Pharmaceutical and Biomedical Analysis*– en revisión

ARTÍCULO 5: **Delivery systems with omega-*O*-acylceramide repair perturbed human stratum corneum.** V. Moner, L. Opálka, K. Vávrová y O. López. *International Journal of Pharmaceutics* – en revisión.

ARTÍCULO 6: **A lipid system containing acylceramides and long chain fatty acids to rebuild stratum corneum lamellar structure.** V. Moner, L. Opálka, P. Pullmannová, K. Talló, K. Vávrová y O. López. *Langmuir* –en revisión.

ARTÍCULO 1

Lamellar body mimetic system: An up-to-down repairing strategy of the stratum corneum lipid structure. V. Moner, E. Fernández, G. Rodríguez, M. Cócera, L. Barbosa-Barros, A. de la Maza y O. López. *International Journal of Pharmaceutics*, 2016, 510(1), 135-143.

La mayoría de enfermedades cutáneas como la dermatitis atópica y la psoriasis presentan cuerpos laminares epidérmicos disfuncionales. En consecuencia, la matriz lipídica del SC presenta deficiencias en ceramidas y ácidos grasos ocasionando una barrera cutánea deteriorada e ineficiente. Además, en dermatitis atópica, la síntesis de péptidos antimicrobianos está reducida y el pH de la piel es más alcalino que en piel sana por lo que la piel atópica es susceptible a la colonización de bacterias.

En éste trabajo se diseñó un sistema lipídico que mimetiza los cuerpos laminares epidérmicos tanto en morfología como composición para reparar la estructura lipídica laminar del SC. Se incluyó Cer3b, ácido esteárico, colesterol, sulfato de colesterol y palmitato de colesterol aproximando la composición del SC. Además, se incluyeron lípidos con efecto antimicrobiano y lípidos que actúan como reguladores del pH. El sistema se caracterizó mediante DLS para determinar su tamaño, crio-TEM para estudiar su morfología y SAXS para determinar su estructura. Los resultados de DLS indicaron que el sistema está formado por una población de partículas grandes con diámetro alrededor de 310nm y una población de partículas pequeñas de aproximadamente 24nm de diámetro. Mediante microscopía electrónica se determinó que las partículas grandes corresponden con vesículas que encapsulan estructuras discoidales y las partículas pequeñas con discos no encapsulados. Mediante SAXS se observaron dos reflexiones (66.1Å y 33.1Å) que están asociadas con el primer y segundo orden de las distancias de Bragg que corresponden con estructuras laminares de la bicapa lipídica. Por lo tanto, la morfología, estructura y composición de éste sistema es muy similar a la de los cuerpos laminares epidérmicos (descritos en la introducción de esta tesis, apartado 1.1.2).

También se evaluó el efecto que tiene éste sistema *in vitro* en piel porcina deslipidizada. Para ello SC nativo, SC deslipidizado y SC deslipidizado después de ser tratado con el sistema se analizó mediante GISAXS y FSTEM. Mediante GISAXS, el SC nativo mostró reflexiones que corresponden con la organización laminar de los lípidos intercelulares, concretamente con la LPP, la SPP y el colesterol. En cambio en SC

deslipidizado no se detectaron estas reflexiones ya que no hay lípidos estructurados en forma de láminas; solo se detectó una reflexión ancha que puede corresponder con los lípidos unidos covalentemente a la envoltura del corneocito y que no son extraídos con disolventes orgánicos. Finalmente, el análisis del SC deslipidizado y posteriormente tratado con el sistema mostró nuevas reflexiones que corresponden con la SPP y el colesterol. Mediante FSTEM se encontraron resultados similares. En SC nativo se observaron lípidos ordenados en forma de láminas entre los corneocitos. En cambio, esta estructura lipídica no fue observada en SC deslipidizado. Finalmente, en SC deslipidizado después del tratamiento con el sistema, se observaron nuevas estructuras lipídicas entre los corneocitos.

Estos resultados indican que el sistema propuesto que imita la morfología y composición de los cuerpos laminares epidérmicos restablece *in vitro* parte de la estructura laminar de SC deslipidizado.

International Journal of Pharmaceutics 510 (2016) 135–143

Contents lists available at ScienceDirect

International Journal of Pharmaceutics

journal homepage: www.elsevier.com/locate/ijpharm

Lamellar body mimetic system: An up-to-down repairing strategy of the stratum corneum lipid structure

Verónica Moner[a,*], Estibalitz Fernández[a], Gelen Rodríguez[b], Mercedes Cócera[b], Lucyanna Barbosa-Barros[b], Alfonso de la Maza[a], Olga López[a]

[a] Department of Chemical and Surfactant Technology, Institute of Advanced Chemistry of Catalonia (IQAC-CSIC), C/Jordi Girona 18-26, 08034 Barcelona, Spain
[b] Bicosome S.L. C/Jordi Girona 18-26, 08034. Barcelona, Spain

ARTICLE INFO

Article history:
Received 28 January 2016
Received in revised form 9 June 2016
Accepted 10 June 2016
Available online 14 June 2016

Keywords:
Lamellar bodies (LBs)
Stratum corneum (SC)
Skin lipids
Lipid composition
Grazing-incidence small-angle scattering (GISAXS)
Freeze substitution transmission electron microscopy (FSTEM)

ABSTRACT

Epidermal lamellar bodies (LBs) are organelles that secrete their content, mainly lipids and enzymes, into the intercorneocyte space of the stratum corneum (SC) to form the lamellar structure of this tissue. Thus, LBs have a key role in permeability and the microbial cutaneous barrier. In this work, a complex lipid system that mimics the morphology, structure and composition of LBs has been designed. To evaluate the effect of this system on delipidized SC, in vitro experiments using porcine skin were performed. The microstructure of SC samples (native, delipidized and, delipidized after treatment) was evaluated by freeze substitution transmission electron microscopy (FSTEM) and grazing-incidence small-angle X-ray scattering (GISAXS). Delipidized SC samples showed no evidence of lipid lamellae after extraction with organic solvents. However, after treatment with the LB mimetic system, new lamellar structures between corneocytes were detected by FSTEM, and high intensity peaks and reflections were found in the GISAXS pattern. These results demonstrate a strong effect of the treatment in repairing part of the lipid lamellar structure of the SC. Accordingly, future research could extend the use of this system to repair skin barrier dysfunction.

1. Introduction

The stratum corneum (SC) is the outermost layer of the skin and acts as barrier that prevents water loss and microbial infection. It consists of 15–20 layers of corneocytes embedded in lipid lamellar regions that mainly contain ceramides (45–50% by weight), cholesterol (25%) and free fatty acids (10–15%), and a smaller amount of cholesterol sulphate (5%) and cholesterol esters (2%).

Lamellar bodies (LBs) are ovoid, membrane-delimited and lamellate organelles measuring 200–300 nm in diameter. These organelles secrete their content (precursors of the SC lipids, hydrolases, protease inhibitors, and antimicrobial peptides) into the intercorneocyte space of the SC to form the lamellar structure of this tissue (Feingold and Elias, 2014; Menon et al., 1992).

A large number of skin diseases have been associated with the absence of or altered functions of LBs. The activity of one or more enzymes involved in the synthesis of barrier lipids is often altered. Consequently, diseased skin is characterized by a reduced barrier function and an altered lipid composition and organization. Harlequin ichthyosis is characterized by the absence of or abnormal LBs and a lack of extracellular lipid lamellae within the SC (Akiyama, 2014; Milner et al., 1992). Type 2 Gaucher disease, with severe defects in β-glucocerebrosidase, results in failure to metabolize LBs glucosylceramide to ceramide (Chan et al., 2011). Netherton syndrome is characterized by premature secretion of LB contents and impaired maturation of lamellar membrane structures (Fartasch et al., 1999). In atopic dermatitis (AD) and psoriasis, the skin has deficient synthesis of certain lipids, especially ceramides and free fatty acids (FFAs) (Elias and Wakefield, 2014; Imokawa et al., 1991; Motta et al., 1993, 1995). In AD but not in skin with psoriasis, the synthesis of antimicrobial peptides that play a role in protecting the skin from microbial infection is reduced (de Jongh et al., 2005). In addition, an alkaline pH of the skin surface is another cause of increased skin susceptibility to bacteria, mainly *Staphylococcus aureus* in AD (Rippke et al., 2004).

Biophysics studies of lipids have allowed us to design complex lipid systems with specific a size, morphology, structure, composition and phase behaviour (Barbosa-Barros et al., 2008; Rodríguez et al., 2011). Bicosomes are lipid aggregates (200–400 nm) formed by disks encapsulated in lipid vesicles.

* Corresponding author at: IQAC-CSIC, Department of Chemical and Surfactant Technology, C/Jordi Girona 18-26. 08034, Barcelona. Spain.
E-mail address: vmmtqt@iqac.csic.es (V. Moner).

http://dx.doi.org/10.1016/j.ijpharm.2016.06.033
0378-5173/

The interaction of these systems with the skin can promote an increase in the permeability of the barrier, reinforcement of the lipid structure and targeted delivery of molecules to specific skin layers, among others effects (Barbosa-Barros et al., 2012; Rodríguez et al., 2015).

The objective of the present work is to formulate a lipid system based on bicosomes that mimics the morphology, structure and composition of LBs and to evaluate the effect of this system on delipidized SC. The lipid components of this system include SC lipids, lipids with antimicrobial characteristics (lysophosphatidylcholine) and lipids focused on the regulation of skin pH (stearic acid). The system was characterized using small angle X-ray scattering (SAXS), cryogenic transmission electron microscopy (Cryo-TEM) and dynamic light scattering (DLS). SAXS was used to determine the lamellar organization of the lipids. Cryo-TEM was valuable for characterizing the dimensional and morphological features of the lipid system and for directly visualizing the sample. Finally, DLS was used to determine the average size of the system.

To evaluate the effect of our system on the skin, in vitro experiments using excised porcine skin were performed. The microstructure of skin samples (native, delipidized and delipidized after treatment) was evaluated by freeze substitution transmission electron microscopy (FSTEM) and grazing-incidence small-angle X-ray scattering (GISAXS). These techniques allow us to observe intercellular lamellar lipid regions and study the lipid organization.

The present work introduces a new lipid system that seems to mimic LB function and works from SC into the epidermis. This system is able to repair part of the lipid lamellar structure of a delipidized SC. Therefore, our work reports new data that are useful for designing specific systems for different diseases in which both the permeability and microbial barrier are compromised.

2. Material and methods

2.1. Chemicals

1,2-Dipalmitoyl-*sn-glycero*-3-phosphocholine (DPPC) and 1,2-dihexanoyl-*sn-glycero*-3-phosphocholine (DHPC) were purchased from Avanti Polar Lipids (Alabaster, US).

Cholesterol from lanolin (Chol), cholesteryl sulphate sodium salt (Schol), cholesteryl palmitate (Echol), stearic acid, trypsin, phosphate-buffered saline tablets, and sodium lauryl ether sulphate (SLES) were acquired from Sigma-Aldrich (Steinheim, Germany). Ceramide IIIb, *N*-oleyl phytosphingosine (Cer) was generously provided by Evonik (Essen, Germany).

Lipoid S100, whose main component (>94%) is soybean phosphatidylcholine (PC) and Lipoid S LPC 80, whose main component (80%) is soybean lysophosphatidylcholine (LysoPC), were obtained from Lipoid GmbH (Ludwigshafen, Germany).

Chloroform and methanol were purchased from Merck (Darmstadt, Germany).

2.2. Preparation and characterization of the lipid systems

2.2.1. Discoidal structures preparation

Four types of discoidal structures were prepared: (a) DPPC/DHPC, q = 3.5 (q = DPPC/DHPC molar ratio) including 10 mol% Cer; (b) DPPC/DHPC, q = 3.5 including 5 mol% Chol; (c) DPPC/DHPC, q = 3.5 including 5 mol% Schol and (d) DPPC/DHPC q = 3.5 including 5 mol% Echol.

For each of the discoidal systems, appropriate amounts of the corresponding lipids were mixed in a chloroform-methanol (2:1) solution and evaporated to dryness using a rotary evaporator. The systems were hydrated with distilled water to obtain a 10% (w/v) total lipid concentration and then subjected to 4 cycles of sonication at room temperature, cooling on ice and heating at 40 °C, with each step lasting one minute.

Then, different volumes of these samples were selected to obtain a mixture in which the molar ratio of Cer, Chol, Schol and Echol was similar to that found in the skin. A 1 ml mixture required 440 μl of (a), 440 μl of (b), 88 μl of (c) and 32 μl of (d).

This mixture was used to prepare the LB mimetic system.

2.2.2. LB mimetic system preparation

A chloroform solution containing 95 mg/ml PC, 5 mg/ml LysoPC and 1.6 mg/ml stearic acid was rota-evaporated to remove the chloroform and thus form a lipid film. The film was hydrated with the previously prepared mixture of discoidal structures approximating the SC lipid composition.

The total lipid concentration in the final system was 20% (w/v) with a Cer:stearic acid: Chol:Schol:Echol molar ratio of 1:1:0.5:0.1:0.04.

2.2.3. Effect of dilution on the LB mimetic system

The sample containing the LB mimetic system was diluted in water from 20% (initial lipid concentration) to 10% (final lipid concentration) to determine the effect of dilution on the size of the particles forming the LB mimetic system. The samples were analysed by DLS.

2.2.4. Dynamic light scattering (DLS)

The hydrodynamic diameter (HD) and polydispersity index (PI) were determined using DLS with a Zetasizer nano ZS (Malvern Instruments, UK). The PI, which is a measure of the homogeneity of the sample, can range from 0.0 (monodisperse) to 1.0 (very heterogeneous).

The DLS technique measures the diffusion coefficient (D) of the particles corresponding to Brownian motion. The relationship between the size of a particle and its D due to Brownian motion is defined by the Stokes-Einstein equation: $HD = kT/3\pi hD$, where HD is the hydrodynamic diameter of a hypothetical hard sphere that diffuses with the same speed as the particle in the experiment, D is the translational diffusion coefficient (m^2/s), k is the Boltzmann constant ($1.3806503 \times 10^{-23}\,m^2\,kg\,s^{-2}\,k^{-1}$), T is the absolute temperature (298 k), and η (mPa s) is the viscosity of the dispersant at 25 °C. The particles sizes were determined from the scattered light that was detected at an angle of 173° when a laser beam of 633 nm wavelength crossed the sample.

The size of the lipid system was determined immediately after preparation and 24 h after preparation. Measurements were performed in triplicate.

2.2.5. Small angle X-ray scattering (SAXS)

SAXS measurements were carried out using a S3-MICRO (Hecus X-ray systems GMBH Graz, Austria) coupled to a GeniX Cu high flux source (Xenocs, Grenoble). The wavelength of the X-rays was 0.1542 nm. Transmitted scattering was detected using a PSD 50 Hecus, and the temperature was controlled by means of a Peltier TCCS-3 Hecus. The sample was inserted in a flow-through glass capillary with a 1 mm diameter and 10 μm wall thickness.

2.2.6. Cryogenic transmission electron microscopy (Cryo-TEM)

The morphology of the LB mimetic system was evaluated by Cryo-TEM. A thin aqueous film was formed by dipping a glow-discharged holey carbon grid in the system suspension and then blotting the grid against a filter paper. The resulting thin sample film spanning the grid holes was vitrified by plunging the grid into ethane, which was maintained at its melting point with liquid nitrogen, using a Vitrobot (FEI Company, Eindhoven, The Netherlands). The vitreous sample film was transferred to a Tecnai F20 TEM (FEI Company, Eindhoven, The Netherlands) using a Gatan

cryotransfer (Barcelona, Spain), and the sample was observed in low-dose mode. Images were acquired at 200 kV at a temperature between −170 °C and −175 °C, using low-dose imaging conditions.

Ten overviews and approximately 50 detailed electron micrographs were taken.

2.3. In vitro study of the skin

2.3.1. Isolation of SC

Pig skin from the back of large Landrace white pigs was obtained immediately after the pigs had been slaughtered at the Bellvitge Animal Facility located at the University of Barcelona campus, Spain. To separate the epidermis from the dermis (Kligman and Christophers, 1963), the excised skin was placed in water at 65 °C for 2–3 min, and the epidermis was scraped off in sheets. Then, the SC was separated by placing the epidermis, with the SC facing up, on filter paper soaked with a 0.5% trypsin in phosphate-buffered saline (PBS) solution, pH 7.4, at 37 °C for 2 h. This procedure digests the epidermal cells. After this time, the SC was washed several times with distilled water.

2.3.2. Extraction of SC lipids

The SC was immobilized without loss of the tissue orientation and placed on filter paper in a plate. For the lipid extraction, we have followed the previously described procedure (Wertz and Downing, 1987). The sample was sequentially immersed in three different chloroform/methanol mixtures (2:1; 1:1 and 1:2, vol/vol) for 2 h each at room temperature and stirred at 60 revolutions/minute (Pselecta unitronic, Barcelona, Spain). Afterwards, the tissue was treated overnight with methanol. The extractions were then repeated for 1 h each, and another overnight extraction with methanol was performed. The extraction in methanol was used to extract any polar lipids that remained in the SC. Finally, the delipidized SC was washed three times with an abundance of distilled water.

2.3.3. Treatment of delipidized SC

The whole area (36 mm^2) of the SC piece was treated with 10 μl of the LB mimetic system, overnight, at room temperature. The sample was placed on wet filter paper in a Petri dish so that it remained hydrated. After the incubation time, the system remaining on the skin surface was removed with a specific wash: first with 10 μl of distilled water, then with 10 μl of SLES solution (at 0.5%, w/v) and finally twice (2 × 10 μl) with distilled water. Afterwards, the skin surface was dried with filter paper to remove excess water (Rubio et al., 2010).

2.3.4. Grazing-incidence small-angle scattering (GISAXS) experiments

GISAXS measurements were carried out using a S3-MICRO (Hecus X-ray systems GMBH Graz, Austria) coupled to a GeniX Cu high flux source (Xenocs, Grenoble). The wavelength of the X-rays was 0.1542 nm. Slit collimation was used to achieve a beam spot that was approximately 200 μm in height and 200 μm in width (z- and y-axes, respectively). The linear detector, a PSD 50 Hecus, covered a range of $0.07\ nm^{-1} < q < 6\ nm^{-1}$.

Hydrated samples were mounted by deposition on an oxidized silicon 111 cut plane wafers and placed on a homemade accessory that allowed a humid atmosphere. Humid air at 22 °C was blown in the sample cell at 99% relative humidity. The wafers were oriented in the scanning direction by a stepping motor with a resolution of 0.01°. The sample-to-detector distance was calibrated with silver behenate, and it was fixed at 268 mm. The exposure time was between 1800 and 3600 s. The sample was aligned between 0.5° and 0.25° of the incident angle.

The GISAXS curves are shown as a function of the scattering vector modulus, $q = (4\pi \sin\theta/2)/\lambda$, in which θ is the scattering angle, and λ the wavelength of the X-rays. The position of the scattering peaks is directly related to the repeat distance of the molecular structure and is calculated from Bragg's law (Bragg, 1913) as $q = 2\pi n/d$, where n and d represent the order of the diffraction peak and the repeat distance, respectively.

2.3.5. Freeze substitution transmission electron microscopy (FSTEM) experiments

The SC (native, delipidized and delipidized-treated) was cut into small ribbons with a size of approximately 2 × 1 mm. The ribbons were fixed in 5% (w/v) glutaraldehyde in a 0.1 M sodium cacodylate buffer at pH 7.2. Next, the ribbons were post-fixed in 0.2% (w/v) RuO_4 in sodium cacodylate buffer at pH 6.8 with 0.25% (w/v) potassium ferrocyanide ($K_4Fe(CN)_6$). After 1 h, the RuO_4 solution was replaced with fresh RuO_4 to establish optimal fixation. After a rinse in buffer, the tissue samples were cryofixed by rapid freezing on a liquid nitrogen-cooled metal mirror (Cryovacublock, Leica) at −196 °C prior to freeze-substitution, which was performed using an AFS (Automatic Freeze Substitution) system (Leica). The tissue samples were cryosubstituted at −90 °C for 48 h using 100% methanol containing 1.0% (w/v) osmium tetroxide (OsO_4), 0.5% (w/v) uranyl acetate and 3.0% (w/v) glutaraldehyde. After the 48 h substitution period, the temperature was increased to −50 °C, and the samples were washed three times in 100% methanol. Subsequently, the methanol solution was gradually replaced with the embedding medium, Lowicryl HM20 (100%). This resin was replaced after 24 and 48 h with freshly prepared embedding medium. Finally, the samples were transferred to a mould containing Lowicryl and were incubated for 48 h at −50 °C under UVA radiation to facilitate polymerization. Ultrathin sections were cut (Ultracut UCT, Leica), transferred to Formvar-coated grids, and examined using a Hitachi 600 transmission electron microscope (Rodríguez et al., 2012).

On average, 10 overviews and approximately 30–40 detailed electron micrographs for each freeze-substitution process were taken.

3. Results

3.1. Characterization of the LB mimetic system

DLS, Cryo-TEM and SAXS were used to characterize the LB mimetic system. The size distribution curves for the system and the diluted system were obtained by DLS. The HD and the

Table 1
Effect of the dilution of the LB mimetic system to the HD analysed by the scattered light intensity.

Lipid concentration of the LBs mimetic system	Particle population 1		Particle population 2	
	HD (nm)	% intensity	HD (nm)	% intensity
20%	24 ± 3	27 ± 2	314 ± 82	73 ± 2
15%	43 ± 17	15 ± 5	1110 ± 354	85 ± 5
10%	45 ± 15	6 ± 3	2423 ± 387	94 ± 3

percentage of light scattered by the different particle populations forming the system are shown in Table 1. The size distribution curve of the system, which was obtained by analysis of the scattered light intensity, shows two peaks corresponding to a population of small particles with an HD of approximately 24 nm that scattered 27% of the light and a population of large particles of approximately 314 nm that scattered 73% of the light. When the system was diluted from a 20% to 15% lipid concentration, the particle sizes increased; the population of small particles (43 nm) scattered 15% of the light, and the population of large particles (1110 nm) 85% of the light. When the lipid concentration of the system was diluted from 20% to 10%, two peaks were obtained at 45 nm (6%) and 2422 nm (94%). The subsequent dilution process involved an increase in the size of the aggregates present in the system and also a modification in the distribution of small and large particles. The percentage of small particles decreased from 27% to 6%, and the percentage of large particles increased from 73% to 94%. Both the system and the diluted system presented a PI of 1. This high value is expected due to the different sizes of the two populations forming the systems.

The morphology of the structures present in the LB mimetic system was studied by Cryo-TEM. Many images were analysed. Fig. 1 shows two Cryo-TEM images of the LB mimetic system. The images confirm the DLS results and showed two types of structures: nonencapsulated disks with diameters of approximately 30 nm and vesicles encapsulating disks (black arrows) with sizes from 200 nm to 500 nm. The discoidal structures are shown in all projections, edge-on (white open arrows) and face-on (white close arrows). In addition, nonencapsulated face-to-face stacking disks were detected (*).

SAXS provided information on the structural features of the LB mimetic system, primarily the lipid bilayer characteristics. The lamellar repeat distance *d* was estimated by analysing the reflections using Bragg's law and was attributed to the bilayer thickness, as in studies of liposomes and other bilayer models (Barbosa-Barros et al., 2008; Wu et al., 2012). Fig. 2 shows the SAXS profile for the LB mimetic system. Two reflections were observed at 66.1 Å and 33.1 Å, which can be attributed to the first- and second-order Bragg scattering, respectively, corresponding to the lipid lamellar organization of the lipid bilayer.

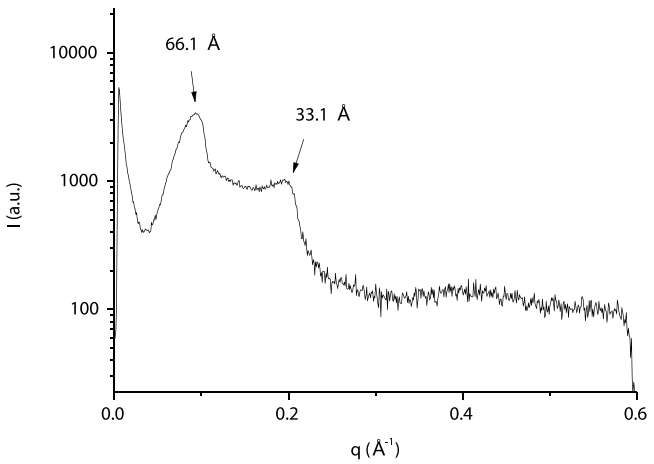

Fig. 2. SAXS profile of the LB mimetic system. Reflections can be attributed to the first- and second-order Bragg scattering, corresponding to the lipid lamellar structure of the lipid bilayer.

3.2. In vitro study results

In this work, the lipid structure of native SC, delipidized SC and delipidized SC after treatment with the LB mimetic system was analysed by two complementary techniques: GISAXS and FSTEM.

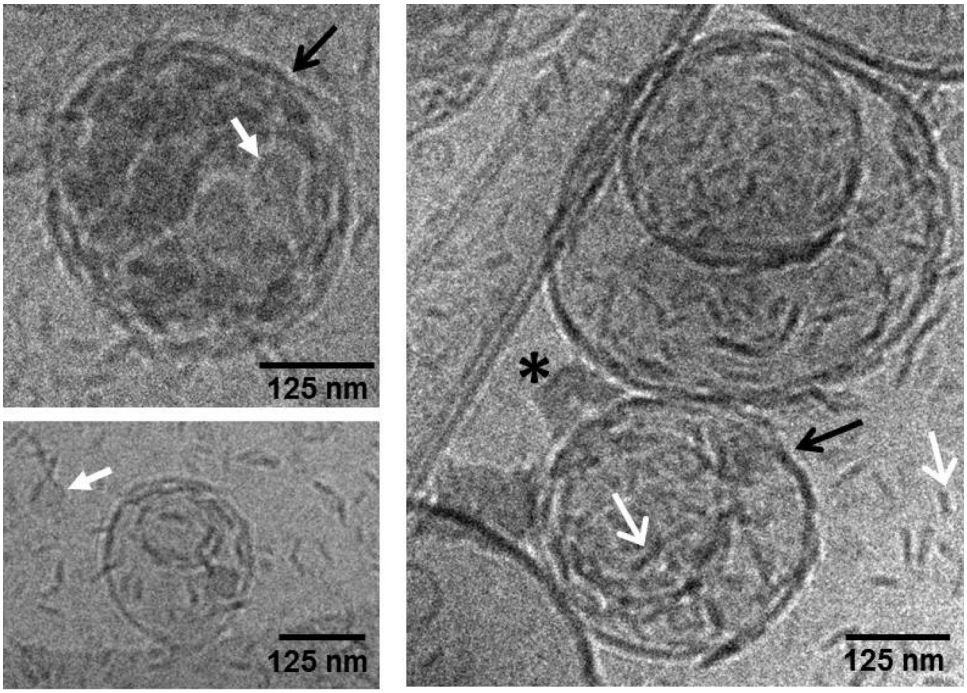

Fig. 1. Cryo-TEM micrographs of the LB mimetic system. The system is formed by different structures, mainly nonencapsulated disks with diameters approximately 30 nm and vesicles encapsulating disks (black arrows) with sizes from 200 to 500 nm. The discoidal structures are shown in all projections, edge-on (white open arrows) and face-on (white close arrows). (*) Stacks of disks.

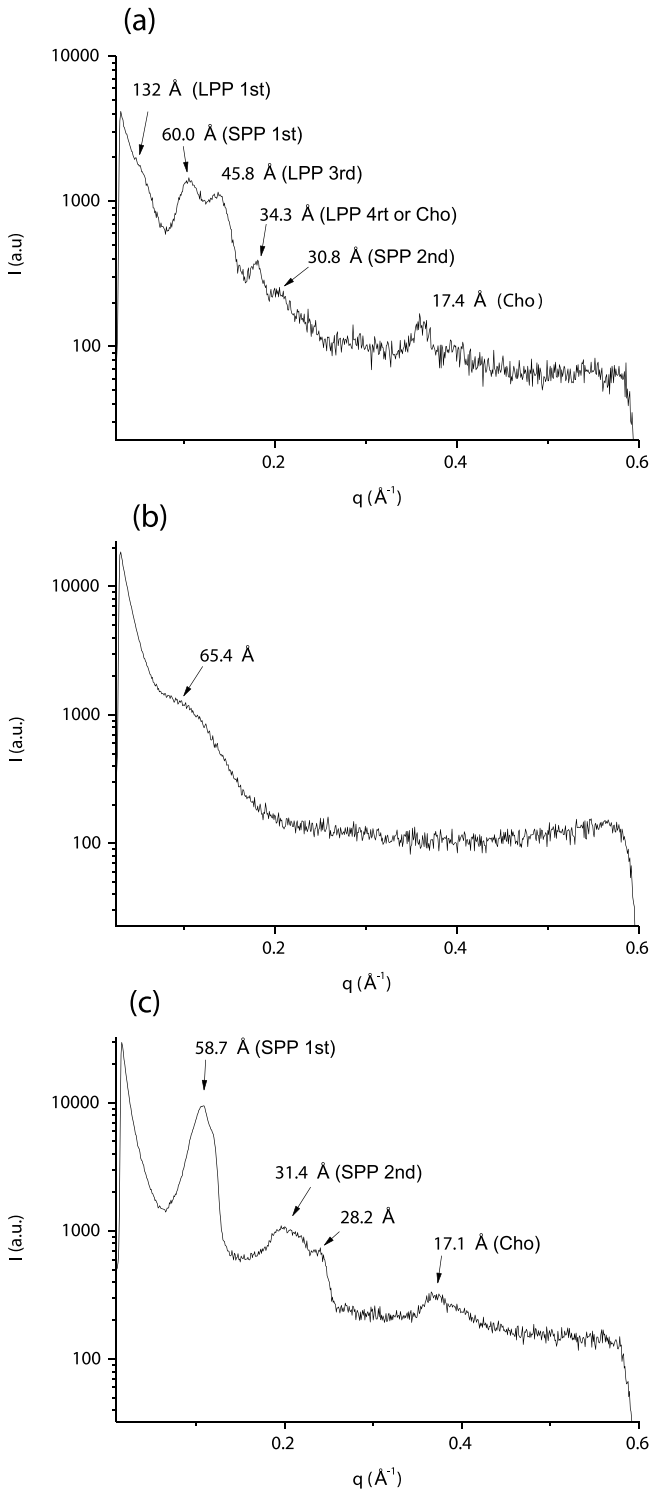

Fig. 3. (a) The GISAXS profile of the native SC shows reflections attributed to the LPP, SPP and crystalline cholesterol (Cho). (b) GISAXS profile for delipidized SC. The broad band observed at a d-spacing of approximately 65.4 Å could correspond to some organization of the lipids that are covalently linked to the corneocyte envelope. (c) GISAXS profile of the delipidized SC after the treatment with the LB mimetic system showing reflections attributed to the SPP and crystalline cholesterol (Cho). The peak at 28.2 Å could not be attributed to a particular phase.

Fig. 3 shows the GISAXS profiles corresponding to native, delipidized and delipidized-treated SC. The scattering pattern of native SC in Fig. 3a shows six peaks corresponding to d-spacings of 132, 60.0, 45.8, 34.3, 30.8 and 17.4 Å. According to Bouswtra et al., these spacing are associated with the intercellular lipid lamellar structure of the SC (Bouwstra and Ponec, 2006). These authors reported that two lamellar phases are present in human and pig SC (Bouwstra et al., 1995, 1991): one lamellar phase with a periodicity of approximately 60 Å referred to as the short periodicity phase (SPP) and another with a periodicity of approximately 132 Å that it is known as the long periodicity phase (LPP). Several weak orders of the LPP described by these authors were not detected in our experiments probably due to their low intensities. The reflections detected at 132, 45.8 and 34.3 Å are associated with the first, third and fourth order of the LPP, respectively. The peak at 34.3 Å also could be attributed to the crystalline cholesterol (Bouwstra et al., 2002). In addition, the reflections detected at 60.0 and 30.8 Å are associated with the first- and second-order of the SPP. Finally, the peak at 17.4 Å could correspond to the crystalline cholesterol (Bouwstra et al., 2002).

The GISAXS profile for delipidized SC after the extraction with organic solvents is shown in Fig. 3b. In this sample, no reflections corresponding to the intercellular lamellar lipids were detected. Only a broad band was observed in the profile (d-spacing of approximately 65.4 Å); this band could correspond to some organization of the lipids covalently linked to the corneocyte envelope (Elias et al., 2014; Madison, 2003). However, the GISAXS profile for delipidized SC after treatment with the LB mimetic system (Fig. 3c) shows four peaks corresponding to d-spacings of 58.7, 31.4, 28.2 and 17.1 Å. The reflections detected at 58.7 and 31.4 Å are associated with the first- and second-order of the SPP. The peak at 28.2 Å could not be attributed to a particular phase. Finally, the reflection at 17.1 Å could correspond to the crystalline cholesterol (Bouwstra et al., 2002).

FSTEM allows observation of the microstructure of the SC samples (Fig. 4): native, delipidized and delipidized after treatment. Several images of each sample were taken to evaluate the effect of the treatment on delipidized SC. The image of native SC (Fig. 4a) shows two layers of corneocytes (C) and the intercorneocyte lipid lamellar structure (L). However, the image of delipidized SC (Fig. 4b) shows two layers of corneocytes and the corneocyte envelope (white arrow) without any lipid lamellar structures between the corneocytes (*). Finally, two images of delipidized SC after treatment with the LB mimetic system are shown in Fig. 4c and Fig. 4d. Both images show new lamellar structures between the corneocytes (black arrows). Fig. 4c shows stacks of lipids bilayers at the surface of the SC (B).

4. Discussion

4.1. LB mimetic system

Keratinocyte differentiation is oriented from the basal layer to the surface of the epidermis. The process results in the transformation of keratinocytes to the corneocytes that form the SC. LBs are produced in the upper stratum spinosum and in the stratum granulosum (SG), and they extrude their content at the SG-SC interface to form the lipid lamellar structure of this tissue (Madison, 2003).

LBs are ovoid, membrane-delimited and lamellate organelles that measure approximately 200 nm in diameter. Based on extensive electron microscopy studies, Landmann proposed that the internal lamellae of the LBs are stacks of disks (Landmann, 1986). Bicosomes are lipid aggregates formed by phospholipids and consist of discoidal structures that are encapsulated into vesicles (Rodríguez et al., 2010). Therefore, the morphology and structure of these systems resemble epidermal LBs. Accordingly, we have designed a system that is similar to LBs: the LB mimetic

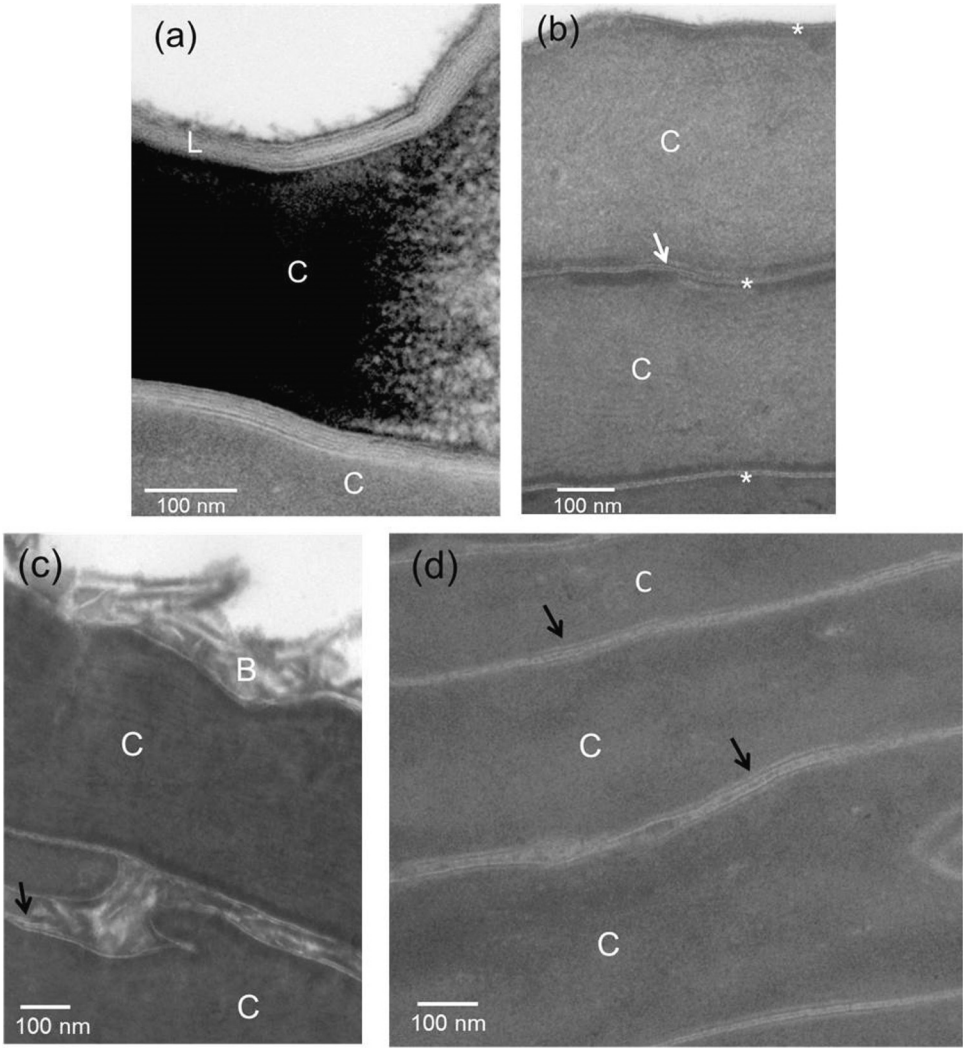

Fig. 4. FSTEM micrograph of the native SC (a), delipidized SC (b) and delipidized SC after treatment with the LB mimetic system (c) and (d). Symbols: C, corneocyte; L, lipid lamellar structure; *, no lipid lamellar structure; B, stacks of lipid bilayers; white arrow, corneocyte envelope; and black arrows, new lamellar structures between corneocytes.

system. This system is based on bicosomes and mimics the morphology, structure and composition of LBs.

The morphology and structure of the LB mimetic system observed in our Cryo-TEM images are quite similar to those of the epidermal LBs observed by other authors in electron micrographs (Madison, 2003; Menon et al., 1992; Wertz, 2015). The LB mimetic system, similarly to epidermal LBs, is organized in a lipid bilayer that contains discoidal structures, although the vesicle sizes are slightly larger than those of LBs. In a recent study using 3-dimensional electron microscopy Norlén et al. suggested that the LBs are not discrete vesicles but are part of a tubuloreticular membrane network (den Hollander et al., 2015; Norlén, 2001). In any case, the LB mimetic system morphologically resembles the epidermal LBs, and their integration into the skin could affect skin microstructure.

Another important point is the composition of the LB mimetic system. Epidermal LBs are composed of lipid lamellae that contain glucosylceramides, phospholipids and cholesterol, which are the precursors of SC intercellular lipids. Complex changes in lipid composition occur through enzymatic actions after the extrusion of their contents. Afterwards, the lipids form the lamellar structure of the SC. The LB mimetic system approximates the SC lipid composition. It includes 3% of the mixture of ceramide IIIb, stearic acid, cholesterol, cholesterol sulphate and cholesterol palmitate to repair the SC lamellar structure. These lipids in the system also have a molar ratio similar to that found in the skin. The LB mimetic system consists of discoidal structures that are encapsulated in vesicles. In this way, the system was designed so that the disks would contain the lipids that form the SC lamellar structure. For disks formation, both the DPPC constituting the flat bilayer and the DHPC stabilizing the rim of the structure are needed (Rodri'guez et al., 2010). Only one of the SC lipids, the FFA stearic acid, was included in the membrane of the vesicle. In addition to participating in the formation of the SC lamellar structure, this lipid also acts as a pH regulator (Fluhr et al., 2001). The vesicle also includes LysoPC, a lipid that could have bactericidal activity (Uchida et al., 1991), and PC, which is necessary to form the vesicular structure. We decided to include stearic acid and LysoPC in the external vesicle for potential future vivo applications of this system. In skin disorders, such as atopic dermatitis, the skin exhibits an alkaline pH and suffers from bacterial infections (Baker, 2006). Therefore, some lipids have been included in the external

vesicle or in the internal disks depending on their function in the skin and on the interactions of the system with skin that we discuss in the Section 4.2.

Additionally, some of the lipids forming the system could have other effects on the skin. DHPC could potentiate the fluidity of SC lipid domains. This effect can be understood by considering the surfactant effect on lipids of this short alkyl chain phospholipid (López-Fontán et al., 2003). LysoPC has an inverted cone shape and acts as a permeation enhancer (Kirjavainen et al., 1996). Cholesterol sulphate affects the SC lipid structure and seems to reduce the cohesion between lipid lamellae (van den Bergh et al., 1998).

Overall, the complex composition of the system together with the sophisticated organization could have great potential for skin applications.

Similarly to our design of a system that mimics epidermal LBs, other authors have developed a system that mimics lung LBs that consists of a vesicle that contains specific phospholipids in proportions similar to those found in lung LBs (Dobbie, 2013). Lung LBs are produced by alveolar type II epithelial cells and are specialized for the storage of surfactant (a mixture of proteins and lipids), which is arranged in tightly packed, concentric, membrane lamellae (Weaver et al., 2002).

4.2. Effect of LB mimetic system on delipidized SC

GISAXS and FSTEM are two complementary techniques that allowed us to evaluate the effect of the LB mimetic system on delipidized pig skin. GISAXS provides information about the SC lipid lamellar structure. Following previous studies of our group (Rodríguez et al., 2012), in the present work we used GISAXS with a convectional source instead of SAXS with a synchrotron source. For the GISAXS measurements, the skin surface was aligned with a certain incident angle, whereas in SAXS, the skin was situated perpendicularly to the incident beam (transmission).

X-ray diffraction data indicate that the native SC is composed of two phases with different repeat distances: 60 Å and 132 Å, corresponding to the SPP and LPP, respectively, described by Bouwstra et al. This scattering profile was compared to the profile obtained from the SC after extraction of the lipids with chloroform-methanol mixtures. After lipid extraction, the diffraction peaks disappeared due to the harsh extraction with the organic solvents. However, the lipids of the corneocyte envelope are resistant to this method because these lipids are covalently linked to the proteins of the envelope. Therefore, the broad band detected in the delipidized SC profile could correspond to these lipids.

The GISAXS profile from the delipidized SC after treatment is quite similar to that of the native SC. This fact indicates that after treatment with the LB mimetic system, the lipid structure of the tissue has recovered part of the organization. Interestingly, the re-establishment of the lamellar structure is mainly related to the SPP. This may be due to the fact that the tail lengths of the ceramides and free fatty acids in the native SC that are involved in the formation of the LPP are much longer than those of the lipids used in our system. Furthermore, ceramide 1 (ceramide EOS C30) is a prerequisite for the formation of the LPP (Groen et al., 2009), and it was absent in our system.

TEM images provide similar evidence. For the SC samples in which no lipid lamellar structure remained after the extraction with organic solvents, treatment with the LB mimetic system led to new lamellar structures between the corneocytes. Therefore, the LB mimetic system seems to rebuild part of the lipid lamellar structure of delipidized SC.

Our results could be explained by a specific interaction mechanism between LB mimetic system and the skin. This system mimics epidermal LBs in morphology, structure and composition. Therefore, the effect exerted by this system on the skin could be due to (a) the composition, (b) the morphology and structure or (c) a combination of both.

In a previous study, we evaluated the effect of liposomes and bicelles with the same lipid composition on the skin. The results showed that the lipid aggregates with different assemblies exerted different effects on the skin (Barbosa-Barros et al., 2009). Therefore, we concluded that the structure of the lipid systems plays a very important role in their effect on the skin. The previous work allowed us to assume that the structure of our LB mimetic system would be involved in the skin effect, which would be different if the same lipids formed another aggregate, such a liposome.

As mentioned previously, the LB mimetic system consists of discoidal structures encapsulated into a vesicle. Discoidal lipid structures have recently been demonstrated to be useful as carriers and modifiers of skin permeability. Because of their small size and discoidal morphology, these structures have the ability to penetrate through the narrow intercellular spaces of the SC (Rodríguez et al., 2015) that are approximately 6–10 nm (Bouwstra et al., 1995) and reinforce its lipid lamellar structure (Barbosa-Barros et al., 2012). This effect on the skin is unique and due to the self-organization of the discoidal structures (Rodri'guez et al., 2010). Additionally, the interaction of liposomes with human skin has been reviewed and indicated that liposomes do not penetrate through the spaces of the SC due to their size. Liposomes mainly burst and fuse with the outer lipid layers of the SC (Dreier et al., 2016). Therefore, our system combines the advantages of the discoidal structures and vesicles that promote a specific effect on the skin. When external vesicles (~300 nm) contact the skin, the bilayer of the vesicle bursts, and the encapsulated disks are released from the inside (Fernández et al., 2015). Once incorporated into the SC, they increase in size as a result of the hydration gradient of the skin, similarly to how our system increased in size due to the effect of the dilution (shown in Section 3.1). These new structures also partially re-establish the original SC lipid lamellar organization.

Other authors have studied the mechanism of the interaction between different lipid systems and the skin. For example, van den Bergh et al. have studied the interaction between liposomes, which had a composition similar to skin lipids, and SC by FSTEM but they did not delipidize the tissue. They observed intercellular vesicular structures in the upper parts of the SC after treatment, similar to those visualized in the samples that we treated with our LB mimetic system. The authors concluded that the migration of these liposomes through the intercellular lipid bilayers of the SC seems very unlikely because of their size. Therefore, they propose that cholesterol sulphate may be responsible for the fusion of the liposomes with the intercellular lipid bilayers. In our experiments, the small discoidal structures would penetrate the skin; once inside, the structures would increase in size and form the new lamellar structures in the skin (Barbosa-Barros et al., 2012), as discussed before.

The composition of the system is also important. To establish whether stratum corneum lipids could form bilayers, Wertz and Abraham prepared liposomes from lipid mixtures approximating the composition of the SC lipids (Abraham and Downing, 1989; Wertz et al., 1986). The interest in these structures is that they are capable of forming bilayers at physiologic pH. Despite the limitations of liposomes, stratum corneum lipid liposomes (SCLLs) have been described as good models for studying the lipid properties of the SC (Hatfield and Fung, 1995). Moreover, SCLLs have been proposed as a topical drug delivery system (Fresta and Puglisi, 1996) because their lipid composition is similar to SC lipids; thus, these systems can penetrate the epidermal barrier to a greater extent than other liposome compositions (El Maghraby, 2016).

Therefore, the effect that our system exerts on the skin possibly is due to a combination of the composition and structure.

5. Conclusions

The characterization of the LB mimetic system demonstrates that this system mimics epidermal LBs in morphology, structure and function. This system includes the main SC lipids in addition to lipids with a bactericidal effect and lipids that regulate skin pH. The images obtained by FSTEM and the GISAXS patterns show a strong effect of the treatment with the LB mimetic system on the intercellular spaces of the delipidized SC; this treatment seems to re-establish the lipid lamellar structure of the SC, mainly the SPP.

A large number of skin diseases have been associated with the absence of or altered functions of LBs. Consequently, diseased skin is characterized by a reduced barrier function and an altered lipid composition and organization. The LB mimetic system seems to facilitate the interaction with the skin by working as an exogenous lipid storage and secretory system. In this way, future research could be directed to designing specific systems for different skin diseases.

Acknowledgments

The authors wish to thank Carmen Lopez-Iglesias, Jaume Caelles and Josep Carilla for expert technical assistance. We also thank Evonik (Essen, Germany) for providing the ceramide and the Bellvitge Animal Facility located at the University of Barcelona Campus (Spain) which is the provider of the pig skin. This work was supported by funds from Comisión Interministerial de Ciencia y Tecnología from Spain (CTQ 2013-44998-P).

References

Abraham, W., Downing, D.T., 1989. Preparation of model membranes for skin permeability studies using stratum corneum lipids. J. Invest. Dermatol. 93, 809–813.
Akiyama, M., 2014. The roles of ABCA12 in epidermal lipid barrier formation and keratinocyte differentiation. Biochim. Biophys. Acta Mol. Cell. Biol. Lipids 1841, 435–440.
Baker, B.S., 2006. The role of microorganisms in atopic dermatitis. Clin. Exp. Immunol. 144, 1–9.
Barbosa-Barros, L., De La Maza, A., López-Iglesias, C., López, O., 2008. Ceramide effects in the bicelle structure. Colloids Surf. A Physicochem. Eng. Asp. 317, 576–584.
Barbosa-Barros, L., Barba, C., Rodríguez, G., Cócera, M., Coderch, L., López-Iglesias, C., De La Maza, A., López, O., 2009. Lipid nanostructures: self-assembly and effect on skin properties. Mol. Pharm. 6, 1237–1245.
Barbosa-Barros, L., Rodríguez, G., Barba, C., Cócera, M., Rubio, L., Estelrich, J., López-Iglesias, C., de la Maza, A., López, O., 2012. Bicelles: lipid nanostructured platforms with potential dermal applications. Small 8, 807–818.
Bouwstra, J.A., Ponec, M., 2006. The skin barrier in healthy and diseased state. Biochim. Biophys. Acta Biomembr. 1758, 2080–2095.
Bouwstra, J.A., Gooris, G.S., van der Spek, J.A., Bras, W., 1991. Structural investigations of human stratum corneum by small-angle X-ray scattering. J. Invest. Dermatol. 97, 1005–1012.
Bouwstra, J.A., Gooris, G.S., Bras, W., Downing, D.T., 1995. Lipid organization in pig stratum corneum. J. Lipid Res. 36, 685–695.
Bouwstra, J.A., Gooris, G.S., Dubbelaar, F.E., Ponec, M., 2002. Phase behavior of stratum corneum lipid mixtures based on human ceramides: the role of natural and synthetic ceramide 1. J. Invest. Dermatol. 118, 606–617.
Bragg, W.L., 1913. The diffraction of short electromagnetic waves by a crystal. Proc. Cambridge Philos. Soc. 17, 43–57.
Chan, A., Holleran, W.M., Ferguson, T., Crumrine, D., Goker-Alpan, O., Schiffmann, R., Tayebi, N., Ginns, E.I., Elias, P.M., Sidransky, E., 2011. Skin ultrastructural findings in type 2 Gaucher disease: diagnostic implications. Mol. Genet. Metab. 104, 631–636.
Dobbie, J., 2013. Lamellar bodies for use in therapeutics treatments, Google Patents. Lamellar Biomedical LTD. (EP20080170973).
Dreier, J., Sørensen, J.A., Brewer, J.R., 2016. Superresolution and fluorescence dynamics evidence reveal that intact liposomes do not cross the human skin barrier. PLoS One 11.
El Maghraby, G.M.M., 2016. Stratum corneum lipid liposomes: drug delivery systems and skin models, percutaneous penetration enhancers. Chemical Methods in Penetration Enhancement. Springer, pp. 111–119.
Elias, P.M., Wakefield, J.S., 2014. Mechanisms of abnormal lamellar body secretion and the dysfunctional skin barrier in patients with atopic dermatitis. J. Allergy Clin. Immunol. 134 (781–791), e781.
Elias, P.M., Gruber, R., Crumrine, D., Menon, G., Williams, M.L., Wakefield, J.S., Holleran, W.M., Uchida, Y., 2014. Formation and functions of the corneocyte lipid envelope (CLE). Biochim. Biophys. Acta Mol. Cell. Biol. Lipids 1841, 314–318.
Fartasch, M., Williams, M.L., Elias, P.M., 1999. Altered lamellar body secretion and stratum corneum membrane structure in Netherton syndrome: differentiation from other infantile erythrodermas and pathogenic implications. Arch. Dermatol. 135, 823–832.
Feingold, K.R., Elias, P.M., 2014. Role of lipids in the formation and maintenance of the cutaneous permeability barrier. Biochim. Biophys. Acta Mol. Cell. Biol. Lipids 1841, 280–294.
Fernández, E., Rodríguez, G., Cócera, M., Barbosa-Barros, L., Alonso, C., López-Iglesias, C., Jawhari, T., de la Maza, A., López, O., 2015. Advanced lipid systems containing β-carotene: stability under UV–vis radiation and application on porcine skin in vitro. Phys. Chem. Chem. Phys. 17, 18710–18721.
Fluhr, J.W., Kao, J., Jain, M., Ahn, S.K., Feingold, K.R., Elias, P.M., 2001. Generation of free fatty acids from phospholipids regulates stratum corneum acidification and integrity. J. Invest. Dermatol. 117, 44–51.
Fresta, M., Puglisi, G., 1996. Application of liposomes as potential cutaneous drug delivery systems. In vitro and in vivo investigation with radioactively labelled vesicles. J. Drug Target. 4, 95–101.
Groen, D., Gooris, G.S., Bouwstra, J.A., 2009. New insights into the stratum corneum lipid organization by X-ray diffraction analysis. Biophys. J. 97, 2242–2249.
Hatfield, R.M., Fung, L.W., 1995. Molecular properties of a stratum corneum model lipid system: large unilamellar vesicles. Biophys. J. 68, 196–207.
Imokawa, G., Abe, A., Jin, K., Higaki, Y., Kawashima, M., Hidano, A., 1991. Decreased level of ceramides in stratum corneum of atopic dermatitis: an etiologic factor in atopic dry skin? J. Invest. Dermatol. 96, 523–526.
Kirjavainen, M., Urtti, A., Jääskeläinen, I., Marjukka Suhonen, T., Paronen, P., Valjakka-Koskela, R., Kiesvaara, J., Mönkkönen, J., 1996. Interaction of liposomes with human skin in vitroäthe influence of lipid composition and structure. Biochim. Biophys. Acta Lipid Met. 1304, 179–189.
Kligman, A.M., Christophers, E., 1963. Preparation of isolated sheets of human stratum corneum. Arch. Dermatol. 88, 702–705.
López-Fontán, J.L., Martínez-Landeira, P., Santamarina, C., Ruso, J.M., Prieto, G., Sarmiento, F., 2003. The surfactant characteristics of short-chain lecithins analyzed through lecithin-lecithin and lecithin-biopolymer interactions. Progress in Colloids and Polymer Science. Springer, pp. 141–148.
Landmann, L., 1986. Epidermal permeability barrier: transformation of lamellar granule-disks into intercellular sheets by a membrane-fusion process, a freeze-fracture study. J. Invest. Dermatol. 87, 202–209.
Madison, K.C., 2003. Barrier function of the skin:la raison d'etre of the epidermis. J. Invest. Dermatol. 121, 231–241.
Menon, G.K., Feingold, K.R., Elias, P.M., 1992. Lamellar body secretory response to barrier disruption. J. Invest. Dermatol. 98, 279–289.
Milner, M.E., O'Guin, W.M., Holbrook, K.A., Dale, B.A., 1992. Abnormal lamellar granules in harlequin ichthyosis. J. Invest. Dermatol. 99, 824–829.
Motta, S., Monti, M., Sesana, S., Caputo, R., Carelli, S., Ghidoni, R., 1993. Ceramide composition of the psoriatic scale. Biochim. Biophys. Acta Mol. Basis Dis. 1182, 147–151.
Motta, S., Sesana, S., Ghidoni, R., Monti, M., 1995. Content of the different lipid classes in psoriatic scale. Arch. Dermatol. Res. 287, 691–694.
Norlén, L., 2001. Skin barrier formation: the membrane folding model. J. Invest. Dermatol. 117, 823–829.
Rippke, F., Schreiner, V., Doering, T., Maibach, H.I., 2004. Stratum corneum pH in atopic dermatitis. Am. J. Clin. Dermatol. 5, 217–223.
Rodríguez, G., Soria, G., Coll, E., Rubio, L., Barbosa-Barros, L., López-Iglesias, C., Planas, A.M., Estelrich, J., De la Maza, A., López, O., 2010. Bicosomes: bicelles in dilute systems. Biophys. J. 99, 480–488.
Rodríguez, G., Barbosa-Barros, L., Rubio, L., Cócera, M., López-Iglesias, C., de la Maza, A., López, O., 2011. Bicellar systems as modifiers of skin lipid structure. Colloids Surf. B Biointerfaces 84, 390–394.
Rodríguez, G., Co'cera, M., Rubio, L., Lo'pez-Iglesias, C., Pons, R., de la Maza, A., Lo'pez, O., 2012. A unique bicellar nanosystem combining two effects on stratum corneum lipids. Mol. Pharm. 9, 482–491.
Rodríguez, G., Barbosa-Barros, L., Rubio, L., Cócera, M., Fernández-Campos, F., Calpena, A., Fernández, E., De La Maza, A., López, O., 2015. Bicelles: new lipid nanosystems for dermatological applications. J. Biomed. Nanotechnol. 11, 282–290.
Rodri'guez, G., Rubio, L., Cócera, M., Estelrich, J., Pons, R., de la Maza, A., López, O., 2010. 2010: Application of bicellar systems on skin: diffusion and molecular organization effects. Langmuir: ACS J. Surf. Colloids 26, 10578–10584.
Rubio, L., Alonso, C., Rodríguez, G., Barbosa-Barros, L., Coderch, L., De la Maza, A., Parra, J.L., Lopez, O., 2010. Bicellar systems for in vitro percutaneous absorption of diclofenac. Int. J. Pharm. 386, 108–113.
Uchida, Y., Ogawa, T., Ohta, M., Kondo, M., Takada, S., Yamamura, M., 1991. Penetration of lysophosphatidylcholine into the dermis. J. Dermatol. 18, 523–527.
Weaver, T.E., Na, C.-L., Stahlman, M., 2002. Biogenesis of lamellar bodies: lysosome-related organelles involved in storage and secretion of pulmonary surfactant. Semin. Cell Dev. Biol. 13, 263–270.
Wertz, P.W., Downing, D.T., 1987. Covalently bound omega-hydroxyacylsphingosine in the stratum corneum. Biochim. Biophys. Acta 917, 108–111.

Wertz, P.W., Abraham, W., Landmann, L., Downing, D.T., 1986. Preparation of liposomes from stratum corneum lipids. J. Invest. Dermatol. 87, 582–584.
Wertz, P.W., 2015. Epidermal lipids and the intercellular pathway. In: Dragicevic-Curic, N., Maibach, H.I. (Eds.), Percutaneous Penetration Enhancers Chemical Methods in Penetration Enhancement. Springer, Berlín, pp. 13–18.
de Jongh, G.J., Zeeuwen, P.L., Kucharekova, M., Pfundt, R., van der Valk, P.G., Blokx, W., Dogan, A., Hiemstra, P.S., van de Kerkhof, P.C., Schalkwijk, J., 2005. High expression levels of keratinocyte antimicrobial proteins in psoriasis compared with atopic dermatitis. J. Invest. Dermatol. 125, 1163–1173.
den Hollander, L., Han, H., de Winter, M., Svensson, L., Masich, S., Daneholt, B., Norlén, L., 2015. Skin lamellar bodies are not discrete vesicles but part of a tubuloreticular network. Acta Dermatol. Venereol..
van den Bergh, B., Salomons-de Vries, I., Bouwstra, J.A., 1998. Interactions between liposomes and human stratum corneum studied by freeze-substitution electron microscopy. Int. J. Pharm. 167, 57–67.
Wu, R.G., Dai, J.D., Wu, F.G., Zhang, X.H., Li, W.F., Wang, Y.R., 2012. Competitive molecular interaction among paeonol-loaded liposomes: differential scanning calorimetry and synchrotron X-ray diffraction studies. Int. J. Pharm. 438, 91–97.

ARTÍCULO 2

Sorption-desorption test for the functional assessment of skin treated with a lipid system that mimics epidermal lamellar bodies. V. Moner, E. Fernández, A. del Pozo, G. Rodríguez, M. Cócera, A. de la Maza y O. López. *Contact Dermatitis*, 2017, 77(1), 25-34.

Considerando los resultados obtenidos *in vitro* en SC deslipidizado, se propuso un trabajo con el objetivo de evaluar el efecto que tiene el LBms *in vivo*. Para ello se realizó en voluntarios el SDT mediante corneómetro, tanto en una zona de piel sana como en una zona de piel irritada por un tensioactivo antes y después de ser tratadas con el sistema lipídico. Este test proporciona información de diferentes parámetros que pueden asociarse con la funcionalidad de la piel como es la capacidad de retener agua, la capacidad de absorción de agua y la cantidad de agua liberada a través del SC durante la fase de desorción.

La piel sana se trató durante 7 días con el sistema lipídico y se realizó el SDT antes de iniciar el tratamiento, después de 4 días de tratamiento y a los 7 días de tratamiento. Después del tratamiento la piel sana aumentó su capacidad de retención de agua.

Para evaluar el efecto del sistema en piel irritada se aplicó sobre la piel un parche con una solución de lauril sulfato de sodio al 2% durante 2h. El SDT indicó que justo después de irritar la piel, ésta aumenta su capacidad de retener agua y de liberarla más lentamente. También aumenta su capacidad de absorción de agua. Se ha descrito que la piel frente a un daño en la barrera como podría ser el producido por el tensioactivo, inicia una respuesta de reparación homeostática para recuperar la función barrera. Este hecho podría explicar los resultados obtenidos. Sin embargo, estas capacidades que adquiere la piel justo después de ser irritada vuelven al equilibrio después de 24h. En cambio, si la piel irritada se trata durante 4 días con el LBms se observa una mejora extra en éstos parámetros no detectada en la piel irritada sin tratar.

Es decir, este trabajo demuestra que el LBms refuerza la función barrera *in vivo* tanto en piel sana como piel irritada por un tensioactivo. Se propone este sistema como posible tratamiento de enfermedades cutáneas las cuales presentan una barrera deteriorada como es el caso de la dermatitis atópica.

Sorption–desorption test for functional assessment of skin treated with a lipid system that mimics epidermal lamellar bodies

Verónica Moner[1], Estibalitz Fernández[2], Alfonso del Pozo[3], Gelen Rodríguez[2], Mercedes Cócera[2], Alfonso de la Maza[1] and Olga López[1]

[1] *Department of Chemical and Surfactant Technology, Institute of Advanced Chemistry of Catalonia (IQAC-CSIC), 08034 Barcelona, Spain,* [2] *Bicosome S.L., 08034 Barcelona, Spain, and* [3] *Faculty of Pharmacy, Department of Pharmacy and Pharmaceutical Technology, University of Barcelona, 08028 Barcelona, Spain*

doi:10.1111/cod.12771

Summary

Background. Many skin diseases are associated with either increases or decreases in lamellar body secretion, or dysfunctional lamellar bodies. Consequently, diseased skin is characterized by reduced barrier function and altered lipid composition and organization. Human skin is commonly evaluated *in vivo* with non-invasive biophysical techniques. The dynamic functions of the skin are evaluated with repeat measurements such as the sorption–desorption test (SDT).

Objectives. The aim of this study was to evaluate *in vivo* skin hydration–dehydration kinetics after treatment with a lipid system that mimics the morphology, structure and composition of lamellar bodies in both healthy and irritated human skin.

Methods. A patch with an aqueous solution of 2% sodium lauryl sulfate (SLS) was used to irritate the skin of the volunteers. The SDT was performed with the CM 820 corneometer.

Results. After treatment with this system, both healthy and SLS-irritated skin increased their ability to retain water and to release water slowly during the desorption phase.

Conclusions. Treatment with this system seems to reinforce the barrier function in both healthy and SLS-irritated human skin. Therefore, the present study provides evidence that this system could be of interest for developing future treatments for protecting and repairing the skin.

Key words: accumulated water decay (AWD); corneometer; skin lipids; sorption–desorption test; water-holding capacity (WHC); water sorption capacity (WSC).

Skin barrier function depends on the composition and lipid organization of the outermost layer of the epidermis, the stratum corneum, whose main functions are to prevent excessive water loss and the penetration of xenobiotics and pathogens. The stratum corneum (10–20 μm in thickness) contains approximately 15–20 layers of corneocytes, which are embedded in a lipid matrix organized in a lamellar structure (1). The whole stratum corneum contains ~15% lipids, mainly ceramides (45–50% of the total lipid mass), cholesterol (25%), and free fatty acids (10–15%), and smaller amounts of cholesterol sulfate (5%) and cholesterol ester (2%) (2).

Epidermal lamellar bodies are produced in the stratum granulosum by keratinocytes, and secrete their contents – precursors of the stratum corneum lipids, hydrolases, protease inhibitors, and antimicrobial peptides – into the intercellular space at the stratum

Correspondence: Verónica Moner, Department of Chemical and Surfactant Technology, Institute of Advanced Chemistry of Catalonia (IQAC-CSIC), C/Jordi Girona 18-26, 08034 Barcelona, Spain. Tel: +34 93 400 61 00. E-mail: vmmtqt@iqac.csic.es

Conflicts of interest: The authors do not have a conflict of interest to declare.

Accepted for publication 9 January 2017

granulosum–stratum corneum interface to form the lamellar structure of this tissue (3). Two models have been proposed for skin barrier formation: the Landmann model, which proposes that lamellar bodies are discrete vesicles (4); and the membrane-folding model, which proposes that lamellar bodies form part of a tubuloreticular membrane network (5, 6).

A large number of skin diseases are associated with either increases or decreases in lamellar body secretion or dysfunctional lamellar bodies (7–11). Consequently, diseased skin is characterized by reduced barrier function and alterations in lipid composition and organization. Atopic dermatitis is a very common skin disease in which there are deficiencies in certain lipids, especially ceramides and free fatty acids (12, 13). Moreover, the synthesis of antimicrobial peptides, which play a role in protecting the skin from microbial infection, is reduced in atopic dermatitis (14). In addition, an alkaline pH of the skin surface is another cause of increased skin susceptibility to bacteria, mainly *Staphylococcus aureus*, in atopic dermatitis (15).

Human skin is commonly evaluated *in vivo* with non-invasive biophysical techniques such as skin hydration, which gives information about the water content, and transepidermal water loss for study of skin barrier function. The dynamic functions of the skin are evaluated with repeat measurements, such as the sorption–desorption test (SDT). This test assesses the behaviour of the skin surface when it is in contact with applied water. Therefore, the SDT provides information about the ability of the skin to take up water (water sorption capacity) and to retain water, counteracting a dehydration process (water-holding capacity) (16). In this way, the SDT is used for the functional assessment of different skin diseases, such as psoriasis (17) and atopic dermatitis (18), and the results are compared with those obtained with healthy skin. In addition, this test is useful for evaluating the efficacy of moisturizers (19, 20).

In previous work, we designed a lipid system based on bicosomes that mimic the morphology, structure and composition of epidermal lamellar bodies. In addition, we performed *in vitro* studies to evaluate the effect of this system on delipidized stratum corneum (21). We concluded that treatment with the lamellar body mimetic system (LBms) re-establishes part of the lipid lamellar structure of delipidized stratum corneum, mainly the short periodicity phase described by Bouwstra et al. (22).

In the present study, we sought to evaluate the effect of the application of the LBms on the skin *in vivo*. Accordingly, we evaluated hydration–dehydration skin kinetics in both healthy and irritated human skin, and how treatment with this system affected water sorption and desorption.

Materials and Methods

Chemicals

1,2-Dipalmitoyl-sn-glycero-3-phosphocholine (DPPC) (CAS no. 63-89-8) and 1,2-dihexanoyl-sn-glycero-3-phosphocholine (DHPC) (CAS no. 34506-67-7) were from Avanti Polar Lipids (Alabaster, AL, USA).

Cholesterol from lanolin (chol) (CAS no. 57-88-5), cholesteryl sulfate sodium salt (Schol) (CAS no. 2864-50-8), cholesteryl palmitate (Echol) (CAS no. 601-34-3) and stearic acid (SA) (CAS no. 57-11-4) were from Sigma-Aldrich (Steinheim, Germany). Ceramide IIIb, *N*-oleyl phytosphingosine (Cer) was from Evonik (Essen, Germany). Lipoid S100, whose main component (>94%) is soybean phosphatidylcholine (PC), and Lipoid S LPC 80, whose main component (80%) is soybean lysophosphatidylcholine (LysoPC) (CAS no. 92128-87-5), were from Lipoid GmbH (Ludwigshafen, Germany).

Chloroform (CAS no. 67-66-3), methanol (CAS no. 67-56-1) and sodium lauryl sulfate (SLS) (CAS no. 151-21-3) were from Merck (Darmstadt, Germany).

Preparation and characterization of the lipid systems

Discoidal structure preparation. Four types of discoidal structure were prepared: (i) DPPC/DHPC, $q = 3.5$ (q = DPPC/DHPC molar ratio), including 10 mol% Cer; (ii) DPPC/DHPC, $q = 3.5$, including 5 mol% chol; (iii) DPPC/DHPC, $q = 3.5$, including 5 mol% Schol; and (iv) DPPC/DHPC, $q = 3.5$, including 5 mol% Echol. For each of the discoidal systems, appropriate amounts of lipids were mixed in a chloroform/methanol (2:1) solution and evaporated to dryness with a rotary evaporator. The systems were hydrated with distilled water to obtain a 10% (wt/vol) total lipid concentration, and then subjected to several cycles of sonication, freezing and heating until the samples became transparent.

Next, different volumes of these samples were selected to obtain a mixture in which the molar ratio of Cer, chol, Schol and Echol was similar to that found in the skin. To obtain 1 ml, 440 µl of (i), 440 µl of (ii), 88 µl of (iii) and 32 µl of (iv) were mixed. This mixture was used to prepare the LBms.

LBms preparation. A chloroform solution containing 95 mg/ml PC, 5 mg/ml LysoPC and 1.6 mg/ml SA was rota-evaporated to remove the chloroform and

thus form a lipid film. The film was hydrated with the previously prepared mixture of discoidal structures approximating the stratum corneum lipid composition. The total lipid concentration in the final system was 20% (wt/vol), with a Cer:SA:chol:Schol:Echol molar ratio of 1:1:0.5:0.1:0.04. The LBms was analysed 24 h after preparation by dynamic light scattering (DLS) and cryogenic transmission electron microscopy (Cryo-TEM). The sample was maintained at 4°C during the 10 days of the experiment.

Dynamic light scattering. The hydrodynamic diameter (HD) was determined by DLS with a Zetasizer nano ZS (Malvern Instruments, Malvern, UK). The DLS technique measures the diffusion coefficient (D) of the particles corresponding to Brownian motion, and converts this to size by using the Stokes–Einstein equation,

$$HD = kT/3\pi\eta D$$

where HD is the hydrodynamic diameter, D is the translational diffusion coefficient (m^2/s), k is the Boltzmann constant ($1.3806503 \times 10^{-23}\ m^2\ kg\ s^{-2}\ K^{-1}$), T is the absolute temperature (298 K), and η is the viscosity of the dispersant at 25°C (water, 0.8872 mPa s). The particle sizes were determined from the scattered light that was detected at an angle of 173° when a laser beam of wavelength 633 nm crossed the sample. Measurements were performed in triplicate.

Cryogenic transmission electron microscopy. The LBms was visualized by the use of Cryo-TEM. A thin aqueous film was formed by dipping a glow-discharged holey carbon grid in the suspension and then blotting the grid against a filter paper. The resulting thin sample film spanning the grid holes was vitrified by plunging the grid into ethane, which was maintained at its melting point with liquid nitrogen, by use of a Vitrobot (FEI Company, Eindhoven, The Netherlands). The vitreous sample film was transferred to a Tecnai F20 transmission electron microscope (FEI Company) by use of a cryotransfer holder (Gatan, Barcelona, Spain), and the sample was observed in low-dose mode. Images were acquired at 200 kV at a temperature between −170°C and −175°C, under low-dose imaging conditions. Ten overviews and ~50 detailed electron micrographs were taken.

In vivo study

Five females aged 29–51 years with healthy skin participated in this study. Written informed consent was obtained from all participants. Four different skin areas ($4\ cm^2$) on the lower leg corresponding to untreated (control), treated with the LBms (treated), irritated with SLS (SLS) and irritated with SLS and treated with the LBms (SLS-treated) were delimited. These areas were randomized on each participant. The participants were not allowed to use moisturizers on the lower leg for 1 week prior to, and during, the period of the experiment. To obtain reliable measurements, the participants were acclimatized for 15 min in a conditioned room at 23 ± 1°C and 50 ± 3% relative humidity before the measurements.

Study design. SDTs on two non-irritated skin areas were performed on days 0, 4, and 7. One of these areas was treated daily with 10 µl of the LBms for 7 days, and the other was not treated.

On irritated skin, SDTs on two skin areas were performed on day 0 (before and 30 min after SLS irritation), day 1, and day 4. Both skin areas were irritated as described: 10 µl of SLS 2% aq. was applied on a filter paper placed in each of two aluminium chambers (diameter = 8 mm; Finn Chambers®; SmartPractice, Phoenix, AZ, USA). The chambers were fixed to the skin for 2 h with adhesive tape. Upon removal of the patches, the skin was gently rinsed with water and dried with a paper towel. One of these areas was treated daily with 10 µl of the LBms for 4 days, and the other was not treated.

Sorption–desorption test. A CM 820 corneometer (Courage & Khazaka, Cologne Germany), which measures skin capacitance in arbitrary units, was used to record the different measurements obtained with the SDT. The SDT was performed as described by Tagami et al. (16), with slight modifications, such as a longer water application time (1 min instead of 10 s). The first capacitance measurement represented the prehydration value. Soaked cotton wool with 1 ml of distilled water was placed onto the skin, left for 1 min, and wiped with a paper towel, and the hydration was immediately measured (60 s). The capacitance was subsequently measured every 30 s for a maximum of 2.5 min. A curve was then constructed, with the value of maximum hydration as 100%, and the other values were calculated accordingly. This test provides information about the ability of the skin to take up water [water sorption capacity (WSC)] and to retain water, counteracting a dehydration process [water-holding capacity (WHC)]. Also, it provides information about the amount of water released from the stratum corneum through the desorption phase [accumulated water decay (AWD)]. These parameters were calculated from the curve as described by Pellacani and Seidenari (18). Figure 1 shows an example of an SDT curve and the different parameters.

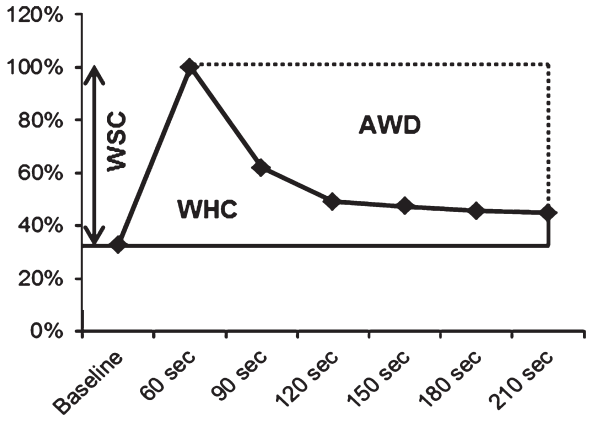

Fig. 1. Example of sorption–desorption test curve indicating the different parameters. AWD, accumulated water decay; WHC, water-holding capacity; WSC, water sorption capacity.

Table 1. Changes in water-holding capacity (WHC), water sorption capacity (WSC) and accumulated water decay (AWD) of healthy skin after 4 and 7 days of treatment with the lamellar body mimetic system

	WHC (%)	WSC (%)	AWD (%)
Day 4	28	−1	−25
Day 7	77	19	−31

The results are expressed as percentage increase or decrease with respect to the initial value at day 0 and the untreated control.

In order to be able to make interpretable statements on the effects of the treatment on WHC, WSC and AWD parameters, the results were calculated by use of the following equation (23):

$$\text{Change in the parameters } (\%) = \left[\left(P_t - P_0\right)/P_0\right] \times 100$$

In Table 1, P_t is the mean of the quotients of the calculated parameters of treated and control areas after the application time t in all participants, and P_0 is the mean of the quotients of the calculated parameters of treated and control areas before application in all participants. In Table 2, P_t is the mean of the calculated parameters of the irritated area after the application time t in all participants, and P_0 is the mean of the calculated parameters before irritation in all participants.

Statistical analysis. Means and standard deviations were calculated. Statistical analysis of the experimental data was performed by use of the Wilcoxon rank-sum test with STATA/SE 12.0 software. Differences were considered to be statistically significant at $p < 0.05$.

Table 2. Changes in water-holding capacity (WHC), water sorption capacity (WSC) and accumulated water decay (AWD) of irritated skin and irritated skin after treatment with the lamellar body mimetic system at day 0 (after irritation), day 1, and day 4

	Irritated skin			Irritated and treated skin		
	WHC (%)	WSC (%)	AWD (%)	WHC (%)	WSC (%)	AWD (%)
Day 0 (SLS)	47	23	−33	57	14	−27
Day 1	4	3	−3	19	−4	−15
Day 4	−6	8	14	43	12	−18

SLS, sodium lauryl sulfate.
On day 0, the two skin areas are equivalent. The results are expressed as percentage increase or decrease with respect to the initial value (before irritation) at day 0 for each skin area.

Results

Characterization of the system

DLS was used to determine the average size of the LBms. The size distribution curve of the system, which was obtained by analysis of the scattered light intensity, showed two peaks corresponding to a population of small particles with an HD of 27 ± 2 nm that scattered $26 \pm 1\%$ of the light, and a population of large particles of 345 ± 17 nm that scattered $74 \pm 1\%$ of the light.

Cryo-TEM allows us to directly visualize the sample and to characterize the dimensions and morphology of the different structures present in the system. Figure 2 shows a micrograph of the LBms. This image shows two types of structures, which is in agreement with the data obtained by DLS, corresponding to non-encapsulated disks (white arrows) with diameters of ~35 nm, and disks encapsulated in vesicles (black arrows) with a size of ~320 nm. This image also shows the disks in edge-on (white open arrows) and face-on (white closed arrows) configuration.

Effect of the treatment on healthy skin

SDTs were performed on healthy skin before treatment (day 0) and after 4 and 7 days of treatment with the LBms. The sorption–desorption curves and the different parameters calculated from the curves are shown in Fig. 3. After the application of water, the relative increase in capacitance values was similar before (black curve) and after (orange and brown curves) treatment with the LBms. The second parts of the sorption–desorption curves show that all of the relative capacitance values were higher after treatment (orange and brown curves), although the differences were not statistically significant. However, the parameter WHC calculated from the curves increased

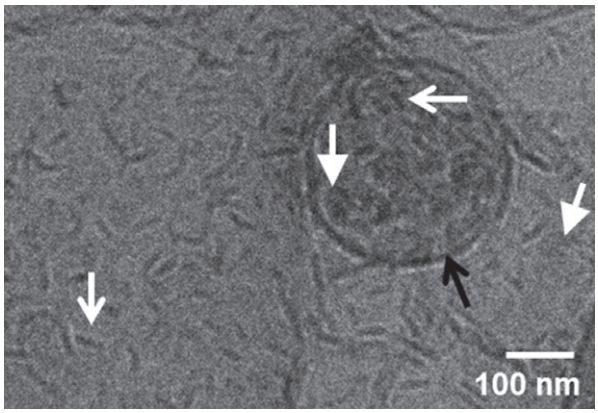

Fig. 2. Cryogenic transmission electron microscopy micrograph of the lamellar body mimetic system. The system is formed by non-encapsulated disks with diameters of ~35 nm, and vesicles encapsulating disks (black arrow) with sizes of ~320 nm. The disks are shown in all projections: edge-on (white open arrows) and face-on (white closed arrows).

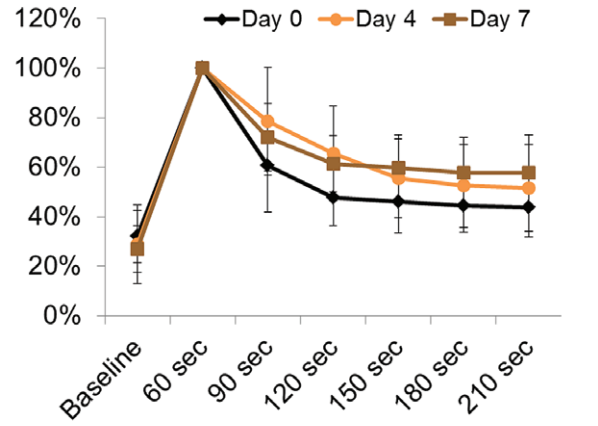

	WHC	WSC	AWD
Day 0	132.6 ± 27.1	68.2± 10.2	64.5 ± 15.2
Day 4	181.9 ± 31.8*	71.2 ± 16.0	49.3 ± 20.0
Day 7	185.1 ± 28.4*	73.2 ± 9.4	47.9 ± 16.7

Fig. 3. Sorption–desorption test performed on healthy skin before treatment (day 0) and after 4 and 7 days of treatment with the lamellar body mimetic system. AWD, accumulated water decay; WHC, water-holding capacity; WSC, water sorption capacity. *Statistically significant differences ($p < 0.05$) as compared with day 0.

significantly after treatment with the LBms, and no differences were detected between days 4 and 7.

In order to be able to make valid statements on the effect of the LBms in healthy skin, the results were doubly evaluated as a percentage of modification with respect to the initial value on day 0, and as a percentage of modification with respect to the untreated control. The results are shown in Table 1. When healthy skin was treated for 4 and 7 days, WHC increased by 28% and 77%, respectively. WSC remained unaltered after 4 days of treatment, but increased by 19% after 7 days. Finally, AWD decreased by 25% and 31% after 4 and 7 days of treatment, respectively.

Therefore, after treatment with the LBms, healthy skin increased its capacity to retain water, and also showed a decrease in the rate of water loss. Additionally, visual inspection of the treated area did not identify any irritant effect or colour change, and no participant of this study perceived irritation of the test areas.

Effect of the treatment on irritated skin

Two skin areas were exposed to SLS on day 0, and one of these areas was then left untreated, whereas the other was treated daily with the LBms for 4 days. The present study aimed to evaluate the effect of the lipid system on the skin. The lipid system is formed in water. However, water is not appropriate as a control, as the effect of water alone could be different from the effect of the water part of the system. Also, in a previous study, we showed that hydration values after treatment with water are almost the same as those in untreated skin (24).

SDTs were performed on day 0 (before and after SLS exposure), day 1 and day 4 on the two areas, and the curves are shown in Fig. 4a and b. Figure 4a shows the different sorption–desorption curves and the corresponding parameters calculated from the curves for the irritated untreated skin. After the application of water, the relative increase in capacitance was higher just after irritation of the skin (grey curve) than before irritation (black curve). In contrast, the amount of water absorbed by the skin 1 day after irritation (green curve) was similar to that before irritation (black curve). Moreover, no differences were detected between days 1 and 4 (green and orange curves). The second parts of the sorption–desorption curves show that all relative capacitance values were higher just after SLS exposure (grey curve) than before irritation (black curve). This indicates that, just after SLS irritation, the skin response is to release water slowly, although the tissue loses this ability in 1 day, as shown by the descending part of the curves at days 1 and day 4 (green and orange curves).

Figure 4b shows the different sorption–desorption curves and the corresponding parameters calculated from the curves for skin irritated and treated with the LBms. The behaviour of the skin after SLS irritation was the same as shown in Fig. 4a. Only after 4 days of treatment did the irritated and treated skin (orange

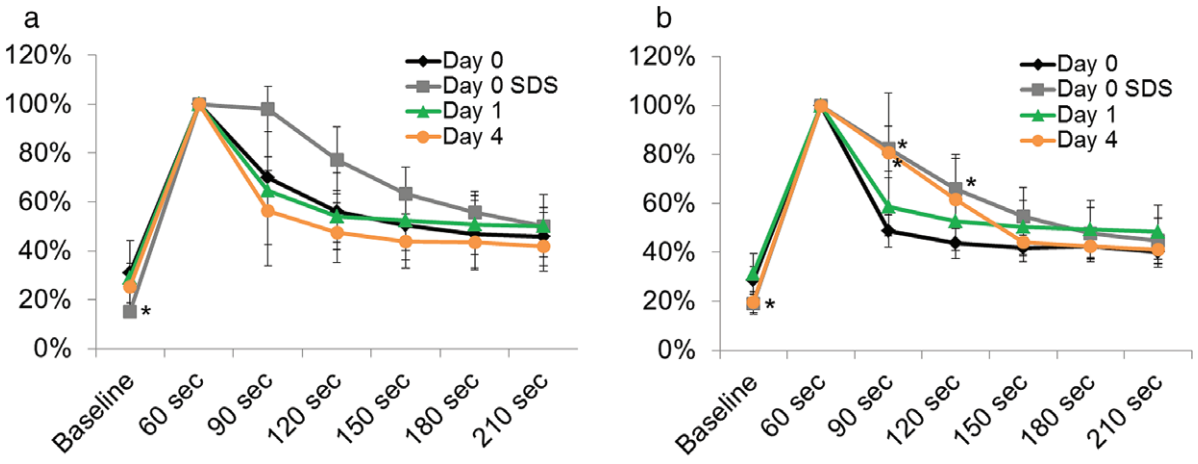

	WHC	WSC	AWD
Day 0	151.3 ± 35.9	69.1 ± 13.4	58.6 ± 16.0
Day 0 SDS	223.1 ± 25.1*	84.9 ± 1.5*	39.4 ± 10.8*
Day 1	158.0 ± 25.9	71.1 ± 5.9	57.0 ± 13.4
Day 4	142.8 ± 29.9	74.8 ± 6.6	66.8 ± 16.4

	WHC	WSC	AWD
Day 0	121.9 ± 20.9	71.4 ± 5.7	70.7 ± 7.5
Day 0 SDS	191.4 ± 26.8*	81.1 ± 4.0*	51.2 ± 13.0*
Day 1	145.3 ± 24.7*	68.9 ± 8.4	60.1 ± 14.2
Day 4	174.8 ± 26.6*	80.3 ± 4.4*	58.1 ± 9.3

Fig. 4. Sorption–desorption test (SDT) performed on irritated skin (a) and irritated skin treated with the lamellar body mimetic system (b). AWD, accumulated water decay; WHC, water-holding capacity; WSC, water sorption capacity. *Statistically significant differences ($p < 0.05$) as compared with day 0.

curve) show a higher amount of water absorbed than before treatment (black curve). The second parts of the sorption–desorption curves show that all of the relative capacitance values were higher after treatment of the skin (green and orange curves) than before treatment (black curve). This indicates that the treatment causes skin to release water slowly. This response was not observed in the irritated untreated skin.

In both skin areas just after SLS exposure, WHC and WSC increased and AWD decreased, with significant differences. As shown in Fig. 4a, if the irritated skin was maintained untreated, these parameters were restored in 1 day and remained unaltered after 4 days. However, after 1 day of treatment, the skin showed a WHC that was higher than on day 0, and both WSC and AWD remained unaltered. After 4 days of treatment, both WHC and WSC increased significantly in comparison with day 0, and AWD decreased, although the differences were not statistically significant.

These results were also evaluated as percentage increase and decrease with respect to the initial values (before SLS exposure) at day 0, as shown in Table 2. Just after skin irritation, WHC and WSC increased by approximately 50% and 20%, respectively, and AWD decreased by approximately 30%. If the skin was left untreated, these parameters were restored in 1 day, and no differences were detected after 4 days. However, the irritated skin showed an increase in WHC after treatment, namely, 19% after one application and 43% after four applications. WSC decreased by 4% after 1 day of treatment, but increased by 12% after 4 days of treatment. Moreover, AWD decreased by 15% and 18% after 1 day and 4 days of treatment, respectively. Therefore, if the irritated skin was treated with the LBms, a notable increase in WHC and a decrease in AWD were observed in comparison with irritated untreated skin.

Therefore, after treatment with the LBms, irritated skin increases its capacity to absorb and retain water, and also shows a decrease in the rate of water loss, in comparison with irritated untreated skin.

Discussion

The LBms

On the basis of extensive electron microscopy studies, Landmann described epidermal lamellar bodies as ovoid, membrane-delimited and lamellate organelles measuring ~200 nm in diameter (4). However, recent studies conducted by Norlen's group suggested that the lamellar body system is composed of a single and coherent tuboreticular membrane network (5). In both models, the presence of stacked lamellar structures seems to be relevant, although these lamellar structures are packed into discrete vesicles

in the Landmann model and into a tubuloreticular membrane system in the Norlen model.

The LBms proposed in this work is also based on lamellar structures, some of them stacked as planar discoidal assemblies that resemble those described in the Landman and Norlen models. Furthermore, these discoidal structures are encapsulated in vesicles. The morphology and structure of the LBms observed in our Cryo-TEM images are quite similar to those of the epidermal lamellar bodies observed by other authors in electron micrographs (25, 26). The LBms, similarly to epidermal lamellar bodies, is organized in a lipid bilayer that contains discoidal lamellar structures and is also similar in structure to bicosomes previously described in other studies (27, 28). Bicosomes formed exclusively by phospholipids have been shown to constitute a good vehicle for incorporating different molecules into the skin, owing to the specific interaction of these structures with the stratum corneum (28).

The LBms proposed here approximates the stratum corneum lipid composition and, in addition, includes phospholipids, among them LysoPC, which has bactericidal activity (29). Unlike epidermal lamellar bodies, which contain the precursors of stratum corneum intercellular lipids (30), the LBms contains lipids that approximate the stratum corneum lipid composition.

In a previous study, the LBms was shown to undergo a specific interaction with the skin *in vitro* (21). Treatment with this system re-established part of the lipid lamellar structure of delipidized stratum corneum, mainly the short-periodicity phase described by Bouwstra et al. (31). This fact could be related to the effect of this system *in vivo* described here.

As in our previous work, the LBms was designed so that the disks would contain the lipids that form the stratum corneum lamellar structure, and the external vesicle would include the compounds that should remain on the skin surface. For disk formation, both the DPPC constituting the flat bilayer and the DHPC stabilizing the rim of the structure are needed (32). Only one of the stratum corneum lipids, stearic acid, was included in the membrane of the vesicle. The rationale for this approach was that this lipid, in addition to participating in the formation of the stratum corneum lamellar structure, acts as a pH regulator (33). The normal pH on the skin surface is in the range of 5.4–5.9, and it is known that changes in skin pH may play a significant role in the pathogenesis, prevention and treatment of dermatitis and other cutaneous conditions. The vesicle also includes PC, which is necessary to form the vesicular structure and LysoPC. Following the mechanism of bicosome–skin interaction previously described (34), when external vesicles contact the skin, the bilayer of the vesicle bursts, and the encapsulated disks are released from the inside. Once incorporated into the stratum corneum, the discoidal structures increase in size as a result of the hydration gradient of the skin, and lipids from the LBms mix with the stratum corneum lipids, supposedly reinforcing the skin barrier. The composition of the LBms, like that of skin lipids, plays an important role in the effect of this system on the skin. It is known that liposomes approximating the stratum corneum lipid composition, despite the limitations of these structures, interact with the epidermal barrier to a greater extent than other liposomes with different compositions (35). In our case, mimicking the composition, and the combination of discoidal and vesicular assemblies forming the LBms, could potentiate the effects of both nanostructures on the cutaneous tissue.

Dynamic hydration tests

In order to study the *in vivo* hydration dynamics of the skin, three tests have been developed: the SDT (16, 36), the moisture accumulation test (37), and the plastic occlusion stress test (38). In the present study, the SDT was used to perform a functional analysis of stratum corneum hydration–dehydration kinetics. This test is simple and quick, and provides information about WHC, WSC, and AWD. With this test, some skin diseases, such as atopic dermatitis and psoriasis, have been investigated (17, 18). This test has also been applied to assess the effects of different moisturizers under different experimental conditions of impairment of skin barrier function (19, 20), and to study the dynamic hydration changes occurring in the skin surface after application of irritants such as SLS (19). Therefore, the SDT appears to be appropriate for studying the effect of treatment with the LBms in healthy and irritated skin.

Effect of the treatment on healthy skin

In the present study, we found an increase in WHC of healthy skin after treatment with the LBms. This result could be explained by the specific structure and composition of the LBms and its interaction with the skin. In order to investigate the role of lipids in WHC of the stratum corneum, some authors removed the lipids from the stratum corneum and studied which lipid is primarily responsible for WHC (39). It is known that lipids themselves have little or no affinity for water molecules (40). However, after application of mixtures of stratum corneum lipids to a depleted stratum corneum, the skin recovered its WHC, suggesting that the lipids that form the lamellar structure of this tissue could be specific modulators of water-retaining properties (41–44). Among these lipids,

ceramides show the highest capacity to recover diminished WHC (45).

In a previous study, we evaluated the effect of the LBms *in vitro* in porcine delipidized stratum corneum. By using grazing-incidence small-angle scattering and freeze substitution transmission electron microscopy, we showed that this system re-established part of the stratum corneum lamellar structure of delipidized stratum corneum (21). We can assume that, in the present study, this system incorporates lipids into the stratum corneum lamellar structure in a similar way as in the *in vitro* assay. Therefore, the incorporation of these lipids into the lamellar structure of the stratum corneum seems to reinforce the skin barrier, increasing its WHC. Both the composition and structure of the LBms would work synergistically to improve the skin condition.

Effect of the treatment on irritated skin

Anionic surfactants such as SLS are used as model irritants in experimentally induced irritant contact dermatitis (46). SLS has been reported to induce epidermal cell proliferation or accelerated stratum corneum turnover, thickening of both the stratum corneum and viable epidermis, and dryness of the outer layers of the former (47).

In general, it has been reported that surfactants partially remove lipids from the stratum corneum, but this depends on the concentration and exposure time. Froebe et al. found that no ceramide and only 8–15% of free fatty acids and cholesterol were removed by a surfactant at a concentration of 2% (48). Studies by Fartasch point in the same direction, as they found that the surfactant at a low concentration of 0.5–1% did not seem to alter the existing lipid structure, but rather the synthesis of new lipids (49). Therefore, in our study, after exposure to 2% of surfactant, we expected a small amount of lipid to be removed but a perturbation of the skin barrier owing to the interaction of SLS with the lipids of the stratum corneum.

In the present study, we found increases in WHC and WSC and a decrease in AWD just after SLS exposure (Fig. 4a and b, day 0 SLS). This is possibly attributable to the action of this surfactant on the cutaneous tissue. SLS could interact with the stratum corneum lipids, increasing lipid fluidity and thereby enhancing skin permeability and allowing greater penetration of the water applied on the skin surface (50). Also, it has been reported that the hydrophobic alkyl chain of SLS interacts with the skin lipid structure, leaving the end sulfate group of the surfactant exposed, and creating additional sites in the membrane. This would result in forces that separate the protein matrix, uncoil the filaments, and expose more water-binding sites, hence increasing the hydration level of skin (51). It is also known that, in healthy skin, perturbation of the barrier function (in this case induced by the surfactant) initiates a sequence of events that rapidly results in the return of lipids to the stratum corneum and the restoration of its barrier function, owing to an increase in lamellar body secretion (52). Furthermore, surfactants also induce changes in the concentrations of several natural moisturizing factor components immediately following exposure. It has been reported that the concentrations of most of these components are decreased, although those of a small group, including ornithine, lactate, and urea, are increased (53). In addition, some authors have reported that creams containing urea increase WHC (20). Therefore, the increases in WHC and WSC and the decrease in AWD detected just after SLS exposure could result from a combination of these mechanisms, re-establishing the normal barrier function.

Regarding the irritated and LBms-treated skin, we found increases in WHC and WSC after 4 days of treatment. This could be attributable to the incorporation of lipids into the stratum corneum lamellar structure in a similar way as in healthy skin, as discussed above. The importance of the intercellular lipids in regulating the water content is well known. Lipid lamellar organization in the stratum corneum are essential for maintaining the WHC of the skin and for regulating the water permeability of the stratum corneum (44).

Probably the most striking finding in skin irritated and then treated with the LBms was the skin behaviour after 4 days of treatment. As described before, just after irritation with SLS, all of the biophysical and biochemical mechanisms of the skin attempt to restore normal conditions (Fig. 4a and b, day 0 SLS) (52). Thereby, skin parameters related to sorption and desorption of water are re-established 1 day after irritation with SLS, regardless of treatment with the LBms (Fig. 4a and b, day 1). However, if the irritated skin is treated with the LBms for 4 days, the parameters point to an extra improvement of the skin condition (Fig. 4b, day 4). Some of the natural repair mechanisms of the skin that had been activated by the effect of the SLS damage and were normalized 1 day after irritation could be supported by the effect of treatment with the LBms.

Conclusions

Treatment with the LBms seems to reinforce the barrier function in both healthy and SLS-irritated human skin. Therefore, the present study provides evidence that this system could be of interest for the development of future treatments for protecting and repairing the skin.

Acknowledgements

The authors wish to thank Evonik (Essen, Germany) for providing the ceramide. We also thank the volunteers who participated in this study. This work was supported by funds from Comisión Interministerial de Ciencia y Tecnología from Spain (CTQ 2013-44998-P).

References

1 Elias P M. Epidermal lipids, barrier function, and desquamation. *J Invest Dermatol* 1983: **80** (Suppl.): 44s–49s.
2 Pons L, Parra J L. La piel y sus anejos como sustrato vivo de la cosmetología. *Ciencia cosmética: bases fisiológicas y criterios prácticos*, (ed.): Madrid, Consejo general de colegios oficiales de farmacéuticos, 1995: pp. 54–60.
3 Elias P M, Menon G K. Structural and lipid biochemical correlates of the epidermal permeability barrier. *Adv Lipid Res* 1991: **24**: 1–26.
4 Landmann L. Epidermal permeability barrier: transformation of lamellar granule-disks into intercellular sheets by a membrane-fusion process, a freeze-fracture study. *J Invest Dermatol* 1986: **87**: 202–209.
5 den Hollander L, Han H, de Winter M et al. Skin lamellar bodies are not discrete vesicles but part of a tubuloreticular network. *Acta Dermatol Venereol* 2016: **96**: 303–308.
6 Norlén L. Skin barrier formation: the membrane folding model. *J Invest Dermatol* 2001: **117**: 823–829.
7 Ghadially R, Reed J T, Elias P M. Stratum corneum structure and function correlates with phenotype in psoriasis. *J Invest Dermatol* 1996: **107**: 558–564.
8 Elias P M, Wakefield J S. Mechanisms of abnormal lamellar body secretion and the dysfunctional skin barrier in patients with atopic dermatitis. *J Allergy Clin Immunol* 2014: **134**: 781–791.e1.
9 Milner M E, O'Guin W M, Holbrook K A, Dale B A. Abnormal lamellar granules in harlequin ichthyosis. *J Invest Dermatol* 1992: **99**: 824–829.
10 Fartasch M, Williams M L, Elias P M. Altered lamellar body secretion and stratum corneum membrane structure in Netherton syndrome: differentiation from other infantile erythrodermas and pathogenic implications. *Arch Dermatol* 1999: **135**: 823–832.
11 Chan A, Holleran W M, Ferguson T et al. Skin ultrastructural findings in type 2 Gaucher disease: diagnostic implications. *Mol Genet Metab* 2011: **104**: 631–636.
12 Imokawa G, Abe A, Jin K et al. Decreased level of ceramides in stratum corneum of atopic dermatitis: an etiologic factor in atopic dry skin? *J Invest Dermatol* 1991: **96**: 523–526.
13 Smeden J, Janssens M, Kaye E C et al. The importance of free fatty acid chain length for the skin barrier function in atopic eczema patients. *Exp Dermatol* 2014: **23**: 45–52.
14 Ong P Y, Ohtake T, Brandt C et al. Endogenous antimicrobial peptides and skin infections in atopic dermatitis. *N Engl J Med* 2002: **347**: 1151–1160.
15 Rippke F, Schreiner V, Doering T, Maibach H I. Stratum corneum pH in atopic dermatitis. *Am J Clin Dermatol* 2004: **5**: 217–223.
16 Tagami H, Kanamaru Y, Inoue K et al. Water sorption–desorption test of the skin in vivo for functional assessment of the stratum corneum. *J Invest Dermatol* 1982: **78**: 425–428.
17 Borroni G, Vignati G, Brazzelli V et al. Changes in the water holding capacity of psoriatic stratum corneum in vivo. *Acta Derm Venereol Suppl (Stockh)* 1989: **146**: 192–194.
18 Pellacani G, Seidenari S. Water sorption–desorption test and moisture accumulation test for functional assessment of atopic skin in children. *Acta Derm Venereol (Stockh)* 2001: **81**: 100–103.
19 Treffel P, Gabard B. Stratum corneum dynamic function measurements after moisturizer or irritant application. *Arch Dermatol Res* 1995: **287**: 474–479.
20 Sindhvananda J, Gritiyarangsan P, Rungrairatanaroij P. Flygroscopicity and water-holding capacity of moisturizing agents: a single-application in vivo study. *J Soc Cosmet Chem* 1993: **44**: 279–288.
21 Moner V, Fernández E, Rodríguez G et al. Lamellar body mimetic system: an up-to-down repairing strategy of the stratum corneum lipid structure. *Int J Pharm* 2016: **510**: 135–143.
22 Bouwstra J A, Gooris G S, van der Spek J A, Bras W. Structural investigations of human stratum corneum by small-angle X-ray scattering. *J Invest Dermatol* 1991: **97**: 1005–1012.
23 Huang H C, Chang T M. Ceramide 1 and ceramide 3 act synergistically on skin hydration and the transepidermal water loss of sodium lauryl sulfate-irritated skin. *Int J Dermatol* 2008: **47**: 812–819.
24 Barbosa-Barros L, Barba C, Cócera M et al. Effect of bicellar systems on skin properties. *Int J Pharm* 2008: **352**: 263–272.
25 Madison K C. Barrier function of the skin: "la raison d'etre" of the epidermis. *J Invest Dermatol* 2003: **121**: 231–241.
26 Wertz P W. Epidermal lipids and the intercellular pathway. In: *Percutaneous Penetration Enhancers Chemical Methods in Penetration Enhancement*, Dragicevic N, Maibach H I (eds): Berlín, Springer-Verlag, 2015: pp. 13–18.
27 Fernández E, Rodríguez G, Cócera M et al. Advanced lipid systems containing β-carotene: stability under UV–vis radiation and application on porcine skin in vitro. *Phys Chem Chem Phys* 2015: **17**: 18710–18721.
28 Fernández E, Hostachy S, Sandt C et al. Monitoring bicosomes containing antioxidants in normal and irradiated skin. *RSC Adv* 2016: **6**: 72559–72567.
29 Uchida Y, Ogawa T, Ohta M et al. Penetration of lysophosphatidylcholine into the dermis. *J Dermatol* 1991: **18**: 523–527.
30 Elias P M, Feingold K R, Fartasch M. The epidermal lamellar body as a multifunctional secretory organelle. In: *Skin Barrier*, Elias P M, Feingold K R (eds): New York: Taylor & Francis Group, 2006: pp. 261–272.
31 Bouwstra J A, Gooris G S, Bras W, Downing D T. Lipid organization in pig stratum corneum. *J Lipid Res* 1995: **36**: 685–695.
32 Rodríguez G, Rubio L, Cócera M et al. Application of bicellar systems on skin: diffusion and molecular organization effects. *Langmuir* 2010: **26**: 10578–10584.
33 Fluhr J W, Kao J, Jain M et al. Generation of free fatty acids from phospholipids regulates stratum corneum acidification and integrity. *J Invest Dermatol* 2001: **117**: 44–51.
34 Barbosa-Barros L, Rodríguez G, Barba C et al. Bicelles: lipid nanostructured platforms with potential dermal applications. *Small* 2012: **8**: 807–818.
35 El Maghraby G M. Stratum corneum lipid liposomes: drug delivery systems and skin models. In: *Percutaneous Penetration Enhancers Chemical Methods in Penetration Enhancement*, Dragicevic N, Maibach H I

(eds): Berlin Heildelberg: Springer-Verlag, 2015: pp. 111–119.
36 Tagami H. Electrical measurement of the hydration state of the skin surface in vivo. *Br J Dermatol* 2014: **171**: 29–33.
37 van Neste D. In vivo evaluation of unbound water accumulation in stratum corneum. *Dermatology* 1990: **181**: 197–201.
38 Berardesca E, Maibach H I. Monitoring the water-holding capacity in visually non-irritated skin by plastic occlusion stress test (POST). *Clin Exp Dermatol* 1990: **15**: 107–110.
39 Imokawa G, Akasaki S, Hattori M, Yoshizuka N. Selective recovery of deranged water-holding properties by stratum corneum lipids. *J Invest Dermatol* 1986: **87**: 758–761.
40 Imokawa G. Ceramides as natural moisturizing factors and their efficacy in dry skin. In: *Skin Moisturization*, Leyden J J, Rawlings A V (eds): New York: CRC Press, 2002: pp. 267–302.
41 Coderch L, De Pera M, Fonollosa J et al. Efficacy of stratum corneum lipid supplementation on human skin. *Contact Dermatitis* 2002: **47**: 139–146.
42 Imokawa G, Akasaki S, Minematsu Y, Kawai M. Importance of intercellular lipids in water-retention properties of the stratum corneum: induction and recovery study of surfactant dry skin. *Arch Dermatol Res* 1989: **281**: 45–51.
43 Imokawa G, Kuno H, Kawai M. Stratum corneum lipids serve as a bound-water modulator. *J Invest Dermatol* 1990: **96**: 845–851.
44 Barba C, Martí M, Semenzato A et al. Effect of lipid modification on stratum corneum permeability. *J Therm Anal Calorim* 2015: **120**: 297–305.
45 Imokawa G, Akasaki S, Kawamata A et al. Water-retaining function in the stratum corneum and its recovery properties by synthetic pseudoceramides. *J Soc Cosmet Chem* 1989: **40**: 273–285.
46 Effendy I, Maibach H I. Surfactants and experimental irritant contact dermatitis. *Contact Dermatitis* 1995: **33**: 217–225.
47 Baker H, Kligman A M. Technique for estimating turnover time of human stratum corneum. *Arch Dermatol* 1967: **95**: 408–411.
48 Froebe C L, Simion F A, Rhein L D et al. Stratum corneum lipid removal by surfactants: relation to in vivo irritation. *Dermatology* 1990: **181**: 277–283.
49 Fartasch M. Ultrastructure of the epidermal barrier after irritation. *Microsc Res Tech* 1997: **37**: 193–199.
50 Downing D T, Abraham W, Wegner B K et al. Partition of sodium dodecyl sulfate into stratum corneum lipid liposomes. *Arch Dermatol Res* 1993: **285**: 151–157.
51 Rhein L, Robbins C, Fernee K. Surfactant structure effects on swelling of isolated human. *J Soc Cosmet Chem* 1986: **37**: 125–139.
52 Menon G K, Feingold K R, Elias P M. Lamellar body secretory response to barrier disruption. *J Invest Dermatol* 1992: **98**: 279–289.
53 Hoffman D R, Kroll L M, Basehoar A et al. Immediate and extended effects of sodium lauryl sulphate exposure on stratum corneum natural moisturizing factor. *Int J Cosmet Sci* 2014: **36**: 93–101.

ARTÍCULO 3

A lamellar body mimetic system for the treatment of oxazolone-induced atopic dermatitis in hairless mice. V. Moner, E. Fernández, A. Calpena, A. Garcia-Herrera, M. Cócera y O. López. *Journal of Dermatological Science*, 2018, 90(2), 172-179.

En éste trabajo se evaluó el efecto que tiene el LBms *in vivo*, en este caso en un modelo de ratón con dermatitis inducida. La aplicación tópica durante varios días de oxazolona en el dorso de ratones después de ser sensibilizados con la misma sustancia provocó una dermatitis comparable a la humana. Una vez los ratones desarrollaron dermatitis por la continua aplicación de oxazolona, se dividieron en dos grupos, un grupo se trató con el sistema lipídico y el otro grupo se trató con agua. Durante los días de tratamiento se efectuaron medidas de TEWL e hidratación y se extrajo sangre de los animales. Después de 10 días de tratamiento los ratones fueron sacrificados y se extrajeron muestras de piel.

La función barrera de la piel se evaluó *in vivo* mediante los valores de TEWL e hidratación. La inflamación se determinó mediante cuantificación de IgE en suero sanguíneo y por análisis histológico de las muestras de piel extraídas. También se estudió la microestructura de la piel mediante FSTEM. Tal como se esperaba, los ratones con dermatitis presentaron alteración de la función barrera cutánea, desorganización y reducción de la estructura lipídica laminar del SC e inflamación. El tratamiento con el LBms mejoró la dermatitis reforzando la función barrera cutánea (disminución de TEWL). En cuanto a la hidratación no se encontró una mejora respecto al grupo sin tratar. El tratamiento con el LBms también redujo considerablemente la inflamación (reducción de IgE en suero, menor grosor epidérmico y reducción de infiltrado de linfocitos), aunque aún se observó paraqueratosis y espongiosis indicando cierto grado de inflamación. Esto podría deberse a que durante el período de tratamiento también se aplicó oxazolona.

El LBms podría tanto incorporar lípidos al SC (tal como se ha descrito en el trabajo 1 y como demuestra el análisis de la microestructura del SC en el presente trabajo) como estimular la producción y secreción de lípidos del SC endógenos ya que el tratamiento en éste caso fue *in vivo*. Por lo tanto, el presente trabajo demuestra que el LBms, que combina composición y estructura apropiadas, puede ser de interés para el desarrollo de nuevos tratamientos para dermatitis atópica. Además, el sistema se podría adaptar

variando su composición para tratar otras enfermedades cutáneas que tengan la función barrera comprometida y a las que se hayan asociado ciertas deficiencias lipídicas.

Journal of Dermatological Science 90 (2018) 172–179

Contents lists available at ScienceDirect

Journal of Dermatological Science

journal homepage: www.jdsjournal.com

A lamellar body mimetic system for the treatment of oxazolone-induced atopic dermatitis in hairless mice

Verónica Moner[a,*], Estibalitz Fernández[b], Ana Cristina Calpena[c], Adriana Garcia-Herrera[d], Mercedes Cócera[b], Olga López[a]

[a] Department of chemical and surfactant technology. Institute of Advanced Chemistry of Catalonia (IQAC-CSIC). C/Jordi Girona 18-26, 08034. Barcelona, Spain
[b] Bicosome S.L. C/Jordi Girona 18-26, 08034. Barcelona, Spain
[c] Department of pharmacy and pharmaceutical technology. Faculty of Pharmacy, University of Barcelona. C/Joan XXII 27-31, 08028. Barcelona, Spain
[d] Hematopathology Section, Hospital Clínic, Villarroel 170, 08036-Barcelona, Spain

ARTICLE INFO

Article history:
Received 26 October 2017
Received in revised form 21 December 2017
Accepted 16 January 2018

Keywords:
Atopic dermatitis
Lamellar body
Oxazolone
Dermatitis mouse model
Skin lipids

ABSTRACT

Background: Atopic dermatitis is a common skin disease characterized by a Th2 cell-dominant inflammatory infiltrate, elevated serum IgE levels and impaired epidermal barrier function. It is associated to abnormal epidermal lamellar body secretion, producing alteration in lipid composition and extracellular lamellar membrane organization.
Objectives: The oxazolone-induced atopic dermatitis in hairless mice was used to evaluate *in vivo* the effect of the application of a lipid system that mimics the morphology, structure and composition of epidermal lamellar bodies.
Methods: The skin barrier function was evaluated measuring TEWL and skin hydration *in vivo*. Inflammation was assessed by analysis of serum IgE levels and histological analysis. The microstructure of the intercellular lipid region was also evaluated before and after treatment.
Results: The skin condition was improved after 10 days of treatment indicated by decreased TEWL, decreased serum IgE levels, reduced epidermal thickness and reduced lymphocyte-dominated infiltrate. However, the treatment did no improve skin hydration.
Conclusions: The treatment with this lipid system seems to improve the skin condition by reinforcing the barrier function and reducing the skin inflammation. Therefore, the present study provides evidence that this lipid system combining appropriate lipid composition and morphology could be of interest for the development of future treatments for atopic dermatitis.

1. Introduction

Atopic dermatitis is a common skin disease characterized by inflammatory, pruritic eczema. It is a multifactorial disease which involves a complex interplay of environmental and genetic factors. Atopic dermatitis shows a Th2 cell-dominant inflammatory infiltrate, elevated serum IgE levels and impaired epidermal barrier function [1], indicated by an increased transepidermal water loss (TEWL) [2] and decreased water-holding capacity [3].

The cutaneous permeability barrier is mediated by extracellular lipids mainly ceramides, free fatty acids and cholesterol, which form extracellular lipid-enriched lamellar membranes between the corneocytes that block the movement of water and electrolytes [4]. These lipids are delivered to the extracellular spaces of the stratum corneum by the secretion of lamellar bodies. Atopic dermatitis is associated to abnormal lamellar body secretion, producing alteration in lipid composition, especially ceramides and free fatty acids [5,6], and in extracellular lamellar membrane organization, as well as dysfunction in antimicrobial defense. Moreover, in atopic dermatitis alkaline pH of the skin surface is another cause of increased skin susceptibility to bacteria, mainly *Staphylococcus aureus* [7].

One animal model that closely reflects these features is the oxazolone-induced atopic dermatitis in hairless mice [8]. When oxazolone is applied to the skin of hairless mice for a period of 3 weeks, mice develop symptoms characteristic for atopic dermatitis including barrier dysfunction, secretion of IgE, epithelial cell hyperplasia, fibrosis and infiltration of inflammatory cells into the dermis and epidermis and secretion of Th2 cytokines.

Bicosomes are lipid aggregates (200–400 nm) formed by disks encapsulated in lipid vesicles [9]. The interaction of these systems with the skin can modify the permeability of the barrier, reinforce

* Corresponding author.
E-mail address: vmmtqt@iqac.csic.es (V. Moner).

https://doi.org/10.1016/j.jdermsci.2018.01.010
0923-1811/

the lipid structure and promote targeted delivery of molecules to specific skin layers, among others effects [10–12]. In a previous study, we designed a lipid system based on bicosomes that mimic the morphology, structure and composition of epidermal lamellar bodies [13]. In addition, we performed *in vitro* studies to evaluate the effect of this system on delipidized stratum corneum. We concluded that the treatment with the lamellar body mimetic system (LBms) re-establishes *in vitro* part of the lipid lamellar structure of delipidized stratum corneum, mainly the short periodicity phase described by Bouwstra et al. [14]. In other study, we evaluate *in vivo* the hydration-dehydration kinetics of human skin after treatment with the LBms [15]. We found that skin increased its ability to retain water. Thus, this lipid system seems to reinforce the barrier function.

Our previous results point to a high potential of the LBms to improve skin conditions. Thus, in the present study, we sought to evaluate the effect of the application of the LBms on oxazolone-induced atopic dermatitis mouse model. Accordingly, we evaluate skin hydration and TEWL to study the skin barrier function. Inflammation was assessed by analysis of IgE levels in serum. In addition, skin biopsies were taken the last day of the experiment for histological analysis by optical microscopy and for evaluating the microstructure of the intercellular lipid regions by freeze substitution transmission electron microscopy (FSTEM).

2. Material and methods

2.1. Chemicals

1,2-Dipalmitoyl-sn-*glycero*-3-phosphocholine (DPPC) and 1,2-dihexanoyl-sn-*glycero*-3-phosphocholine (DHPC) were from Avanti Polar Lipids (Alabaster, United States). Cholesterol from lanolin (chol), cholesteryl sulphate sodium salt (Schol), cholesteryl palmitate (Echol), stearic acid (SA), oxazolone, hematoxylin solution Gill 2, eosin Y alcoholic solution, lithium carbonate, xylene and DPX mountant for histology were from Sigma-Aldrich (Steinheim, Germany). Ceramide IIIb (cer3) and ceramide VI (cer6) were from Evonik (Essen, Germany). Lipoid S100, whose main component (>94%) is soybean phosphatidylcholine (PC) and Lipoid S LPC 80 whose main component (80%) is soybean lysophosphatidylcholine (lysoPC) were from Lipoid GmbH (Ludwigshafen, Germany). Chloroform, formaldehyde solution 4% and acetic acid were from Merck (Darmstadt, Germany). Acetone and ethanol absolute were from Panreac (Barcelona, Spain). Optimal cutting temperature compound (OCT) was from Sakura Finetek (Torrance, United States).

2.2. Preparation and characterization of the system

2.2.1. Discoidal structures preparation

Four types of discoidal structures were prepared: (a) DPPC/DHPC, q = 3.5 (q = DPPC/DHPC molar ratio) including 5 mol% cer3 and 5 mol% cer6; (b) DPPC/DHPC, q = 3.5 including 5 mol% chol; (c) DPPC/DHPC, q = 3.5 including 5 mol% Schol and (d) DPPC/DHPC q = 3.5 including 5 mol% Echol.

For each of the discoidal systems, appropriate amounts of lipids were mixed in chloroform and evaporated to dryness using a rotary evaporator. The systems were hydrated with distilled water to obtain a 10% (w/v) total lipid concentration and then subjected to several cycles of sonication, freezing and heating until the samples became transparent.

Next, different volumes of these samples were selected to obtain a mixture in which the molar ratio of cer, chol, Schol and Echol was similar to that found in the skin. To obtain 1 ml, 440 μl of (a), 440 μl of (b), 88 μl of (c) and 32 μl of (d) were mixed. This mixture was used to prepare the LBms.

2.2.2. LBms preparation

A chloroform solution containing 95 mg/ml PC, 5 mg/ml lysoPC and 1.6 mg/ml SA was rota-evaporated to remove the chloroform and thus form a lipid film. The film was hydrated with the previously prepared mixture of discoidal structures.

The total lipid concentration in the final system was 20% (w/v) with a cer:SA:chol:Schol:Echol molar ratio of 1:1:0.5:0.1:0.04.

The LBms was analysed 24 h after preparation by dynamic light scattering (DLS) and cryogenic transmission electron microscopy (Cryo-TEM).

2.2.3. DLS

The hydrodynamic diameter (HD) was determined by DLS with a Zetasizer nano ZS (Malvern Instruments, UK). The DLS technique measures the diffusion coefficient (D) of the particles corresponding to Brownian motion, and converts this to size by using the Stokes-Einstein equation,

$$HD = kT/3\pi hD$$

where HD is the hydrodynamic diameter, D is the translational diffusion coefficient (m^2/s), k is the Boltzmann constant ($1.3806503 \times 10^{-23}\ m^2\ kg\ s^{-2}\ K^{-1}$), T is the absolute temperature (298 K), and η is the viscosity of the dispersant at 25 °C (water, 0.8872 mPa s). The particles sizes were determined from the scattered light that was detected at an angle of 173° when a laser beam of 633 nm wavelength crossed the sample. Measurements were performed in triplicate.

2.2.4. Cryo-TEM

The morphology of the LBms was evaluated by Cryo-TEM. A thin aqueous film was formed by dipping a glow-discharged holey carbon grid in the suspension and then blotting the grid against a filter paper. The resulting thin sample film spanning the grid holes was vitrified by plunging the grid into ethane, which was maintained at its melting point with liquid nitrogen, by use of a Vitrobot (FEI Company, Eindhoven, The Netherlands). The vitreous sample film was transferred to a Tecnai F20 TEM (FEI Company, Eindhoven, The Netherlands) by use of a cryotransfer holder (Gatan, Barcelona, Spain), and the sample was observed in low-dose mode. Images were acquired at 200 kV at a temperature between −170 °C and −175 °C, under low-dose imaging conditions. Ten overviews and approximately 50 detailed electron micrographs were taken.

2.3. Animals and study protocol

The study protocol was approved by the Animal Experimentation Ethics Committee of the University of Barcelona according to the regulations of the local government (Decree 214/1997, July 30th). Female hairless mice SKH-1 (n = 8; Charles River, Germany) of 8–9 weeks old were housed in two cages (n = 4) in a room with controlled temperature and humidity. Food and water were provided *ad libitum*. Atopic dermatitis was induced by topical application of oxazolone in acetone. The design of the study is summarized in Fig. 1. The animals were sensitized on dorsal skin with 10 μl of 5% oxazolone in acetone (D0). A week later, the dorsal skin of the mice was treated with 60 μl of 0.1% oxazolone in acetone for 20 days (from D7 to D26). In addition, one group was treated with 30 μl of LBms (treated-dermatitis group) whereas the other was treated with 30 μl of water (dermatitis group) for 10 days (from D17 to D26). Treatment with LBms or water was applied one hour after oxazolone application. Twenty four hours after the last treatment, animals were euthanized and biopsies from the dorsal skin of the mice were taken (D27).

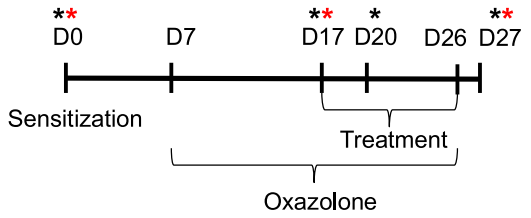

Fig. 1. Study design. The mice were sensitized with 5% oxazolone in acetone on day 0 (D0). A week later, the dorsal skin of the mice was treated with 0.1% oxazolone in acetone for 20 days (from D7 to D26). Treatment with LBms or water was applied during 10 days (from D17 to D26). Black asterisk indicates TEWL and hydration measurements, and red asterisk indicates blood sample collection.

TEWL was measured with a tewameter TM 210 (Courage & Khazaka, Germany) to assess the skin barrier disruption. Skin hydration was determined with a corneometer CM 820 (Courage & Khazaka, Germany) which measures skin capacitance in arbitrary units (a.u). Both TEWL and skin hydration were measured on day 0, 17, 20 and 27 prior to the application of oxazolone and the treatment.

Blood samples were collected from mice tails on day 0, 17 and 27. These samples were centrifuged (3000 rpm, 15 min, 4 °C) and serum was stored at −80 °C. Serum IgE concentration was determined with a mouse IgE ELISA quantification kit from Thermo Scientific (Waltham, United States) following instructions provided by the manufacturer.

2.4. FSTEM

The skin biopsies were cut into small ribbons with a size of approximately 2 × 1 mm. The ribbons were fixed in 5% (w/v) glutaraldehyde in a 0.1 M sodium cacodylate buffer at pH 7.2. Next, the ribbons were post-fixed in 0.2% (w/v) RuO_4 in sodium cacodylate buffer at pH 6.8 with 0.25% (w/v) potassium ferrocyanide ($K_4Fe(CN)_6$). After 1 h, the RuO_4 solution was replaced with fresh RuO_4 to establish optimal fixation. After a rinse in buffer, the tissue samples were cryofixed by rapid freezing on a liquid nitrogen-cooled metal mirror (Cryovacublock, Leica) at −196 °C prior to freeze-substitution, which was performed using an AFS (Automatic Freeze Substitution) system (Leica). The tissue samples were cryosubstituted at −90 °C for 48 h using 100% methanol containing 1.0% (w/v) osmium tetroxide (OsO_4), 0.5% (w/v) uranyl acetate and 3.0% (w/v) glutaraldehyde. After the 48 h substitution period, the temperature was increased to −50 °C, and the samples were washed three times in 100% methanol. Subsequently, the methanol solution was gradually replaced with the embedding medium, Lowicryl HM20 (100%). This resin was replaced after 24 and 48 h with freshly prepared embedding medium. Finally, the samples were transferred to a mould containing Lowicryl and were incubated for 48 h at −50 °C under UVA radiation to facilitate polymerization. Ultra-thin sections were cut (Ultracut UCT, Leica), transferred to Formvar-coated grids, and examined using a Hitachi 600 transmission electron microscope.

On average, 10 overviews and approximately 30–40 detailed electron micrographs for each freeze-substitution process were taken.

2.5. Histological analysis

First, skin samples were covered with aluminium foil and then with OCT. The aluminium foil was used to avoid the direct contact between the skin and the OCT. Then, skin samples were frozen in liquid N_2 and cut into transverse 6 μm thick sections. The cuts were performed using a Cryostat CM3050 S (Leyca Biosystems, Nussloch, Germany). Tissue sections were then stained with hematoxylin-eosin (H&E). Epidermal thickness was measured in ten randomly selected areas from the basement membrane to the base of the stratum corneum.

2.6. Statistical analysis

Means and standard deviations (SD) were calculated. Statistical analysis of the experimental data was performed by Wilcoxon rank-sum test using STATA/SE 12.0 software. Differences were considered to be statistically significant at $p \leq 0.05$.

3. Results

3.1. Characterization of the system

DLS was used to determine the average size of the LBms. The size distribution curve of the system which was obtained by analysis of the scattered light intensity, showed two peaks corresponding to a population of small particles with a diameter of 53 ± 12 nm that scattered 28 ± 5% of the light and a population of large particles of 267 ± 21 nm that scattered 72 ± 5% of the light.

Cryo-TEM allows us to directly visualize the sample and to characterize the morphology of the different structures present in the system. Two representative Cryo-TEM images of the LBms are shown in Fig. 2. These images show two types of structures, which is in agreement with the data reported by DLS, corresponding to discoidal structures (white arrows) with diameter of approximately 40 nm and vesicles encapsulating disks (black arrow) with size approximately 300 nm. Moreover, disks are shown in all dispositions, edge-on (white open arrows) and face-on (white close arrow).

3.2. TEWL and hydration

TEWL of animals on D0 was 12.1 ± 0.7 g/m^2 h (n = 8). The oxazolone treatment resulted in a marked increase in TEWL value being of 30.8 ± 4.8 g/m^2 h (n = 8) on D17 as shown in Fig. 3A. The

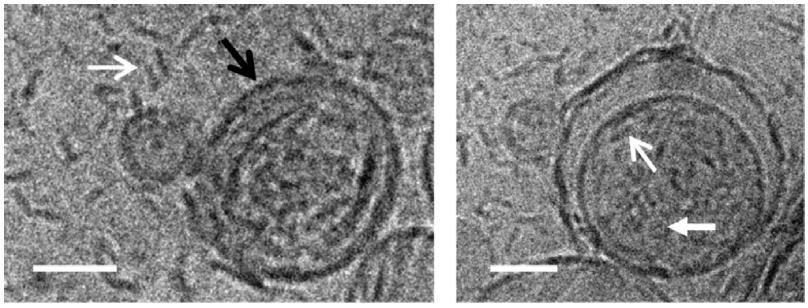

Fig. 2. Cryo-TEM micrographs of the LBms. The system is formed by encapsulated and non-encapsulated disks with diameters of ~40 nm, and vesicles encapsulating disks (black arrow) with size of ~300 nm. The disks are shown in all projections: edge-on (white open arrows) and face-on (white close arrow). Bar = 100 nm.

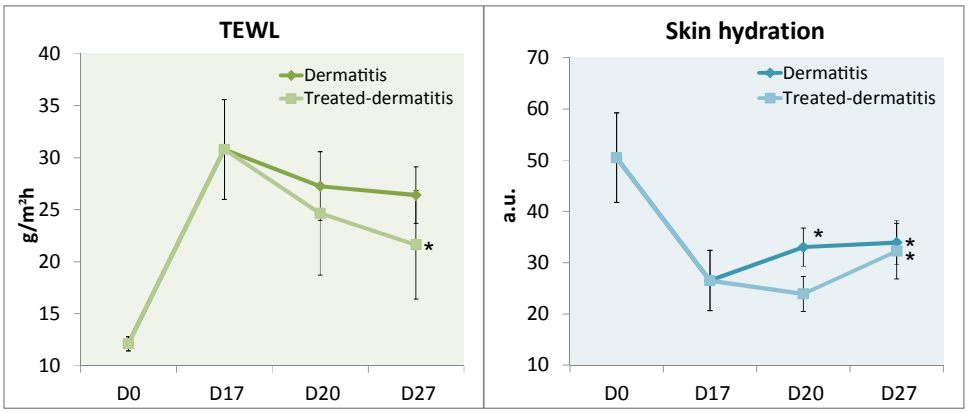

% of decrease with respect to D17		
	D20	D27
Dermatitis	12	14
Treated-dermatitis	20	30

% of increase with respect to D17		
	D20	D27
Dermatitis	25	28
Treated-dermatitis	-10	22

Fig. 3. Values of TEWL and skin hydration in both dermatitis and treated-dermatitis group along the experiment. The tables show the percentage of difference with respect to the day before starting treatment with the LBms or water (D17). *Statistically significant differences ($p \leq 0.05$) compared with D17.

dermatitis group (n = 4) presented a TEWL of 27.3 ± 3.3 g/m^2·h (D20) and 26.4 ± 2.7 g/m^2 h (D27) whereas the treated-dermatitis group (n = 4) presented a TEWL of 24.7 ± 6.0 g/m^2 h (D20) and 21.6 ± 5.2 g/m^2 h (D27). After 10 days of treatment (D27), TEWL was reduced significantly, approximately 30% compared to D17. This difference is not found in the untreated group. The reduction in TEWL value is associated with an improvement of skin barrier function.

Regarding hydration values (Fig. 3B), the mice presented a capacitance of 50.5 ± 8.7 a.u (n = 8) on D0. After 10 oxazolone challenges (D17), the capacitance was reduced being 26.5 ± 5.9 a.u (n = 8). On D20, the dermatitis group (n = 4) presented a capacitance of 33.0 ± 3.7 a.u whereas in the treated-dermatitis group (n = 4) was 23.9 ± 3.4 a.u. This small difference between treated and untreated group could be related with the initial interaction of the LBms with the skin involving a re-arrangement of the skin lipids by effect of the LBms lipids. However, the last day of the experiment (D27) the capacitance of both groups was similar being of 33.9 ± 4.3 a.u (dermatitis group) and 32.3 ± 5.4 a.u (treated-dermatitis group) and increased significantly 22–28% compared to D17. Given that skin capacitance is directly related to skin hydration, these results indicate that the treatment did not affect the hydration with respect the normal behaviour of the skin.

Therefore, 10 oxazolone challenges induce atopic dermatitis generating impairment of the epidermal barrier function indicated by markedly increased TEWL and declined hydration. The treatment with the LBms (10 days) reduced TEWL but did not affect the hydration.

3.3. Serum IgE measurements

Basal serum IgE level (n = 8) was 0.22 ± 0.06 μg/ml. After 10 oxazolone challenges (D17) the serum IgE increased markedly being of 140 ± 77 μg/ml (n = 8). The last day of the experiment (D27), serum IgE decrease 19% in the treated-dermatitis group being of 114 ± 71 μg/ml (n = 4) whereas was similar, 140 ± 32 μg/ml (n = 4), in the dermatitis group compared to the IgE value on D17.

3.4. FSTEM

The microstructure of the skin was observed by FSTEM. Representative micrographs of healthy skin, dermatitis skin and treated-dermatitis skin are shown in Fig. 4. The micrographs of healthy skin (Fig. 4a–c) show normal intercorneocyte lipid lamellar structure (white close arrows). The lamellar bodies are well-organized in compact sheets and secrete their contents at the stratum granulosum-stratum corneum interface (Fig. 4c, black arrow). The intercorneocyte spaces appeared wide and almost empty in the dermatitis skin (Fig. 4d,e) and showed disorganized lipid structures (white open arrow). Also, dermatitis skin showed entombed lamellar body contents within the corneocytes cytosol (white asterisks) indicating incomplete lamellar body secretion [16]. Therefore, these contents would be unavailable to form lamellar membranes. The treated-dermatitis skin (Fig. 4f,g) shows a stratum corneum more compact than the dermatitis skin indicating that the extracellular lamellar lipids almost entirely filled the intercorneocyte spaces. However, entombed lamellar body contents within the corneocytes cytosol were also shown after treating the dermatitis skin with the LBms. In addition, abundant vesicular structures similar to lamellar bodies were visualized within the corneocytes (black asterisks). Given that these structures were not observed in the dermatitis group we assume that this effect was consequence of the treatment with the lipid system.

3.5. Histological analysis

Histologic analysis of skin sections (healthy, dermatitis and treated-dermatitis) are shown in Fig. 5 in two different magnitudes (20× and 60×). Skin sections stained with H&E show marked thickening of the epidermis in dermatitis skin ($66.4\ \mu m \pm 6.6\ \mu m$) compared to healthy skin ($17.1\ \mu m \pm 3.1\ \mu m$). However, the epidermal thickness was reduced significantly ($34.7\ \mu m \pm 3.4\ \mu m$) after treating the dermatitis skin with the LBms. These results are represented in the graph of Fig. 6. In addition, dermatitis skin exhibits lymphocyte-dominated infiltrate (indicated by an asterisk in Fig. 5b). However, a reduced lymphocyte infiltration was observed after treating the dermatitis skin with the LBms. Despite this, both dermatitis and treated-dermatitis skin show parakeratosis (retention of keratinocyte nuclei in the stratum corneum, red arrows) and spongiosis (intercellular edema, white arrows).

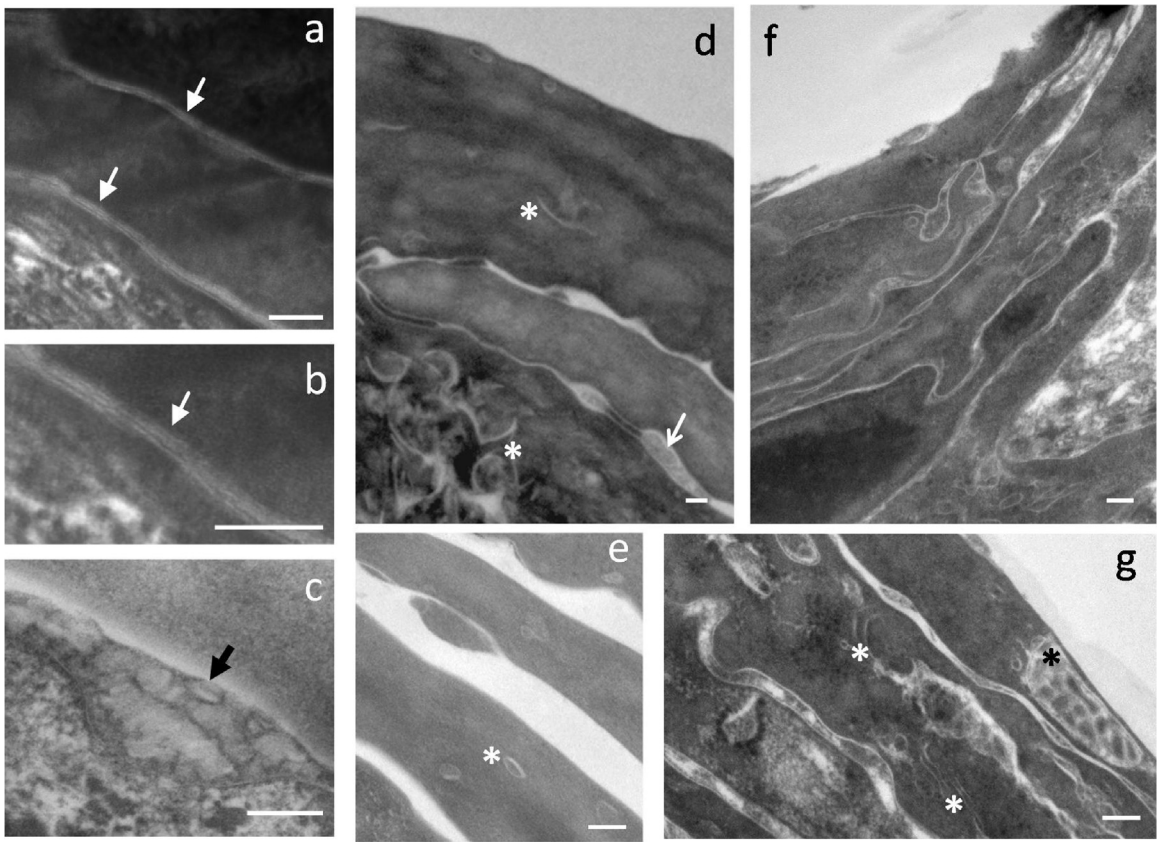

Fig. 4. Microstructure of the skin observed by FSTEM. The micrographs of healthy skin (a–c) show normal intercorneocyte lipid lamellar structure (a,b, close white arrows) and normal lamellar bodies secreting their content at the SG-SC interface (c, black arrow). Dermatitis skin (d,e) shows wide and almost empty intercorneocyte spaces, disorganized lipid structures (d, open white arrow) and entombed lamellar body contents within the corneocytes cytosol (white asterisks). The treated-dermatitis skin (f,g) shows extracellular lamellar lipids almost entirely filling the intercorneocytes spaces and, abundant vesicular structures similar to lamellar bodies (black asterisk). Entombed lamellar body contents are also observed (white asterisks). (Bar = 100 nm).

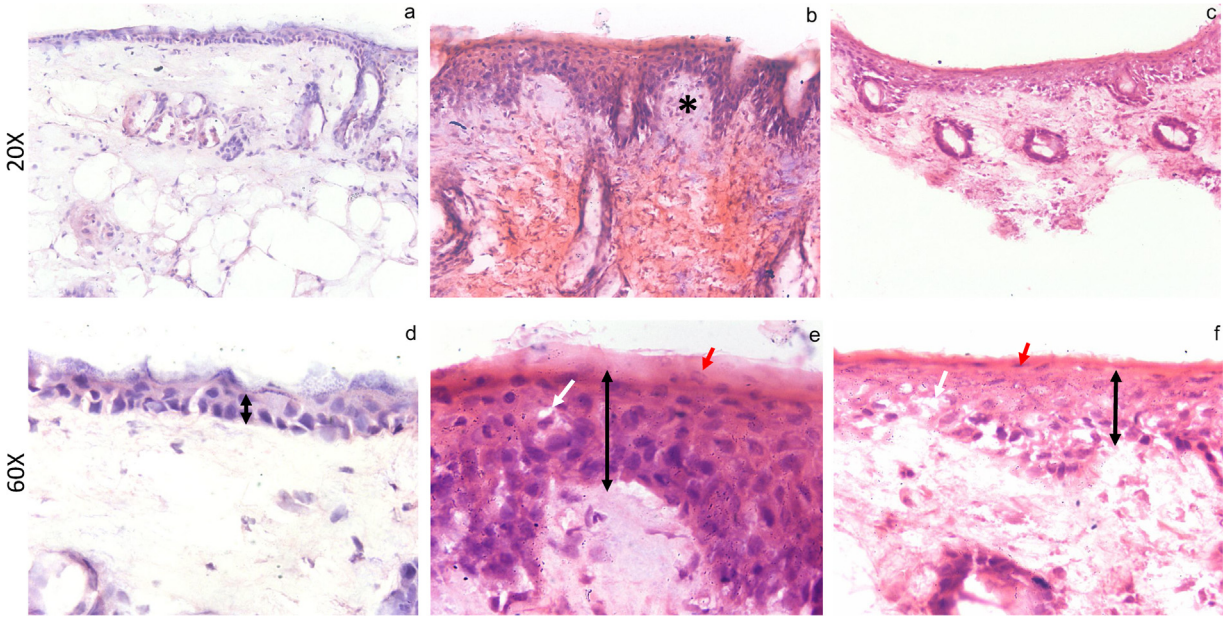

Fig. 5. Histologic analysis of the skin sections stained with hematoxylin-eosin (20× and 60×): healthy skin (a,d), dermatitis skin (b,e) and treated-dermatitis skin (c,f). Measurement of epidermal thickness is indicated by black arrows (d,e,f). The lymphocyte-dominated infiltrate is indicated by an asterisk (b). Parakeratosis and edema are indicated by red and white arrows, respectively. (For interpretation of the references to colour in this figure legend, the reader is referred to the web version of this article.)

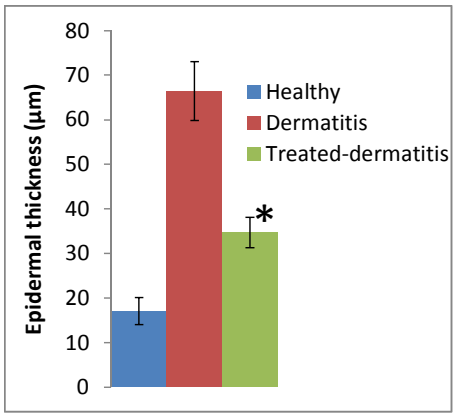

Fig. 6. Epidermal thickness of healthy, dermatitis and treated-dermatitis skin. Mean of ten randomly measurements. *Statistically significant differences ($p \leq 0.05$) compared with dermatitis group.

4. Discussion

4.1. The LBms

The formation of the skin barrier depends on deposition of lipids into the extracellular space between the viable and cornified epidermis [17]. Prior deposition, the lipids are located to, and delivered by, membrane-delimited organelles called epidermal lamellar bodies [18]. The morphology and structure of the LBms observed in our Cryo-TEM images (Fig. 2) are quite similar to those of the epidermal lamellar bodies observed by other authors in electron micrographs [19–21]. The LBms, similarly to epidermal lamellar bodies, is organized in a lipid bilayer that contains discoidal lamellar structures and also is similar in structure to bicosomes previously described in other studies [9,11]. Bicosomes formed exclusively by phospholipids have shown to constitute a good vehicle for incorporating different molecules into the skin, owing to the specific interaction of these structures with the stratum corneum [10,12].

The LBms contains lipids that approximate the stratum corneum lipid composition unlike epidermal lamellar bodies, which contain the precursors of stratum corneum intercellular lipids [22]. In addition, the LBms includes phospholipids, among them LysoPC, which has bactericidal activity [23]. This fact makes LBms appropriate for skin treatment, it is known that patients with atopic dermatitis frequently suffer from bacterial infections [24].

The LBms was designed as described in our previous study [13]. The disks would contain the lipids that form the stratum corneum lamellar structure, and the external vesicle would include the compounds that should remain on the skin surface. Following the mechanism of bicosome-skin interaction previously described [12,25], when external vesicles contact the skin, the bilayer of the vesicle bursts, and the encapsulated disks are released from the inside. These disks exhibit size small enough to penetrate into the stratum corneum and once incorporated, the discoidal structures increase in size as a result of the hydration gradient of the skin, and lipids from the LBms mix with the stratum corneum lipids reinforcing the skin barrier [15].

4.2. Characterization of induced atopic dermatitis condition

Atopic dermatitis is a skin disease associated with disturbances of skin barrier function as evidenced by an increase in TEWL, a decrease in water-binding properties, a reduction in skin lipids, specifically levels of ceramides, and impaired lamellar body secretion [1,18]. Furthermore, it is associated with abnormal immune response including increased serum IgE levels.

Various mouse models have been used in the literature to study the mechanism of atopic dermatitis and the usefulness of specific treatments. For instance, the dry skin mouse model is produced by repetitive exposure of the skin to acetone, diethyl ether and water. Consequently, the mice show marked increase in TEWL, reduced hydration, increased induction of scratching behaviour, epidermal hyperplasia and parakerotosis, but dry skin model does not show infiltration of inflammatory cells [26]. On the other hand, the oxazolone-induced atopic dermatitis mouse model used in this work is produced by treating the skin with an allergen (oxazolone). Oxazolone is an hapten, a small reactive molecule that covalently modifies proteins in the skin, thereby triggering allergic responses [27]. Multiple oxazolone challenges to normal murine skin produce a chronic Th2-like hypersensitivity reaction with multiple features of human atopic dermatitis [8], including barrier dysfunction and lipid abnormalities in addition to variations in biophysical parameters as TEWL and hydration. Therefore, we decided to evaluate the effect of the LBms in the oxazolone model because this model reproduces very well human atopic dermatitis features in clinical, histological and also immunological aspect.

This mouse model is common to assess a therapy for atopic dermatitis [28–30]. Some authors applied the oxazolone on the dorsal skin of the mice [29] and others on the ears [28,30]. In the present study, 10 oxazolone-challenges were applied on the dorsal skin of hairless mice which lead to profound changes in skin barrier function similar as other studies [8,31,32]. The oxazolone-challenges were applied also every day during the 10 days of treatment with the LBms in order to maintain the induced dermatitis during all the treatment period.

The skin barrier function was assessed by measuring TEWL which gives information about water loss across the stratum corneum. It is described that atopic dermatitis patients display a 2–5-fold increase in basal TEWL, in both lesional and non-lesional skin [33]. In the present study, basal TEWL was about 12 g/m^2 h, and after atopic dermatitis induction TEWL increased to 30 g/m^2 h. This fact may be explained by disruption of the stratum corneum lamellar structure due to deficiency in certain lipids. Man et al. [8] found in mice that after 10 oxazolone-challenges, total free fatty acid content declined, cholesterol increased and ceramide 3 declined although the total amount of ceramides did not changed. Lipid analysis of human skin affected by atopic dermatitis has also shown similar results [34]. This fact allows to associate dermatitis condition with stratum corneum lipids disorders.

Another parameter useful to determine skin barrier function is skin capacitance, which reflects water content of stratum corneum. The corneometer measures the change in the dielectric constant due to skin surface hydration changing the capacitance of a precision capacitator. Basal hydration of the stratum corneum was about 50 a.u, and after atopic dermatitis induction the hydration was significantly reduced to 27 a.u. The reduced water content in the stratum corneum after 10 oxazolone-challenges may be explained by perturbations in stratum corneum proteins that could affect the natural moisturizing factor. In addition, perturbations in stratum corneum lipids could also affect due to lipids serve a water-holding function through the formation of lamellar structures within the stratum corneum [35]. Studies of electron microscopy from previous authors show abnormalities in the stratum corneum lamellar structure in atopic dermatitis [36,37]. Our results of FSTEM show similar results. The microstructure of the induced-dermatitis skin showed disorganized and decreased number of lamellar bilayers compared to healthy skin. Besides, the partial removal of the stratum corneum lipids by action of the acetone applied with the oxazolone should not be excluded.

In addition, as we discussed before 10 oxazolone-challenges in hairless mice produced a chronic Th2 dominated inflammatory response that is similar to human atopic dermatitis [8]. In the present study, the inflammation was characterized by epidermal thickness, parakeratosis, spongiosis and lymphocyte-dominated infiltrate as shown the histological analysis and also by highly elevated serum IgE levels. Our SKH-1 hairless mice exhibited basal IgE levels of 0.22 ± 0.06 μg/ml and reached values of 140 ± 77 μg/ml after 10 oxazolone-challenges.

4.3. Effect of the LBms on the induced atopic dermatitis condition

The dermatitis-induced mice were used to evaluate the effect of the LBms. The skin condition was improved after 10 days of treatment as shown the results of TEWL, FSTEM, histological analysis and serum IgE levels.

The effect of the LBms reducing TEWL is not as big as other common moisturizers as Vaseline. It is known that Vaseline reduces TEWL by more than 98% by an occlusion effect [38]. The Vaseline forms a layer on the surface of the skin and moisturize by retarding the evaporation of water. However, the LBms penetrates the skin and once incorporated in the lipid matrix mix with the stratum corneum lipids (described in section 4.1). The effect that the LBms exerts on the skin possibly is due to a combination of appropriate lipid composition and structure. Our LBms would avoid limiting factors associated with Vaseline and other occlusives like odor, potential allergenicity and acneiform eruptions [39].

The microstructure of the skin after treatment shows the intercorneocyte spaces almost entirely filled with extracellular lamellar lipids in contrast to the untreated dermatitis skin. This finding accords with our previous *in vitro* study in which the LBms was shown to have a specific interaction with the skin [13]. Treatment with this system *in vitro* re-established part of the lipid lamellar structure of delipidized stratum corneum, mainly the short-periodicity phase described by Bouwstra et al. [14]. Therefore, in the present study, the improvement of the skin condition *in vivo* could be related with a similar effect. The incorporation of lipids from the LBms into the stratum corneum lamellar structure would reinforce the skin barrier function indicated by decreased TEWL. In addition, the treatment with the LBms *in vivo* could stimulate the production and secretion of endogenous stratum corneum lipids in a similar way as other studies [37,40]. Mao et al. proposed that lipids from preparations containing ceramides, cholesterol and free fatty acids can penetrate impaired stratum corneum, and once absorbed by keratinocytes, the extrinsic lipids may be used by the cells and integrated into nascent lamellar bilayers [40]. Therefore, we assume that our lipid system could exert similar effect. The presence of abundant vesicular structures similar to lamellar bodies within the corneocytes in our FSTEM images (Fig. 4g, black asterisk) could be related of this. On one hand, the lipids from LBms applied on the skin could penetrate and remain into the tissue (described in Section 4.1), and on the other the system could stimulate the production of new epidermal lamellar bodies, although we found these structures within the corneocytes instead of the upper keratinocytes layers.

The inflammation was reduced after treatment (reduced epidermal thickness, reduced lymphocyte-dominated infiltrate and decreased serum IgE levels), although the treated group still showed parakeratosis and spongiosis, which is associated with inflammation. It is important to note that during the treatment period, the oxazolone was also applied which could explain this result and the fact that although the amount of IgE is reduced after treatment, it is still high compared to the basal value. Studies on atopic dermatitis and barrier repair treatment, either in animal model or in humans, showed that adequate lipid replacement therapy restores epidermal barrier function [41,42] and reduces inflammation comparable to a mid-potency steroid (fluticasone cream) [43]. In previous studies we demonstrated that the LBms penetrates into the skin and is retained mainly in the stratum corneum and upper layers of the epidermis [13]. Therefore, considering that skin immune cells are mainly located in the epidermis and especially in the dermis, we do not foresee that our system directly affects these cells, since it would remain in more external layers. However, our LBms mimicking the stratum corneum lipid composition is able to re-establish the lipid structure of damaged skin reinforcing the barrier and could indirectly participate in the immune skin response. It has been described that correction of the barrier abnormality is anti-inflammatory by different mechanisms: down-regulates of signaling mechanisms for barrier repairing that are pro-inflammatory and decreases further penetration of haptens that drive Th2 inflammation. Additionally, the inclusion of free fatty acids impart an acidic pH, which further improves barrier function and blocks activation of proinflammatory serine proteases [44].

Moreover, Schwarz et al. have recently suggested that the topical application of short chain fatty acids (SCFAs) may be used to control inflammatory disorders in the skin due to they have a specific role on skin regulatory T cells. These authors demonstrated that the topical application of sodium butyrate, a representative SCFAs, prevents the expression of hapten-specific skin inflammation in previously sensitized mice [45]. These authors also showed that sodium butyrate application was still effective even when applied after elicitation of the CHS response, suggesting a "curative" potential once inflammation has developed.

According to these results, we would expect that stearic acid forming the LBms could act in a similar way. Moreover, ceramides, in addition to structural roles also play an important role in intracellular signaling and regulates a variety of biological processes, including proliferation, differentiation, apoptosis, inflammation and immune responses [46].

Nevertheless, the dermatitis-induced mice exhibited similar skin hydration after treatment with the LBms as the dermatitis group. It is known that moisturizers improve skin hydration using a combination of occlusive, humectant, and emollient ingredients. In our case, the LBms is formed by lipids organized as bilayer structures in water. Therefore, an improvement of skin hydration is not expected due to the lipids themselves have little or no affinity for water molecules [47]. However, the lipids that form the stratum corneum lamellar structure could be specific modulators of water-retaining properties [35,48]. Our previous study using the sorption-desorption test showed that the treatment with the LBms *in vivo* increase the ability of the skin to retain water in both healthy and irritated human skin [15]. For that reason, the formulation of the LBms in an appropriate base cream could potentiate and complement the effect of this system.

5. Conclusions

The oxazolone-induced atopic dermatitis in hairless mice reflects similar characteristics as human atopic dermatitis including barrier dysfunction, elevated serum IgE levels and a Th2 cell dominant inflammatory infiltrate. This animal model is normally used to assess a therapy for atopic dermatitis. The treatment with the LBms improves the dermatitis skin condition *in vivo* by reinforcing the skin barrier function and reducing the skin inflammation. Therefore, the present study provides evidence that this lipid system combining appropriate lipid composition and morphology could be of interest for the development of future treatments for atopic dermatitis.

Conflict of interest

The authors have not conflict of interest to declare.

Acknowledgments

The authors wish to thank Evonik (Essen, Germany) for providing the ceramides. This work was supported by the Spanish Ministry of Economy, Industry and Competitiveness, grant number CTQ 2013-44998-P.

References

[1] E. Proksch, R. Fölster-Holst, J.-M. Jensen, Skin barrier function epidermal proliferation and differentiation in eczema, J. Dermatol. Sci. 43 (3) (2006) 159–169.
[2] Y. Werner, M. Lindberg, Transepidermal water loss in dry and clinically normal skin in patients with atopic dermatitis, Acta Derm. Venereologica 65 (2) (1985) 102–105.
[3] H. Tagami, Y. Kanamaru, K. Inoue, S. Suehisa, F. Inoue, K. Iwatsuki, K. Yoshikuni, M. Yamada, Water sorption-desorption test of the skin in vivo for functional assessment of the stratum corneum, J. Invest. Dermatol. 78 (5) (1982) 425–428.
[4] K.R. Feingold, Thematic review series: skin lipids. The role of epidermal lipids in cutaneous permeability barrier homeostasis, J. Lipid Res. 48 (12) (2007) 2531–2546.
[5] G. Imokawa, A. Abe, K. Jin, Y. Higaki, M. Kawashima, A. Hidano, Decreased level of ceramides in stratum corneum of atopic dermatitis: an etiologic factor in atopic dry skin? J. Invest. Dermatol. 96 (4) (1991) 523–526.
[6] J. Smeden, M. Janssens, E.C. Kaye, P.J. Caspers, A.P. Lavrijsen, R.J. Vreeken, J.A. Bouwstra, The importance of free fatty acid chain length for the skin barrier function in atopic eczema patients, Exp. Dermatol. 23 (1) (2014) 45–52.
[7] F. Rippke, V. Schreiner, T. Doering, H.I. Maibach, Stratum corneum pH in atopic dermatitis, Am. J. Clin. Dermatol. 5 (4) (2004) 217–223.
[8] M.-Q. Man, Y. Hatano, S.H. Lee, M. Man, S. Chang, K.R. Feingold, D.Y. Leung, W. Holleran, Y. Uchida, P.M. Elias, Characterization of a hapten-induced murine model with multiple features of atopic dermatitis: structural, immunologic, and biochemical changes following single versus multiple oxazolone challenges, J. Invest. Dermatol. 128 (1) (2008) 79–86.
[9] G. Rodríguez, G. Soria, E. Coll, L. Rubio, L. Barbosa-Barros, C. López-Iglesias, A. M. Planas, J. Estelrich, A. de la Maza, O. López, Bicosomes: bicelles in dilute systems, Biophis. J. 99 (2) (2010) 480–488.
[10] E. Fernández, S. Hostachy, C. Sandt, G. Rodríguez, H.C. Bertrand, S. Clède, M. Cócera, A. de la Maza, F. Lambert, C. Policar, Monitoring bicosomes containing antioxidants in normal and irradiated skin, RSC Adv. 6 (76) (2016) 72559–72567.
[11] E. Fernández, L. Fajarí, G. Rodríguez, C. López-Iglesias, M. Cócera, L. Barbosa-Barros, A. de la Maza, O. López, Bicelles and bicosomes as free radical scavengers in the skin, RSC Adv. 4 (95) (2014) 53109–53121.
[12] E. Fernández, G. Rodríguez, S. Hostachy, S. Clède, M. Cócera, C. Sandt, F. Lambert, A. de la Maza, C. Policar, O. López, A rhenium tris-carbonyl derivative as a model molecule for incorporation into phospholipid assemblies for skin applications, Colloids Surf. B 131 (2015) 102–107.
[13] V. Moner, E. Fernández, G. Rodríguez, M. Cócera, L. Barbosa-Barros, A. de la Maza, O. López, Lamellar body mimetic system: an up-to-down repairing strategy of the stratum corneum lipid structure, Int. J. Pharm. 510 (1) (2016) 135–143.
[14] J.A. Bouwstra, G.S. Gooris, J.A. van der Spek, W. Bras, Structural investigations of human stratum corneum by small-angle X-ray scattering, J. Invest. Dermatol. 97 (6) (1991) 1005–1012.
[15] V. Moner, E. Fernández, A. del Pozo, G. Rodríguez, M. Cócera, A. de la Maza, O. López, Sorption-desorption test for functional assessment of skin treated with a lipid system that mimics epidermal lamellar bodies, Contact Dermatitis 77 (2017) 25–34.
[16] P.M. Elias, J.S. Wakefield, Mechanisms of abnormal lamellar body secretion and the dysfunctional skin barrier in patients with atopic dermatitis, J. Allergy Clin. Immunol. 134 (4) (2014) 781–791 (e1).
[17] P.M. Elias, T. Mauro, U. Rassner, L. Kömüves, B.E. Brown, G.K. Menon, C. Cullander, The secretory granular cell: the outermost granular cell as a specialized secretory cell, J. Invest. Dermatol. Symp. Proc. 3 (2) (1998) 87–100.
[18] K.R. Feingold, P.M. Elias, Role of lipids in the formation and maintenance of the cutaneous permeability barrier, Biochim. Biophys. Acta Mol. Cell. Biol. Lipids 1841 (3) (2014) 280–294.
[19] K.C. Madison, Barrier function of the skin:la raison d'etre of the epidermis, J. Invest. Dermatol. 121 (2) (2003) 231–241.
[20] G.K. Menon, K.R. Feingold, P.M. Elias, Lamellar body secretory response to barrier disruption, J. Invest. Dermatol. 98 (3) (1992) 279–289.
[21] P.W. Wertz, Epidermal lipids and the intercellular pathway, in: N. Dragicevic-Curic, H.I. Maibach (Eds.), Percutaneous Penetration Enhancers Chemical Methods in Penetration Enhancement, Springer, Berlín, 2015, pp. 13–18.
[22] P.M. Elias, K.R. Feingold, M. Fartasch, The epidermal lamellar body as a multifunctional secretory organelle, in: P.M. Elias, K.R. Feingold (Eds.), Skin Barrier, CRC Press, 2005, pp. 261–272.
[23] Y. Uchida, T. Ogawa, M. Ohta, M. Kondo, S. Takada, M. Yamamura, Penetration of lysophosphatidylcholine into the dermis, J. Dermatol. 18 (9) (1991) 523–527.
[24] K. Breuer, A. Kapp, T. Werfel, Bacterial infections and atopic dermatitis, Allergy 56 (11) (2001) 1034–1041.
[25] L. Barbosa-Barros, G. Rodríguez, C. Barba, M. Cócera, L. Rubio, J. Estelrich, C. López-Iglesias, A. de la Maza, O. López, Bicelles: lipid nanostructured platforms with potential dermal applications, Small 8 (6) (2012) 807–818.
[26] T. Miyamoto, H. Nojima, T. Shinkado, T. Nakahashi, Y. Kuraishi, Itch-associated response induced by experimental dry skin in mice, Jpn. J. Pharmacol. 88 (3) (2002) 285–292.
[27] B. Liu, J. Escalera, S. Balakrishna, L. Fan, A.I. Caceres, E. Robinson, A. Sui, M.C. McKay, M.A. McAlexander, C.A. Herrick, TRPA1 controls inflammation and pruritogen responses in allergic contact dermatitis, FASEB J. 27 (9) (2013) 3549–3563.
[28] M.-Q. Man, M. Hupe, R. Sun, G. Man, T.M. Mauro, P.M. Elias, Topical apigenin alleviates cutaneous inflammation in murine models, J. Evid. Based Complementary Altern Med. 2012 (2012).
[29] H.-J. Lee, M. Jung, J.-H. Kim, N.Y. Yoon, E.H. Choi, The effect of adipose-derived stem cell-cultured media on oxazolone treated atopic dermatitis-like murine model, Ann. Dermatol. 24 (2) (2012) 181–188.
[30] M.S. Tsang, D. Jiao, B.C. Chan, K.-L. Hon, P.C. Leung, C. Lau, E.C. Wong, L. Cheng, C.K. Chan, C.W. Lam, Anti-inflammatory activities of pentaherbs formula, berberine, gallic acid and chlorogenic acid in atopic dermatitis-like skin inflammation, Molecules 21 (4) (2016) 519.
[31] Y. Hatano, M.-Q. Man, Y. Uchida, D. Crumrine, T.M. Mauro, K.R. Feingold, P.M. Elias, W.M. Holleran, Murine atopic dermatitis responds to peroxisome proliferator-activated receptors α and β/δ (but not γ) and liver X receptor activators, J. Allergy Clin. Immunol. 125 (1) (2010) 160–169.
[32] N.R. Lee, H.-J. Lee, N.Y. Yoon, D. Kim, M. Jung, E.H. Choi, Application of topical acids improves atopic dermatitis in murine model by enhancement of skin barrier functions regardless of the origin of acids, Ann. Dermatol. 28 (6) (2016) 690–696.
[33] J.-M. Jensen, R. Fölster-Holst, A. Baranowsky, M. Schunck, S. Winoto-Morbach, C. Neumann, S. Schütze, E. Proksch, Impaired sphingomyelinase activity and epidermal differentiation in atopic dermatitis, J. Invest. Dermatol. 122 (6) (2004) 1423–1431.
[34] A. di Nardo, P. Wertz, A. Gianneti, S. Seidenari, Ceramide and cholesterol composition of the skin of patients with atopic dermatitis, ACTA Dermato-Venereologica (Stockholm) 78 (1998) 27–30.
[35] G. Imokawa, H. Kuno, M. Kawai, Stratum corneum lipids serve as a bound-water modulator, J. Invest. Dermatol. 96 (6) (1990) 845–851.
[36] S.L. Chamlin, J. Kao, I.J. Frieden, M.Y. Sheu, A.J. Fowler, J.W. Fluhr, M.L. Williams, P.M. Elias, Ceramide-dominant barrier repair lipids alleviate childhood atopic dermatitis: changes in barrier function provide a sensitive indicator of disease activity, J. Am. Acad. Dermatol. 47 (2) (2002) 198–208.
[37] A. Piekutowska, D. Pin, C. Rème, H. Gatto, M. Haftek, Effects of a topically applied preparation of epidermal lipids on the stratum corneum barrier of atopic dogs, J. Comp. Pathol. 138 (4) (2008) 197–203.
[38] A. Rawlings, D.A. Canestrari, B. Dobkowski, Moisturizer technology versus clinical performance, Dermatol. Ther. 17 (s1) (2004) 49–56.
[39] A. Sethi, T. Kaur, S. Malhotra, M. Gambhir, Moisturizers the slippery road, Indian J. Dermatol. 61 (3) (2016) 279.
[40] M. Mao-Qiang, B.E. Brown, S. Wu-Pong, K.R. Feingold, P.M. Elias, Exogenous nonphysiologic vs physiologic lipids: divergent mechanisms for correction of permeability barrier dysfunction, Arch. Dermatol. 131 (7) (1995) 809–816.
[41] P.M. Elias, Barrier-repair therapy for atopic dermatitis: corrective lipid biochemical therapy, Expert Rev. Dermatol. 3 (4) (2008) 441–452.
[42] Y. Valdman-Grinshpoun, D. Ben-Amitai, A. Zvulunov, Barrier-restoring therapies in atopic dermatitis: current approaches and future perspectives, Dermatol. Res. Pract. 2012 (2012).
[43] J.L. Sugarman, The epidermal barrier in atopic dermatitis, Semin. Cutan. Med. Surg. 27 (2) (2008) 108–114.
[44] P.M. Elias, Barrier repair trumps immunology in the pathogenesis and therapy of atopic dermatitis, Drug Discov. Today Dis. Mech. 5 (1) (2008) e33–e38.
[45] A. Schwarz, A. Bruhs, T. Schwarz, The short-chain fatty acid sodium butyrate functions as a regulator of the skin immune system, J. Invest. Dermatol. 137 (4) (2017) 855–864.
[46] A. Huwiler, T. Kolter, J. Pfeilschifter, K. Sandhoff, Physiology and pathophysiology of sphingolipid metabolism and signaling, Biochim. Biophys. Acta Mol. Cell Biol. Lipids 1485 (2) (2000) 63–99.
[47] G. Imokawa, Ceramides as natural moisturizing factors and their efficacy in dry skin, in: J.J. Leyden, A.V. Rawlings (Eds.), Skin Moisturization, CRC Press, 2002, pp. 267–302.
[48] G. Imokawa, S. Akasaki, Y. Minematsu, M. Kawai, Importance of intercellular lipids in water-retention properties of the stratum corneum: induction and recovery study of surfactant dry skin, Arch. Dermatol. Res. 281 (1) (1989) 45–51.

ARTÍCULO 4

Synchrotron FTIR microspectroscopy to study different skin conditions. V. Moner, I. Yousef, E. Fernández, M. Cócera, K. Talló, A. Calpena y O. López. *Journal of Pharmaceutical and Biomedical Analysis* - en revisión

El LBms mejora la función barrera cutánea *in vivo* tanto en voluntarios con piel irritada por un tensioactivo (trabajo 2) como en un modelo animal de dermatitis (trabajo 3). Además, reduce la inflamación como se ha descrito en el trabajo 3. Sin embargo, se desconoce el efecto que produce el LBms en la piel a nivel bioquímico. Por lo tanto, en éste trabajo se utilizó FTIRM usando fuente de radiación sincrotrón para estudiar el efecto que tiene el sistema lipídico en piel con dermatitis inducida a nivel bioquímico.

El análisis de la piel por FTIRM permite obtener espectros de absorción de infrarrojo que proporcionan información de la estructura y concentración de las diferentes biomoléculas de la piel, ya que estas presentan bandas de absorción características. Además, con estos datos se pueden generar mapas químicos del tejido que permiten visualizar la distribución de estas biomoléculas. Mediante ésta técnica se estudiaron las muestras de piel obtenidas en el trabajo 3 correspondientes a piel sana, piel con dermatitis y piel con dermatitis después del tratamiento con el sistema lipídico. Se utilizó un análisis estadístico multivariante, el PCA, para estudiar diferencias entre las muestras en el rango espectral de los lípidos (3030-2800 cm^{-1}), las proteínas (1800-1483 cm^{-1}) y los carbohidratos-DNA (1481-1000 cm^{-1}).

Los resultados de PCA indicaron que la piel con dermatitis es bioquímicamente diferente a la piel sana tanto en el rango de los lípidos, las proteínas, como en el de los carbohidratos-DNA. Las diferencias son debidas a que la piel con dermatitis presenta una menor cantidad y un mayor ordenamiento de los lípidos en la zona del SC-epidermis, un aumento de la estructura en lámina beta del colágeno y cambios en el DNA. Sin embargo, se encontró que la piel tratada con el sistema lipídico es espectralmente similar a la piel sana. Este hecho podría indicar que el sistema incorpora lípidos en el SC y que podría estimular la producción y secreción de lípidos endógenos. Esto podría proteger las capas más profundas de la piel de los cambios bioquímicos que se producen en dermatitis inducida.

Manuscript Details

Manuscript number	JPBA_2018_1725
Title	Synchrotron FTIR microspectroscopy to study different skin conditions
Article type	Full length article

Abstract

Atopic dermatitis is a common skin disease that affects up to 20% of children and up to 4% of adults worldwide. It has been associated with dysfunctional epidermal lamellar bodies, secretory organelles key in the correct formation of the skin barrier function. Synchrotron fourier transform infrared microspectroscopy is a vibrational molecular technique able to provide information of the biological tissues generating a high resolution chemical map of the sample. Here, this technique was used to study the vibrational characteristics of the skin at different conditions (healthy and dermatitis) and to evaluate how a topical treatment with a lipid system that mimics epidermal lamellar bodies improves the dermatitis condition. Multivariate analysis of the spectra recorded using principal component analysis reveals clear differences in the lipid, protein and sugar-DNA regions in dermatitis skin compared to healthy skin. Interestingly, these biochemical modifications were restored after treating dermatitis skin with the lipid system. Future studies evaluating skin samples at different stages of the disease and after different treatments could report data that helps to understand how dermatitis develops. This would be very useful for the investigation of new, better targeted treatments.

Keywords	Atopic dermatitis; dermatitis mouse model; synchrotron fourier transform infrared microspectroscopy; chemical mapping; principal component analysis
Taxonomy	Pharmaceutical Application, Skin Pharmacology
Manuscript category	Pharmaceutical Applications
Corresponding Author	Verónica Moner
Order of Authors	Verónica Moner, Ibraheem Yousef, Estibalitz Fernández, Mercedes Cócera, Kirian Talló, ANA CRISTINA CALPENA, Olga López
Suggested reviewers	

Submission Files Included in this PDF

File Name [File Type]

Cover letter.docx [Cover Letter]

Highlights.doc [Highlights]

Graphical abstract.ppt [Graphical Abstract]

Manuscript.doc [Manuscript File]

Figure1.pptx [Figure]

Figure2.pptx [Figure]

Figure3.pptx [Figure]

Supplementary data.pdf [Supplementary Material]

To view all the submission files, including those not included in the PDF, click on the manuscript title on your EVISE Homepage, then click 'Download zip file'.

Synchrotron FTIR microspectroscopy to study different skin conditions

Verónica Moner[a], Ibraheem Yousef[b], Estibalitz Fernández[c], Mercedes Cócera[c], Kirian Talló[a], Ana Cristina Calpena[d] and Olga López[a]

[a] Institute of Advanced Chemistry of Catalonia (IQAC-CSIC), Carrer Jordi Girona 18-26, 08034, Barcelona, Spain.

[b] Alba Synchrotron, Carrer de la Llum 2-26, 08290, Cerdanyola del Vallès, Barcelona, Spain.

[c] Bicosome S.L, Carrer Jordi Girona 18-26, 08034, Barcelona, Spain.

[d] Department of Pharmacy and Pharmaceutical Technology, Faculty of Pharmacy, University of Barcelona, Carrer Joan XXII 27-31, 08028, Barcelona, Spain.

Corresponding author: Verónica Moner. E-mail: vmmtqt@iqac.csic.es

Abstract

Atopic dermatitis is a common skin disease that affects up to 20% of children and up to 4% of adults worldwide. It has been associated with dysfunctional epidermal lamellar bodies, secretory organelles key in the correct formation of the skin barrier function. Synchrotron fourier transform infrared microspectroscopy is a vibrational molecular technique able to provide information of the biological tissues generating a high resolution chemical map of the sample. Here, this technique was used to study the vibrational characteristics of the skin at different conditions (healthy and dermatitis) and to evaluate how a topical treatment with a lipid system that mimics epidermal lamellar bodies improves the dermatitis condition. Multivariate analysis of the spectra recorded using principal component analysis reveals clear differences in the lipid, protein and sugar-DNA regions in dermatitis skin compared to healthy skin. Interestingly, these biochemical modifications were restored after treating dermatitis skin with the lipid system. Future studies evaluating skin samples at different stages of the disease and after different treatments could report data that helps to understand how dermatitis develops. This would be very useful for the investigation of new, better targeted treatments.

Keywords: Atopic dermatitis, dermatitis mouse model, synchrotron fourier transform infrared microspectroscopy, chemical mapping, principal component analysis

1. Introduction

The stratum corneum (SC) is the uppermost epidermal layer. It is composed of keratin-rich corneocytes embedded in a lipid intercellular matrix organized in a lamellar structure. This lipid matrix consists of ceramides, cholesterol and free fatty acids with a minor amount of cholesteryl sulfate [1]. The specific structure of the SC acts as a barrier preventing water loss and bacterial infection. Epidermal lamellar bodies are secretory organelles responsible of the correct formation of the SC lipid barrier. Many skin diseases like atopic dermatitis has dysfunctional lamellar bodies, producing alteration in SC lipid composition [2].

Atopic dermatitis affects up to 20% of children and up to 3-4% of adults and presents different causes and symptoms. In all cases a deterioration of the skin barrier function occurs [2]. Consequently, a treatment focused in restoring the barrier function could be very appropriate. In this way, in previous work we have designed a lipid system that mimics the morphology and structure of epidermal lamellar bodies and approximates the SC lipid composition [3]. *In vitro,* this system re-establishes part of the SC lamellar structure in damaged skin [3]. Moreover, *in vivo,* this system increases the capacity of the skin to retain water in human volunteers [4] and reduces transepidermal water loss and skin inflammation in a dermatitis mouse model [5]. Therefore, all these results point to a high potential of this system improving the skin condition. Although the effect of these systems is clear, the impact they have at biochemical level on *in vivo* treatments is still unknown. Elucidation of these aspects could shed light on the biochemical bases of the disease and on the healing process of dermatitis lesions. Additionally, knowledge generated would allow applying these systems for the treatment of other cutaneous diseases.

Synchrotron fourier transform infrared (FTIR) microspectroscopy provides biochemical information of the cells and biological tissues generating a high resolution chemical map of the main biomolecules such as lipids, proteins and nucleic acids [6]. This technique has also demonstrated to be a useful tool to visualize the penetration and distribution of exogenous substances through the skin layers [7]. Moreover, equipped with multivariate analysis, this technique has been useful to investigate the effect of different penetration enhancers on the SC biochemical structure [8] and to identify biochemical changes at very early stages of melanoma [9].

The aim of this work is to study the vibrational characteristics of the skin at different conditions (healthy and dermatitis) and to evaluate how the topical application of a lipid system mimicking epidermal lamellar bodies improves the dermatitis condition.

The principal component analysis (PCA), a type of multivariate statistical analysis, was used to find out in what one sample is different from another. The main differences in the three samples are related to the conformation order and packing geometry of the lipids, the secondary structure of the proteins and the DNA.

2. Material and methods

2.1. Chemicals

1,2-Dipalmitoyl-sn-glycero-3-phosphocholine (DPPC) and 1,2-dihexanoyl-sn-glycero-3-phosphocholine (DHPC) were supplied from Avanti Polar Lipids (Alabaster, United States). Cholesterol from lanolin (chol), cholesteryl sulphate sodium salt (Schol), cholesteryl palmitate (Echol), stearic acid (SA) and oxazolone were purchased from Sigma-Aldrich (Steinheim, Germany). Ceramide IIIb (cer3) and ceramide VI (cer6) were generously provided by Evonik (Essen, Germany). Lipoid S100, whose main component (>94%) is soybean phosphatidylcholine (PC) and Lipoid S LPC 80 whose main component (80%) is soybean lysophosphatidylcholine (lysoPC) were supplied from Lipoid GmbH (Ludwigshafen, Germany). Chloroform was obtained from Merck (Darmstadt, Germany). Acetone was purchased from Panreac (Barcelona, Spain). Optimal cutting temperature compound (OCT) was acquired from Sakura Finetek (Torrance, United States).

2.2. Preparation of the lipid system

Formation of the lipid system mimicking epidermal lamellar bodies that we called Lamellar Body mimetic system (LBms) consists in two steps. Firstly, different discoidal structures with diverse lipid composition are prepared. Subsequently, these disks are encapsulated in lipid vesicles forming a vesicular structure enclosing lamellar disks inside, similar to the structure of epidermal lamellar bodies. The system was prepared according to a published procedure [5]. Briefly, four types of discoidal structures were prepared. The total lipid concentration of each system was 10% (w/v).

- DPPC/DHPC, q=3.5 (q= DPPC/DHPC molar ratio) including 5 mol% cer3 and 5 mol% cer6
- DPPC/DHPC, q=3.5 including 5 mol% chol
- DPPC/DHPC, q=3.5 including 5 mol% Schol
- DPPC/DHPC q=3.5 including 5 mol% Echol

To complete the preparation of LBms, a chloroform solution containing 95 mg/ml PC, 5 mg/ml lysoPC and 1.6 mg/ml SA was rota-evaporated to remove the chloroform. The lipid film formed was hydrated with the mixture of discoidal structures previously formed [5]. The LBms includes Cer:SA:Chol:SChol:EChol in a molar ratio of 1:1:0.5:0.1:0.04, respectively. The total lipid concentration of the final system was 20% (w/v).

2.3. Cryogenic transmission microscopy (cryo-TEM)

The lipid system was visualized by cryo-TEM. A thin, aqueous sample film was formed by dipping a glow-discharged holey carbon grid in the lipid suspension and then blotting the grid against a filter paper. The resulting thin sample film spanning the grid holes was vitrified by plunging the grid into ethane, which was maintained at its melting point with liquid nitrogen, by use of a Vitrobot (FEI Company, Eindhoven, The Netherlands). The vitreous sample film was transferred to a Tecnai F20 TEM (FEI Company, Eindhoven, The Netherlands) by the use of a cryotransfer holder (Gatan, Barcelona, Spain), and the sample was observed in low-dose mode. Images were acquired at 200 kV at a temperature between -170 °C and -175 °C, under low-dose imaging conditions. Five overviews and approximately 30 detailed electron micrographs were taken.

2.4. Animals and study protocol

The study protocol was approved by the Animal Experimentation Ethics Committee of the University of Barcelona according to the regulations of the local government (Decree 214/1997, July 30th). Female hairless mice SKH-1 (n = 8; Charles River, Germany) of 8-9 weeks old were housed in two cages (n = 4) in a room with controlled temperature and humidity. Food and water were provided *ad libitum*. Atopic dermatitis was induced by topical application of oxazolone in acetone. The animals were sensitized on dorsal skin with 10 µl of 5% oxazolone in acetone (day 0). A week later, the dorsal skin of the mice was treated with 60 µl of 0.1% oxazolone in acetone for 20 days (from day 7 to 26). In addition, one group was treated with 30 µl of LBms (treated-dermatitis group) whereas the other was treated with 30 µl of water (dermatitis group) for 10 days (from day 17 to 26). Treatment with LBms or water was applied one hour after oxazolone application. Twenty four hours after the last treatment, animals were euthanized and biopsies from the dorsal skin of the mice were taken (day 27).

2.5. FTIR sample preparation

Whole skin biopsies were covered firstly with aluminium foil and then with OCT. The aluminium foil was used to avoid the direct contact between the skin and the OCT. Then, skin samples were frozen in liquid N_2 and cut into transverse 6 μm thick sections (Cryostat CM3050 S, Leyca Biosystems, Nussloch, Germany) and mounted on CaF_2 circular windows (Crystran Ltd, UK).

2.6. FTIR microspectroscopy

FTIR microspectroscopy measurements were performed at the MIRAS beamline at Alba synchrotron (Barcelona, Spain) using a Hyperion 3000 microscope coupled to a Vertex 70 spectrometer (Bruker, Germany). The microscope is equipped with a 36x magnification Schwarzschild objective (NA = 0.65) and a matching 36X condenser. A mercury cadmium telluride 50 microns MCT-A detector was used. The microscope and spectrometer were continuously purged with nitrogen gas. The spectra were obtained in the spectral range 3500-1000 cm^{-1} and the spectra collection was carried out in transmission mode at 4 μm spectral resolution, 8 μm x 8 μm single masking aperture dimensions, step size of 6 μm x 6 μm and 256 co-added scans.

2.7. FTIR data treatment and statistical analysis

Maps of healthy skin, dermatitis skin and treated-dermatitis skin sections were acquired and the chemical image of each sample was generated. According to our previous results [5], epidermal thickness is ~20 μm in healthy skin, ~65 μm in dermatitis skin and ~35 μm in dermatitis skin after treatment with the LBms. Therefore, the depth of the maps from SC-epidermis area was selected according to these results. To obtain the map of the dermis area, it was selected an area deeper into the skin. The maps obtained were split to yield a data set (SC-epidermis area or dermis area) of each sample. Each data set contained approximately 50 spectra from the SC-epidermis area and approximately 120 from the dermis area. The resulting raw spectra of all data sets were pre-processed using the Unscrambler X 10.5 software (CAMO software) as described by Mansour et al. [8]. Three ranges of interest in the spectral domain corresponding to lipids (3030-2800 cm^{-1}), proteins (1800-1483 cm^{-1}) and sugar-DNA (1481-1000 cm^{-1}) were identified. Savitsky-Golay second derivatives of all the spectra were then calculated using third polynomial order and 11 smoothening points. Each defined range was then separately range normalized. PCA was performed on each of the predefined spectral ranges in all data sets and the results were represented in the form of score plots. The normalized reduced average spectrum and its corresponding Savitsky-Golay second derivative (third polynomial order and 11

smoothening points) for each data set, in each corresponding spectral range, were obtained.

3. Results and Discussion

3.1. Characterization of LBms

Cryo-TEM allows us to characterize the morphology of the different structures present in the system and to determine their size. A representative cryo-TEM micrograph and a schematic diagram of the LBms are shown in Fig. S1. The cryo-TEM image shows two types of structures corresponding to discoidal structures (white arrows) with diameter of approximately 40 nm and vesicles encapsulating disks (black arrow) with size approximately 300 nm. It is interesting to note that the morphology and structure of the LBms observed in Fig. S1 is quite similar to epidermal lamellar bodies observed by other authors in electron micrographs [10, 11]. However, the LBms contains lipids that approximate the SC lipid composition unlike epidermal lamellar bodies, which contain the precursors of SC lipids [2]. In addition, the LBms includes lysoPC which has been reported to have bactericidal activity [12].This fact could have a positive effect in the treatment of dermatitis, since patients with atopic dermatitis frequently suffer from bacterial infections [13].

3.2. Visual skin evaluation

Fig. S2 shows representative photographs of the mice corresponding to (a) healthy, (b) dermatitis and (c) dermatitis after treatment with the LBms. The photographs were taken the last day of the experiment. The dermatitis group shows red, scaly skin which is absent in healthy skin. The treated-dermatitis group shows a marked reduction of the skin lesions indicating an improvement of the skin condition. This result correlates with our previous findings which demonstrated that this system reinforces the skin barrier function and reduces the skin inflammation in the oxazolone-induced dermatitis mouse model [5].

The effect that LBms exerts on the skin possibly is due to the combination of appropriate lipid composition and structure of this lipid system. Our system contains ceramides, among other SC lipids. Ceramides have an important role in the maintenance of the barrier function, which is clearly deteriorated in diseased skin. Then, the application of these lipids would help to restore the compositional balance in dermatitis skin. The nanostructure used to apply these lipids that mimic the SC lipid

composition is also important. Many studies have reported that structures of sizes larger than 70-100 nm are not able to penetrate healthy skin, although inflamed skin or with dermatitis may have higher permeability [14]. The LBms could interact with the skin in a similar way as other lipid systems [3]. Although the external vesicle is too large (300 nm in diameter) to penetrate through the intercellular spaces of the SC (between 6-10 nm), these vesicles could break on the skin surface and deliver the discoidal structures. The disks have a size more appropriate for passing between the intercellular SC spaces.

3.3. Skin characterization by synchrotron FTIR microspectroscopy

Synchrotron FTIR microspectroscopy is a vibrational molecular technique that provide biochemical information of the skin generating a high resolution chemical map of the sample. Fig. S3A shows a typical spectrum of healthy skin collected in the 3500-1000 cm^{-1} range. CH_3 and CH_2 stretching bands are associated with lipids [15]; Amide I&II bands are associated with proteins [7, 16] and PO_2 stretching band is mainly associated with nucleic acids although it is also associated with phospholipids [17]. These vibration modes, the frequency range, and their sensitivity are summarized in Table S1.

Fig. S3B shows the optical image of healthy skin where we can differentiate the SC, epidermis and dermis layers. The chemical maps obtained, superimposed to the optical images, show the distribution of the skin components along the tissue. The pink areas represent the highest concentration of each molecule; while in the blue areas these molecules are not detected. Consequently, the lipids are mainly found in the SC-epidermis zone, whereas the proteins and DNA are mainly found in dermis zone.

This technique allows us to identify biochemical signals in healthy skin and disease skin, and to relate biochemical changes with the disease. In this study, the PCA was used to find out differences between healthy, dermatitis and treated-dermatitis skin in the spectral range of lipids (3030-2800 cm^{-1}), proteins (1800-1483 cm^{-1}) and sugar-DNA (1481-1000 cm^{-1}).

3.3.1. PCA analysis on the spectral range of lipids

The bands between 3030 and 2800 cm^{-1} are of particular interest for studying the lipids of the skin. In this spectral range, the lipids exhibit four peaks around 2955, 2920, 2870 and 2850 cm^{-1} which are assigned to asymmetric CH_3 stretching, asymmetric CH_2 stretching, symmetric CH_3 stretching and symmetric CH_2 stretching, respectively. The CH_2 stretching frequencies reflect both lipid chain conformational order and packing geometry [15]. Although the symmetric stretching vibration of CH_2 is more sensitive

than the asymmetric vibration to packing changes [18], this latter is also used in some studies for similar purposes [19].

In this work, the PCA on the spectral range of lipids (3030-2800 cm^{-1}) was performed. The results of PCA analysis are represented in the form of scores plot and corresponding loadings. Each point (score) in the score plot corresponds to one spectrum. The results are shown in Fig. 1. In the SC-epidermis area, clustering of each of the three groups (healthy, dermatitis and treated dermatitis) is clear and, 70% of the variability is explained by principal component 1 (PC-1). The treated-dermatitis group and healthy group are located on the positive side of PC-1 while the dermatitis group is located on the negative side. This implies that treated-dermatitis group is spectrally more similar to healthy group than dermatitis group. By PC-2, which explains only the 15% of the variance, the samples are not well separated. In PCA, the spectral origins of the variation which differentiate the data groups according to the wavenumbers are represented in the loadings with positive and negative loadings correlate to the positive and negative scores, respectively [8]. The loadings show that CH_2 stretching vibrations are the responsible for the variation. The comparison of the asymmetric and symmetric CH_2 stretching peaks in the average spectra show a shift to less frequency in dermatitis group (2924 and 2852 cm^{-1}) compared to healthy group (2926 and 2854 cm^{-1}). This indicates an increase in the order of lipids in induced-dermatitis skin, rather than a higher conformational disordering that has been described in human dermatitis skin disease [20]. However, our result is in accordance with Bommannan et al. which found an increase in the order of lipids after treating human SC with ethanol [21]. Ethanol could have a similar interaction with skin lipids as oxazolone that we used to induce the dermatitis condition in our work. Our results show that this alteration in lipid order is restored after treatment with the LBms. Moreover, considering that the intensity of a particular FTIR peak reflects the amount of the assigned compound for that wavenumber [22], induced-dermatitis could suffer a loss of lipids that would be recovered after treatment with the LBms.

We concluded here that the treatment re-establishes the changes on the lipid spectral region. This fact could be due to the introduction of lipids from the LBms into the SC lamellar structure. Moreover, the treatment with LBms could stimulate *in vivo* the production and secretion of endogenous lipids in a similar way as other studies [23]. Mao et al. proposed that lipids from preparations containing SC lipids could penetrate impaired SC, and once absorbed by keratinocytes, the extrinsic lipids may be used by cells and integrated into nascent lamellar bilayers [23]. Thus, the LBms could exert similar effect.

In the dermis area, the dermatitis group is located mainly in the positive side of PC-1 whereas the healthy group is located in the negative side. However, the treated-dermatitis group seems to be mixed with both samples, part with healthy and part with dermatitis group. By PC-2, which explains 33% of the variance, the samples are not well separated. The comparison of the asymmetric and symmetric CH_2 stretching peaks in the average spectra show the same frequency for the three samples around 2925 and 2854 cm^{-1}, respectively. This indicates that the lipids in the dermis are packet similarly, in a disordered conformation, in healthy, dermatitis and treated-dermatitis skin. The intensity of these peaks could indicate a reduction of the amount of lipids in induced dermatitis skin compared to normal skin which would be recovered after treatment.

3.3.2. PCA analysis on the spectral range of proteins

The main IR features of the skin that correspond to its protein content are the Amide I and Amide II bands. The Amide I at 1610-1690 cm^{-1} arises mainly from C=O stretching of amide groups of the peptide backbone in proteins. The Amide II at 1520-1560 cm^{-1} arises mainly from N-H bending (60%) and C-N stretching (40%) vibrations of amide groups of the peptide backbone in proteins. Both bands, particularly the Amide I band, are sensitive to protein secondary structure [16]. Another band related to proteins is the Amide III (40% C-N stretching, 30% N-H bending, 20% methyl-C stretching) located in the spectral range 1350-1200 cm^{-1}. However, this band is rarely used for conformational studies of proteins due to the presence of other bands in this spectral region [24].

In this work, the PCA analysis on the spectral range of proteins (1800-1483 cm^{-1}) was performed in dermis area (Fig. 2). Clustering of each of the three groups is clear and 62% of the variability is explained by PC-1. Healthy group and treated-dermatitis group are located predominately on the positive side of PC-1 while the dermatitis group is located in the negative side. This implies that dermatitis group is spectrally the most different. By PC-2, which explains only the 17% of the variance, the samples are not well separated. The analysis of the loadings reveals that most of the variance involves changes in the Amide I and Amide II bands. The comparison of the Amide I band on the average spectra show a shift to high frequency in dermatitis group (1658.5 cm^{-1}) compared to healthy group (1654.6 cm^{-1}). However, the treated-dermatitis group presented this band at 1656.6 cm^{-1}, closest to the vibration of the sample of healthy skin. Moreover, the Amide I band shows a shoulder at 1635 cm^{-1} in the three groups. Regarding the Amide II, the comparison of this band on the average spectra shows similar results as Amide I. This band was located at 1549.0 cm^{-1} in healthy group, 1552.4 cm^{-1} in dermatitis group and 1550 cm^{-1} in treated-dermatitis group. It can be

concluded here that the treatment seems to recover partially the changes on the protein spectral region.

Second derivative spectrum analysis is used to enhance the resolution of overlapping IR bands and it is one of the most popular approaches used for analysis of Amide I peak of proteins in solution [25]. This approach allows the identification of various secondary structures present in the proteins since most of the peak positions can be easily found. In dermis, the Amide I arises from collagen and it is sensitive to collagen structural changes. In the present work, we studied the second derivative of the Amide I peak (Fig. 2D). The Amide I had 5 sub-peaks: at 1695 cm^{-1} (aggregated strand), 1679 cm^{-1} (anti-parallel β-sheets and β-turns), 1654 cm^{-1} (α-helix), 1635 cm^{-1} (β-sheets) and 1612 cm^{-1} (intermolecular β-sheets) [26]. The three samples showed an intense band at 1659-1655 cm^{-1} related to triple-helical structure of the collagen. The peak at 1635 cm^{-1} is slightly more intense in dermatitis and treated-dermatitis group than healthy group suggesting a partially increase of β-sheet structure of collagen.

Additionally, in the spectral range 1800-1483 cm^{-1}, two other bands are found. These bands correspond to the carbonyl ester group (C=O) stretching of lipids. The band at 1745 cm^{-1} corresponds to triglycerides and/or phospholipids and the band at 1711 cm^{-1} corresponds to fatty acids [27]. These vibrational modes showed the same frequency in healthy, dermatitis and treated-dermatitis group. However, the intensity is lower in dermatitis group indicating a reduction of these lipids in diseased skin.

3.3.3. PCA on the spectral range of sugar-DNA

The PCA analysis on the spectral range of sugar-DNA (1481-1000 cm^{-1}) was performed in dermis area in order to evaluate the possible affectation of this type of biomolecules in dermatitis condition with and without treatment with the LBms (Fig. 3). PC-1, which explains most of the variance (81%), shows that treated-dermatitis group is spectrally similar in sugar-DNA range to healthy group while dermatitis group is the most different. The analysis of the loadings reveals that most of the variance involves changes in the PO_2 stretching vibration related mainly to DNA. The comparison of asymmetric PO_2 stretching (peak VII) on the average spectra shows the peak at 1236.1 cm^{-1} on healthy, dermatitis and treated-dermatitis group. However, we observed an increase in the intensity of this peak in dermatitis group compared to healthy group. This increase in intensity is reduced after treatment. Regarding the symmetric PO_2 stretching (peak XI) a small change in position and intensity is observed in dermatitis group and treated-dermatitis group compared to healthy group.

The average absorbance spectra in this spectral range also show other bands. Peak assignment of these bands is given in table S2. The band (I) at 1463.7 cm^{-1} is mainly due to the CH_2 scissoring mode [18]. This band gives information concerning the acyl chain of lipids. However, the skin displays a strong CH_3 bending mode (II) related to proteins in the immediate vicinity of the CH_2 scissoring [28]. Therefore, it is difficult to estimate the exact positions of the scissoring components although it seems similar in the three samples. The band III is related to the COO^- stretching of proteins [24]. The band IV is due to the CH_3 bending of proteins [28]. The band V is related to the CH_2 wagging of proteins [24]. The bands VI and VIII are due to the amide III of proteins [29]. The band IX is due to the C-O stretching of proteins and carbohydrates [24]. Finally, the bands X, XII and XIII are mainly due to the vibrational modes of C-O stretching coupled with C-O bending of carbohydrates [24]. In general, we observed slight variations in these bands in dermatitis skin compared to healthy skin. In particular, these changes are related to the intensity of these bands. After treatment the intensity of these bands are similar to healthy skin.

The results obtained in the present study indicate that different biomolecules are altered in induced-dermatitis skin. The recovery of the spectral behavior after topical treatment with the LBms may be indicative of the efficacy of this treatment. Possibly, the improvement of the barrier function in dermatitis skin by our lipid system, previously demonstrated [5], would protect the deeper layers of the skin to biochemical changes produced by an irritant as the oxazolone. Additionally, the improved barrier function in upper skin layers would stimulate the natural mechanisms of skin recovery having effect on deeper layers.

4. Conclusion

Synchrotron FTIR microspectroscopy technique is useful to study the vibrational characteristics of the skin at different conditions (healthy and dermatitis) and to evaluate the effect of treatments. The PCA analysis on the spectral range of lipids, proteins and sugar-DNA shows differences in induced-dermatitis skin compared to healthy skin. It was found an increase in the ordering of lipids in the SC-epidermis zone, whereas the lipids in dermis zone are packed similarly. In addition, the induced-dermatitis skin has a loss of lipids. Our results also suggest that the collagen is affected in induced-dermatitis skin indicated by a partially increase of β-sheet structure. DNA is also partially affected; we found an increase in the PO_2 asymmetric band. These differences are restored after treatment with the LBms. This fact could be due to the

introduction of lipids from the LBms into the SC lamellar structure inducing an improvement of the barrier function. In addition, the treatment could stimulate the production and secretion of endogenous lipids and other mechanisms of skin recovery. The barrier function improvement would protect the deeper layers of the skin to biochemical changes produced by the oxazolone. Future studies evaluating skin samples at different stages of the disease could report data that helps to understand how dermatitis develops. This would be very useful for the investigation of new, better targeted treatments.

Acknowledgements

The authors wish to thank Lidia Delgado from the unit of electron cryomicroscopy of CCiTUB for expert technical assistance. We also thank Evonik (Essen, Germany) for kindly providing the ceramides. These experiments were performed at Miras beamline at ALBA Synchrotron with the collaboration of ALBA staff. This work was supported by the Spanish Ministry of Economy, Industry and Competitiveness; grant numbers CTQ 2013-44998-P and RTC-2016-4957-1.

Figures

Figure 1

PCA analysis on the spectral range of lipids (3030-2800 cm^{-1}) on SC-epidermis area (left) and dermis area (right). The scores (top), loading plots (middle) and average absorbance spectra (unit vector normalized; bottom) are presented. Color code: healthy skin (blue), dermatitis skin (red) and dermatitis skin after treatment (green).

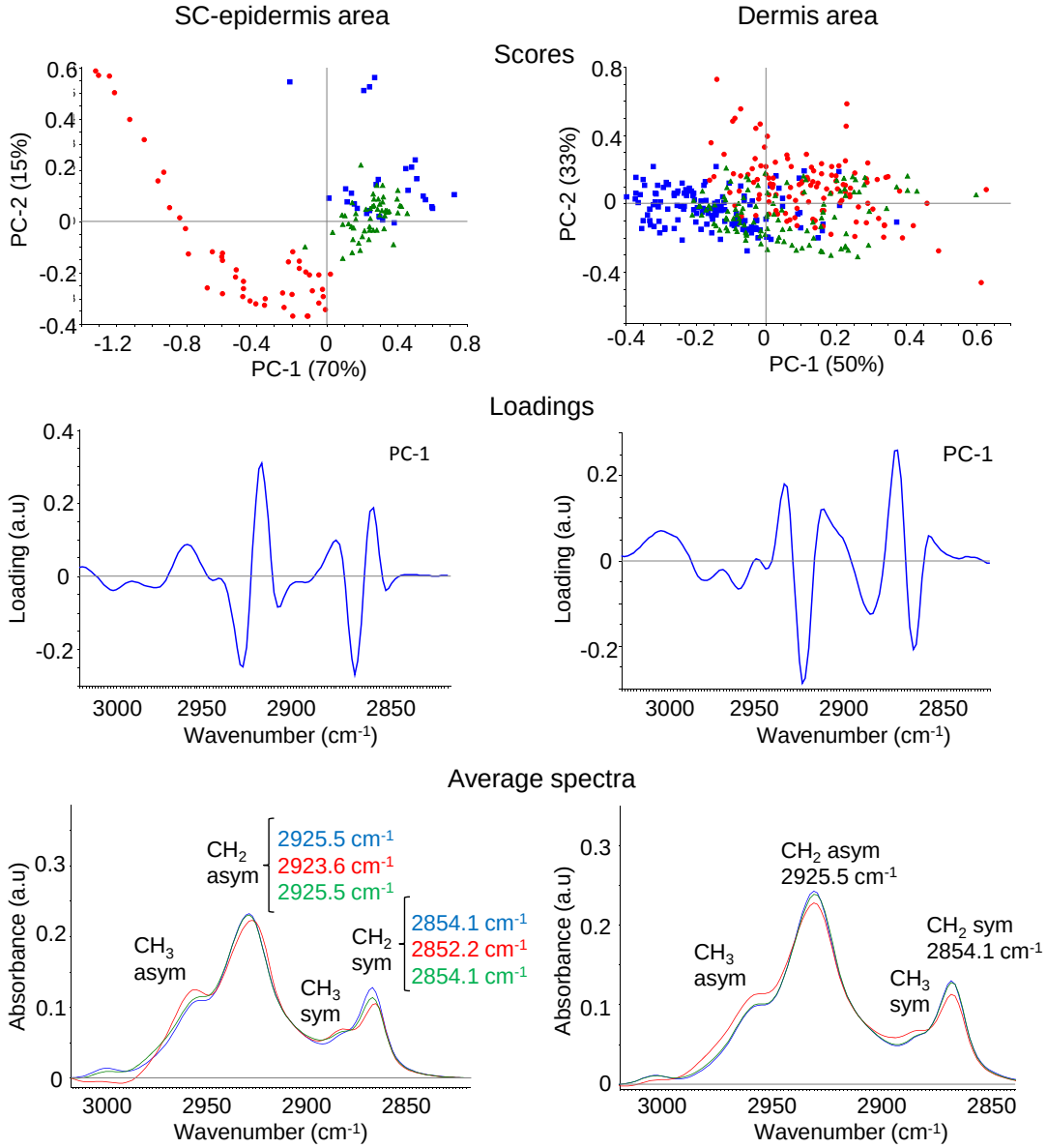

Figure 2

PCA analysis on the spectral range of proteins (1483-1800 cm^{-1}) on dermis area. (A) Scores, (B) loading plots, (C) average absorbance spectra (unit vector normalized) and (D) range normalized average second derivative spectra of Amide I. Color code: healthy skin (blue), dermatitis skin (red) and dermatitis skin after treatment (green).

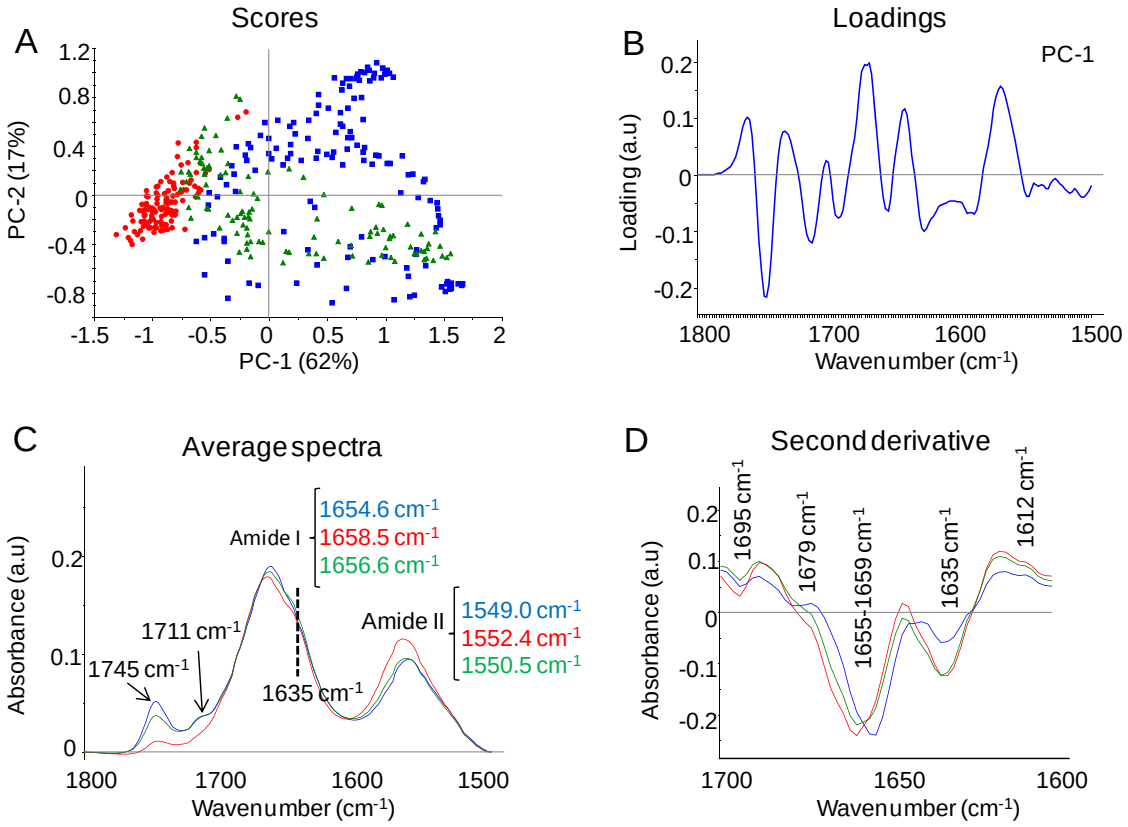

Figure 3

PCA analysis on the spectral range of sugar-DNA (1481-1000 cm^{-1}) on dermis area. Scores (top), loading plots (middle) and average absorbance spectra (unit vector normalized; bottom) are presented. Refer to table 2 for peak numbers and their assignment. (Color code: healthy skin (blue), dermatitis skin (red) and dermatitis skin after treatment (green).

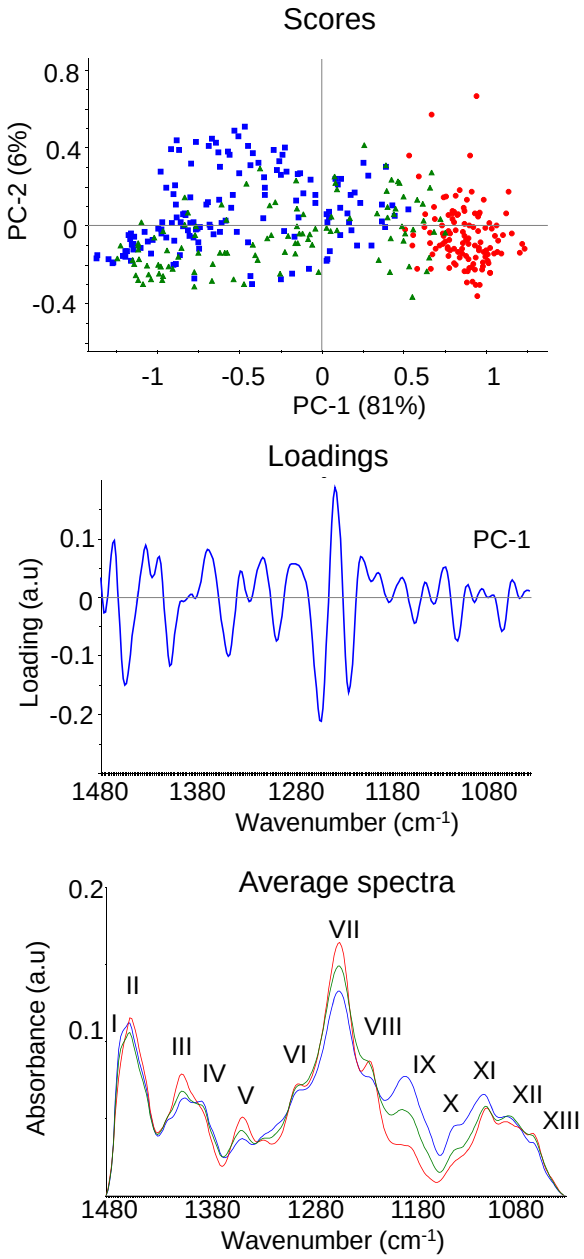

[1] P.M. Elias, Epidermal lipids, barrier function, and desquamation, J. Invest. Dermatol. 80 (1983) Suppl:44s-49s.

[2] P.M. Elias, J.S. Wakefield, Mechanisms of abnormal lamellar body secretion and the dysfunctional skin barrier in patients with atopic dermatitis, J. Allergy Clin. Immunol. 134(4) (2014) 781-791 e1.

[3] V. Moner, E. Fernández, G. Rodríguez, M. Cócera, L. Barbosa-Barros, A. de la Maza, O. López, Lamellar body mimetic system: an up-to-down repairing strategy of the stratum corneum lipid structure, Int. J. Pharm. 510(1) (2016) 135-143.

[4] V. Moner, E. Fernández, A. del Pozo, G. Rodríguez, M. Cócera, A. de la Maza, O. López, Sorption–desorption test for functional assessment of skin treated with a lipid system that mimics epidermal lamellar bodies, Contact Dermatitis 77 (2017) 25-34.

[5] V. Moner, E. Fernández, A.C. Calpena, A. Garcia-Herrera, M. Cócera, O. López, A lamellar body mimetic system for the treatment of oxazolone-induced atopic dermatitis in hairless mice, J. Dermatol. Sci. (90) 172-179.

[6] L.M. Miller, P. Dumas, Chemical imaging of biological tissue with synchrotron infrared light, Biochim. Biophys. Acta Biomembr. 1758(7) (2006) 846-857.

[7] M. Cotte, P. Dumas, M. Besnard, P. Tchoreloff, P. Walter, Synchrotron FT-IR microscopic study of chemical enhancers in transdermal drug delivery: example of fatty acids, J Control. Release 97(2) (2004) 269-281.

[8] R.S. Mansour, A.A. Sallam, I.I. Hamdan, E.A. Khalil, I. Yousef, Elucidation of penetration enhancement mechanism of Emu oil using FTIR microspectroscopy at EMIRA laboratory of SESAME synchrotron, Spectrochim. Acta Part A 185 (2017) 1-10.

[9] G. Zhang, D.J. Moore, C.R. Flach, R. Mendelsohn, Vibrational microscopy and imaging of skin: from single cells to intact tissue, Anal. Bioanal. Chem. 387(5) (2007) 1591-1599.

[10] P.W. Wertz, Epidermal Lipids and the Intercellular Pathway, in: N. Dragicevic-Curic, H.I. Maibach (Eds.), Percutaneous Penetration Enhancers Chemical Methods in Penetration Enhancement, Springer, Berlín, 2015, pp. 13-18.

[11] G.K. Menon, K.R. Feingold, P.M. Elias, Lamellar body secretory response to barrier disruption, J. Invest. Dermatol. 98(3) (1992) 279-289.

[12] Y. Uchida, T. Ogawa, M. Ohta, M. Kondo, S. Takada, M. Yamamura, Penetration of lysophosphatidylcholine into the dermis, J. Dermatol. 18(9) (1991) 523-527.

[13] K. Breuer, A. Kapp, T. Werfel, Bacterial infections and atopic dermatitis, Allergy 56(11) (2001) 1034-1041.

[14] C. Try, B. Moulari, A. Béduneau, O. Fantini, D. Pin, Y. Pellequer, A. Lamprecht, Size dependent skin penetration of nanoparticles in murine and porcine dermatitis models, Eur. J. Pharm. Biopharm. 100 (2016) 101-108.

[15] G.M. Golden, D.B. Guzek, R.R. Harris, J.E. McKie, R.O. Potts, Lipid thermotropic transitions in human stratum corneum, J. Investig. Dermatol. 86(3) (1986) 255-259.

[16] M. Jackson, H.H. Mantsch, The use and misuse of FTIR spectroscopy in the determination of protein structure, Crit. Rev. Biochem. Mol. 30(2) (1995) 95-120.

[17] P. Wong, E. Papavassiliou, B. Rigas, Phosphodiester stretching bands in the infrared spectra of human tissues and cultured cells, J. Appl. Spectrosc. 45(9) (1991) 1563-1567.

[18] R. Mendelsohn, C.R. Flach, D.J. Moore, Determination of molecular conformation and permeation in skin via IR spectroscopy, microscopy, and imaging, Biochim. Biophys. Acta Biomembr. 1758(7) (2006) 923-933.

[19] L. Coderch, M. De Pera, N. Perez-Cullell, J. Estelrich, A. De la Maza, J. Parra, The effect of liposomes on skin barrier structure, Skin Pharmacol. Physiol. 12(5) (1999) 235-246.

[20] M. Janssens, J. van Smeden, G.S. Gooris, W. Bras, G. Portale, P.J. Caspers, R.J. Vreeken, T. Hankemeier, S. Kezic, R. Wolterbeek, Increase in short-chain ceramides correlates with an altered lipid organization and decreased barrier function in atopic eczema patients, J. Lipid Res. 53(12) (2012) 2755-2766.

[21] D. Bommannan, R.O. Potts, R.H. Guy, Examination of the effect of ethanol on human stratum corneum in vivo using infrared spectroscopy, J. Control. Release 16(3) (1991) 299-304.

[22] N. Igci, P. Sharafi, D.O. Demiralp, C.O. Demiralp, A. Yuce, S. Emre, Application of Fourier transform infrared spectroscopy to biomolecular profiling of cultured fibroblast cells from Gaucher disease patients: A preliminary investigation, Advances in Clinical and Experimental Medicine 26(7) (2017) 1053-1061.

[23] M. Mao-Qiang, B.E. Brown, S. Wu-Pong, K.R. Feingold, P.M. Elias, Exogenous nonphysiologic vs physiologic lipids: divergent mechanisms for correction of permeability barrier dysfunction, Arch. Dermatol. 131(7) (1995) 809-816.

[24] S. Olsztyńska-Janus, A. Pietruszka, Z. Kiełbowicz, M. Czarnecki, ATR-IR study of skin components: Lipids, proteins and water. Part I: Temperature effect, Spectrochim. Acta A Mol. Biomol. Spectrosc. 188 (2018) 37-49.

[25] J. Kong, S. Yu, Fourier transform infrared spectroscopic analysis of protein secondary structures, Acta Biochim. Biophys. Sin. 39(8) (2007) 549-559.

[26] R. Tang, V. Samouillan, J. Dandurand, C. Lacabanne, F. Nadal-Wollbold, C. Casas, A.-M. Schmitt, Thermal and vibrational characterization of human skin, J. Therm. Anal. Calorim. 127(2) (2017) 1143-1154.

[27] P. Garidel, Mid-FTIR-Microspectroscopy of stratum corneum single cells and stratum corneum tissue, Phys. Chem. Chem. Phys. 4(22) (2002) 5671-5677.

[28] M. Boncheva, F. Damien, V. Normand, Molecular organization of the lipid matrix in intact Stratum corneum using ATR-FTIR spectroscopy, Biochim. Biophys. Acta Biomembr. 1778(5) (2008) 1344-1355.

[29] C. Eklouh-Molinier, T. Happillon, N. Bouland, C. Fichel, M.-D. Diébold, J.-F. Angiboust, M. Manfait, S. Brassart-Pasco, O. Piot, Investigating the relationship between changes in collagen fiber orientation during skin aging and collagen/water interactions by polarized-FTIR microimaging, Analyst 140(18) (2015) 6260-6268.

Supplementary data

Synchrotron FTIR microspectroscopy to study different skin conditions

Verónica Moner[a], Ibraheem Yousef[b], Estibalitz Fernández[c], Mercedes Cócera[c], Kirian Talló[a], Ana Cristina Calpena[d] and Olga López[a]

[a] *Institute of Advanced Chemistry of Catalonia (IQAC-CSIC), Carrer Jordi Girona 18-26, 08034, Barcelona, Spain.*

[b] *Alba Synchrotron, Carrer de la Llum 2-26, 08290, Cerdanyola del Vallès, Barcelona, Spain.*

[c] *Bicosome S.L, Carrer Jordi Girona 18-26, 08034, Barcelona, Spain.*

[d] *Department of Pharmacy and Pharmaceutical Technology, Faculty of Pharmacy, University of Barcelona, Carrer Joan XXII 27-31, 08028, Barcelona, Spain.*

*Corresponding author: Verónica Moner. E-mail: vmmtqt@iqac.csic.es

Fig. S1. Cryo-TEM micrograph and diagram of the LBms. The system is formed by encapsulated and non-encapsulated disks with diameters of ~ 40 nm (white arrows), and vesicles encapsulating disks (black arrow) with size of ~ 300 nm. Bar = 100 nm.

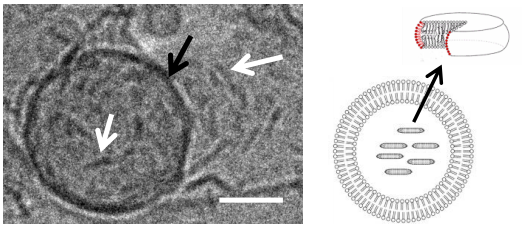

Fig. S2. Representative photographs of the mice: (A) healthy, (B) dermatitis and (C) dermatitis after treatment with the LBms.

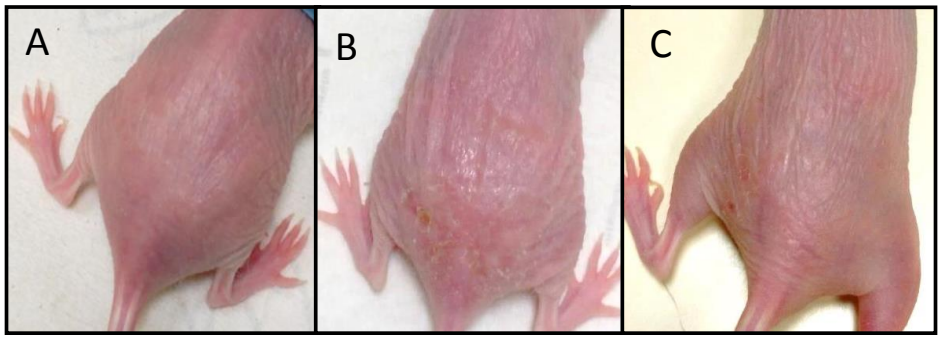

Fig. S3. (A) Typical FTIR spectrum obtained from healthy skin in the spectral range 3500-1000 cm^{-1}, showing CH_3 and CH_2 stretching vibrations of lipids, Amide I&II vibrations of proteins and PO_2 stretching vibration mainly of nucleic acids. (B) Chemical maps with the corresponding optical image of the skin section showing the distribution of lipids, proteins and DNA along the tissue. Bar = 20 µm.

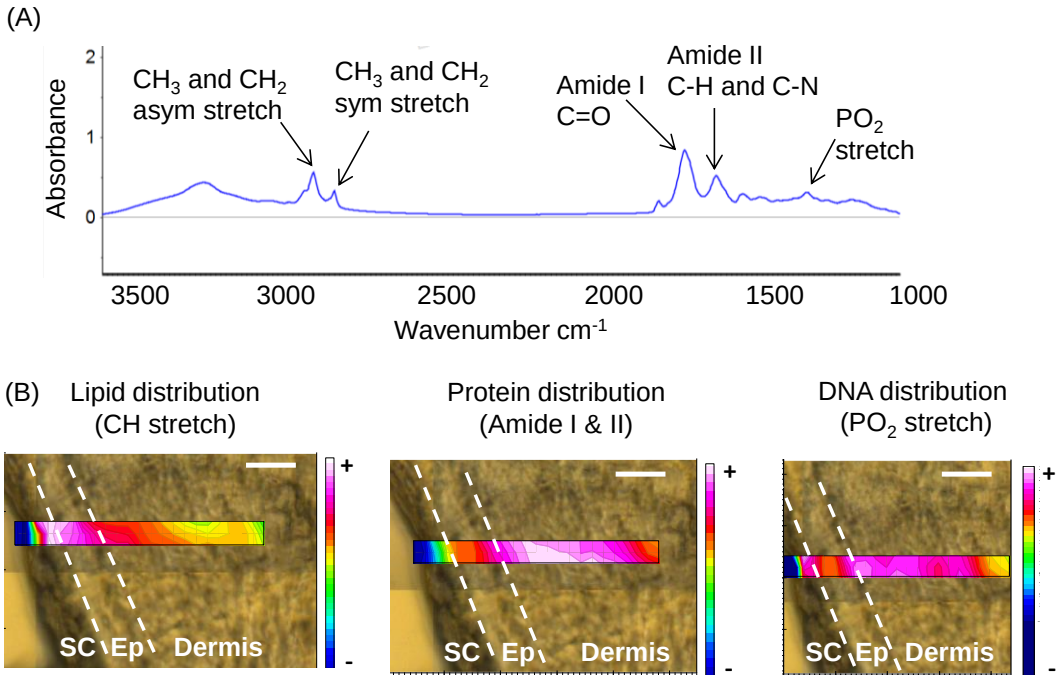

Table S1. Characteristic frequencies of different skin components (lipids, proteins and nucleic acids) by FTIR and their meaning.

Vibrational mode		Frequency (cm^{-1}) Literature[1-3]	Sensitivity
Lipids	CH_3 asym stretch	2955-2960	The CH_2 sym stretching frequencies are more sensitive than asym vibrations and reflect both lipid chain conformation order and packing geometry.
	CH_2 asym stretch	2915-2924	
	CH_3 sym stretch	2872-2875	
	CH_2 sym stretch	2847-2855	
Proteins	Amide I (80% C=O stretch)	1610-1690	Both bands, particularly the amide I band, are sensitive to protein secondary structure.
	Amide II (60% N-H in plane bend, 40% C-N stretch)	1520-1560	
Nucleic acids	PO_2 asym stretch	1239-1240	These bands are mainly related to DNA.
	PO_2 sym stretch	1082-1086	

Table S2. FTIR spectra peak attributions on the spectral range of sugar-DNA (1481-1000 cm^{-1}). Literature[2, 4-7]

Peak number	Wavenumber (cm^{-1})	Possible vibrations	Assignment
I	1463.7	CH_2 scissoring	Lipids
II	1455.9	CH_3 bending asym	Proteins
III	1400.0	COO^- stretch	Proteins
IV	1380.8	CH_3 bending sym	Proteins
V	1340.0	CH_2 wagging	Proteins
VI	1280.5	Amide III	Proteins
VII	1236.1	PO_2 asym	Nucleic acids, phospholipids
VIII	1203.3	Amide III	Proteins
IX	1166.7	C-O stretch	Proteins and carbohydrates
X	1116.8	C-O stretch, C-O bending	Carbohydrates
XI	1083.8	PO_2 sym	Nucleic acids, phospholipids
XII	1058.8	C-O stretch, C-O bending	Carbohydrates
XIII	1030.7	C-O stretch, C-O bending	Carbohydrates

[1] G.M. Golden, D.B. Guzek, R.R. Harris, J.E. McKie, R.O. Potts, Lipid thermotropic transitions in human stratum corneum, J. Investig. Dermatol. 86(3) (1986) 255-259.

[2] R. Mendelsohn, C.R. Flach, D.J. Moore, Determination of molecular conformation and permeation in skin via IR spectroscopy, microscopy, and imaging, Biochim. Biophys. Acta Biomembr. 1758(7) (2006) 923-933.

[3] J. Kong, S. Yu, Fourier transform infrared spectroscopic analysis of protein secondary structures, Acta Biochim. Biophys. Sin. 39(8) (2007) 549-559.

[4] P. Wong, E. Papavassiliou, B. Rigas, Phosphodiester stretching bands in the infrared spectra of human tissues and cultured cells, J. Appl. Spectrosc. 45(9) (1991) 1563-1567.

[5] S. Olsztyńska-Janus, A. Pietruszka, Z. Kiełbowicz, M. Czarnecki, ATR-IR study of skin components: Lipids, proteins and water. Part I: Temperature effect, Spectrochim. Acta A Mol. Biomol. Spectrosc. 188 (2018) 37-49.

[6] M. Boncheva, F. Damien, V. Normand, Molecular organization of the lipid matrix in intact Stratum corneum using ATR-FTIR spectroscopy, Biochim. Biophys. Acta Biomembr. 1778(5) (2008) 1344-1355.

[7] C. Eklouh-Molinier, T. Happillon, N. Bouland, C. Fichel, M.-D. Diébold, J.-F. Angiboust, M. Manfait, S. Brassart-Pasco, O. Piot, Investigating the relationship between changes in collagen fiber orientation during skin aging and collagen/water interactions by polarized-FTIR microimaging, Analyst 140(18) (2015) 6260-6268.

ARTÍCULO 5

Delivery systems with omega-O-acylceramide repair perturbed human stratum corneum. V. Moner, L. Opálka, K. Vávrová y O. López. *International Journal of Pharmaceutics* – en revisión.

Las ceramidas son un grupo de lípidos heterogéneo, se han descrito 15 subclases en humanos. Las ceramidas del SC se diferencian unas de otras por la arquitectura de su grupo cabeza y por la longitud de la cadena del ácido graso. Predominan las ceramidas con ésteres de ácido graso ω-hidroxi unidos a ácido linoleico y amida unida a esfingosina (ceramida 1, también denominada EOS). Ésta ceramida tiene un papel imprescindible en la organización característica de los lípidos del SC y por lo tanto en el mantenimiento de la función barrera de la piel.

El LBms debe su acción a su composición lipídica semejante a la del SC sano. En base a los resultados obtenidos en nuestros trabajos previos y el conocimiento del papel relevante de la CerEOS, en éste trabajo, se incluyó la CerEOS en el LBms con el objetivo que este sistema sea capaz de reparar en mayor medida la estructura lipídica del SC.

Se incluyó la CerEOS tanto en estructuras discoidales (discos CerEOS) como en el LBms (LBms CerEOS). Estos sistemas se compararon con los descritos en el trabajo 1, que incluían Cer3b. Los discos CerEOS presentaron una gran variabilidad de tamaños y en general tenían un diámetro mayor que los discos Cer3b. El LBms EOS al igual que el que incluye Cer3b, está formado por vesículas que encapsulan estructuras discoidales y discos no encapsulados. Sin embargo, este sistema también presentó tubos multilaminares no observados en el LBms Cer3b.

En este trabajo también se estudió el efecto de los sistemas lipídicos sobre la permeabilidad de SC deslipidizado utilizando celdas de Franz. Para ello se trató SC humano previamente deslipidizado con discos CerEOS, LBms CerEOS o vesículas (estructura externa del LBms). Se estudió el perfil de penetración de la teofilina y la pérdida de agua transepidérmica. El SC deslipidizado presentó un flujo de teofilina y una pérdida de agua mayores que el SC sano. Después del tratamiento con discos CerEOS o vesículas se redujo el flujo de teofilina pero la pérdida de agua no varió. Sin embargo después del tratamiento con el LBms CerEOS, el flujo de teofilina se redujo en mayor medida hasta alcanzar un valor similar al del SC sano y la pérdida de agua se redujo significativamente. Esto indica que el sistema repara la barrera cutánea.

Finalmente se comparó el efecto del tratamiento con LBms CerEOS con el que incluye Cer3b (artículo 1) o una mezcla de las dos ceramidas. El estudio de permeabilidad demostró que los sistemas que incluyen CerEOS mejoran la función barrera en mayor medida que el que incluye solo la Cer3b. Este hecho se correlaciona bien con el papel crucial descrito para la CerEOS en el SC.

Delivery systems with omega-*O*-acylceramide repair perturbed human stratum corneum

V. Moner[1]; L. Opálka[2]; K. Vavrová[2] and O. López[1]

[1] Institute of Advanced Chemistry of Catalonia (IQAC-CSIC), Barcelona, 08034, Spain.

[2] Skin Barrier Research Group, Charles University, Faculty of Pharmacy, Hradec Králové, 50005, Czech Republic.

Keywords: defective epidermal barrier, skin lipids, acylceramide, ceramide, lamellar body mimetic system, permeability

Abstract

Skin diseases such as atopic dermatitis, psoriasis, and ichthyoses have dysfunctional epidermal lamellar bodies and, consequently, impaired permeability barrier. Ceramide (Cer) subclasses with omega-hydroxylated ultra-long acyl chains and linoleic acid esterified to the omega-hydroxyl, also named acylceramides (acylCer) are essential for the organization and barrier function of the skin lipids. The aim of this study was to evaluate the barrier repair effects of nanostructured lipid systems containing the most abundant acylCer subclass, Cer EOS. The lipids were formulated into disks and systems that mimic the epidermal lamellar bodies and applied on solvent-extracted human stratum corneum with various degrees of barrier damage. The *in vitro* permeability experiments showed that the lamellar body mimetic system containing Cer EOS can recover 48% of water loss and completely restore the barrier to the flux of a model permeant theophylline. These delivery systems provided stronger barrier recovery than disks with Cer EOS, Cer EOS suspension or lamellar body mimetic systems with Cer3b. Thus, Cer EOS can be successfully incorporated in nanostructured lipid systems and delivered into perturbed skin. We propose the lamellar body mimetic system with Cer EOS as a novel therapeutic strategy for the treatment of skin barrier disorders.

1. Introduction

Stratum corneum (SC) extracellular domain is filled with a lipid-enriched lamellar structure, which is essential for the functional skin permeability barrier (Elias et al., 1977). This lipid matrix consists of an approximately equimolar mixture of ceramides (Cer), free fatty acids, and cholesterol (Chol), along with a minor amount of cholesteryl sulfate (SChol). These lipids are delivered to the SC through specialized organelles called lamellar bodies. The lamellar bodies are vesicles responsible for the transport, accumulation, and secretion of the SC lipid precursors and enzymes that eventually process these lipids at the stratum granulosum/SC interface. The lipids released from the precursors then fill the extracellular SC spaces and form the skin permeability barrier (Feingold and Elias, 2014). Several skin diseases, such as atopic dermatitis, psoriasis, and ichthyoses have dysfunctional epidermal lamellar bodies and, consequently, defective skin permeability barrier (Elias and Wakefield, 2014; Fartasch et al., 1999; Ghadially et al., 1996). The reduced skin barrier function is manifested by an increased transepidermal water loss (TEWL), disorganized SC lipid structure and aberrant keratinocyte differentiation (Amen et al., 2013).

Cer are the dominant permeability barrier lipids, constituting 50% of the SC lipids by weight. SC Cer are a structurally heterogeneous group: 15 subclasses of SC Cer have so far been identified in humans (Rabionet et al., 2014). AcylCer are a unique epidermal Cer subclass essential for the skin barrier. In acylCer, the *N*-acyl chain is composed of ω-hydroxylated ultra-long chain fatty acid esterified at the ω-position with linoleic acid (Breiden and Sandhoff, 2014). Major defects in acylCer biosynthesis lead to neonatal death due to an enormous TEWL (Jennemann et al., 2011). Recently, it has been discovered that PNPLA1 (patatin-like phospholipase domain-containing 1), an enzyme expressed in differentiated keratinocytes, plays a crucial role in the biosynthesis of acylCer (Hirabayashi et al., 2017; Ohno et al., 2017; Pichery et al., 2017). In addition to their essential function in the lipid lamellae formation, acylCer are also important as the precursors of protein-bound Cer in the corneocyte lipid envelope, which connect lipid lamellae and corneocytes (Wertz and Downing, 1987; Zheng et al., 2011). The topical application of acylCer has a promising potential in an adjuvant therapy in the skin barrier-related diseases, which is documented in a recent report (Mauldin et al., 2018).

The broader use of acylCer in research or therapy has been hampered by the commercial unavailability of these lipids and their extremely low solubility, which makes their efficient delivery to the skin a challenge. Recently, we have reported an efficient and scalable synthesis of acylCer (Opálka et al., 2015). Here, we aim to address

the latter point by formulating these lipids, namely a sphingosine-based acylCer, Cer EOS, into nanostructured delivery systems.

In our previous work, we designed a lipid system that mimics epidermal lamellar bodies in their morphology and structure: The lamellar body mimetic system (LBms) (Moner et al., 2016). This system consists of discoidal lamellar structures encapsulated into vesicles. The LBms contained Cer3b, stearic acid (SA), Chol, SChol and cholesteryl palmitate (EChol) in a ratio similar to human SC lipid composition. Studies of grazing-incidence small-angle X-ray scattering (GISAXS) and electron microscopy demonstrated that this lipid system can re-establish a substantial part of the lipid lamellar structure of delipidated SC (Moner et al., 2016). Additionally, treatment with this system improved the skin condition in an oxazolone-induced dermatitis mouse model by reinforcing the skin barrier function and reducing the skin inflammation (Moner et al.).

Based on the above results and the fact that acylCer are critical lipids that mediate the permeability barrier, we proposed to incorporate the acylCer EOS in the LBms with the aim to improve the barrier repair potency of the previous system. In this study, two different lipid system types (disks or LBms) were prepared. These systems were characterized by dynamic light scattering (DLS) to determine their size and by cryogenic transmission electron microscopy (cryo-TEM) in order to visualize their structure and morphology. The prepared LBms containing acylCer EOS was applied on a human SC *in vitro* with various degrees of barrier perturbation to simulate various skin barrier disorders. The effects of this formulation were compared to the treatment with disks containing Cer EOS, empty vesicles (LBms shells) and Cer EOS suspension. Moreover, the effect of LBms containing Cer EOS was compared to particles with the same nanostructure but different Cer content: LBms with Cer3b, and LBms with a 9:1 mixture of Cer3b/Cer EOS. The barrier function was assessed using two permeability markers: the flux of theophylline as a model exogenous permeant and water loss through the SC.

2. Materials and methods

2.1. Materials

1,2-Dipalmitoyl-sn-glycero-3-phosphocholine (DPPC) and 1,2-dihexanoyl-sn-glycero-3-phosphocholine (DHPC) were supplied from Avanti Polar Lipids (Alabaster, USA). Cholesterol from lanolin (Chol), cholesteryl sulfate sodium salt (SChol), cholesteryl

palmitate (EChol), stearic acid (SA), trypsin, propylene glycol (PG), theophylline (TH), sodium phosphate dibasic dodecahydrate, gentamicin, chloroform ($CHCl_3$), ethanol (EtOH) and methanol (MeOH) were purchased from Sigma-Aldrich (Schnelldorf, Germany). Ceramide IIIb (oleoyl phytosphingosine, Cer3b) was generously provided by Evonik (Essen, Germany). Acylceramide EOS (*N*-(32-linoleoyloxydotriacontanoyl)-sphingosine, acylCer EOS) was prepared according to a published procedure (Opálka et al., 2015). Lipoid S100, whose main component (>94%) is soybean phosphatidylcholine (PC) and Lipoid S LPC 80 whose main component (80%) is soybean lysophosphatidylcholine (lysoPC) were supplied from Lipoid GmbH (Ludwigshafen, Germany). Water was purified using a Milli-Q system (Merck Millipore, Billerica, USA).

2.2. Preparation of the lipid systems

First, discoidal structures were prepared according to a published procedure (Moner et al., 2016). Five types of discoidal structures based on DPPC/DHPC in 3.5 molar ratio, including the following additives were prepared: 10 mol% Cer3b (Disks Cer3b), 5 mol% EOS (Disks EOS), 5 mol% Chol (Disks Chol), 5 mol% SChol (Disks SChol), 5 mol% EChol (Disks EChol). For each system, appropriate amounts of lipids were mixed in $CHCl_3$ and evaporated to dryness with a rotary evaporator. The total lipid concentration of each lipid system was 10% (w/v). Then, different volumes of these samples were selected to obtain a mixture in which the molar ratio of Cer, Chol, SChol and EChol was similar to that found in the skin (Wertz, 2000).

To prepare the empty vesicles (LBms shells) and LBms, chloroform solutions of 95 mg/ml PC, 5 mg/ml lysoPC and 1.6 mg/ml SA were mixed and rota-evaporated to remove the chloroform. The lipid film was hydrated with H_2O to prepare the empty vesicles or with a mixture of pre-formed discoidal structures (Moner et al., 2016) to prepare the LBms. The total lipid concentrations in the empty vesicles and LBms were 10% and 20% (w/v), respectively. Three different LBms were prepared with the final Cer/SA/Chol/SChol/EChol molar ratio of 1:1:0.5:0.1:0.04, where the Cer was Cer3b (LBms Cer3b), Cer EOS (LBms EOS), and a 1:9 (v/v) mixture of Cer EOS:Cer3b (LBms EOS-Cer3b). Additionally, a suspension of Cer EOS in PG/EtOH (7:3, v/v) was prepared as a control with the final Cer EOS concentration being 3.7 mg/ml, same as in the LBms EOS.

2.3. Dynamic light scattering (DLS)

The DLS technique measures the diffusion coefficient of the particles corresponding to their Brownian motion, which is converted to size by the Stokes–Einstein equation (Edwards and Baeumner, 2006). Particle size distribution was measured with a

Zetasizer Nano ZS (Malvern Instruments, Malvern, UK). Refractive index of the medium and viscosity of the sample were approximated to the respective water values. Particle sizes were determined from the scattered light that was detected at an angle of 173° when a laser beam of wavelength 633 nm crossed the sample. Measurements were performed in triplicate at 25 °C.

2.4. Cryogenic transmission electron microscopy (Cryo-TEM)

The lipid systems were visualized by cryo-TEM. A thin, aqueous sample film was formed by dipping a glow-discharged holey carbon grid in the lipid suspension and then blotting the grid against a filter paper. The resulting thin sample film spanning the grid holes was vitrified by plunging the grid into ethane, which was maintained at its melting point with liquid nitrogen, by the use of a Vitrobot (FEI Company, Eindhoven, Netherlands). The vitreous sample film was transferred to a Tecnai F20 TEM (FEI Company, Eindhoven, Netherlands) by the use of a cryotransfer holder (Gatan, Barcelona, Spain), and the sample was observed in low-dose mode. Images were acquired at 200 kV at a temperature between -170 °C and -175 °C, under low-dose imaging conditions. Five overviews and 30 detailed electron micrographs of each sample were taken.

2.5. Isolation of the human SC

The human abdominal skin was obtained from Caucasian women (age 40 ± 10 years), who had undergone plastic surgery. The procedure was approved by the Ethics Committee of the First Private Surgical Center Sanus, Hradec Králové, Czech Republic, and was conducted according to the Declaration of Helsinki Principles.

The SC for each experiment was obtained from a single donor and was isolated using a modified procedure described by Kligman and Christophers (Kligman and Christophers, 1963). Human skin was immersed in 60 °C Milli-Q water for 2 min and the epidermis was peeled off using tweezers. Then, the epidermis was incubated overnight at 32 °C with the basal layer facing downward in a solution of 0.5 % trypsin in phosphate-buffered saline (PBS) at pH 7.4 with 50 mg/L gentamicin. The residual epidermis cells were gently removed from the SC using cotton swabs. The SC was washed several times in Milli-Q water, once briefly in acetone to remove surface lipids, and finally with PBS.

2.6. Delipidation of the SC

The SC was immersed in a Petri dish filled with a $CHCl_3$/MeOH solution (2:1 v/v) for different time periods (2 h, 15 min or 5 min). Afterward, the SC was washed several times with PBS buffer, cut into 1.5 × 1.5 cm pieces, immediately placed on supporting 0.45 μm nylon membrane disks (Thomas Scientific, Swedesboro, USA), and mounted in Teflon holders with a diffusion area of 1 cm^2 for permeability experiments.

2.7. Permeation experiments

Franz diffusion cells with an acceptor volume of 6.6 ± 0.4 ml (the precise volume was measured for each cell and was included in the flux calculation) were used for the permeability experiments. Control and delipidated SC pieces fixed in Teflon holders were mounted in the cells with the SC facing the donor compartment. The acceptor compartment was filled with PBS at pH 7.4 with 50 mg/L of gentamicin, and the assembled cells were equilibrated at 32 °C for 12 h.

The delipidated SC samples were treated with 100 μl of disks EOS, empty vesicles, different LBms, and Cer EOS suspension for 12 h. After 12 h, any systems remaining on the SC surface were removed by washing twice with 0.5 ml of PBS. Then, the SC samples were equilibrated at 32 °C for 2 h; and then the SC water loss was measured (see below).

Next, 200 μl of 5% TH in 60% PG was applied on the SC. Samples of the acceptor phase (300 μl) were collected every 15 min during the first hour and then every hour over 5 h. The removed volume was always replaced with the same amount of fresh acceptor solution (PBS).

2.8. Water loss

The water loss through the SC was measured using Aqua Flux model AF200 (Biox Systems Ltd, London, U.K.). The probe was placed on top of the Teflon holder (after the donor part of the cell was temporarily removed). The measuring time was approximately 1 min until the steady-state was reached, and the average steady-state value (g/h/cm^2) was recorded. The measurements were repeated twice and were carried out at 25-27°C and 27-35% relative humidity.

2.9. HPLC

The collected samples from the TH permeation experiments were analyzed using isocratic reverse-phase HPLC using a Shimadzu Prominence instrument (Shimadzu,

Kyoto, Japan) consisting of LC-20AD pumps with a DGU-20A3 degasser, SIL-20A HT autosampler, CTO-20AC column oven, SPDM20A diode array detector, and CBM-20A communication module. Data were analyzed using the LCsolution 1.22 software. Reverse-phase separation of TH was achieved on a LiChroCART 250-4 column (LiChrospher 100 RP18, 5um, Merck, Darmstadt, Germany) at 35 °C using 4:6 methanol/0.1 M NaH_2PO_4 (v/v) as a mobile phase at a flow rate of 1.2 ml/min. An acceptor-phase sample (20 µl) was injected into the column, and the UV absorption of the effluent was measured at 272 nm, with a bandwidth of 4 nm.

2.10. Data treatment

The cumulative amounts of TH that penetrated through the SC were calculated from the concentration measured using HPLC and the Franz cell volume and were corrected for the acceptor-phase replacement. The cumulative amounts were plotted against time, and the steady-state flux of TH (µg/cm²/h) was calculated as the slope obtained using Microsoft Excel. All data are presented as the mean with the standard error of the mean (SEM). One-way analysis of variance (ANOVA) or *t*-test as indicated in the pertinent figures was used for statistical analysis, and $p < 0.05$ was considered significant.

3. Results

3.1. Characterization of the lipid systems

The particle size distribution of the studied lipid systems was determined by DLS (Table 1). The DPPC/DHPC structures containing Cer3b were approximately 13 nm in diameter. When Cer3b was replaced with Cer EOS, the system showed two particle sizes around 40 nm and 430 nm in diameter. Similar particle sizes were detected for the LBms containing CerEOS, Cer3b or a mixture of Cer EOS-Cer3b as well. All three LBms systems showed two peaks corresponding to a population of large particles with sizes between 380-460 nm that scattered 80% light and a population of small particles between 30-40 nm that scattered 20% light. Therefore, the change in composition related to Cer in the LBms does not affect the particle size. Concerning the empty vesicles, only one peak at approximately 220 nm was observed.

The morphology of the lipid systems (DPPC/DHPC structures containing Cer3b or Cer EOS, empty vesicles and LBms EOS) was studied by cryo-TEM. Fig. 1.A shows a representative image of the DPPC/DHPC structures with Cer3b. This micrograph

shows that these structures are disks with uniform size around 13-18 nm in diameter. The DPPC/DHPC structures with Cer EOS (Fig. 1.B) are also disk-shaped with diameter ranges from 40 to 260 nm corresponding to small disks and large disk-like sheets. Some disks are folded due to their large size, which is indicated by an arrowhead. Both discoidal structures containing Cer3b or Cer EOS are observed in edge-on (white open arrow) and face-on (white close arrow) disposition. Fig. 1.C shows a representative image of the LBms EOS. This image shows vesicles encapsulating disks (black arrow) with sizes from 85 to 210 nm and non-encapsulated disks (white arrow) with size from 35 to 80 nm. Therefore, although the lipid systems DPPC/DHPC containing Cer EOS (Fig. 1.B) and LBms EOS (Fig. 1.C) showed two particle populations with similar size by DLS, the cryo-TEM shows that these systems are formed by different structures. The morphology of the LBms EOS was found to be similar to the LBms Cer3b characterized in our previous work (Moner et al., 2016) with a single difference, that the LBms EOS also formed multilamellar tubules (indicated by an asterisk), which were not found in the LBms Cer3b. Finally, the sample containing empty vesicles is shown in Fig. 1.D. This image confirms the DLS results and shows vesicles (black close arrow) with sizes from 70 to 270 nm.

3.2. The effects of the studied lipid systems on the permeability of delipidated SC

The permeability of delipidated SC after the treatments with disks EOS, LBms EOS and empty vesicles (external shell of the LBms) was studied using water loss and permeability to TH as a model permeant (Fig. 2). Two controls were used: untreated normal SC and SC treated with a simple suspension of Cer EOS in PG/EtOH (7:3, v/v) to distinguish between the effects of free Cer EOS or Cer EOS included in the lipid systems.

The isolated human SC was delipidated using the mixture of $CHCl_3$/MeOH (2:1 v/v) for different times (2 h, 15 min or 5 min) to create various degrees of barrier disruption. Fig. 2.A shows the permeabilities of the SC delipidated for 2 h. The TH flux through the native control SC was 2.9 ± 2.0 μg/cm²/h. After SC delipidation for 2 h, the TH flux increased by two orders-of-magnitude to 455.3 ± 89.8 μg/cm²/h. The treatments of the delipidated SC with disks EOS, LBms EOS, empty vesicles and Cer EOS in suspension decreased the TH flux values to 287.5 ± 49.3 (not significant compared to delipidated control), 137.9 ± 44.4 (significant at $p < 0.001$, ANOVA), 401.0 ± 47.6 (not significant) and 321.8 ± 66.8 μg/cm²/h (not significant), respectively. The water loss of native untreated SC was 20.6 ± 1.4 g/m²/h, and the 2-h delipidation increased this value significantly to 104.4 ± 0.9 g/m²/h. The water loss values after the treatment of

delipidated SC with disks EOS, LBms EOS, empty vesicles and Cer EOS in suspension decreased to 101.1 ± 0.6 ($p < 0.05$ compared to delipidated control, t-test), 97.7 ± 1.6 ($p < 0.05$, ANOVA), 105.9 ± 0.4 (not significant) and 100.8 ± 0.3 g/m²/h ($p < 0.05$, t-test), respectively. For both permeability markers, the best result was achieved using the LBms particles containing Cer EOS.

Similar trends were observed in the SC that was delipidated for 15 min (Fig. 2.B). This delipidation time resulted in a considerable damage to the barrier, which was only slightly less pronounced compared to the 2-h delipidation procedure. The TH flux through the native control was 2.8 ± 1.1 μg/cm²/h and increased upon delipidation to 245.0 ± 29.0 μg/cm²/h. The treatments of the delipidated SC with disks EOS, LBms EOS, empty vesicles and EOS in suspension resulted in a decrease in TH flux to 149.0 ± 23.4 ($p < 0.05$ compared to delipidated control, ANOVA), 33.0 ± 15.5 ($p < 0.0001$, ANOVA), 196.0 ± 94.0 (not significant) and 205.7 ± 31.0 μg/cm²/h (not significant), respectively. The water loss of the native SC in this experiment was 23.0 ± 1.6 g/m²/h and it increased after the delipidation to 93.7 ± 1.3 g/m²/h. The treatments of the delipidated SC with disks EOS, LBms EOS, empty vesicles and EOS in suspension resulted in the water loss values of 95.1 ± 1.5 (not significant compared to delipidated control), 84.8 ± 3.0 ($p < 0.05$, t-test), 91.8 ± 4.5 (not significant) and 88.5 ± 5.8 g/m²/h (not significant), respectively.

Fig. 2.C shows the results of the last experiment using SC delipidated for 5 min. This delipidation had only mild (but significant) disrupting effect on the SC barrier as judged by the two studied markers. In this experiment, the TH flux values through the native and delipidated SC were 2.8 ± 1.3 μg/cm²/h and 15.8 ± 5.8 μg/cm²/h, respectively. The TH flux was again reduced by the treatment of delipidated SC with the different lipid systems to 6.9 ± 1.6 (disks EOS, not significant compared to delipidated control), 1.1 ± 0.3 (LBms EOS, $p < 0.05$, ANOVA), 7.5 ± 2.5 (empty vesicles, not significant) and 5.2 ± 1.0 μg/cm²/h (Cer EOS suspension, not significant). The water loss increased from 14.6 ± 1.7 g/m²/h of the native SC to 41.9 ± 4.2 g/m²/h after delipidation, and then decreased after the treatments with the lipid systems to 36.7 ± 3.6 (disks EOS, not significant compared to delipidated control), 28.7 ± 1.4 (LBms EOS, $p < 0.05$, ANOVA), 31.4 ± 43.4 (empty vesicles, not significant) and 33.8 ± 1.7 g/m²/h (Cer EOS suspension, not significant).

In order to compare the permeability results between all three experiments, the results were recalculated as a percent recovery Eq.(1) of TH flux (Table 2A) and water loss (Table 2B) of the treated SC compared to the delipidated control.

% Recovery = (Delipidated control - Treated SC) / (Delipidated control – Normal control) x 100

Eq.(1)

The best ability to repair the damaged SC was found for LBms EOS, which led to the almost full recovery of the barrier function in both the 15-min and 5-min delipidated SC. In the completely delipidated SC (2-h delipidation), the barrier recovery still reached 70%. The effects of other studied lipid systems were much weaker compared to LBms EOS. These results also indicate that the time of delipidation (and, consequently, the amount of residual SC barrier lipids) plays an important role in the recovery, as the greatest reduction in the TH flux after the treatment with lipid systems was found in the mildly damaged SC delipidated for 5 min. Similar trends were observed for the water loss (Table 2B): In the SC delipidated for 5 min, the treatment with the LBms EOS recovered almost 50% of the original water barrier, whereas in the SC delipidated for 2 h or 15 min, the effects of this formulation were only minor (8 – 13%).

3.3. Comparison of the barrier repair effects of the LBms with Cer3b and Cer EOS

To compare the barrier recovery potencies of Cer EOS and Cer3b, LBms containing Cer EOS, Cer3b or a 1:9 mixture of Cer EOS-Cer3b were prepared. The effects of these systems on the permeability of the SC perturbed by a 5-min delipidation were assessed using the same permeability markers: flux of TH and water loss through the SC (Fig. 3). LBms Cer3b apparently but not significantly reduced TH flux from 15.8 ± 5.8 μg/cm²/h in the delipidated control to 8.3 ± 3.3 μg/cm²/h upon treatment. Replacement of 10% Cer3b in this system by Cer EOS (that is, Cer EOS/Cer3b in a 1:9 ratio) resulted in a significant decrease in TH flux to 2.5 ± 0.5 μg/cm²/h. Although this permeability to TH was not as low as for the LBms that contained 10 times higher concentration of Cer EOS (1.1 ± 0.3 μg/cm²/h), it was not different from the native SC before delipidation (2.8 ± 1.3 μg/cm²/h).

A similar trend was found for water loss (Fig. 3.B). Treatment of the delipidated SC control (41.9 ± 4.2 g/m²/h) with LBms EOS, LBms Cer3b and LBms EOS-Cer3b, decreased the water loss to 28.7 ± 1.4 ($p < 0.05$ compared to delipidated control, ANOVA), 36.5 ± 3.9 (not significant) and 32.7 ± 1.8 g/m²/h (not significant), respectively. Thus, LBms EOS is the most effective system for repairing the disrupted water barrier under the experimental conditions used here.

4. Discussion

4.1. Influence of Cer EOS on the parameters of the studied lipid systems

In our previous work, we designed a lipid system, LBms, that mimicked the structure and morphology of epidermal lamellar bodies, which are lipid bilayer vesicles from the trans-Golgi network, necessary for the transport of barrier lipid precursors to the SC extracellular spaces (Fartasch et al., 1993). A mixture of Cer3b, SA, Chol, SChol and EChol approximating the SC lipid composition was used to construct this lipid system (Moner et al., 2016). Cer, in particular the subgroup of acylCer (*e.g.*, Cer EOS), are essential components of the skin permeability barrier. AcylCer are crucial for the formation of the corneocyte lipid envelope that anchors the free SC lipids to keratinocytes (Moore and Rawlings, 2017) and for the formation of the long periodicity lamellar phase (Bouwstra et al., 1998); both these structural features are necessary to prevent excessive TEWL and entry of potentially harmful environmental substances. Defects in the acylCer synthesis are related to several skin disorders, such as atopic dermatitis, psoriasis or ichthyoses (Di Nardo et al., 1998; Motta et al., 1993; Paige et al., 1994). Therefore, in this study, we included Cer EOS in our LBms systems to probe the barrier repair effects of such systems using artificially damaged human SC.

Although samples containing discoidal structures are usually transparent under visual inspection, in this study, the sample containing disks EOS was slightly translucent probably due to the presence of large disks or sheets in addition to small disks. Cer EOS may not be homogenously distributed in each of the structures, which might explain the variety of disks present in this system. The sample containing disks Cer3b was transparent and formed by homogeneous small disks only, which indicates that the incorporation of Cer with different acyl chain lengths (50C in Cer EOS and 18C in Cer3b) in the discoidal structures significantly affects their size. Regarding the LBms containing Cer EOS or Cer3b both systems were formed by vesicles encapsulating disks and non-encapsulated disks. Interestingly, the cryo-TEM image of the LBms EOS showed multilamellar tubules that were not observed before in the LBms Cer3b. DLS results showed that some disks EOS are larger than the vesicles; thus, the encapsulation of these structures during the formation of the LBms EOS would not be possible. We suggest that these disks rich in Cer EOS could have mixed with other lipids during the LBms preparation forming the multilamellar tubules. The formation of tubular structures after the inclusion of very long chain Cer in phosphatidylcholine model membranes was described before, and likely arose from the ability of very long chain Cer to interdigitate (Pinto et al., 2011). The tubular structures observed by cryo-TEM could be identified as large particles affecting the hydrodynamic diameter

measured by DLS, which could explain the discrepancies in size estimation using those techniques.

4.2. Effect of the studied lipid nanostructures on the permeability of delipidated SC

Next, permeability experiments were conducted to investigate the effects of the treatment of the delipidated SC with disks EOS, LBms EOS, empty vesicles, and Cer EOS in suspension. The TH flux and water loss through the SC were used as the permeability markers. TH with its small molecule and balanced hydrophilic/lipophilic character has been used as a permeability marker in previous studies (Opálka et al., 2016; Vavrova et al., 2007; Yoshiike et al., 1993), and the measurement of water loss is commonly used to assess the skin barrier integrity (Nangia et al., 1998; Werner and Lindberg, 1985).

It has been described that skin delipidation with $CHCl_3$/MeOH (2:1, v/v) mixtures alters the SC lipid composition or organization (Barba et al., 2016), resulting in a decreased or lost barrier function. The degree of barrier perturbation correlates with the number of lipids removed. Intact SC is characterized by a low water loss, which generally does not exceed 25 g/m²/h. A severe damage to the SC, such as tape stripping, results in water loss values of 70-100 g/m²/h (Kalia et al., 2000). In our study, after 2-h or 15-min delipidation, the water loss through the SC reached values of 90-105 g/m²/h indicating that the barrier function was severely damaged. After the 5-min delipidation, the water loss was 40 g/m²/h, which is close to the values found in patients with atopic dermatitis (approximately 34-54 g/m²/h) (Angelova - Fischer et al., 2005).

Our results showed that the barrier repair effects of the lipid systems (as judged by the two studied permeability markers) were the strongest on the SC delipidated for 5-min (compared to 2-h or 15-min delipidation). We speculate that the remaining lipids after a short delipidation course may provide a template for the multilamellar arrangement of the topically added lipids. 2-h delipidation likely removed higher amount of SC lipids, although it is not enough to completely remove the free SC lipids and the lipids covalently bound to corneocyte. To extract the free lipids exhaustively, a succession of $CHCl_3$/MeOH mixtures (2:1, 1:1 and 1:2 v/v) for longer time is commonly used (López et al., 2001; Swartzendruber et al., 1987). Alternatively, longer exposure of SC to the potent solvent mixture may result in an additional damage than just simple lipid extraction (Abrams et al., 1993). In contrast, the 5-min delipidation likely removed a smaller fraction of lipids causing a partial disruption of the SC lamellar structure without compromising the barrier completely. The remaining SC lipids likely facilitated

the relipidation effects of the lipid systems leading to the most pronounced improvement of the SC permeability.

Previous studies described that vesicles do not penetrate through the SC extracellular spaces due to their large size and that they only act on the skin surface (Dreier et al., 2016). However, we observed a marked improvement of the repair effects of Cer EOS incorporated in the LBms compared to that in the disks. Thus, the external coating structures of the LBms (vesicles) likely interact only with the skin surface, where they may increase the partitioning of their cargo into the SC. Indeed, empty vesicles did not result in a significant barrier repair. As described above, disks EOS contain both small and large discoidal structures. The smaller disks could penetrate through the narrow spaces of the SC (6-10 nm) due to their size and discoidal morphology and mix with the lipids of this tissue leading to a reinforcement of the barrier function (Barbosa - Barros et al., 2012). The penetration of larger disks is not expected in their intact form (or at least their penetration would be much more difficult). The LBms combines the advantages of the discoidal structures (non-encapsulated disks) and vesicles (also containing disks), promoting a barrier repair effect of this system that, in the case of the LBms EOS result in a complete recovery of the TH flux and a significantly decreased water loss. This double system may act in two stages: first, the non-encapsulated disks penetrate through the SC spaces, and second, the vesicles fuse with the SC surface to release the encapsulated disks (Fernández et al., 2015). These released disks then also penetrate the SC and mix with the residual lipids of this tissue. As this LBms system was designed to mimic the SC lipid composition (it contains Cer EOS, SA, Chol, SChol and EChol), the effects of LBms EOS on the skin likely result from a combination of their morphology, structure and lipid composition.

4.3. Effect of LBms with different Cer on the permeability of 5-min delipidated SC

GISAXS and electron microscopy previously demonstrated that LBms Cer3b re-established a part of the lipid lamellar structure of delipidated SC (Moner et al., 2016). The *in vivo* treatment with LBms Cer3b reinforced the skin barrier function and reduced the skin inflammation in an oxazolone-induced dermatitis mouse model (Moner et al.). We confirmed here that the treatment with the LBms Cer3b partly restored the damaged SC barrier function, which is in agreement with our previous work. This barrier repair effect was even more pronounced with the treatment with LBms EOS or LBms EOS-Cer3b, where the flux of TH normalized to values comparable to normal SC before delipidation and the water loss through the treated SC was

markedly reduced. Therefore, the systems comprising Cer EOS are more effective in repairing damaged SC than LBms based on Cer3b alone.

The Cer incorporated in these three LBms affected their structure. The LBms EOS partly formed multilamellar tubules that were not found in the LBms Cer3b. It is possible that these tubular structures may also play a role in the observed barrier regeneration upon LBms EOS treatment along with the effect of Cer EOS on the lamellar arrangement of the SC lipids. Although further work is certainly needed, this proof-of-concept study showed that Cer EOS can be successfully incorporated in LBms and these systems have a strong potential to deliver lipids to perturbed SC. Furthermore, these LBms containing a naturally occurring human acylCer have an excellent barrier repair potency and could be beneficial in the treatment of skin disorders with a perturbed permeability barrier, such as atopic dermatitis or ichthyoses.

5. Conclusions

AcylCer are essential for the functional organization of lipids in the SC interstices, and thereby to maintain the barrier function of the skin. In this study, acylCer (Cer EOS) was incorporated into discoidal structures and LBms. The permeability study on the delipidated SC showed that the treatment with LBms EOS reduced water loss and abolished the increased flux of a model permeant. Thus, topical treatment with LBms EOS is a potentially useful approach to restoring the damaged SC barrier function, which may be fine-tuned in future to serve as a potential novel therapeutic strategy for the treatment of skin barrier disorders.

6. Acknowledgments

The authors would like to thank Evonik Industries for kindly providing the Cer3b and Lipoid GmbH for providing the PC and lysoPC. This work was supported by the project EFSA-CDN (No. CZ.02.1.01/0.0/0.0/16_019/0000841) co-funded by ERDF, the Czech Science Foundation (16-25687J), and the Spanish Ministry of Economy, Industry and Competitiveness (CTQ 2013-44998-P and RTC-2016-4957-1).

Figures

Figure 1. Cryo-TEM micrograph showing the morphology of the different lipid systems: (A) disks Cer3b, (B) disks EOS, (C) LBms EOS and (D) empty vesicles. The disks are observed in edge-on (white open arrows) and face-on (white closed arrows) disposition. The arrow head indicates a folded disk. The black open arrow indicates vesicles encapsulating disks while the black closed arrow indicates only empty vesicles. The asterisk indicates multilamellar tubules. Bar = 100 nm.

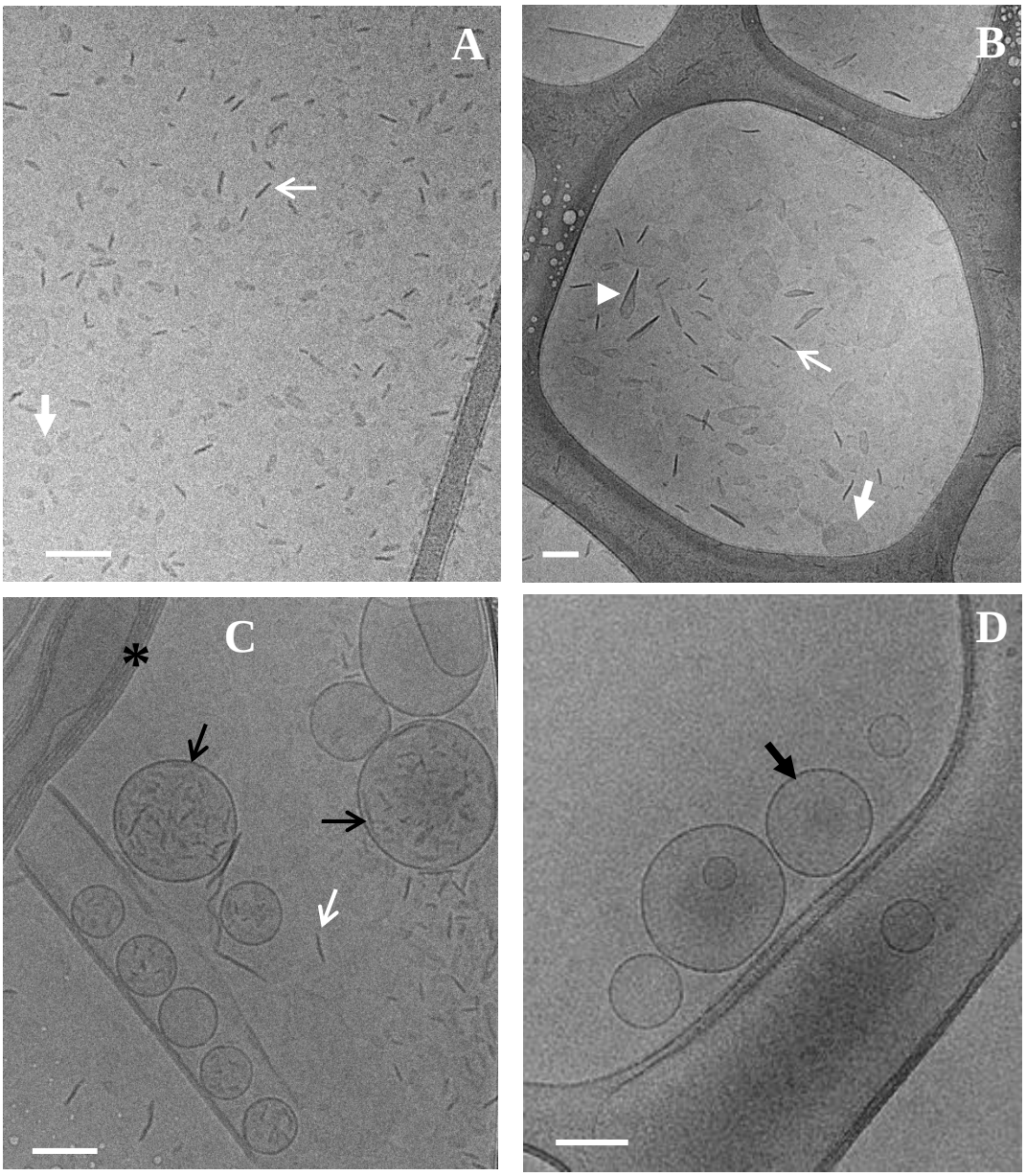

Figure 2. Permeability of human SC assessed by the steady-state flux of TH and water loss. (A) 2-h delipidation, (B) 15-min delipidation and (C) 5-min delipidation. Data are presented as means ± SEM; n = 6. Asterisks indicate statistically significant differences compared with delipidated control (second column) at $p < 0.05$ (*), $p < 0.01$ (**), $p < 0.001$ (***) and $p < 0.0001$ (****) using ANOVA. The symbol (#) indicates statistically significant differences compared with delipidated control at $p < 0.05$ using t-test.

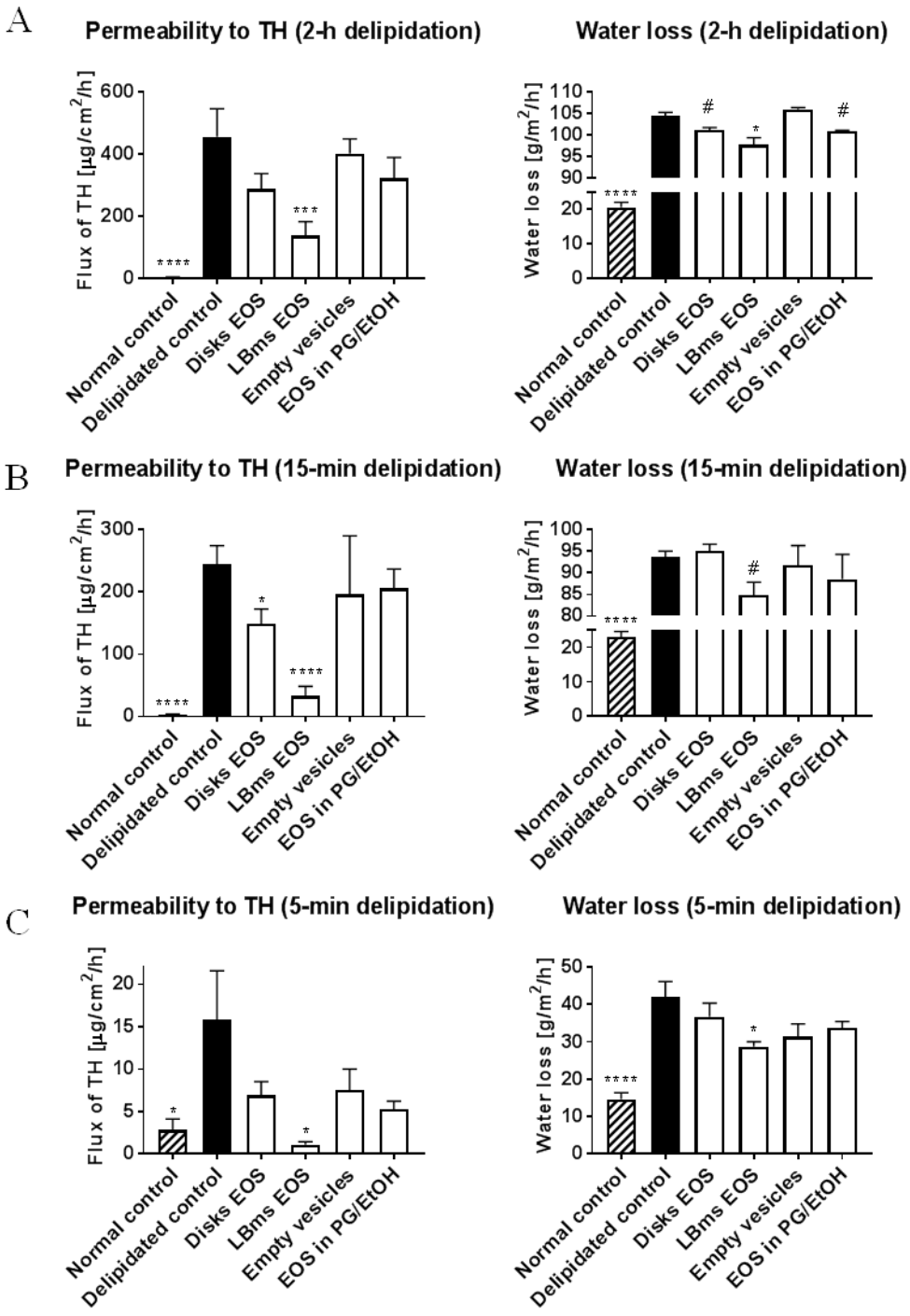

Figure 3. Permeability of human SC delipidated for 5 min treated with LBms EOS, LBms Cer3b and LBms EOS-Cer3b: (A) Steady-state flux of TH, (B) water loss through the SC. Data are presented as means ± SEM; n = 6. Asterisks indicate statistically significant differences compared with delipidated control (second column) at $p < 0.05$ (*) and $p < 0.0001$ (****) using ANOVA.

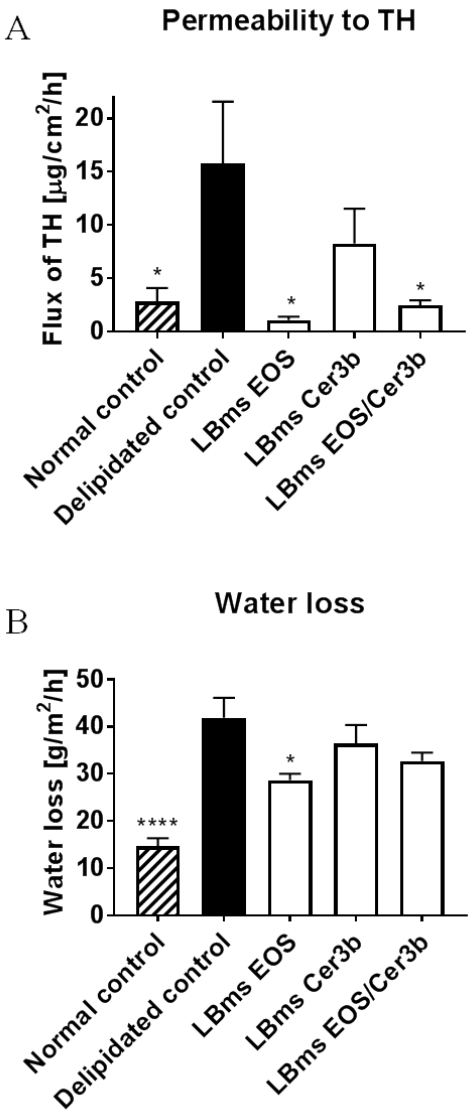

Table 1. Particle size distribution in terms of scattering intensity. The results are shown as means ± SEM; n = 3.

	Peak 1		**Peak 2**	
System	Size (nm)	% Intensity	Size (nm)	% Intensity
Disks Cer3b			13 ± 0.3	100
Disks EOS	429 ± 39	89 ± 3	41 ± 8	11 ± 3
LBms Cer3b	458 ± 16	81 ± 2	32 ± 6	19 ± 2
LBms EOS	414 ± 26	78 ± 2	43 ± 5	22 ± 2
LBms EOS-Cer3b	379 ± 12	77 ± 1	41 ± 2	23 ± 1
Empty vesicles	221 ± 22	100		

Table 2: Percent recovery in (A) flux of TH, (B) water loss through the SC after the treatments compared with delipidated control. % recovery = (Delipidated control - Treated SC with the studied systems) / (Delipidated control - Normal control) x 100

A

Delipidated SC	Disks EOS	LBms EOS	Empty vesicles	EOS in PG/EtOH
2 h	37.0	70.0	12.0	29.5
15 min	39.6	87.5	20.2	16.2
5 min	68.5	113.0	63.8	81.5

B

Delipidated SC	Disks EOS	LBms EOS	Empty vesicles	EOS in PG/EtOH
2 h	3.9	8.0	-0.7	4.3
15 min	-2.0	12.6	2.7	7.4
5 min	19.0	48.4	38.5	29.7

References:

Abrams, K., Harvell, J.D., Shriner, D., Wertz, P., Maibach, H., Maibach, H.I., Rehfeld, S., 1993. Effect of organic solvents on in vitro human skin water barrier function. Journal of investigative dermatology 101.

Amen, N., Mathow, D., Rabionet, M., Sandhoff, R., Langbein, L., Gretz, N., Jäckel, C., Gröne, H.-J., Jennemann, R., 2013. Differentiation of epidermal keratinocytes is dependent on glucosylceramide: ceramide processing. Human molecular genetics 22, 4164-4179.

Angelova-Fischer, I., Bauer, A., Hipler, U., Petrov, I., Kazandjieva, J., Bruckner, T., Diepgen, T., Tsankov, N., Williams, M., Fischer, T., 2005. The objective severity assessment of atopic dermatitis (OSAAD) score: validity, reliability and sensitivity in adult patients with atopic dermatitis. British Journal of Dermatology 153, 767-773.

Barba, C., Alonso, C., Marti, M., Manich, A., Coderch, L., 2016. Skin barrier modification with organic solvents. Biochimica et Biophysica Acta (BBA)-Biomembranes 1858, 1935-1943.

Barbosa‐Barros, L., Rodríguez, G., Barba, C., Cócera, M., Rubio, L., Estelrich, J., López‐Iglesias, C., de la Maza, A., López, O., 2012. Bicelles: lipid nanostructured platforms with potential dermal applications. Small 8, 807-818.

Bouwstra, J.A., Gooris, G., Dubbelaar, F., Weerheim, A., Ijzerman, A., Ponec, M., 1998. Role of ceramide 1 in the molecular organization of the stratum corneum lipids. J. Lipid Res. 39, 186-196.

Breiden, B., Sandhoff, K., 2014. The role of sphingolipid metabolism in cutaneous permeabilitybarrier formation. Biochim. Biophys. Acta Mol. Cell. Biol. Lipids 1841, 441-452.

Di Nardo, A., Wertz, P., Giannetti, A., Seidenari, S., 1998. Ceramide and cholesterol composition of the skin of patients with atopic dermatitis. Acta Derm.-Venereol. 78, 27-30.

Dreier, J., Sørensen, J.A., Brewer, J.R., 2016. Superresolution and Fluorescence Dynamics Evidence Reveal That Intact Liposomes Do Not Cross the Human Skin Barrier. PloS one 11.

Edwards, K.A., Baeumner, A.J., 2006. Analysis of liposomes. Talanta 68, 1432-1441.

Elias, P.M., Goerke, J., Friend, D.S., 1977. Mammalian epidermal barrier layer lipids: composition and influence on structure. J. Investig. Dermatol. 69, 535-546.

Elias, P.M., Wakefield, J.S., 2014. Mechanisms of abnormal lamellar body secretion and the dysfunctional skin barrier in patients with atopic dermatitis. J. Allergy Clin. Immunol. 134, 781-791 e781.

Fartasch, M., Bassukas, I., Diepgkn, T., 1993. Structural relationship between epidermal lipid lamellae, lamellar bodies and desmosomes in human epidermis: an ultrastructural study. British Journal of Dermatology 128, 1-9.

Fartasch, M., Williams, M.L., Elias, P.M., 1999. Altered lamellar body secretion and stratum corneum membrane structure in Netherton syndrome: differentiation from

other infantile erythrodermas and pathogenic implications. Arch. Dermatol. 135, 823-832.

Feingold, K.R., Elias, P.M., 2014. Role of lipids in the formation and maintenance of the cutaneous permeability barrier. Biochim. Biophys. Acta Mol. Cell. Biol. Lipids 1841, 280-294.

Fernández, E., Rodríguez, G., Cócera, M., Barbosa-Barros, L., Alonso, C., López-Iglesias, C., Jawhari, T., de la Maza, A., López, O., 2015. Advanced lipid systems containing β-carotene: stability under UV-vis radiation and application on porcine skin in vitro. Phys. Chem. Chem. Phys. 17, 18710-18721.

Ghadially, R., Reed, J.T., Elias, P.M., 1996. Stratum corneum structure and function correlates with phenotype in psoriasis. J. Invest. Dermatol. 107, 558-564.

Hirabayashi, T., Anjo, T., Kaneko, A., Senoo, Y., Shibata, A., Takama, H., Yokoyama, K., Nishito, Y., Ono, T., Taya, C., 2017. PNPLA1 has a crucial role in skin barrier function by directing acylceramide biosynthesis. Nat. Commun. 8, 14609.

Jennemann, R., Rabionet, M., Gorgas, K., Epstein, S., Dalpke, A., Rothermel, U., Bayerle, A., van der Hoeven, F., Imgrund, S., Kirsch, J., 2011. Loss of ceramide synthase 3 causes lethal skin barrier disruption. Hum. Mol. Genet., ddr494.

Kalia, Y.N., Alberti, I., Sekkat, N., Curdy, C., Naik, A., Guy, R.H., 2000. Normalization of stratum corneum barrier function and transepidermal water loss in vivo. Pharmaceutical research 17, 1148-1150.

Kligman, A.M., Christophers, E., 1963. Preparation of isolated sheets of human stratum corneum. Arch. Dermatol. 88, 702-705.

López, O., Cócera, M., Walther, P., Wehrli, E., Coderch, L., Parra, J.L., de la Maza, A., 2001. Effect of liposomes on delipidized stratum corneum structure: an 'in vitro'study based on high resolution low temperature scanning electron microscopy. Colloids and Surfaces A: Physicochemical and Engineering Aspects 182, 35-42.

Mauldin, E.A., Crumrine, D., Casal, M.L., Jeong, S., Opálka, L., Vavrova, K., Uchida, Y., Park, K., Craiglow, B., Choate, K.A., 2018. Cellular and Metabolic Basis for the Ichthyotic Phenotype in NIPAL4 (Ichthyin)–Deficient Canines. The American journal of pathology 188, 1419-1429.

Moner, V., Fernández, E., Calpena, A.C., Garcia-Herrera, A., Cócera, M., López, O., A lamellar body mimetic system for the treatment of oxazolone-induced atopic dermatitis in hairless mice. J. Dermatol. Sci., 172-179.

Moner, V., Fernández, E., Rodríguez, G., Cócera, M., Barbosa-Barros, L., de la Maza, A., López, O., 2016. Lamellar body mimetic system: an up-to-down repairing strategy of the stratum corneum lipid structure. Int. J. Pharm. 510, 135-143.

Moore, D.J., Rawlings, A.V., 2017. The chemistry, function and (patho)physiology of stratum corneum barrier ceramides. Int. J. Cosmetic Sci. 39, 366-372.

Motta, S., Monti, M., Sesana, S., Caputo, R., Carelli, S., Ghidoni, R., 1993. Ceramide composition of the psoriatic scale. Biochim. Biophys. Acta 1182, 147-151.

Nangia, A., Patil, S., Berner, B., Boman, A., Maibach, H., 1998. In vitro measurement of transepidermal water loss: a rapid alternative to tritiated water permeation for assessing skin barrier functions. International journal of pharmaceutics 170, 33-40.

Ohno, Y., Kamiyama, N., Nakamichi, S., Kihara, A., 2017. PNPLA1 is a transacylase essential for the generation of the skin barrier lipid ω-O-acylceramide. Nature Commun. 8, 14610.

Opálka, L., Kováčik, A., Maixner, J., Vávrová, K.i., 2016. Omega-O-acylceramides in skin lipid membranes: effects of concentration, sphingoid base, and model complexity on microstructure and permeability. Langmuir : the ACS journal of surfaces and colloids 32, 12894-12904.

Opálka, L., Kováčik, A., Sochorová, M., Roh, J., Kunes, J., Lenčo, J., Vávrová, K.i., 2015. Scalable Synthesis of Human Ultralong Chain Ceramides. Org. Lett. 17, 5456-5459.

Paige, D., Morse‐Fisher, N., Harper, J., 1994. Quantification of stratum corneum ceramides and lipid envelope ceramides in the hereditary ichthyoses. Brit. J. Dermatol. 131, 23-27.

Pichery, M., Huchenq, A., Sandhoff, R., Severino-Freire, M., Zaafouri, S., Opálka, L., Levade, T., Soldan, V., Bertrand-Michel, J., Lhuillier, E., 2017. PNPLA1 defects in patients with Autosomal Recessive Congenital Ichthyosis and KO mice sustain PNPLA1 irreplaceable function in epidermal omega-O-acylceramide synthesis and skin permeability barrier. Hum. Mol. Genet.

Pinto, S.N., Silva, L.C., Futerman, A.H., Prieto, M., 2011. Effect of ceramide structure on membrane biophysical properties: the role of acyl chain length and unsaturation. Biochim.Biophis. Acta Biomembr. 1808, 2753-2760.

Rabionet, M., Gorgas, K., Sandhoff, R., 2014. Ceramide synthesis in the epidermis. Biochim. Biophys. Acta Mol. Cell. Biol. Lipids 1841, 422-434.

Swartzendruber, D.C., Wertz, P.W., Madison, K.C., Downing, D.T., 1987. Evidence that the corneocyte has a chemically bound lipid envelope. Journal of Investigative Dermatology 88, 709-713.

Vavrova, K., Hrabalek, A., Mac‐Mary, S., Humbert, P., Muret, P., 2007. Ceramide analogue 14S24 selectively recovers perturbed human skin barrier. Br. J. Pharmacol. 157, 704-712.

Werner, Y., Lindberg, M., 1985. Transepidermal water loss in dry and clinically normal skin in patients with atopic dermatitis. Acta Derm. Venereol. 65, 102-105.

Wertz, P.W., 2000. Lipids and barrier function of the skin. Acta Dermato-Venereologica 80.

Wertz, P.W., Downing, D.T., 1987. Covalently bound omega-hydroxyacylsphingosine in the stratum corneum. Biochim. Biophys. Acta 917, 108-111.

Yoshiike, T., Aikawa, Y., Sindhvananda, J., Suto, H., Nishimura, K., Kawamoto, T., Ogawa, H., 1993. Skin barrier defect in atopic dermatitis: increased permeability of the stratum corneum using dimethyl sulfoxide and theophylline. J. Dermatol. Sci. 5, 92-96.

Zheng, Y., Yin, H., Boeglin, W.E., Elias, P.M., Crumrine, D., Beier, D.R., Brash, A.R., 2011. Lipoxygenases mediate the effect of essential fatty acid in skin barrier formation a proposed role in releasing omega-hydroxyceramide for construction of the corneocyte lipid envelope. J. Biol. Chem. 286, 24046-24056.

ARTÍCULO 6

A lipid system containing acylceramides and long chain fatty acids to rebuild stratum corneum lamellar structure. V. Moner, L. Opálka, P. Pullmannová, K. Talló, K. Vávrová y O. López. *Langmuir –en revisión.*

Aunque los lípidos de la epidermis sólo forman el 15% del peso total del SC, son componentes esenciales para conseguir una función barrera adecuada. Se ha descrito que tanto la composición como la cantidad de ceramidas, ácidos grasos libres y colesterol son esenciales para una correcta organización de los lípidos del SC. Los lípidos del SC se organizan en dos fases laminares coexistentes denominadas LPP y SPP. En el trabajo 1 se vio que el LBms restablece parte de la estructura laminar de SC deslipidizado, en concreto la SPP. No se consiguió restablecer la LPP. Una posible razón podría ser que el sistema del artículo 1 no incluía ceramidas ni ácidos grasos libres de cadena alquílica larga que se ha descrito que son esenciales para la formación de esta fase. Con el objetivo de conseguir restablecer la LPP en SC deslipidizado, en éste trabajo se preparó un sistema mimético que incorporaba una mezcla de ceramidas extraídas de SC humano que contenía CerEOS (~4% en peso), CerNS (~10%), CerEOP (~2%), CerNP+CerEOH (~46%), CerAS+CerNH (~25%), CerAP (~6%) y CerAH (~7%), una mezcla de ácidos grasos que contenía ácido palmítico (1.33% en peso), ácido esteárico (3.30%), ácido oleico (6.84%), ácido behénico (47.1%) y ácido lignocérico (41.38%), además de colesterol.

El sistema se caracterizó mediante crio-TEM y SAXS. Se observaron nanoagregados de morfología y estructura similar al sistema previo (trabajo 1). En este trabajo también se determinó si el nuevo sistema era capaz de restablecer *in vitro* la LPP de SC deslipidizado. Para ello se trató SC deslipidizado con el nuevo sistema lipídico y se analizó el tejido mediante GISAXS de igual manera que en el trabajo 1. Lo interesante en este caso es que el nuevo sistema que incluye una composición lipídica más compleja que el sistema previo es capaz de restablecer no solo la SPP sino también la LPP. Por lo tanto, este sistema restablece una organización lipídica semejante a la que presenta la piel sana. Este resultado confirma el papel de las ceramidas utilizadas en la formación de una estructura laminar adecuada y además nos permite tener por primera vez un sistema lipídico que es capaz de reconstruir completamente la estructura laminar.

A lipid system containing acylceramides and long chain fatty acids to rebuild stratum corneum lamellar structure

V. Moner[1], O. Opálka[2], P. Pullmannová[2], K. Talló[1], K. Vávrová[2], O. López[1]

[1] Institute of Advanced Chemistry of Catalonia (IQAC-CSIC), Barcelona, 08034, Spain.

[2] Skin Barrier Research Group, Charles University, Faculty of Pharmacy, Hradec Králové, 50005, Czech Republic.

Keywords: extracted human ceramides, stratum corneum lipids, skin treatment, cryogenic transmission electron microscopy (cryo-TEM), grazing-incidence small-angle scattering (GISAXS)

Abstract

A proper stratum corneum (SC) lipid organization is relevant for correct skin barrier functionality. The lipids in this tissue are assembled in two lamellar phases referred to as long periodicity phase (LPP) and short periodicity phase (SPP). Alterations in the LPP, such as shortening of the repeat distance or a complete lack of this phase are found in different skin diseases. In our previous work, a lipid system that mimics the morphology and structure of epidermal lamellar body (LBms) was designed. We demonstrated that this system re-establishes the SPP of delipidated SC. However, the LPP was not re-built. Given the importance of this LPP in the correct functionality of the barrier function and the involvement of acylceramides and long chain free fatty acids in the formation of this phase, in the present work we include these lipids in addition to cholesterol and cholesterol sulfate in a new category of LBms. This system has demonstrated to re-establish also the LPP.

1. Introduction

The stratum corneum (SC) contains layers of corneocytes embedded in an intercellular lipid matrix consisting in ceramides, free fatty acids (FFAs) and cholesterol with a minor amount of cholesterol sulfate. These intercellular lipids are assembled in two lamellar phases, with a repeat distance of either 130 or 60 Å, referred to as long periodicity phase (LPP) or short periodicity phase (SPP), respectively [1]. This organization is relevant for the proper skin barrier functionality.

During the skin differentiation process, the lipids are delivered to the extracellular spaces of the SC by the secretion of epidermal lamellar bodies [2]. Several skin diseases have been associated with absence or altered function of these organelles [3]. Consequently, diseased skin is characterized by a reduced barrier function, altered lipid composition, especially in ceramides and free fatty acids, and deficiencies in lipid organization. Alterations in the LPP, such as shortening of the repeat distance or a complete lack of this phase, were found in atopic dermatitis [4], lamellar ichthyosis [5], psoriasis [6] and netherton syndrome [7]. Therefore, the normalization of the SC lipid composition and organization may improve the skin barrier function.

In a previous study, we designed a lipid system formed by discoidal lamellar structures encapsulated into vesicles mimicking the morphology and structure of epidermal lamellar body. That system includes ceramide 3b, stearic acid, cholesterol and cholesteryl sulfate approximating the SC lipid composition. Studies of electron microscopy and grazing-incidence small-angle X-ray scattering (GISAXS) demonstrated that this system re-establishes part of the SC lamellar structure of delipidized SC [8]. However, this system only restored the SPP. Due to the importance of acylceramides and the chain length of ceramides and FFAs in the formation of the LLP, in this work we improve our lipid system by including ceramides extracted from human SC and a mixture of FFAs approximating the SC lipid composition. The morphology and the size of this lipid system was studied by cryogenic transmission electron microscopy (cryo-TEM), and the lamellar organization of the lipids was determined by small angle X-ray scattering (SAXS). The aim of this work was to determine *in vitro* if the new lipid system is able to restore the LPP of delipidized human skin. For that, the SC lipid organization of native skin, delipidized skin and delipidized skin after treatment with this system was studied by GISAXS.

2. Material and methods

2.1. Chemicals

1,2-Dipalmitoyl-sn-glycero-3-phosphocholine (DPPC) and 1,2-dihexanoyl-sn-glycero-3-phosphocholine (DHPC) were purchased from Avanti Polar Lipids (Alabaster, USA). Cholesterol from lanolin (chol), sodium cholesterol sulfate (Schol), hexadecanoic acid, octadecanoic acid, eicosanoic acid, docosanoic acid, tetracosanoic acid and trypsin were acquired from Sigma-Aldrich (Schnelldorf, Germany). Lipoid S100, whose main component (>94%) is soybean phosphatidylcholine (PC) and Lipoid S LPC 80, whose main component (80%) is soybean lysophosphatidylcholine (lysoPC) were obtained from Lipoid GmbH (Ludwigshafen, Germany).

2.2. Isolation of the SC

Human abdominal skin from plastic surgery patients was provided by the University Hospital Hradec Králové, Clinics of Plastic Surgery. The procedure was approved by the Ethics Committee of the University Hospital Hradec Kralové, Czech Republic, and was conducted according to the Declaration of Helsinki Principles. The SC was isolated using a modified procedure described by Kligman and Christophers [9]. Human skin was immersed in 60 °C Milli-Q water for 30 s. The epidermis was peeled off using tweezers. Then, the epidermis was incubated overnight with the basal layer down in a solution of 0.5% trypsin in PBS at pH 7.4 and 32 °C. The residual epidermal cells were gently removed from the SC using cotton swabs. The SC was washed several times in Milli-Q water.

2.3. Isolation of human SC lipids

The SC was dried in vacuum over P_4O_{10} and solid paraffin in a desiccator and stored in nitrogen environment at -20 °C. The SC lipids were extracted from pooled SC of 6 subjects by a modified method of Bligh and Dyer [10] with a series of chloroform:methanol mixtures (2:1, 1:1, and 1:2 v/v) for 2 h each. The solvent from the combined extracts was removed using a rotary vacuum evaporator.

2.4. Isolation of human SC Cer (hCer)

The obtained human SC lipids were redissolved in a suitable volume of chloroform-methanol (2:1 v/v) and applied to a silica gel column (Silicagel 60, Merck, Darmstadt, Germany). The SC lipid classes were eluted sequentially using gradient elution with solvent mixtures (v/v) in the following sequence: chloroform-acetic acid 99:1 and then chloroform-methanol in ratios of 100:1, 50:1, 10:1, 3:1, 2:1, 1:1 and 1:2. The lipid

composition of the individual fractions was established by one-dimensional thin layer chromatography that was run in parallel with standards. To ensure complete separation of the least polar Cer and FFA, the separation of these fractions was repeated [11]. The fractions containing the eluted Cer were collected, and the solvent was removed using a rotary vacuum evaporator and then in high vacuum over P_4O_{10} and solid paraffin. The isolated hCer were stored under nitrogen at -20 °C.

2.5. High performance thin layer chromatography (HPTLC) analysis of hCer

Qualitative and quantitative analysis of the isolated hCer was performed using high performance thin layer chromatography (HPTLC) according to Pullmannová et al. [11]. The HPTLC glass plate (silica gel 60, Merck, Darmstadt, Germany) was washed with 2:1 chloroform-methanol (v/v), dried and equilibrated at 120 °C for 30 min in a drying oven before use. hCer was dissolved at a concentration of 0.5 mg/mL in 2:1 chloroform-methanol, and the standards were dissolved at a concentration of 1 mg/mL in 2:1 chloroform-methanol (v/v). The samples and standards were sprayed on an HPTLC glass plate under a stream of nitrogen using Linomat V (Camag, Muttenz, Switzerland). The standards were applied to an HPTLC plate together with the analyzed samples to generate calibration curves from 10 μg to 0.1 μg. The HPTLC plate was developed twice with 190:9:1.5 chloroform-methanol-acetic acid (v/v/v) in a solvent-saturated horizontal developing chamber (Camag, Muttenz, Switzerland). The dried plate was immersed in an aqueous solution of 10% $CuSO_4$, 8% H_3PO_4 (v/v), and 5% methanol for 10 s and then charred in a drying oven at 160 °C for 30 min.

A small portion of the hCer was hydrolyzed with 1:9 10 M NaOH-methanol at 60 °C for 1 h. Afterward, the solution was adjusted to pH 4 with 2 M HCl and extracted twice with chloroform. The chloroform layer was concentrated under a stream of nitrogen. The lipids were dried in vacuum over P_4O_{10} and solid paraffin in a desiccator. The hydrolyzed Cer were applied to the HPTLC plate in the same manner as described above. The hydrolysis indicated the presence of acylCer in the hCer fraction because the bands belonging to the acylCer were absent from the sequence of the hydrolyzed hCer.

The (semi)quantification was conducted using densitometry with a TLC Scanner 3 (Camag, Muttenz, Switzerland) at a wavelength of 350 nm. The peak areas were integrated and quantified using CATS software (Camag, Muttenz, Switzerland). The following standards were used to quantify the results: CerNS for the Cer classes NS and EOS; CerNP for NP, EOP and EOH; CerAS for AS, AH and NH; and CerAP for AP.

2.6. Preparation of the lipid system

First, a mixture of FFAs was prepared. It was selected 1.33% hexadecanoic acid, 3.30% octadecanoic acid, 6.84% eicosanoic acid, 47.10% docosanoic acid and 41.38% tetracosanoic acid (in weight) corresponding to the composition of human SC FFAs [12].

Then, four different discoidal structures were prepared. DPPC/DHPC at molar ratio of 3.5 was dissolved in chloroform and either hCer or FFAs or chol or Schol was added in the amount of 5wt% of total lipids. Solvent was rota-evaporated and the dry film was hydrated with Mili-Q water. The total lipid concentration of each system was 10% (w/v).

The final lipid system was prepared mixing 95% of PC and 5% of lysoPC (in weigh) in chloroform to reach 10% (w/v) of lipid concentration. The solvent was evaporated with a rotary evaporator until a lipid film was obtained. Then, the lipid film was hydrated with a mixture of discoidal structures by stirring (50% of disks hCer, 20% disks mix FFAs, 25% disks chol and 5% Schol, in weigh).

2.7. Characterization of the lipid system

2.7.1. Cryogenic transmission electron microscopy (Cryo-TEM)

The lipid system was visualized by cryo-TEM. A thin, aqueous sample film was formed by dipping a glow-discharged holey carbon grid in the lipid suspension. Immediately after, the sample excess liquid was blotted with a Whatman No. 4 filter paper between 1 and 4 seconds. The blotted grids were plunged into liquid ethane cooled with liquid nitrogen using a Leica EM GP (Leica, Germany) at room temperature and 99% humidity. The specimen grid under liquid nitrogen was mounted on a Gatan 626 cryotransfer system. Images were obtained using a Jeol JEM 2011 cryo-electron microscope operated at 200 kV, under low-dose conditions, and using different degrees of defocus (500–700 nm) to obtain an adequate phase contrast image. During image acquisition, several grids of the sample were used and different holes in the perforated carbon film were examined. Images presented on this work correspond to a representative fraction of the micrographs saved during the microscopy session.

2.7.2. Small angle X-ray scattering (SAXS)

This technique was used to determine the structure of the lipid system. SAXS measurements were carried out using a S3-MICRO (Hecus X-ray systems GMBH Graz, Austria) coupled to a GeniX Cu high flux source (Xenocs, Grenoble). The wavelength of

the X-rays was 0.1542 nm. Transmitted scattering was detected using a PSD 50 Hecus, and the temperature was controlled by means of a Peltier TCCS-3 Hecus. The sample was inserted and measured in a flow-through glass capillary 1 mm diameter with 10 μm wall thickness.

2.8. Treatment of delipidated SC

The SC was delipidated using chloroform:methanol mixtures (2:1, 1:1 and 1:2 v/v) for 2 hours each [13]. The delipidated SC was washed several times with distilled water. Then, delipidated SC pieces of 36 mm^2 were treated with 10 μl of the lipid system, overnight, at room temperature. After that incubation time, the system remaining on the SC surface was removed with distilled water. Then, the excess of water was dried with a filter paper.

2.9. Grazing-incidence small-angle scattering (GISAXS)

This technique was used to study the effect of the lipid system on delipidated SC. GISAXS measurements were carried out using a S3-MICRO (Hecus X-ray systems GMBH Graz, Austria) coupled to a GeniX Cu high flux source (Xenocs, Grenoble). The wavelength of the X-rays was 0.1542 nm. Slit collimation was used to achieve a resulting beam spot that was approximately 200 μm in height and 200 μm in width (the z- and y-axes, respectively). The linear detector, PSD 50 Hecus, covered a range of $0.07\ nm^{-1} < q < 6\ nm^{-1}$.

Hydrated SC samples were mounted by deposition on oxidized silicon 111 cut plane wafers and placed on a homemade accessory that allowed a humid atmosphere. Humid air at 22 °C was blown in the sample cell at 99% relative humidity. The wafers were oriented in the scanning direction by a stepping motor with a resolution of 0.01°. The sample-to-detector distance was calibrated with silver behenate, and it was fixed at 268 mm. The exposure time was between 1800 and 3600 s. The sample was aligned between 0.5° and 0.25° of the incident angle.

The GISAXS curves are shown as a function of the scattering vector modulus, $q = (4\pi \sin\theta/2)/ \lambda$, in which θ is the scattering angle, and λ the wavelength of the X-rays. The position of the scattering peaks is directly related to the repeat distance of the molecular structure and is calculated from Bragg's law [14] as $q = 2\pi n/d$, where n and d represent the order of the diffraction peak and the repeat distance, respectively.

3. Results and discussion

3.1. Lipid system

The composition of the SC lipid matrix is dominated by three lipid classes: ceramides, FFAs and cholesterol. Ceramides are a structurally heterogeneous lipid group: 15 subclasses of ceramides have been identified in humans [15]. The FFAs are essentially linear and saturated, with the acyl chain length varying from C14 to C30. In our previous work, a lipid system that mimics the morphology and structure of epidermal lamellar body (LBms) was designed. That system included ceramide 3b, stearic acid, cholesterol and cholesterol sulfate. Thus, only one lipid of each class and short chain lipids were included. This system re-establishes part of the lipid organization of damage SC, corresponding to the SPP [8]. However, the LPP was not re-built. In the present work, we prepared a new LBms with a lipid composition more complex than the previous one with the purpose to re-establish the LPP of delipidated SC. For that, the new lipid system was prepared with ceramides isolated from human SC, a mixture of FFAs, cholesterol and cholesterol sulfate. HPTLC analysis confirmed that the isolated Cer fraction contained Cer in similar proportions to those of the human SC, including the very long acylceramides of the EO classes. We found the following composition of human SC Cer fraction in weight % (mean±SEM, 2 analyses of the hCer sample pooled from 6 subjects): CerEOS 4±0.7%; CerNS 10.2±0.25%; CerEOP 2.3±1.1%; CerNP+CerEOH 46.4±0.2%; CerAS+CerNH 24.6±3.3%; CerAP 5.6±0.6%; and CerAH 6.9±2.1%. Therefore, the LBms prepared here mimics the lipid composition of human SC.

This lipid system was observed by cryo-TEM (Figure 1). It is formed by two types of structures: encapsulated and non-encapsulated disks (white arrows) from 25 to 40 nm, and vesicles encapsulating disks (black arrows) from 100 to 400 nm as our previous system. Thus, the change of lipid composition does not affect the morphology or the size of the lipid system. The structure of this lipid system was determined by SAXS. The lamellar repeat distance *d* was estimated by analyzing the reflections using Bragg's law and was attributed to the bilayer thickness, as in studies of liposomes and other bilayer models [16, 17]. The SAXS profile of this lipid system is shown in Figure 2. Two reflections were observed at 71.6 Å and 34.1 Å, which can be attributed to the first- and second-order Bragg scattering, respectively, corresponding to the lipid lamellar organization of the lipid system.

3.2. The LBms restores the lamellar structure of human delipidated SC

The results of GISAXS experiments are shown in figure 3. Panel A shows the scattering pattern of native human SC which has five peaks corresponding to 133.9, 63.0, 48.0, 33.0 and 29.9 Å. According to Bouwstra et al. these spacing are associated with the intercellular lipid lamellar structure of the SC. These authors reported that two lamellar phases are present in human SC the SPP and the LPP with repeat distances of 60 Å and 132 Å, respectively [1]. The reflections detected at 133.9, 48.0 and 33.0 Å are associated with the first-, third- and fourth-order of the LPP, respectively. The peak at 33.0 Å also could be attributed to the crystalline cholesterol [18]. In addition, the reflections detected at 63.0 and 29.9 Å are associated with the first- and second-order of the SPP. After extraction of SC lipids with organic solvents, no reflections are observed (panel B) suggesting an exhaustive delipidation. Interestingly, after treatment with our lipid system, the scattering pattern is quite similar to native pattern showing reflections related to the LPP and SPP (panel C). Reflections at 131.7, 66.1 and 46.0 Å are associated to the first-, second- and third-order of the LPP, respectively, while the reflections at 66.1 and 27.3 are associated to the first- and second-order of the SPP. Therefore, the LBms prepared in this work is able to re-establish the LPP and SPP of delipidated SC.

The effect that this system exerts on the SC maybe is due to its structure and a proper lipid composition. As mentioned previously, the lipid system is formed by non-encapsulated disks and disks encapsulated in vesicles. The non-encapsulated disks are small enough to penetrate through the narrow intercellular spaces of the SC. Once incorporated into the SC, these new structures re-establish the lipid lamellar structure of delipidated SC. The vesicles do not penetrate through the SC due to their large size [19]. Thus, when the vesicle contacts the SC, the bilayer of the vesicle bursts and fuses with the SC surface and the encapsulated disks are released from the inside. These released disks then also penetrate the SC in a similar way as the non-encapsulated disks. The composition of this lipid system is also important. Our previous lipid system only re-established the SPP of delipidated SC [8]. However, the system that includes acylceramides and long chain FFAs also re-establishes the LPP. This may be due to these lipids have great influence on the formation of the LPP [20]. This fact and its specific interaction to the skin described before makes this system able to repair the lipid organization of damage SC. Moreover, this result confirms the relevance of acylceramides and long chain FFAs in the correct formation of the SC lamellar structure.

Acknowledgments

The authors wish to thank Martí de Cabo and Jaume Caelles for expert technical assistance. This work was supported by the Spanish Ministry of Economy, Industry and Competitiveness (CTQ 2013-44998-P and RTC-2016-4957-1) and the Czech Science Foundation (16-25687J).

Figures

Figure 1: Cryo-TEM image of the lipid system. The system is formed by encapsulated and non-encapsulated disks (white arrows) from 25 to 40 nm, and vesicles encapsulating disks (black arrows) from 100 to 400 nm. Bar = 100 nm.

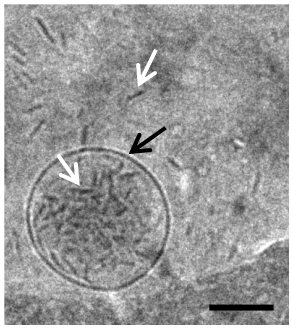

Figure 2: SAXS profile of the lipid system. Reflections can be attributed to the first- and second-order Bragg scattering, respectively.

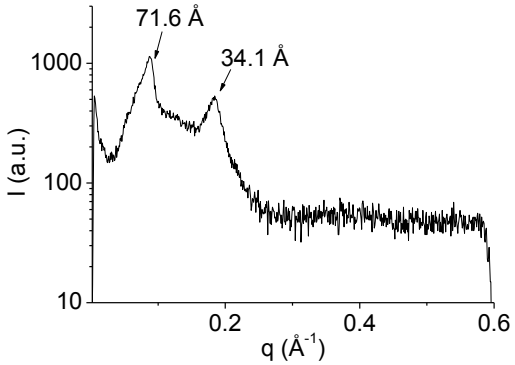

Figure 3: (A) The GISAXS profile of native human SC shows reflections attributed to the LPP, SPP and crystalline cholesterol (Cho). (B) In the GISAXS profile of delipidized SC no reflections were observed. (C) GISAXS profile of delipidized SC after treatment with the lipid system. It shows reflections attributed to the LPP and SPP. Thus, the topical treatment with our lipid system results in relipidization of human SC and leads to a re-establishment of the lamellar organization.

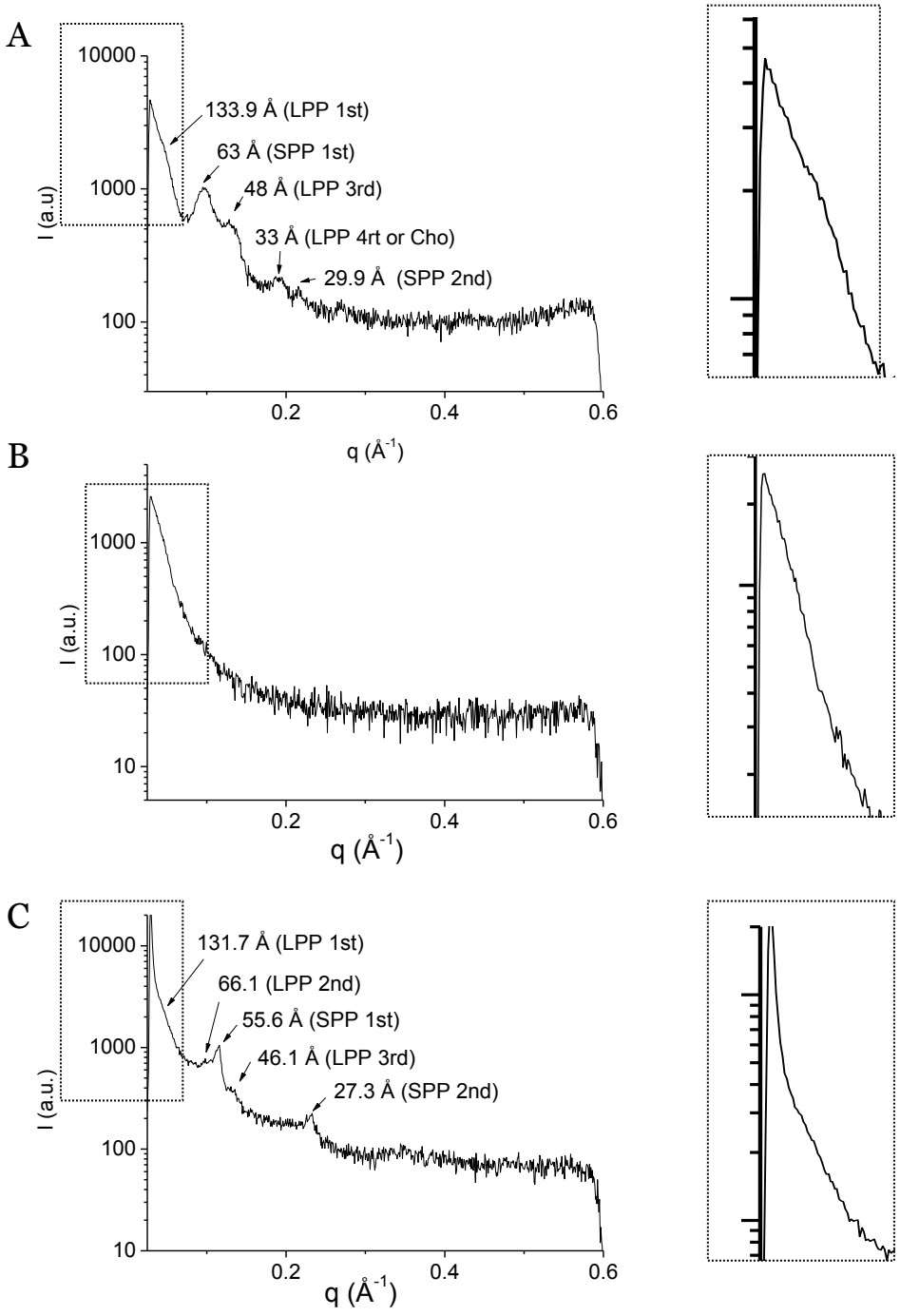

References:

1. Bouwstra, J.A., et al., *Structural investigations of human stratum corneum by small-angle X-ray scattering*. J. Invest. Dermatol., 1991. **97**(6): p. 1005-1012.
2. Elias, P.M., K.R. Feingold, and M. Fartasch, *The epidermal lamellar body as a multifunctional secretory organelle*, in *Skin barrier*, P.M. Elias and K.R. Feingold, Editors. 2005, CRC Press. p. 261-272.
3. Elias, P.M. and J.S. Wakefield, *Mechanisms of abnormal lamellar body secretion and the dysfunctional skin barrier in patients with atopic dermatitis*. J. Allergy Clin. Immunol., 2014. **134**(4): p. 781-791 e1.
4. di Nardo, A., et al., *Ceramide and cholesterol composition of the skin of patients with atopic dermatitis*. Acta Derm. Venereol. (Stockh), 1998. **78**: p. 27-30.
5. Paige, D., N. Morse - Fisher, and J. Harper, *Quantification of stratum corneum ceramides and lipid envelope ceramides in the hereditary ichthyoses*. Br. J. Pharmacol. , 1994. **131**(1): p. 23-27.
6. Motta, S., et al., *Ceramide composition of the psoriatic scale*. Biochim. Biophys. Acta Mol. Basis Dis., 1993. **1182**(2): p. 147-151.
7. van Smeden, J., et al., *Intercellular skin barrier lipid composition and organization in Netherton syndrome patients*. J. Investig. Dermatol. , 2014. **134**(5): p. 1238-1245.
8. Moner, V., et al., *Lamellar body mimetic system: an up-to-down repairing strategy of the stratum corneum lipid structure*. Int. J. Pharm., 2016. **510**(1): p. 135-143.
9. Kligman, A.M. and E. Christophers, *Preparation of isolated sheets of human stratum corneum*. Arch. Dermatol., 1963. **88**(6): p. 702-705.
10. Bligh, E.G. and W.J. Dyer, *A rapid method of total lipid extraction and purification*. Can. J. Biochem. Phis., 1959. **37**(8): p. 911-917.
11. Pullmannová, P., et al., *Effects of sphingomyelin/ceramide ratio on the permeability and microstructure of model stratum corneum lipid membranes*. Biochim.Biophis. Acta Biomembr., 2014. **1838**(8): p. 2115-2126.
12. Groen, D., G.S. Gooris, and J.A. Bouwstra, *Model membranes prepared with ceramide EOS, cholesterol and free fatty acids form a unique lamellar phase*. Langmuir, 2010. **26**(6): p. 4168-4175.
13. Wertz, P.W. and D.T. Downing, *Covalently bound omega-hydroxyacylsphingosine in the stratum corneum*. Biochim. Biophys. Acta, 1987. **917**(1): p. 108-111.
14. Bragg, W.L., *The diffraction of short electromagnetic waves by a crystal*. Proc. Cambridge Philos. Soc., 1913. **17**: p. 43-57.
15. Rabionet, M., K. Gorgas, and R. Sandhoff, *Ceramide synthesis in the epidermis*. Biochim. Biophys. Acta Mol. Cell. Biol. Lipids 2014. **1841**(3): p. 422-434.
16. Barbosa-Barros, L., et al., *Ceramide effects in the bicelle structure*. Colloids Surf. A Physicochem. Eng. Asp., 2008. **317**(1): p. 576-584.
17. Wu, R.G., et al., *Competitive molecular interaction among paeonol-loaded liposomes: differential scanning calorimetry and synchrotron X-ray diffraction studies*. Int. J. Pharm., 2012. **438**(1): p. 91-97.
18. Bouwstra, J.A., et al., *Phase behavior of stratum corneum lipid mixtures based on human ceramides: the role of natural and synthetic ceramide 1*. J. Invest. Dermatol., 2002. **118**(4): p. 606-617.
19. Dreier, J., J.A. Sørensen, and J.R. Brewer, *Superresolution and fluorescence dynamics evidence reveal that intact liposomes do not cross the human skin barrier*. PloS one, 2016. **11**(1).
20. Mojumdar, E., et al., *Stratum corneum lipid matrix: location of acyl ceramide and cholesterol in the unit cell of the long periodicity phase*. Biochim. Biophys. Acta Biomembr., 2016. **1858**(8): p. 1926-1934.

4. DISCUSIÓN

4. DISCUSIÓN

4.1. Nueva estrategia para reparar la barrera cutánea

La piel sana frente a un daño en la barrera cutánea inducido por una fuerza mecánica o por contacto con disolventes, tensioactivos y otras sustancias químicas, inicia una respuesta de reparación homeostática que resulta en una rápida recuperación de la función barrera. Esta respuesta se debe a la rápida acción de los cuerpos laminares epidérmicos que secretan en minutos su contenido entre el estrato granuloso y el SC y en la rápida formación y posterior secreción de nuevos cuerpos laminares (30-60 minutos). Los lípidos secretados al espacio extracelular del SC se procesan mediante la acción de enzimas y en unas 2 horas ya se pueden encontrar nuevas láminas lipídicas en los espacios intercelulares del SC (Elias y col., 1998; Menon y col., 1992).

Por otro lado, diferentes enfermedades cutáneas presentan un aumento o disminución de la formación y secreción de cuerpos laminares o bien una deficiencia en las enzimas que procesan los precursores de los lípidos intercelulares del SC (Chan y col., 2011; Elias y col., 2014; Fartasch y col., 1999; Ghadially y col., 1996; Milner y col., 1992). Así, la piel enferma se caracteriza por ser deficiente en ciertos lípidos, principalmente ceramidas y FFAs, y por consiguiente presenta una barrera cutánea alterada (Bouwstra y col., 2006). Una manera de reparar la barrera cutánea consiste en aplicar diferentes mezclas lipídicas sobre la piel dañada. Se pueden aplicar mezclas de lípidos fisiológicos o lípidos no fisiológicos. Los lípidos fisiológicos (ceramidas, colesterol y FFAs) se aplican básicamente dispersos en propilenglicol (Mao-Qiang y col., 1996) o en emulsiones de aceite en agua (Chamlin y col., 2002). En cuanto a los lípidos no fisiológicos, por ejemplo vaselina (mezcla de hidrocarburos derivados del petróleo) o lanolina (cera natural que se obtiene de la lana) son utilizados como base en muchos productos cosméticos aunque actúan de forma oclusiva formando una película de lípidos sobre el SC (Mao-Qiang y col., 1995).

En esta tesis se ha desarrollado una nueva estrategia dirigida a la reparación de la barrera cutánea. Se ha diseñado un sistema lipídico mimético de los cuerpos laminares epidérmicos con el propósito de que pueda imitar también la función de estos orgánulos. La estructura de los cuerpos laminares epidérmicos así como su mecanismo de secreción de lípidos al espacio extracelular del SC es actualmente objeto de debate. En la literatura se han publicado diferentes modelos que explican la formación de la función barrera, como el modelo de Landman (Landmann, 1986) o el modelo de Norlén (Norlén, 2015). El LBms desarrollado en esta tesis intenta reproducir el modelo de Landman que propone que los cuerpos laminares están formados por vesículas que

contienen en su interior múltiples láminas. Según este modelo, durante la diferenciación de los queratinocitos, los cuerpos laminares derivados del aparato de Golgi se mueven hasta el ápice de las células, se fusionan con la membrana plasmática y secretan su contenido al espacio extracelular entre el estrato granuloso y el SC. Así, los cuerpos laminares epidérmicos reparan la barrera desde las capas internas de la piel. El sistema lipídico que se presenta en esta tesis actuaría en sentido inverso ya que el objetivo es que se aplique sobre la piel y pueda penetrar a través del SC reparando la barrera. Los resultados obtenidos mediante cryo-TEM mostraron que el sistema está formado por vesículas que encapsulan estructuras discoidales y discos no encapsulados. Mediante SAXS y DLS se vio que estas estructuras se organizan en bicapas y que tienen unas dimensiones que oscilan entre los 10nm y los 300nm, observándose variaciones en función de la composición de los sistemas. Así, el LBms al igual que los orgánulos endógenos está organizado por una vesícula lipídica que contiene estructuras laminares. Ver figura 15.

Otro punto importante es la composición de este sistema mimético. Los cuerpos laminares epidérmicos contienen los precursores de los lípidos intercelulares del SC, enzimas necesarias para su posterior procesado y péptidos antimicrobianos. En este sentido y para mimetizar en lo posible la composición de estos orgánulos, en el sistema se incluyó una mezcla de lípidos con composición similar a la del SC, además de lisofosfatidilcolina, un lípido que tiene efecto antimicrobiano (Uchida y col., 1991). A diferencia de los orgánulos endógenos, este sistema también incluye los fosfolípidos (DPPC, DHPC y otras fosfatidilcolinas) necesarios para formar las diferentes nanoestructuras que forman el sistema lipídico.

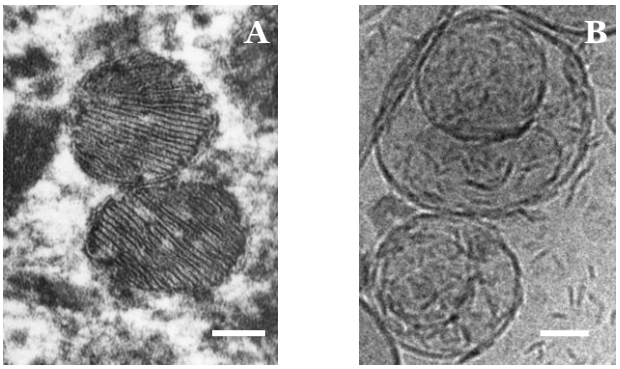

Figura 15. Micrografía de (A) cuerpo laminar epidérmico observado mediante microscopía electrónica de transmisión (Démarchez, 2018) y (B) LBms observado mediante cryo-TEM. Barra = 100nm.

4.2. Desarrollo de LBms de diferente complejidad

La intención de este trabajo fue producir un sistema mimético de los orgánulos endógenos que representara su complejidad pero que tuviera una composición y morfología reproducible. Como se ha explicado en el apartado anterior, el LBms está formado por vesículas que encapsulan discos; estas dos nanoestructuras interaccionan de forma diferente con la piel y por ese motivo se incluyeron moléculas diferentes en cada una de ellas, en función de donde se quería que dicha molécula actuara. En las estructuras discoidales se incorporaron los lípidos del SC, ya que estos discos son estructuras pequeñas que pueden penetrar a través de los espacios intercelulares de la piel (Barbosa-Barros y col., 2008). En cambio, en la vesícula externa se incluyó el lípido antimicrobiano, ya que la vesícula al tener un tamaño mayor no penetra (Dreier y col., 2016) aunque si tiene una interacción a nivel superficial que podría favorecer el efecto antimicrobiano en la superficie cutánea. En estudios previos se intentó preparar las estructuras discoidales utilizando los fosfolípidos (DPPC y DHPC) más una mezcla de cer3b, ácido esteárico y colesterol, pero aunque estas mezclas formaron distintas estructuras de bicapa, no se formaron discos. Por este motivo, se decidió incluir cada uno de los lípidos del SC en un sistema discoidal diferente. Finalmente, se prepararon 4 sistemas discoidales que incluían cer3b, colesterol, sulfato de colesterol o palmitato de colesterol. Estos sistemas se mezclaron en volúmenes adecuados para reproducir las proporciones de estos lípidos en el SC y se encapsularon en vesículas formadas por fosfatidilcolina, lisofosfatidilcolina y ácido esteárico. El ácido esteárico aunque es un lípido que forma parte de la estructura laminar del SC también puede actuar como regulador del pH (Fluhr y col., 2001), parámetro que suele estar alterado en dermatitis atópica. Por lo que se incluyó en la vesícula con la intención de fomentar su localización y acción a nivel superficial. Un punto importante es que en el sistema final, los lípidos del SC tenían una relación molar entre ellos similar a la que presenta la piel con el fin de reproducir el equilibrio composicional cutáneo (Wertz, 2000). Por otro lado, aunque el sistema se diseñó para incluir en los discos y las vesículas unos lípidos concretos, hay que asumir que durante la formación del sistema se puede producir un intercambio de lípidos entre las dos nanoestructuras. Estudios futuros podrían dirigirse a la investigación de la localización concreta de estos lípidos.

Inicialmente, en el sistema lipídico se incluyó la Cer3b porque es una ceramida disponible comercialmente aunque tiene una cadena alquílica corta (artículo 1). Es bien conocido que las ceramidas que tienen cadenas alquílicas largas como la CerEOS tienen un papel imprescindible en la organización característica de los lípidos del SC. Sin embargo, su uso se ha visto obstaculizado por la falta de disponibilidad comercial de

este tipo de ceramidas y su solubilidad extremadamente baja. Recientemente, se ha descrito un método escalable para la síntesis de la CerEOS (Opálka y col., 2015). Así, se sintetizó la CerEOS y se incluyó en el sistema lipídico en lugar de la Cer3b (artículo 5). Mediante cryo-TEM (artículo 5, figura 1) se vio que las estructuras discoidales que incluyen CerEOS presentan una gran variabilidad de tamaños (entre 40-260nm de diámetro) comparado con las formadas con Cer3b (13-18nm de diámetro). Este hecho es debido probablemente a que la CerEOS no se distribuye homogéneamente en las estructuras discoidales por lo que forman discos de diferente tamaño. Además, estos discos son en general de diámetro mayor que los discos que incluyen Cer3b. Por lo tanto, la longitud de la cadena alquílica de la ceramida (50 carbonos en CerEOS y 18 carbonos en Cer3b) afecta al tamaño de las estructuras discoidales. En cuanto al LBms que incluye CerEOS al igual que el que incluye Cer3b, está formado por vesículas que encapsulan estructuras discoidales y discos no encapsulados. Sin embargo, este sistema también presentó tubos multilaminares no observados en el LBms que incluye Cer3b. La formación de estos tubos podría deberse a que el sistema contiene CerEOS y como se ha demostrado en estudios con modelos de membrana de fosfatidilcolina, las ceramidas de cadena larga son capaces de promover la formación de fases interdigitadas e inducir fuertes alteraciones morfológicas, formándose así este tipo de estructuras tubulares (Pinto y col., 2011). En cuanto al tamaño de las nanoestructuras presentes en el LBms EOS, se observó mediante cryo-TEM que el diámetro de las vesículas variaba ente 85-210nm y los discos entre 35-80nm. En cambio, mediante DLS se encontró una población de partículas de 414±26nm y otra de 43±5nm. Esta discrepancia entre las dos técnicas, especialmente para las estructuras de tamaño mayor, puede ser debida a la presencia de las estructuras tubulares observadas por cryo-TEM que se podrían identificar como partículas grandes en las medidas de DLS afectando al diámetro obtenido por esta técnica.

Finalmente, para mimetizar en mayor medida la complejidad composicional del SC se preparó un sistema mimético que incorporaba tanto una mezcla de ceramidas extraídas del SC humano como una mezcla de FFAs (artículo 6). El análisis mediante HPTLC de la mezcla de ceramidas extraídas del SC humano reveló que contenía CerEOS (~4% en peso), CerNS (~10%), CerEOP (~2%), CerNP+CerEOH (~46%), CerAS+CerNH (~25%), CerAP (~6%) y CerAH (~7%). Considerando que los FFAs en el SC humano son predominantemente saturados con una longitud de la cadena alquílica en el rango de 14-28 carbonos, se seleccionó para formar estos sistemas más complejos una mezcla que contenía: ácido palmítico (C16:0, 1.33% en peso), esteárico (C18:0, 3.30%), oleico (C18:1ω9, 6.84%), behénico (C22:0, 47.1%) y lignocérico (C24:0, 41.38%). En este caso, se prepararon 4 sistemas discoidales conteniendo la mezcla de ceramidas, la mezcla de

FFAs, colesterol o sulfato de colesterol. Estos sistemas se mezclaron en los volúmenes adecuados para reproducir las proporciones de estos lípidos en el SC y se encapsularon en vesículas formadas por fosfatidilcolina y lisofosfatidilcolina. El sistema final contenía ceramidas, FFAs, colesterol y sulfato de colesterol con una relación molar de 1:1:0.5:0.1 respectivamente, similar a la que presenta la piel. Las imágenes de este sistema lipídico obtenidas mediante cryo-TEM revelaron que al igual que los LBms previos, este sistema también estaba formado por vesículas que encapsulan estructuras discoidales y discos no encapsulados (artículo 6, figura 1), por lo que la adición de mezclas complejas de ceramidas y FFAs no afecta a su formación ni morfología final.

En resumen, se preparó inicialmente el sistema con una única clase de ceramida, la Cer3b, y el resto de los lípidos del SC, que llamamos LBms Cer3b. Se substituyó la Cer3b por CerEOS para formar el sistema LBms CerEOS. Y finalmente se utilizó una mezcla de ceramidas extraídas del SC humano y una mezcla de FFAs para formar el sistema más complejo.

4.3. Efecto de los sistemas LBms en la piel

4.3.1. Interacción con la microestructura del SC

El grado de penetración del sistema mimético en la piel se determinó mediante la técnica FTIRM. Para ello se trató *in vitro* SC sano con el LBms Cer3b preparado con lípidos deuterados para poder diferenciar las vibraciones de los lípidos correspondientes al sistema (enlaces C-D) de las vibraciones propias de la piel (C-H). Nuestros resultados mostraron que el sistema mimético penetra a través de los espacios del SC y queda retenido en esta capa de la piel. En el anexo 1 se puede ver la distribución del sistema (enlaces C-D) en el mapa químico obtenido de la muestra de piel. La escala de color desde el azul al rosa indica la concentración de lípido deuterado. El color rosa indica una concentración máxima y el azul indica ausencia.

Para analizar la microestructura del SC se utilizó la técnica FSTEM. Mediante esta técnica se pudieron observar claramente los corneocitos, las bicapas lipídicas de los espacios intercelulares y los corneodesmosomas del SC nativo. También se confirmó que la deslipidización del SC fue efectiva ya que no se observaron bicapas lipídicas entre los corneocitos de las muestras extraídas con disolventes orgánicos. Después de tratar el SC deslipidizado con el LBms Cer3b se observaron nuevas estructuras entre los corneocitos sugiriendo que el sistema penetra a través del SC y vuelve a formar bicapas

lipídicas (figura 4, artículo 1). Por lo tanto, esta técnica confirma los resultados obtenidos mediante FTIRM.

Bouwstra y col. proponen el "modelo de sándwich" para explicar cómo está organizada la estructura laminar lipídica en el SC (Bouwstra y col., 2000). Dicho modelo describe una organización lipídica en tres capas: una capa central formada por lípidos en fase líquido-cristalina y una o dos capas de lípidos en fase gel situadas a ambos lados de esta capa central. Esta organización laminar de sándwich muestra dos periodicidades mediante SAXS con luz sincrotrón: una distancia larga (LPP) de 130Å entre las dos capas gel y una corta (SPP) de 60Å entre las capas líquido-cristalina y gel. Nuestros resultados no se obtuvieron con luz sincrotrón sino con fuente de rayos x convencional utilizando la disposición de incidencia rasante para maximizar la intensidad detectada. Aun así mostraron en SC nativo reflexiones correspondientes con la LPP, la SPP y también reflexiones asociadas al colesterol. Esta reflexiones no se detectaron en SC deslipidizado. En esta muestra únicamente se detectó una reflexión ancha posiblemente asociada con los lípidos unidos covalentemente a la envoltura del corneocito que no es posible extraer con el protocolo de disolventes orgánicos utilizado. Después de tratar el SC deslipidizado con el LBms Cer3b se detectaron nuevas reflexiones que corresponden con la SPP y el colesterol (artículo 1). Y cuando se trató con el LBms más complejo, el que incluía la mezcla de ceramidas extraídas del SC y una mezcla de FFAs, se consiguió reconstruir además de la SPP, la LPP (artículo 6). El interés de este resultado se debe a que hasta el momento no se había conseguido restablecer la LPP en ensayos con piel *in vitro*. Algunos autores han descrito la formación de esta fase trabajando con modelos lipídicos multilaminares (Eichner y col., 2016; Mojumdar y col., 2016) pero nuestros resultados muestran por primera vez la reconstrucción de esta fase en piel. En la formación de la LPP principalmente están implicadas ceramidas y ácidos grasos de cadena larga (Mojumdar y col., 2016). Además, la ceramida EOS es imprescindible para su formación (Bouwstra y col., 1998). Probablemente, no se detectó esta fase cuando se trató la piel con el sistema que contenía Cer3b debido a que las cadenas alquílicas en esta ceramida son cortas. Sin embargo, si se detectó al tratar la piel con el sistema más complejo que tiene una composición lipídica más cercana a la del SC nativo.

El LBms podría interaccionar con la piel de una manera similar a como lo hacen los bicosomas, sistemas lipídicos formados por vesículas que encapsulan discos (Fernández y col., 2014). Para entender el mecanismo de interacción hay que considerar las diferentes nanoestructuras presentes en el LBms. Como se ha descrito anteriormente, el LBms está formado por dos tipos de nanoestructuras: vesículas que

encapsulan estructuras discoidales y discos no encapsulados. Estas vesículas tienen tamaños de entre 300-450nm de diámetro, por lo tanto, no son capaces de penetrar entre los espacios intercelulares del SC (6-13nm) y permanecen sobre la piel pudiendo tener una acción sobre la capa más externa del tejido. Al aplicarlas sobre la piel, la vesícula externa podría romperse, desagregarse o fundirse con la superficie de la piel, y es previsible que las estructuras discoidales se liberen. Estas estructuras son suficientemente pequeñas (espesor 4nm y diámetro 10-40nm) para penetrar entre los espacios del SC. La piel exhibe un gradiente de hidratación que aumenta desde las capas más exteriores a las más internas (Elias y col., 1992). Por lo tanto, a mayor profundidad, el contenido de agua es mayor. Así pues, una vez los pequeños discos penetran en el SC, van pasando entre los espacios intercelulares y van encontrando zonas de mayor contenido en agua debido al gradiente de hidratación natural de la piel. Con la dilución, parte de las moléculas de DHPC pasan al agua debido a la parcial solubilidad de esta molécula que dejaría de ocupar su posición en el borde del disco. Este fenómeno y la alta hidrofobicidad del DPPC inducen un incremento de la relación molar en las estructuras y un aumento en el diámetro del disco pudiéndose formar estructuras vesiculares o láminas (Barbosa-Barros y col., 2008) que quedarían retenidas entre los espacios intercelulares de la piel mezclándose con los lípidos endógenos. Además, considerando que el LBms también contiene discos que no se han encapsulado durante el proceso de formación del sistema, estas estructuras también podrían penetrar mediante el mismo mecanismo que los discos encapsulados. Una hipótesis es que primero podrían penetrar los discos no encapsulados, luego las vesículas interaccionarían con la piel y liberarían los discos encapsulados que también penetrarían. Por lo tanto, un punto muy importante que facilita la interacción del sistema mimético con la piel es su morfología y estructura.

4.3.2. Efecto sobre la función barrera y parámetros biofísicos

4.3.2.1. *In vitro*

La integridad de la barrera cutánea se estudió *in vitro* mediante experimentos de permeabilidad con teofilina en celdas de Franz y mediante monitorización de la pérdida de agua transepidérmica (artículo 5). La teofilina es una molécula pequeña que se utiliza comúnmente como marcador de la permeabilidad (Opálka y col., 2016; Yoshiike y col., 1993). Nuestros resultados mostraron un flujo de teofilina en torno a 3µg/cm^2/h en SC sano, mientras que en SC dañado por exposición del tejido a disolventes orgánicos, el flujo de teofilina aumentó en función del tiempo de exposición a los

disolventes. Así, se encontró un flujo de teofilina de 16, 245 o 455µg/cm²/h después de 5min, 15min o 2h de exposición, respectivamente (artículo 5, figura 2). Este aumento del flujo de teofilina está relacionado con el hecho que los disolventes orgánicos utilizados (mezclas de cloroformo y metanol) pueden extraer parte de los lípidos del SC alterando la composición y la organización de los lípidos del tejido (Barba y col., 2016) lo que resulta en un deterioro de la función barrera. La pérdida de agua transepidérmica es otro parámetro comúnmente utilizado para evaluar la integridad de la piel (Nangia y col., 1998). La pérdida transepidérmica de agua de la piel sana no suele exceder los 25g/m²/h. Nuestros resultados (artículo 5, figura 2) mostraron que después de aplicar disolventes orgánicos al SC durante 2h o 15min, la pérdida de agua a través del SC alcanzaba valores de 90-105g/m²/h, indicando un daño severo en la barrera cutánea. Cuando el SC se expuso durante 5min a disolventes orgánicos se detectó una pérdida de agua de alrededor 40g/m²/h, valor similar al que presentan los pacientes con dermatitis atópica (34-54g/m²/h) (Angelova - Fischer y col., 2005).

El SC con diferente grado de perturbación se trató con los sistemas lipídicos y se vio que cuanto menos dañado estaba el tejido, mayor reducción de los parámetros de permeabilidad ejercía el tratamiento. Posiblemente, la cantidad de lípidos extraídos al exponer el SC durante 5min a disolventes orgánicos es mucho menor que con 2h. Por lo que estos lípidos no extraídos podrían servir como anclaje de los nuevos lípidos introducidos por los sistemas lipídicos aplicados. Comparando el efecto del tratamiento con discos CerEOS, LBms CerEOS y un sistema que contenía la misma composición que la vesícula externa del LBms se vio que los tres tratamientos reducían los parámetros de permeabilidad, aunque el LBms CerEOS los reducía en mayor medida (artículo 5, tabla2). Este hecho sería consecuencia del mecanismo de interacción que tienen los diferentes sistemas con la piel (descrito en el apartado 4.3.1) que potencia una mayor interacción del sistema formado por los LBms que por las nanoestructuras que lo forman separadamente. Así, el LBms EOS en SC poco alterado (5min) redujo casi un 50% la pérdida de agua y el flujo de teofilina se normalizó hasta valores similares a los que muestra la piel sana. Esto indica que este sistema mejora la función barrera como consecuencia de la reparación de la estructura laminar como se ha mencionado en apartados anteriores.

Comparando el efecto del LBms CerEOS con el que incluye Cer3b o una mezcla de la dos ceramidas en SC poco perturbado (5min de exposición a disolventes), se observó que tanto el LBms EOS como el que incluye las dos ceramidas reducen los parámetros de permeabilidad en mayor medida que el que incluye Cer3b (artículo 5, figura 3).

Posiblemente porque ambos sistemas incluyen CerEOS que es esencial para conseguir una función barrera adecuada (Bouwstra y col., 1998).

4.3.2.2. *In vivo*

El efecto de los sistemas lipídicos objeto de estudio *in vivo* se evaluó en experimentos con voluntarios humanos y también en un modelo de ratón con dermatitis inducida.

Los ensayos en voluntarios humanos permitieron evaluar el efecto del sistema LBms Cer3b en piel sana y piel con barrera cutánea comprometida. Para ello, se utilizó el SDT ya que es un test simple y rápido que permite evaluar la cinética de hidratación-deshidratación de la piel y determinar diferentes parámetros que pueden asociarse con la funcionalidad de la piel, como es la capacidad de retener agua (WHC), la capacidad de absorción de agua (WSC) y la cantidad de agua liberada a través del SC durante la fase de desorción (AWD) (Pellacani y col., 2001). Nuestros resultados indicaron que la piel sana de voluntarios presenta un aumento en el parámetro WHC después de ser tratada durante 7 días con el LBms Cer3b. Para evaluar el efecto del LBms Cer3b en piel de voluntarios comprometida, primero se aplicó el tensioactivo lauril sulfato de sodio mediante un parche en una zona delimitada de la pierna del voluntario. Este tensioactivo podría interaccionar con los lípidos del SC incrementando la fluidez de las membranas lipídicas por solubilización de algunos lípidos o por alteración del empaquetamiento laminar de estos (Lichtenberg y col., 2013). Estos hechos podrían aumentar la permeabilidad de la piel. La extracción de lípidos del SC por parte de los tensioactivos depende de la concentración y tiempo de exposición al agente. En nuestro estudio, aplicando el tensioactivo al 2% durante 2h esperamos un daño leve en la barrera. Después de 2h de exposición de la piel a un parche con el tensioactivo, ésta presentó un aumento de los parámetros WHC y WSC y una disminución de AWD debido a los diferentes mecanismos que se desencadenan para restablecer la barrera cutánea como se ha descrito en el apartado 4.1. Sin embargo, estos parámetros cutáneos volvían a los valores iniciales en 24h. Nuestros estudios demuestran que si la piel perturbada por el tensioactivo se trata durante 4 días con el LBms se produce un aumento especialmente remarcable en el parámetro WHC. Este valor fue mayor que el observado en la piel perturbada sin tratar, es decir, en la piel que tiene que recuperarse por sí sola (artículo 2, tabla 2). Así, nuestros resultados demuestran que el tratamiento con el sistema mimético refuerza la barrera cutánea en voluntarios tanto en piel sana como irritada por un tensioactivo.

Con el fin de evaluar el potencial del sistema mimético como tratamiento de la dermatitis se realizó un estudio en un modelo de ratón de dermatitis inducida por oxazolona. Este modelo es útil para evaluar terapias para la dermatitis ya que reproduce la dermatitis humana a nivel clínico, histológico e inmunológico (Man y col., 2008). Se indujo dermatitis mediante la aplicación de oxazolona en el dorso de ratones sin pelo y las lesiones se trataron durante 10 días con el LBms Cer3b. La integridad de la barrera cutánea se evaluó mediante medidas de TEWL e hidratación. Los ratones con dermatitis presentaron un aumento del 60% en el valor de TEWL y una disminución cerca del 50% en el valor de hidratación respecto a los valores basales (antes de inducir la dermatitis) (artículo 3, figura 3). Estos resultados indican un deterioro de la función barrera. El análisis de la microestructura de la piel de los ratones con dermatitis demostró un menor número y desorganización de las láminas que forman la estructura lipídica del SC comparado con la piel sana. Esto se debe a un cambio en la composición de los lípidos del SC (disminución de ceramidas y FFAs) (Man y col., 2008).

Las lesiones cutáneas mejoraron después de 10 días de tratamiento con el LBms Cer3b (artículo 4, figura S2). Los ratones tratados presentaron un valor de TEWL significativamente menor que los ratones sin tratar indicando que el sistema lipídico repara la barrera (artículo 3, figura 3). El efecto que produce el sistema mimético se debe a la introducción de lípidos dentro de la estructura del SC, como reflejan nuestros resultados obtenidos *in vitro* mediante microscopía y GISAXS que sugieren una reparación estructural de la barrera. Cuando se analizó la microestructura de la piel de estos animales tratados con el sistema mimético se observó un mayor número de cuerpos laminares epidérmicos que en el grupo sin tratar (artículo 3, figura 4) que podría indicar que el LBms también estimula la producción y secreción de lípidos endógenos. En cuanto a la hidratación no se obtuvo una mejora en el grupo tratado con el sistema lipídico respecto al grupo sin tratar (artículo 3, figura 3). Se ha descrito que los agentes hidratantes mejoran la hidratación utilizando una combinación de ingredientes oclusivos, humectantes y emolientes. Hay que considerar que el LBms no es una formulación final, está compuesto por lípidos organizados en bicapas en solución acuosa, y los lípidos por ellos mismos tienen poca o nula afinidad por las moléculas de agua (Imokawa, 2002). Así pues, es esperable que por sí solo el sistema mimético no tenga un efecto sobre la hidratación.

Para inducir dermatitis en los ratones se utilizó la oxazolona, una molécula de peso molecular pequeño, que puede modificar covalentemente las proteínas de la piel, desencadenando respuestas alérgicas (Liu y col., 2013). La aplicación tópica y continua de este hapteno (al menos durante 10 días) en ratones produce una respuesta de

hipersensibilidad crónica mediada por linfocitos Th2 que producen citocinas e IgE similar a la que presentan las personas con dermatitis atópica (Man y col., 2008). En nuestro estudio, la inflamación se caracterizó mediante análisis histológico de las muestras de piel extraídas después de sacrificar a los ratones el último día del experimento. Además, se evaluó el grado de inflamación a lo largo del experimento mediante el análisis de IgE en el suero sanguíneo. Ambas metodologías demostraron que el tratamiento con el LBms Cer3b reduce la inflamación en piel con dermatitis inducida. El análisis histológico mediante la tinción H&E reveló una disminución del grosor epidérmico del 50% y un menor infiltrado de linfocitos, indicando una reducción de la inflamación, aunque aún se observó paraqueratosis y espongiosis indicativo de que la piel no se había recuperado totalmente (artículo 3, figura 5). En este experimento durante el período de tratamiento con el LBms también se aplicó oxazolona, hecho que podría explicar que la piel aún presentase cierto grado de inflamación y que aunque el valor de IgE en suero sanguíneo se redujera significativamente seguía siendo alto comparado con el valor basal, antes de inducir dermatitis (artículo 5). La reducción de la inflamación podría ser debida a que el sistema mimético repara la barrera cutánea dañada. Por un lado, al reparar la barrera podría disminuir la penetración del hapteno y por el otro, los FFAs que incorpora el sistema podrían ayudar al SC a mantener el pH ácido de la piel ayudando a su vez a mejorar la función barrera por bloqueo de la activación de serina proteasas proinflamatorias (Elias, 2008).

La técnica de FTIRM combinada con el PCA nos permitió identificar cambios en los lípidos, proteínas y ácidos nucleicos de la piel con dermatitis respecto a la sana y relacionarlos con la enfermedad. Además nos permitió determinar si el tratamiento con el LBms mejora las condiciones de la piel a nivel bioquímico. Para ello se analizaron las muestras de piel de los ratones correspondientes a piel sana, piel con dermatitis y piel con dermatitis después de ser tratada con el LBms Cer3b. Los resultados del PCA en el rango espectral de los lípidos (3030-2800cm^{-1}) mostraron que la piel con dermatitis es espectralmente diferente a la sana. Sin embargo, la piel tratada mostró un comportamiento espectral similar a la piel sana, principalmente en la zona SC-epidermis (artículo 4, figura 1). El análisis de los loadings demostró que la vibración "stretching" o de estiramiento del CH_2 es la responsable de las diferencias. Esta vibración presentó una menor frecuencia en piel con dermatitis que en piel sana. Esto indica un incremento en el orden de los lípidos en la muestra de piel con dermatitis inducida en lugar de un aumento en el desorden, como ha sido descrito en la dermatitis humana (Janssens y col., 2012). En nuestro caso la dermatitis se indujo mediante una solución de oxazolona en acetona que podría incrementar el orden igual que se ha

descrito que hace el etanol (Bommannan y col., 1991). Hay que destacar que esta alteración no se observó después de tratar la piel con el LBms Cer3b. Además, la piel con dermatitis presentó una menor cantidad de lípidos ya que la intensidad de la banda de estiramiento del CH_2 fue menos intensa que en la piel sana. Sin embargo, después del tratamiento la intensidad de la banda fue semejante a la piel sana indicando una recuperación de los lípidos.

Los resultados del PCA en el rango espectral de las proteínas (1800-1483cm^{-1}) en la zona de la dermis mostraron que la piel con dermatitis es espectralmente diferente a la sana. Sin embargo, después de ser tratada con el sistema mimético mostró un comportamiento espectral similar a la sana (artículo 4, figura 2). El análisis de los loadings reveló que los cambios se deben a la banda Amida I. En la dermis, la Amida I se debe al colágeno y es sensible a los cambios estructurales de esta proteína (Jackson y col., 1995). Normalmente, se utiliza el análisis de la segunda derivada del espectro para determinar los subpicos asociados a esta banda que permite identificar las diferentes estructuras secundarias de las proteínas (Kong y col., 2007). Nuestros resultados (artículo 4, figura 2D) demostraron que el colágeno mayoritariamente tiene una estructura triple-hélice en las tres muestras ya que todas presentaron una banda intensa entre 1659-1655cm^{-1}. Sin embargo, en las muestras con dermatitis (sin tratar y tratada), la banda a 1635cm^{-1} fue ligeramente más intensa que en piel sana sugiriendo un incremento en la estructura en lámina beta del colágeno.

Los resultados del PCA en el rango espectral de los carbohidratos-DNA (1481-1000cm^{-1}) tanto en la zona de la epidermis como de la dermis mostraron de nuevo que la piel con dermatitis tiene un espectro diferente a la piel sana, y de nuevo la señal espectral de la piel tratada guarda similitud con la piel sana. El análisis de los loadings reveló que los cambios se deben mayoritariamente al stretching del PO_2 que está relacionado con el DNA. El aumento de la intensidad de este pico en piel con dermatitis sugirió un aumento de la síntesis de DNA que se reflejaría en una hiperplasia epidérmica. Sin embargo, después del tratamiento este pico presentó una intensidad semejante a la que presenta la piel sana indicando una reducción de la síntesis de DNA. Este resultado está de acuerdo con lo observado en las histologías donde se vio un aumento del grosor epidérmico en piel con dermatitis respecto la sana y como este grosor era menor después del tratamiento con el sistema mimético (artículo 5, figura 3). En este rango espectral también se observaron otras bandas; la asignación de cada pico está detallada en la tablaS2 del artículo 4. En general se observaron pocas diferencias en estas bandas entre las tres muestras.

Se podría concluir que el LBms penetra a través del SC y queda retenido en esta capa donde repara la barrera cutánea dañada. La recuperación de la integridad y funcionalidad del SC protegería las capas más profundas de la piel de los cambios bioquímicos que se producen en dermatitis inducida.

4.4. Potencial aplicación en dermatitis atópica

La dermatitis atópica es una enfermedad cutánea multifactorial que resulta de la interacción de factores genéticos, ambientales, defectos en la función barrera y una serie de factores inmunológicos (Spergel y col., 2003). Se han propuesto diferentes hipótesis para explicar la patogenia de la dermatitis. Primero se propuso la hipótesis "inside-outside" que sostiene que la dermatitis se debe a una alteración inmunológica, siendo la alteración de la función barrera una consecuencia de la inflamación local. Luego se propuso la hipótesis "outside-inside" que considera que la alteración de la función barrera es la que desencadena la respuesta inmunológica. Dichas hipótesis no se excluyen mutuamente por lo que luego se integraron en una hipótesis más completa. La hipótesis "outside-inside-outside" está basada en la idea de que un defecto en la barrera cutánea conduce a una mayor penetración de alérgenos y microorganismos que podrían estimular en exceso la inmunidad local y a su vez dicha estimulación excesiva desencadena la liberación de mediadores inflamatorios que aumentan aún más la disfunción de la barrera (Elias y col., 2008). La disrupción de la barrera se asocia a una disminución de cuerpos laminares epidérmicos que resulta principalmente en una disminución de ceramidas y ácidos grasos libres en la estructura laminar del SC tanto en zonas lesionadas como no lesionadas llevando a la pérdida de agua y a la deshidratación de la piel.

Para tratar la dermatitis normalmente se utilizan lociones, cremas o geles con agentes antiinflamatorios (corticoides), antimicrobianos (mupirocina) o inmunomoduladores (tacrolimus, pimecrolimus). Sin embargo, el uso de corticoides principalmente a largo plazo puede tener efectos adversos. Además, los inmunomoduladores aunque reducen la inflamación comprometen la función barrera (Kao y col., 2003; Kim y col., 2010). También se ha propuesto la reparación de la barrera como estrategia para el tratamiento de la dermatitis. Se ha demostrado que la aplicación tópica de ceramidas, ácidos grasos libres y colesterol en relación equimolar mejora la función barrera de la piel ya que inducen la formación de nuevos lípidos endógenos (Mao-Qiang y col., 1995). En los últimos años se han desarrollado diversas formulaciones incluyendo mezclas de estos lípidos para tratar la dermatitis.

En esta tesis se propone una nueva estrategia para tratar la dermatitis que se basa en utilizar un sistema lipídico que imite a los cuerpos laminares epidérmicos. Como se ha descrito el LBms incluye una composición lipídica similar al SC, además incluye un lípido que tiene efecto antimicrobiano y lípidos que podrían regular el pH de la piel. Esto es importante ya que se sabe que los pacientes con dermatitis presentan anomalías en la composición lipídica del SC, pH básico y déficit en péptidos antimicrobianos. También hay que destacar la importancia de la estructura del sistema mimético ya que tiene un papel relevante en la interacción del sistema con la piel. Por ejemplo, cuando se trató la piel con estructuras discoidales que incluían CerEOS o simplemente esta ceramida en solución (sin estructurar) no se obtuvo el mismo efecto. Nuestros resultados tanto *in vitro* como *in vivo* muestran que el sistema mimético repara la barrera cutánea por lo que actuaría de manera similar que los orgánulos endógenos. Pero en vez de reparar la barrera transportando y secretando lípidos desde las capas internas de la piel hasta el SC, el LBms la repararía desde la superficie. Nuestros resultados también sugieren que al recuperar la función barrera se podrían inhibir las alteraciones provocadas por las citocinas que se vería reflejado en una reducción de la inflamación. Además, la recuperación de la barrera podría proteger las capas más profundas de la piel de los cambios bioquímicos que se producen en la piel con dermatitis.

Por todo esto, el LBms puede ser de interés para el desarrollo de nuevos tratamientos para dermatitis atópica o para otras disfunciones cutáneas que impliquen un deterioro de la barrera.

5. CONCLUSIONES

5. CONCLUSIONES

I. En esta tesis se ha conseguido formar un sistema lipídico (LBms) mimético de los cuerpos laminares epidérmicos en cuanto a morfología, estructura y composición. El LBms está organizado por vesículas lipídicas que contienen estructuras laminares. El sistema está formado por una composición lipídica similar a la del SC de la piel. Además, incluye un lípido con efecto antimicrobiano y lípidos que podrían regular el pH de la piel.

II. Se han desarrollado LBms de diferente complejidad para mimetizar en lo posible la composición lipídica del SC. Todos los sistemas están formados por vesículas que encapsulan discos y discos no encapsulados. El LBms que incluye CerEOS además de estas dos nanoestructuras también presenta tubos multilaminares.

III. Mediante microespectroscopía de IR se ha determinado que el LBms Cer3b penetra a través del SC y queda retenido en esta capa de la piel.

IV. El LBms Cer3b es capaz de restablecer *in vitro* parte de la estructura lipídica laminar de SC deslipidizado, correspondiente a la SPP. Los resultados de FSTEM demostraron que este sistema introduce láminas lipídicas entre los corneocitos de SC deslipidizado.

V. El LBms de mayor complejidad composicional (mezcla de ceramidas extraídas de SC humano y mezcla de FFAs) restableció tanto la SPP como la LPP de SC deslipidizado, hecho que indica que la estructura laminar lipídica restablecida está organizada de manera muy similar a la de la piel sana.

VI. *In vitro*, el tratamiento con el LBms CerEOS en SC ligeramente alterado reduce alrededor de 50% la pérdida de agua y normaliza el flujo de teofilina hasta valores similares a los que presenta la piel sana. Así, este sistema recupera la integridad de la barrera.

VII. *In vivo*, el tratamiento con el LBms Cer3b aumenta la capacidad de la piel de retener agua tanto en piel de voluntarios sana como perturbada por un tensioactivo. Por lo tanto, el tratamiento refuerza la barrera cutánea. En ratones con dermatitis inducida, el tratamiento con el LBms Cer3b reduce el TEWL significativamente por lo que recupera la integridad de la barrera cutánea. Además, se observa una mejora de las lesiones de dermatitis después del tratamiento.

VIII. El tratamiento con el LBms Cer3b reduce la inflamación en ratones con dermatitis inducida. Las histologías de las secciones de piel muestran una

reducción del grosor epidérmico y un menor infiltrado de linfocitos comparado con la piel sin tratar. El tratamiento reduce significativamente el valor de IgE en suero sanguíneo.

IX. La piel de ratones con dermatitis inducida presenta cambios bioquímicos con respecto a la piel sana en cuanto a los lípidos, proteínas y DNA de la piel. Estos cambios no se observan cuando se trata la piel con el LBms Cer3b. El sistema lipídico repara la barrera y este hecho podría proteger las capas más profundas de la piel de los cambios bioquímicos producidos en dermatitis inducida.

X. El efecto que produce el sistema mimético en la piel es debido tanto a su morfología y estructura como a su composición. La interacción de este sistema con la piel se establece en un mecanismo de dos pasos; la vesícula exterior se funde con la superficie de la piel y los discos penetran al interior del tejido. Así, el sistema introduce lípidos al SC, reparando o reforzando la barrera cutánea. *In vivo*, también podría estimular la producción y secreción de lípidos endógenos, mediante la formación de nuevos cuerpos laminares.

XI. El sistema mimético como se demuestra a lo largo de esta tesis tendría una función similar a la de los orgánulos endógenos, aunque actuaría reparando la barrera desde la superficie de la piel. Por lo tanto, se propone este sistema lipídico como nueva estrategia para el tratamiento de la dermatitis atópica aunque aún se necesitan hacer más estudios y realizar ensayos clínicos utilizando el sistema en una formulación.

6. BIBLIOGRAFÍA

6. BIBLIOGRAFÍA

Almgren, M., Edwards, K., Karlsson, G., 2000. Cryo transmission electron microscopy of liposomes and related structures. Colloids Surf. A Physicochem. Eng. Asp. 174, 3-21.

Angelova - Fischer, I., Bauer, A., Hipler, U., Petrov, I., Kazandjieva, J., Bruckner, T., Diepgen, T., Tsankov, N., Williams, M., Fischer, T., 2005. The objective severity assessment of atopic dermatitis (OSAAD) score: validity, reliability and sensitivity in adult patients with atopic dermatitis. Br. J. Dermatol. 153, 767-773.

Bäckman, A., Ny, A., Edlund, M., Ekholm, E., Hammarström, B.E., Törnell, J., Wallbrandt, P., Egelrud, T., Hansson, L., Wennbo, H., 2002. Epidermal overexpression of stratum corneum chymotryptic enzyme in mice: a model for chronic itchy dermatitis. J. Invest. Dermatol. 118, 444-449.

Bangham, A., Hill, M., Miller, N., 1974. Preparation and use of liposomes as models of biological membranes, Methods in Membrane Biology. Springer, pp. 1-68.

Barba, C., Alonso, C., Martí, M., Manich, A., Coderch, L., 2016. Skin barrier modification with organic solvents. Biochim. Biophys. Acta Biomembr. 1858, 1935-1943.

Barbosa-Barros, L., de La Maza, A., Estelrich, J., Linares, A., Feliz, M., Walther, P., Pons, R., López, O., 2008. Penetration and growth of DPPC/DHPC bicelles inside the stratum corneum of the skin. Langmuir : the ACS journal of surfaces and colloids 24, 5700-5706.

Barbosa - Barros, L., de la Maza, A., Walther, P., Estelrich, J., López, O., 2008. Morphological effects of ceramide on DMPC/DHPC bicelles. J. Microsc. 230, 16-26.

Barbosa - Barros, L., Rodríguez, G., Barba, C., Cócera, M., Rubio, L., Estelrich, J., López - Iglesias, C., de la Maza, A., López, O., 2012. Bicelles: lipid nanostructured platforms with potential dermal applications. Small 8, 807-818.

Barel, A.O., Clarys, P., 2013. Skin Capacitance, in: Berardesca, E., Maibach, H.I., Wilhelm, K.-P. (Eds.), Non invasive diagnostic techniques in clinical dermatology. Springer Science & Business Media, pp. 357-366.

Berardesca, E., Maibach, H.I., 1990. Monitoring the water - holding capacity in visually non - irritated skin by plastic occlusion stress test (POST). Clin. Exp. Dermatol. 15, 107-110.

Bommannan, D., Potts, R.O., Guy, R.H., 1991. Examination of the effect of ethanol on human stratum corneum in vivo using infrared spectroscopy. J. Control. Release 16, 299-304.

Borroni, G., Vignati, G., Brazzelli, V., Vignoli, G.P., Gabba, P., Gatti, M., Berardesca, E., Cosseta, A., Rabbiosi, G., 1989. Changes in the water holding capacity of psoriatic stratum corneum in vivo. Acta Derm. Venereol. Suppl (Stockh) 146, 192-194.

Bouwstra, J.A., Dubbelaar, F., Gooris, G., Ponec, M., 2000. The lipid organisation in the skin barrier. Acta Derm. Venereol. Suppl., 23-30.

Bouwstra, J.A., Gooris, G., Dubbelaar, F., Weerheim, A., Ijzerman, A., Ponec, M., 1998. Role of ceramide 1 in the molecular organization of the stratum corneum lipids. J. Lipid Res. 39, 186-196.

Bouwstra, J.A., Gooris, G.S., 2010. The lipid organisation in human stratum corneum and model systems. Open Dermatol. J. 4, 10-13.

Bouwstra, J.A., Gooris, G.S., van der Spek, J.A., Bras, W., 1991. Structural investigations of human stratum corneum by small-angle X-ray scattering. J. Invest. Dermatol. 97, 1005-1012.

Bouwstra, J.A., Ponec, M., 2006. The skin barrier in healthy and diseased state. Biochim. Biophys. Acta Biomembr. 1758, 2080-2095.

Bragg, W.L., 1913. The diffraction of short electromagnetic waves by a crystal. Proc. Cambridge Philos. Soc. 17, 43-57.

Branco, N., Lee, I., Zhai, H., Maibach, H.I., 2005. Long ‐ term repetitive sodium lauryl sulfate ‐ induced irritation of the skin: an in vivo study. Contact Dermatitis 53, 278-284.

Clarys, P., Barel, A.O., Gabard, B., 1999. Non ‐ invasive electrical measurements for the evaluation of the hydration state of the skin: comparison between three conventional instruments ‐ the Comeometer®, the Skicon® and the Nova DPM®. Skin Res. Technol. 5, 14-20.

Costa, M., Benseny-Cases, N., Cócera, M., Teixeira, C., Alsina, M., Cladera, J., López, O., Fernández, M., Sabés, M., 2009. Diagnosis applications of non-crystalline diffraction of collagen fibres: breast cancer and skin diseases, Applications of Synchrotron Light to Scattering and Diffraction in Materials and Life Sciences. Springer, pp. 265-280.

Chamlin, S.L., Kao, J., Frieden, I.J., Sheu, M.Y., Fowler, A.J., Fluhr, J.W., Williams, M.L., Elias, P.M., 2002. Ceramide-dominant barrier repair lipids alleviate childhood atopic dermatitis: changes in barrier function provide a sensitive indicator of disease activity. J. Am. Acad. Dermatol. 47, 198-208.

Chan, A., Holleran, W.M., Ferguson, T., Crumrine, D., Goker-Alpan, O., Schiffmann, R., Tayebi, N., Ginns, E.I., Elias, P.M., Sidransky, E., 2011. Skin ultrastructural findings in type 2 Gaucher disease: diagnostic implications. Mol. Genet. Metab. 104, 631-636.

Chan, L.S., Robinson, N., Xu, L., 2001. Expression of interleukin-4 in the epidermis of transgenic mice results in a pruritic inflammatory skin disease: an experimental animal model to study atopic dermatitis. J. Investig. Dermatol. 117, 977-983.

Chapman, S., Walsh, A., 1990. Desmosomes, corneosomes and desquamation. An ultrastructural study of adult pig epidermis. Arch. Dermatol. Res. 282, 304-310.

Démarchez, M., 2018.
http://biologiedelapeau.fr/spip.php?page=forum&id_article=3&lang=en.

den Hollander, L., Han, H., de Winter, M., Svensson, L., Masich, S., Daneholt, B., Norlén, L., 2015. Skin lamellar bodies are not discrete vesicles but part of a tubuloreticular network. Acta Dermatol. Venereol. 96, 303-308.

Deo, N., Somasundaran, P., 2001. Mechanism of mixed liposome solubilization in the presence of sodium dodecyl sulfate. Colloids Surf. A: Physicochem. Eng. Asp. 186, 33-41.

di Nardo, A., Wertz, P., Gianneti, A., Seidenari, S., 1998. Ceramide and cholesterol composition of the skin of patients with atopic dermatitis. Acta Dermato-Venereologica (Stockh) 78, 27-30.

Downing, D.T., Stewart, M.E., Wertz, P.W., Colton, S.W., Abraham, W., Strauss, J.S., 1987. Skin lipids: An update. J. Investig. Dermatol. 88, 2s-6s.

Dreier, J., Sørensen, J.A., Brewer, J.R., 2016. Superresolution and fluorescence dynamics evidence reveal that intact liposomes do not cross the human skin barrier. PloS one 11.

Eichner, A., Sonnenberger, S., Dobner, B., Hauss, T., Schroeter, A., Neubert, R.H., 2016. Localization of methyl-branched ceramide [EOS] species within the long-periodicity phase in stratum corneum lipid model membranes: A neutron diffraction study. Biochim. Biophys. Acta Biomembr. 1858, 2911-2922.

Effendy, I., Maibach, H.I., 1995. Surfactants and experimental irritant contact dermatitis. Contact dermatitis 33, 217-225.

El Maghraby, G.M., Williams, A.C., Barry, B.W., 2000. Oestradiol skin delivery from ultradeformable liposomes: refinement of surfactant concentration. Int. J. Pharm. 196, 63-74.

El Maghraby, G.M.M., 2016. Stratum corneum lipid liposomes: drug delivery systems and skin models, Percutaneous Penetration Enhancers Chemical Methods in Penetration Enhancement. Springer, pp. 111-119.

Elias, P.M., 1988. Structure and function of the stratum corneum permeability barrier. Drug Dev. Res. 13, 97-105.

Elias, P.M., 1991. Epidermal barrier function: intercellular lamellar lipid structures, origin, composition and metabolism. J. Control Release 15, 199-208.

Elias, P.M., 2008. Barrier repair trumps immunology in the pathogenesis and therapy of atopic dermatitis. Drug Discov. Today Dis. Mech. 5, e33-e38.

Elias, P.M., Feingold, K., 1992. Lipids and the epidermal water barrier: metabolism, regulation, and pathophysiology, Seminars in Dermatology, pp. 176-182.

Elias, P.M., Feingold, K.R., Fartasch, M., 2005. The epidermal lamellar body as a multifunctional secretory organelle, in: Elias, P.M., Feingold, K.R. (Eds.), Skin barrier. CRC Press, pp. 261-272.

Elias, P.M., Hatano, Y., Williams, M.L., 2008. Basis for the barrier abnormality in atopic dermatitis: outside-inside-outside pathogenic mechanisms. J . Allergy Clin. Immunol. 121, 1337-1343.

Elias, P.M., Mauro, T., Rassner, U., Kömüves, L., Brown, B.E., Menon, G.K., Cullander, C., 1998. The secretory granular cell: the outermost granular cell as a specialized secretory cell. J. Invest. Dermatol. Symp. Proc. 3, 87-100.

Elias, P.M., Wakefield, J.S., 2014. Mechanisms of abnormal lamellar body secretion and the dysfunctional skin barrier in patients with atopic dermatitis. J. Allergy Clin. Immunol. 134, 781-791 e781.

Fartasch, M., Williams, M.L., Elias, P.M., 1999. Altered lamellar body secretion and stratum corneum membrane structure in Netherton syndrome: differentiation from other infantile erythrodermas and pathogenic implications. Arch. Dermatol. 135, 823-832.

Feingold, K.R., Elias, P.M., 2014. Role of lipids in the formation and maintenance of the cutaneous permeability barrier. Biochim. Biophys. Acta Mol. Cell. Biol. Lipids 1841, 280-294.

Fernández, E., Fajarí, L., Rodríguez, G., Cócera, M., Moner, V., Barbosa-Barros, L., Kamma-Lorger, C.S., de la Maza, A., López, O., 2016a. Reducing the harmful effects of infrared radiation on the skin using bicosomes incorporating β-carotene. Skin Pharmacol. Physiol. 29, 169-177.

Fernández, E., Fajarí, L., Rodríguez, G., López-Iglesias, C., Cócera, M., Barbosa-Barros, L., de la Maza, A., López, O., 2014. Bicelles and bicosomes as free radical scavengers in the skin. RSC Adv. 4, 53109-53121.

Fernández, E., Hostachy, S., Sandt, C., Rodríguez, G., Bertrand, H.C., Clède, S., Cócera, M., de la Maza, A., Lambert, F., Policar, C., 2016b. Monitoring bicosomes containing antioxidants in normal and irradiated skin. RSC Adv. 6, 72559-72567.

Fernández, E., Rodríguez, G., Hostachy, S., Clède, S., Cócera, M., Sandt, C., Lambert, F., de la Maza, A., Policar, C., López, O., 2015. A rhenium tris-carbonyl derivative as a model molecule for incorporation into phospholipid assemblies for skin applications. Colloids Surf. B 131, 102-107.

Fluhr, J.W., Kao, J., Jain, M., Ahn, S.K., Feingold, K.R., Elias, P.M., 2001. Generation of free fatty acids from phospholipids regulates stratum corneum acidification and integrity. J. Invest. Dermatol. 117, 44-51.

Ghadially, R., Reed, J.T., Elias, P.M., 1996. Stratum corneum structure and function correlates with phenotype in psoriasis. J. Invest. Dermatol. 107, 558-564.

Goldburg, W., 1999. Dynamic light scattering. Am. J. Phys. 67, 1152-1160.

Hoffman, D.R., 1973. Estimation of serum IgE by an enzyme-linked immunosorbent assay (ELISA). J. Allergy. Clin. Immunol. 51, 303-307.

Imokawa, G., 2002. Ceramides as natural moisturizing factors and their efficacy in dry skin, in: Leyden, J.J., Rawlings, A.V. (Eds.), Skin moisturization. CRC Press, pp. 267-302.

Jackson, M., Mantsch, H.H., 1995. The use and misuse of FTIR spectroscopy in the determination of protein structure. Crit. Rev. Biochem. Mol. 30, 95-120.

Janssens, M., van Smeden, J., Gooris, G.S., Bras, W., Portale, G., Caspers, P.J., Vreeken, R.J., Hankemeier, T., Kezic, S., Wolterbeek, R., 2012. Increase in short-chain ceramides correlates with an altered lipid organization and decreased barrier function in atopic eczema patients. J. Lipid Res. 53, 2755-2766.

Jensen, J.-M., Fölster-Holst, R., Baranowsky, A., Schunck, M., Winoto-Morbach, S., Neumann, C., Schütze, S., Proksch, E., 2004. Impaired sphingomyelinase activity and epidermal differentiation in atopic dermatitis. J. Invest. Dermatol. 122, 1423-1431.

Kao, J.S., Fluhr, J.W., Man, M.-Q., Fowler, A.J., Hachem, J.-P., Crumrine, D., Ahn, S.K., Brown, B.E., Elias, P.M., Feingold, K.R., 2003. Short-term glucocorticoid treatment compromises both permeability barrier homeostasis and stratum corneum integrity: inhibition of epidermal lipid synthesis accounts for functional abnormalities. J. Investig. Dermatol. 120, 456-464.

Kim, M., Jung, M., Hong, S.P., Jeon, H., Kim, M.J., Cho, M.Y., Lee, S.H., Man, M.Q., Elias, P.M., Choi, E.H., 2010. Topical calcineurin inhibitors compromise stratum corneum integrity, epidermal permeability and antimicrobial barrier function. Exp. Dermatol. 19, 501-510.

Knepp, V.M., Szoka Jr, F.C., Guy, R.H., 1990. Controlled drug release from a novel liposomal delivery system. II. Transdermal delivery characteristics. J. Control. Res. 12, 25-30.

Kong, J., Yu, S., 2007. Fourier transform infrared spectroscopic analysis of protein secondary structures. Acta Biochim. Biophys. Sin. 39, 549-559.

Konishi, H., Tsutsui, H., Murakami, T., Yumikura-Futatsugi, S., Yamanaka, K.-i., Tanaka, M., Iwakura, Y., Suzuki, N., Takeda, K., Akira, S., 2002. IL-18 contributes to the spontaneous development of atopic dermatitis-like inflammatory skin lesion independently of IgE/stat6 under specific pathogen-free conditions. Proc. Natl. Acad. Sci. 99, 11340-11345.

Kuo, I.-H., Yoshida, T., De Benedetto, A., Beck, L.A., 2013. The cutaneous innate immune response in patients with atopic dermatitis. J. Allergy Clin. Immunol. 131, 266-278.

Landmann, L., 1986. Epidermal permeability barrier: transformation of lamellar granule-disks into intercellular sheets by a membrane-fusion process, a freeze-fracture study. J. Invest. Dermatol. 87, 202-209.

Lasic, D.D., 1992. Mixed micelles in drug delivery. Nature 355, 279-280.

Lazo, N.D., Meine, J.G., Downing, D.T., 1995. Lipids are covalently attached to rigid corneocyte protein envelopes existing predominantly as β-sheets: a solid-state nuclear magnetic resonance study. J. Investig. Dermatol. 105, 296-300.

Levine, J.R., Cohen, J., Chung, Y., Georgopoulos, P., 1989. Grazing - incidence small - angle X - ray scattering: new tool for studying thin film growth. J. Appl. Crystallogr. 22, 528-532.

Lichtenberg, D., Ahyayauch, H., Goñi, F.M., 2013. The mechanism of detergent solubilization of lipid bilayers. Biophys. J. 105, 289-299.

Liu, B., Escalera, J., Balakrishna, S., Fan, L., Caceres, A.I., Robinson, E., Sui, A., McKay, M.C., McAlexander, M.A., Herrick, C.A., 2013. TRPA1 controls inflammation and pruritogen responses in allergic contact dermatitis. FASEB J. 27, 3549-3563.

Liu, Y., Li, M., Yang, Y., Xia, Y., Nieh, M.-P., 2014. The effects of temperature, salinity, concentration and PEGylated lipid on the spontaneous nanostructures of bicellar mixtures. Biochim. Biophys. Acta Biomembr. 1838, 1871-1880.

López, O., de la Maza, A., Coderch, L., López-Iglesias, C., Wehrli, E., Parra, J.L., 1998. Direct formation of mixed micelles in the solubilization of phospholipid liposomes by Triton X - 100. FEBS Lett. 426, 314-318.

Losonczi, J.A., Prestegard, J.H., 1998. Improved dilute bicelle solutions for high-resolution NMR of biological macromolecules. J. Biomol. NMR 12, 447-451.

Macheleidt, O., Sandhoff, K., Kaiser, H.W., 2002. Deficiency of epidermal protein-bound ω-hydroxyceramides in atopic dermatitis. J. Investig. Dermatol. 119, 166-173.
Madison, K.C., 2003. Barrier function of the skin: “la raison d'etre” of the epidermis. J. Invest. Dermatol. 121, 231-241.

Man, M.-Q., Hatano, Y., Lee, S.H., Man, M., Chang, S., Feingold, K.R., Leung, D.Y., Holleran, W., Uchida, Y., Elias, P.M., 2008. Characterization of a hapten-induced, murine model with multiple features of atopic dermatitis: structural, immunologic, and biochemical changes following single versus multiple oxazolone challenges. J. Invest. Dermatol. 128, 79-86.

Mao-Qiang, M., Brown, B.E., Wu-Pong, S., Feingold, K.R., Elias, P.M., 1995. Exogenous nonphysiologic vs physiologic lipids: divergent mechanisms for correction of permeability barrier dysfunction. Arch. Dermatol. 131, 809-816.

Mao-Qiang, M., Feingold, K.R., Thornfeldt, C.R., Elias, P.M., 1996. Optimization of physiological lipid mixtures for barrier repair. J. Invest. Dermatol. 106, 1096-1101.

Marekov, L.N., Steinert, P.M., 1998. Ceramides are bound to structural proteins of the human foreskin epidermal cornified cell envelope. J. Biol. Chem. 273, 17763-17770.

Masukawa, Y., Narita, H., Shimizu, E., Kondo, N., Sugai, Y., Oba, T., Homma, R., Ishikawa, J., Takagi, Y., Kitahara, T., 2008. Characterization of overall ceramide species in human stratum corneum. J. Lipid Res. 49, 1466-1476.

Matsumoto, K., Mizukoshi, K., Oyobikawa, M., Ohshima, H., Tagami, H., 2004. Establishment of an atopic dermatitis - like skin model in a hairless mouse by repeated elicitation of contact hypersensitivity that enables to conduct functional analyses of the stratum corneum with various non - invasive biophysical instruments. Skin Res. Technol. 10, 122-129.

Menon, G.K., Feingold, K.R., Elias, P.M., 1992. Lamellar body secretory response to barrier disruption. J. Invest. Dermatol. 98, 279-289.

Mezei, M., Gulasekharam, V., 1982. Liposomes-a selective drug delivery system for the topical route of administration: gel dosage form. J. Pharm. Pharmacol. 34, 473-474.

Milner, M.E., O'Guin, W.M., Holbrook, K.A., Dale, B.A., 1992. Abnormal lamellar granules in harlequin ichthyosis. J. Invest. Dermatol. 99, 824-829.

Mojumdar, E., Gooris, G., Groen, D., Barlow, D.J., Lawrence, M., Deme, B., Bouwstra, J., 2016. Stratum corneum lipid matrix: location of acyl ceramide and cholesterol in the unit cell of the long periodicity phase. Biochim. Biophys. Acta Biomembr. 1858, 1926-1934.

Mordechai, S., Sahu, R., Hammody, Z., Mark, S., Kantarovich, K., Guterman, H., Podshyvalov, A., Goldstein, J., Argov, S., 2004. Possible common biomarkers from FTIR microspectroscopy of cervical cancer and melanoma. J. Microsc. 215, 86-91.

Motta, S., Monti, M., Sesana, S., Caputo, R., Carelli, S., Ghidoni, R., 1993. Ceramide composition of the psoriatic scale. Biochim. Biophys. Acta Mol. Basis Dis. 1182, 147-151.

Nangia, A., Patil, S., Berner, B., Boman, A., Maibach, H., 1998. In vitro measurement of transepidermal water loss: a rapid alternative to tritiated water permeation for assessing skin barrier functions. Int. J. Pharm. 170, 33-40.

Nielsen, J.B., 2005. Percutaneous penetration through slightly damaged skin. Arch. Dermatol. Res. 296, 560-567.

Norlén, L., 2015. Molecular structure and function of the skin barrier, in: Dragicevic, N., Maibach, H. (Eds.), Percutaneous Penetration Enhancers Chemical Methods in Penetration Enhancement. Springer, Berblin, Heidelberg, pp. 39-42.

Nutten, S., 2015. Atopic dermatitis: global epidemiology and risk factors. Ann. Nutr. Metab. 66, 8-16.

Opálka, L.s., Kováčik, A., Maixner, J., Vávrová, K.i., 2016. Omega-O-acylceramides in skin lipid membranes: effects of concentration, sphingoid base, and model complexity on microstructure and permeability. Langmuir : the ACS journal of surfaces and colloids 32, 12894-12904.

Opálka, L.s., Kováčik, A., Sochorová, M., Roh, J., Kunes, J., Lenčo, J., Vávrová, K.i., 2015. Scalable synthesis of human ultralong chain ceramides. Org. Lett. 17, 5456-5459.

Pellacani, G., Seidenari, S., 2001. Water sorption-desorption test and moisture accumulation test for functional assessment of atopic skin in children. Acta Dermato-Venereologica (Stockholm) 81, 100-103.

Pinto, S.N., Silva, L.C., Futerman, A.H., Prieto, M., 2011. Effect of ceramide structure on membrane biophysical properties: the role of acyl chain length and unsaturation. Biochim.Biophis. Acta Biomembr. 1808, 2753-2760.

Ponec, M., Weerheim, A., Lankhorst, P., Wertz, P., 2003. New acylceramide in native and reconstructed epidermis. J. Investig. Dermatol. 120, 581-588.

Pons Gimier, L., Parra Juez, J.L., 1995. Ciencia cosmética.

Pons Pons, R., 2012. Dispositivo para alojar una muestra en el interior de una cámara de dispersión o difracción de rayos X.

Rabionet, M., Gorgas, K., Sandhoff, R., 2014. Ceramide synthesis in the epidermis. Biochim. Biophys. Acta Mol. Cell. Biol. Lipids 1841, 422-434.

Rappolt, M., Amenitsch, H., Strancar, J., Teixeira, C.V., Kriechbaum, M., Pabst, G., Majerowicz, M., Laggner, P., 2004. Phospholipid mesophases at solid interfaces: in-situ X-ray diffraction and spin-label studies. Adv. Colloids Interface 111, 63-77.

Rippke, F., Schreiner, V., Doering, T., Maibach, H.I., 2004. Stratum corneum pH in atopic dermatitis. Am. J. Clin. Dermatol. 5, 217-223.

Robson, K.J., Stewart, M.E., Michelsen, S., Lazo, N.D., Downing, D.T., 1994. 6-Hydroxy-4-sphingenine in human epidermal ceramides. J. Lipid. Res. 35, 2060-2068.

Rodríguez, G., Barbosa-Barros, L., Rubio, L., Cócera, M., Fernández-Campos, F., Calpena, A., Fernández, E., de La Maza, A., López, O., 2015. Bicelles: new lipid nanosystems for dermatological applications. J. Biomed. Nanotechnol. 11, 282-290.

Rodríguez, G., Cócera, M., Rubio, L., Alonso, C., Pons, R., Sandt, C., Dumas, P., López-Iglesias, C., de la Maza, A., López, O., 2012. Bicellar systems to modify the phase behaviour of skin stratum corneum lipids. Phys. Chem. Chem. Phys. 14, 14523-14533.

Rodríguez, G., Rubio, L., Cócera, M., Estelrich, J., Pons, R., de la Maza, A., López, O., 2010. Application of bicellar systems on skin: diffusion and molecular organization effects. Langmuir : the ACS journal of surfaces and colloids 26, 10578-10584.

Rodríguez, G., Soria, G., Coll, E., Rubio, L., Barbosa-Barros, L., López-Iglesias, C., Planas, A.M., Estelrich, J., de la Maza, A., López, O., 2010. Bicosomes: bicelles in dilute systems. Biophis. J. 99, 480-488.

Rubio, L., Alonso, C., Rodríguez, G., Barbosa-Barros, L., Coderch, L., de la Maza, A., Parra, J.L., Lopez, O., 2010. Bicellar systems for in vitro percutaneous absorption of diclofenac. Int. J. Pharm. 386, 108-113.

Rubio, L., Rodríguez, G., Alonso, C., López-Iglesias, C., Cócera, M., Coderch, L., de la Maza, A., Parra, J., Lopez, O., 2011. Structural effects of flufenamic acid in DPPC/DHPC bicellar systems. Soft Matter 7, 8488-8497.

Sanders, C.R., Landis, G.C., 1994. Facile acquisition and assignment of oriented sample NMR spectra for bilayer surface-associated proteins. J. Am. Chem. Soc. 116, 6470-6471.

Sanders, C.R., Schwonek, J.P., 1992. Characterization of magnetically orientable bilayers in mixtures of dihexanoylphosphatidylcholine and dimyristoylphosphatidylcholine by solid-state NMR. Biochem. 31, 8898-8905.

Schaefer, H., Redelmeier, T., 1996. Skin barrier: Principles in percutaneous penetration. Karger, Basel, Switzerland.

Schurer, N.Y., Elias, P.M., 1991. The biochemistry and function of stratum corneum lipids, Advances in Lipid Research. Elsevier, pp. 27-56.

Sekkat, N., Kalia, Y., Guy, R.H., 2004. Development of an in vitro model for premature neonatal skin: biophysical characterization using transepidermal water loss. J. Pharm. Sci. 93, 2936-2940.

Serre, G., Mils, V., Haftek, M., Vincent, C., Croute, F., Réano, A., Ouhayoun, J.-P., Bettinger, S., Soleihavoup, J.-P., 1991. Identification of late differentiation antigens of human cornified epithelia, expressed in re-organized desmosomes and bound to cross-linked envelope. J. Investig. Dermatol. 97, 1061-1072.

Simonsen, L., Fullerton, A., 2007. Development of an in vitro skin permeation model simulating atopic dermatitis skin for the evaluation of dermatological products. Skin Pharmacol. Physiol. 20, 230-236.

Sindhvananda, J., Gritiyarangsan, P., Rungrairatanaroij, P., 1993. Flygroscopicity and water-holding capacity of moisturizing agents: A single-application in vivo study. Journal of the Society os Cosmetic Chemists 44, 279-288.

Smeden, J., Janssens, M., Kaye, E.C., Caspers, P.J., Lavrijsen, A.P., Vreeken, R.J., Bouwstra, J.A., 2014. The importance of free fatty acid chain length for the skin barrier function in atopic eczema patients. Exp. Dermatol. 23, 45-52.

Smith, W.P., Christensen, M.S., Nacht, S., Gans, E.H., 1982. Effect of lipids on the aggregation and permeability of human stratum corneum. J. Investig. Dermatol. 78, 7-11.

Spergel, J.M., Paller, A.S., 2003. Atopic dermatitis and the atopic march. J. Allergy Clin. Immunol. 112, S118-S127.

Stewart, M.E., Downing, D.T., 1999. A new 6-hydroxy-4-sphingenine-containing ceramide in human skin. J. Lipid Res. 40, 1434-1439.

Struppe, J., Vold, R.R., 1998. Dilute bicellar solutions for structural NMR work. Journal of Magnetic Resonance 135, 541-546.

Suto, H., Matsuda, H., Mitsuishi, K., Hira, K., Uchida, T., Unno, T., Ogawa, H., Ra, C., 1999. NC/Nga mice: a mouse model for atopic dermatitis. Int. Arch. Allergy Immunol. 120, 70-75.

Tagami, H., 2014. Electrical measurement of the hydration state of the skin surface in vivo. Br. J. Dermatol. 171, 29-33.

Tagami, H., Kanamaru, Y., Inoue, K., Suehisa, S., Inoue, F., Iwatsuki, K., Yoshikuni, K., Yamada, M., 1982. Water sorption-desorption test of the skin in vivo for functional assessment of the stratum corneum. J. Invest. Dermatol. 78, 425-428.

Tfayli, A., Piot, O., Durlach, A., Bernard, P., Manfait, M., 2005. Discriminating nevus and melanoma on paraffin-embedded skin biopsies using FTIR microspectroscopy. Biochim. Biophys. Acta Gen. Subj. 1724, 262-269.

Touitou, E., Dayan, N., Bergelson, L., Godin, B., Eliaz, M., 2000. Ethosomes - novel vesicular carriers for enhanced delivery: characterization and skin penetration properties. J. Control. Release 65, 403-418.

Treffel, P., Gabard, B., 1995. Stratum corneum dynamic function measurements after moisturizer or irritant application. Arch. Dermatol. Res. 287, 474-479.

Tsai, J.C., Sheu, H.M., Hung, P.L., Cheng, C.L., 2001. Effect of barrier disruption by acetone treatment on the permeability of compounds with various lipophilicities: implications for the permeability of compromised skin. J. Pharm. Sci. 90, 1242-1254.

Uchida, Y., Ogawa, T., Ohta, M., Kondo, M., Takada, S., Yamamura, M., 1991. Penetration of lysophosphatidylcholine into the dermis. J. Dermatol. 18, 523-527.

van Dam, L., Karlsson, G., Edwards, K., 2006. Morphology of magnetically aligning DMPC/DHPC aggregates perforated sheets, not disks. Langmuir : the ACS journal of surfaces and colloids 22, 3280-3285.

van den Bergh, B., Swartzendruber, D., Bos - Van der Geest, A., Hoogstraate, J., Schrijvers, A., Boddé, H., Junginger, H., Bouwstra, J., 1997. Development of an optimal protocol for the ultrastructural examination of skin by transmission electron microscopy. J. Microsc. 187, 125-133.

van Neste, D., 1990. In vivo evaluation of unbound water accumulation in stratum corneum. Dermatology 181, 197-201.

van Smeden, J., Hoppel, L., van der Heijden, R., Hankemeier, T., Vreeken, R.J., Bouwstra, J.A., 2011. LC-MS analysis of stratum corneum lipids: ceramide profiling and discovery. J. Lipid Res. 52, 1211-1221.

Varani, J., Dame, M.K., Rittie, L., Fligiel, S.E., Kang, S., Fisher, G.J., Voorhees, J.J., 2006. Decreased collagen production in chronologically aged skin: roles of age-dependent alteration in fibroblast function and defective mechanical stimulation. Am. J. Pathol. 168, 1861-1868.

Vávrová, K., Hrabalek, A., Mac ‐ Mary, S., Humbert, P., Muret, P., 2007. Ceramide analogue 14S24 selectively recovers perturbed human skin barrier. Br. J. Pharmacol. 157, 704-712.

Waller, J.M., Maibach, H.I., 2006. Age and skin structure and function, a quantitative approach (II): protein, glycosaminoglycan, water, and lipid content and structure. Skin Res. Technol. 12, 145-154.

Werner, Y., Lindberg, M., 1985. Transepidermal water loss in dry and clinically normal skin in patients with atopic dermatitis. Acta Derm. Venereol. 65, 102-105.

Wertz, P.W., 2000. Lipids and barrier function of the skin. Acta Derm. Venereol. Suppl (Stockh) 208, 7-11.

Wertz, P.W., Madison, K.C., Downing, D.T., 1989. Covalently bound lipids of human stratum corneum. J. Invest. Dermatol. 92, 109-111.

Wertz, P.W., Miethke, M.C., Long, S.A., Strauss, J.S., Downing, D.T., 1985. The composition of the ceramides from human stratum corneum and from comedones. J. Invest. Dermatol. 84, 410-412.

Yoshiike, T., Aikawa, Y., Sindhvananda, J., Suto, H., Nishimura, K., Kawamoto, T., Ogawa, H., 1993. Skin barrier defect in atopic dermatitis: increased permeability of the stratum corneum using dimethyl sulfoxide and theophylline. J. Dermatol. Sci. 5, 92-96.

7. ANEXOS

SYNCHROTRON INFRARED SPECTROSCOPY TO STUDY SKIN CONDITIONS

Moner V[1], Fernández E[1], Cócera M[2], Yousef I[3] and López O[1]
[1] Institute of Advanced Chemistry of Catalonia (IQAC–CSIC), [2]Bicosome S.L. [3]NCD-BL11 ALBA Synchrotron. Barcelona, Spain

Fourier Transform Infrared spectroscopy (FTIR) provides biochemical information about intracellular biomolecules such as proteins and lipids in biological tissues. Coupling **FTIR to Microscopy and Synchrotron Radiation** with high resolution and large brightness allows to generate a chemical map of the sample[1].

In **Atopic Dermatitis,** skin has deficiencies in stratum corneum (SC) lipids, especially ceramides and free fatty acids, showing reduced barrier function and alterations in lipid composition and organization[2]. Treatments focused in re-establishing lipid equilibrium could be very appropriated. The **Lamellar Body Mimetic System (LBms)** that mimics the morphology, structure and composition of epidermal lamellar bodies has demonstrated a repairing effect of lipid structure *in vitro*.[3]

[1]Fernández et al RSC Adv 2016, [2] Elias et al J Allergy Clin Inmunol, [3]Moner at al Int J Pharm 2016

This work uses synchrotron FTIR microspectroscopy to study different skin conditions : healthy skin, skin affected by dermatitis and, dermatitis skin after treatment with LBms

Lamellar body mimetic system (LBms) reduces irritation in oxazolone-induced dermatitis mice in vivo

LBms is formed by discoidal structures encapsulated in vesicles. This system includes SC lipids, lipids with antimicrobial characteristics and lipids focused on regulation of skin pH[3].

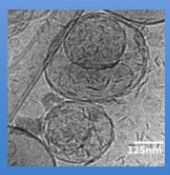

-Atopic dermatitis was induced by oxazolone in hairless mice.

-LBms was applied *in vivo* on dermatitis areas for 10 days.

-Skin biopsies included in OCT and sectioned were examined using FTIR microspectroscopy.

FTIR microspectroscopy allows to obtain chemical maps of skin sections

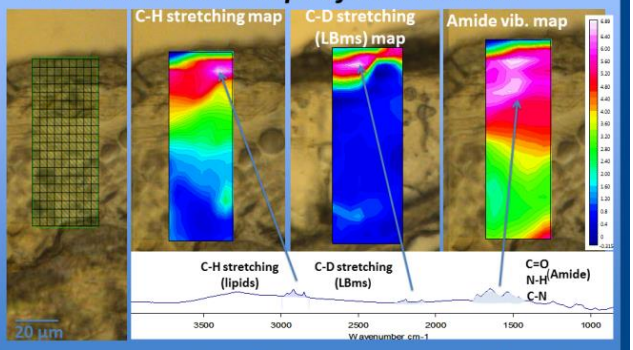

LBms is retained into SC-upper epidermis

Synchrotron infrared spectra forming the skin maps represent a huge amount of data. The procedure PCA (principal component analysis) using Unscrambler software helps to find out differences between samples.

PCA procedure shows the effect of LBms on induced dermatitis skin

PCA analysis:

-After correction of base line and normalization a spectrum with n peaks can be plotted as a point in a n-dimensional space. Each point is called score.
-The original coordinate system is transformed in a new one.
-The new coordinates are called principal components (PC1, PC2) and are related with the direction of highest variances.
-The origin of the new axis is located at the center of datapoints.
-Location and clustering of datapoints allows to determine similarities in spectral behavior.

PCA applied at each region separately (lipid and proteins) from SC-epidermis and dermis spectra are represented in the form of ***score plots.***

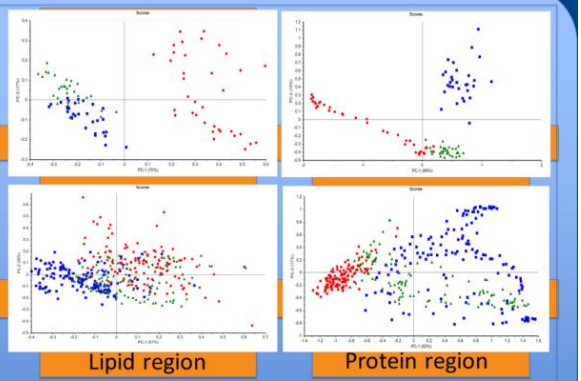

- **PCA shows clear similarities between healthy and dermatitis-treated skin, in both SC-epidermis and dermis zones.**
- **Skin affected by dermatitis without any treatment exhibited, in general, the most different behaviour in comparison with healthy and dermatitis-treated samples.**
- **It is interesting to note that in the protein region of dermis, the dermatitis-treated sample shows similar behaviour as healthy sample. This fact could indicate an effect of the treatment in the dermis, although the system did not penetrate so deep. Probably the effect *in vivo* of the LBms on the upper layers impacts the deeper layers conditions.**

- **FTIR microspectroscopy is an excelent methodology that allows:**
  - **-To obtain chemical maps of skin components.**
  - **-To monitor molecules with characteristic vibrational signatures applied on the skin.**
  - **-To be use as diagnosis tool for skin disfunctions and probably for evaluation of other tissues.**
- **LBms is retained in the SC and upper layers of the epidermis.**
- **Application of this system *in vivo* on skin affected by dermatitis reduces visual signs of irritation and recovers the skin vibrational behaviour.**